Dissertation zur Erlangung des Doktorgrades
der Fakultät für Chemie und Pharmazie
der Ludwig-Maximilians-Universität München

Circumventing the Limits of the Superacid HF/SbF$_5$: Synthesis of Elusive Cations

Christoph Jessen
aus
Rosenheim, Deutschland
2023

Erklärung

Diese Dissertation wurde im Sinne von § 7 der Promotionsordnung vom 28. November 2011 von Herrn Prof. Dr. Andreas J. Kornath betreut.

Eidesstattliche Versicherung

Diese Dissertation wurde selbstständig und ohne unerlaubte Hilfe erarbeitet.

München, den 24.04.2023

…………………………………

Christoph Jessen

Dissertation eingereicht am	22.02.2023
1. Gutachter:	Prof. Dr. Andreas J. Kornath
2. Gutachter:	Prof. Dr. Thomas M. Klapötke
Mündliche Prüfung am	22.03.2023

Danksagung

An erster Stelle bedanke ich mich bei meinem Doktorvater, Herrn Prof. Andreas J. Kornath, für die Betreuung dieser Doktorarbeit. Insbesonders bedanke ich mich für die Aufnahme in den Arbeitskreis, die Möglichkeit eine Vielzahl an interessanten Projekten zu bearbeiten und daran mitzuwirken, den großen Freiraum für eigene Ideen, die Unterstützung bei Fragen jeglicher Art, und für die tollen Erfahrungen auch außerhalb des Labors.

Des Weiteren möchte ich Herrn Prof. Thomas M. Klapötke für die Übernahme der Zweitkorrektur danken.

Großer Dank gebührt dem gesamten Arbeitskreis: Gaby, Manu, Flo, Ines, Yvonne, Domi, Fabi, Steffi, Alan, Marie, Alex, Basti, Dirk, Valentin, Julian und Ulli. An die schöne Zeit und die lustigen Momente mit euch werde ich mich immer gerne zurückerinnern. Dabei möchte ich mich besonders bei Gaby für die administrativen Angelegenheiten, bei Flo für den Aufwand mir quantenchemische Berechnungen beizubringen, bei Alex für das Vorbereiten und Messen von NMR Spektren und bei Alan und Marie für das pedantische Korrigieren meiner Manuskripte bedanken.

Steffi und Alan, vielen Dank, dass ich mich immer auf euch verlassen konnte und wir füreinander da waren. Bessere Doktorgeschwister und Freunde hätte ich mir nicht wünschen können für diese Zeit.

Außerdem bedanke ich mich bei meinen Praktikanten Basti, Hannah und Dirk für das experimentelle Mitwirken an dieser Arbeit.

Darüber hinaus gilt auch ein riesen Dank einigen Menschen außerhalb der Uni. Meiner ganzen Familie danke ich für die Unterstützung und das Vertrauen in mich und besonders für die Gewissheit immer für mich da zu sein. Die Sicherheit, die mir dieses Fundament gibt, ist für mich unersetzlich. Abschließend gebührt Milica ein besonders großer Dank. Du bist mit mir durch einen großen Teil der Zeit dieser Doktorarbeit gegangen und hast mich immer unterstützt, wenn es mal nicht so gut gelaufen ist. Viel Dank für deine Geduld, dein Verständnis und deinen guten Zuspruch.

Table of Contents

1. Introduction 1

2. Objectives 4

3. Summary 5

  3.1 The Reaction of Acetylenedicarboxylic Acid in Superacidic Media 5

  3.2 Elusive and Highly Acidic Sulfur(IV)-Oxo Cations 7

    3.2.1 Formation of the $FS(OH)_2^+$ Cation 7

    3.2.2 Isolation of Protonated Sulfur Dioxide 10

    3.2.3 Isolation of Protonated Thionyl Fluoride 12

  3.3 Isolation and Characterization of Cations Based on Malonyl Difluoride 14

    3.3.1 Protonation of Malonyl Difluoride in Superacidic Media 14

    3.3.2 Isolation of Acylium Cations Based on the Malonyl Backbone 17

4. Conclusion 23

5. References 25

6. Appendix 29

  6.1 List of Publications and Conference Contributions 29

    6.1.1 Publications and Manuscripts 29

    6.1.2 Publications not Included in this Thesis 29

    6.1.3 Conference Contributions 31

  6.2 Manuscripts, Supporting Information, and Cover Pictures 32

    6.2.1 Syntheses and Structures of Protonated Acetylenedicarboxylic Acid 32

    6.2.2 Synthesis and Structure of Protonated Sulfur Dioxide 53

    6.2.3 Characterization of Two Cationic Siblings: The Fluorodihydroxy- and Difluorohydroxysulfonium Cations Are Put to the Acid Test 72

    6.2.4 A Neutron Makes the Difference - Structures of Malonyl Difluoride and its Protonated Species in Condensed Media 105

    6.2.5 Acylium Cations of Malonyl Difluoride: Synthesis and Characterization of the $C_3O_2H^+$ Cation 144

1. Introduction

The term superacid was first introduced by HALL and CONANT in 1927.[1] A commonly used definition of superacids was given later by GILLESPIE as acids with a higher acidity than 100% sulfuric acid or perchloric acid.[2] Even in superacids, the proton is not isolated as H^+ but rather associated with the respective solvent or the acid itself.[3] This is described by Equation 1.[3]

$$B + H^+ \rightleftharpoons BH^+ \tag{1}$$

A quantitative classification of the strength of superacids is described by the HAMMETT acidity function H_0 (Equation 2).[4]

$$H_0 = -log\, a_{H^+} \cdot \frac{f_B}{f_{BH^+}} = -log\, K_{BH^+} + log \frac{C_B}{C_{BH^+}} \tag{2}$$

The H_0 values of the Brønsted superacids sulfuric acid (−12.1), fluorosulfuric acid (−15.1), or hydrogen fluoride (−15.1), are drastically decreased by the addition of strong Lewis acids.[3,5] Among the strongest superacids are the binary systems FSO_3H/SbF_5 (“magic acid”) and HF/SbF_5 with measured H_0 values of approximately −23.[3] In the binary superacidic system HF/SbF_5 the high acidity is based on the influence of the Lewis acid on the autoprotolysis equilibrium of HF (Equations 3-4).[6]

$$3\,HF \rightleftharpoons H_2F^+ + HF_2^- \tag{3}$$

$$HF_2^- + SbF_5 \longrightarrow HF + SbF_6^- \tag{4}$$

The field of superacid chemistry was probably shaped by no one as much as OLAH. He used the unique features of superacids to investigate carbocations, which are key intermediates of many organic reactions.[3] For his contribution to carbocation chemistry, he was awarded the Nobel Prize in 1994.[7] In addition to the investigation of reactive intermediates, the enormous acidity of superacids offers an opportunity to study the protonation of compounds with extremely low basicity. Thus, even common Brønsted acids are protonated in superacidic media and were isolated as salts.[8–10] An extreme example of the high acidity of the superacidic system HF/SbF_5 is the successful isolation of protonated fluorosulfuric acid as the salt $[FSO_3H_2][SbF_6]$.[11] Examples of the protonation of other weakly basic molecules by HF/SbF_5 are also found in the literature. HORVATH *et al.* attempted to protonate carbon monoxide in this superacidic system. They found strong evidence for the formation of the formyl cation, however only in solution and under high pressure of carbon monoxide.[12] The reactivity of sulfur dioxide was investigated in the superacidic system HF/SbF_5 by KORNATH *et al.* However, instead of protonated SO_2, the salt $[FS(OH)_2][SbF_6]$ was obtained as the product.[13]

A similar approach towards the protonation of molecules with extremely low basicity was introduced by REED and STOYANOV, using solid carborane superacids. The general formula of these compounds is described as $H(CHB_{11}X_5Y_6)$ (X = H, Me, F, Cl; Y = F, Cl, Br, I).[14] Even protonation of the molecules sulfur dioxide, carbon monoxide, and nitrous oxide are reported with the strongest carborane acid $H(CHB_{11}F_{11})$, based on results from IR spectroscopic measurements.[15–17] A determination of their H_0 value is, however, impossible since carborane acids are solids. Therefore, outside of solid-gas or solid-liquid reactions, carborane acids depend on the use of a solvent, limiting the absolute acidity of the respective system. For example, the acidity of carborane acids in an SO_2 solution is most likely limited by the proton disolvate $(SO_2)_2H^+$, which is the hemiprotonated species of SO_2.[18–20]

The availability of anhydrous hydrogen fluoride (*a*HF) as a versatile solvent for the superacidic system HF/SbF_5 is a great advantage over the solid carborane superacids, especially with respect to the isolation and particularly the crystallization of the protonated species as salts. Moreover, hydrogen fluoride acts as both solvent and reactant in the binary superacidic system HF/SbF_5. This property is applied profitably in synthetic chemistry as explained in the following.[21–24] Since HF is a poor nucleophile, a highly activated electrophile is needed for a reaction with the solvent *a*HF. Here an outstanding trademark of superacidic media comes into play: the generation and stabilization of electron-deficient cationic species.[25] Highly electrophilic di- or polycationic species are classified as superelectrophiles.[25,26] Concerning the reaction with *a*HF, superelectrophiles are used in synthetic chemistry to allow hydrofluorination reactions on a variety of substrates in the superacidic system HF/SbF_5, for example onto C=C double and C≡C triple bonds.[21–24]

Often discussed drawbacks of the binary superacid HF/SbF_5 are its high toxicity, corrosivity, and the high oxidation potential of the Lewis acid SbF_5.[6,27] An overlooked limitation of the system HF/SbF_5 is the mentioned reactivity of the solvent toward strong electrophiles. Namely, this reactivity makes the isolation of certain interesting cationic species from the solvent *a*HF very difficult, if not impossible. For example, attempting to protonate the molecules SO_3, SO_2, COF_2, or COH_2 with the superacidic system HF/SbF_5 leads instead to the cationic species $FSO_3H_2^+$,[11] $FS(OH)_2^+$,[13] $F_3COH_2^+$,[28,29] and $H_2COCH_2OH^+$,[30] respectively. For sulfur trioxide, carbonyl difluoride, and other perfluorinated ketones a reaction with HF is observed even without the addition of a Lewis acid.[11,28,31,32] The equilibrium of HF addition and elimination between the compounds carbonyl difluoride and trifluoromethanole is thoroughly investigated (Equation 5).[28,29,33,34]

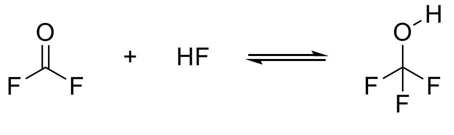

(5)

Surprisingly, the utilization of the HF addition and HF elimination equilibrium has been widely ignored for cationic, protonated species. Understanding how to manipulate this equilibrium to the side of HF elimination is a new approach toward the isolation of highly reactive and elusive cations.

An example is the difficult-to-access cation $C_3O_2H^+$, which is the monoprotonated species of carbon suboxide. Protonated species of carbon suboxide have been observed in the gas phase in mass spectrometry experiments, but not in the condensed phase.[35–39] The difficulty of protonating carbon suboxide arises mainly from its high reactivity. It readily reacts with hydrogen chloride, water, and poor nucleophiles like carboxylic acids.[40–43] Therefore, the successful isolation of protonated carbon suboxide from the superacidic system HF/SbF_5 seems unlikely. OLAH proposed a different approach toward the preparation of protonated carbon suboxide.[26,44] By abstraction of two fluoride anions from malonyl difluoride upon reaction with SbF_5, a diacylium cation is formed according to Scheme 1.[26,44]

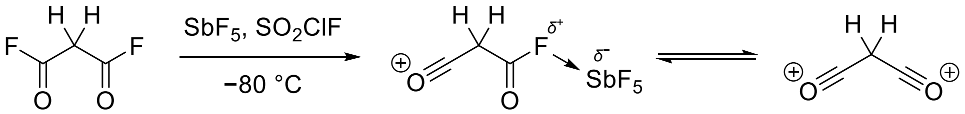

Scheme 1. Preparation of diprotonated carbon suboxide as proposed by OLAH. [26,44]

The shown diacylium cation is the diprotonated species of carbon suboxide. However, in the cited work the resulting products of the reaction could not be characterized due to their low stability.[45] This makes malonyl difluoride an interesting starting material for the investigation in superacidic media and for the reinvestigation of the reported reaction with SbF_5.

2. Objectives

This thesis aims to investigate the limitations of the binary superacidic system HF/SbF_5, concerning the preparation and isolation of small, cationic species. Depending on the target molecule, different approaches will be investigated to circumvent said limitations, with a special focus on formal HF addition and elimination reactions. With this premise in mind, the thesis is subdivided into three parts.

The first issue to address is the reactivity of acetylenedicarboxylic acid in superacidic media. Due to the structural similarity to oxalic acid, which is diprotonated by the superacidic system HF/SbF_5,[10] a possible protonation of acetylenedicarboxylic acid is promising. It will be investigated if protonated species of acetylenedicarboxylic acid can be isolated from the superacidic system, or if the protonation leads to a sufficient activation of the C≡C triple bond to allow further reactions with the solvent *a*HF.

The second part of the thesis addresses limiting factors concerning the protonation of weakly basic molecules in the superacidic medium HF/SbF_5. The reaction of SO_2 in HF/SbF_5 will be investigated to better understand the formation of the $FS(OH)_2^+$ cation, in search of a route to isolate protonated SO_2 in the solid state (Scheme 2, left). In the series of the sulfur(IV) cations, $FS(OH)_2^+$[13] – F_2SOH^+ – F_3S^+,[46] only protonated thionyl fluoride has not been isolated in the solid state so far (Scheme 2, right). A synthesis of the F_2SOH^+ cation will be attempted.

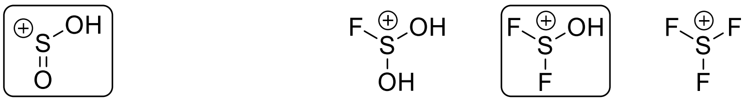

Scheme 2. Lewis structures (left to right) of protonated SO_2 and the three related cations $FS(OH)_2^+$, F_2SOH^+, and F_3S^+.

In the last part of the thesis, malonyl difluoride will be applied as starting material for the synthesis and isolation of cationic species which are based on the malonyl backbone. The basicity of malonyl difluoride will be investigated by reaction with the superacidic system HF/SbF_5 (Scheme 3). Furthermore, the reaction of malonyl difluoride with SbF_5 will be thoroughly investigated to isolate and characterize the obtained products. The objective is the isolation of acylium cations and, in particular, the synthesis of protonated carbon suboxide, which has been inaccessible from acidic solutions so far.

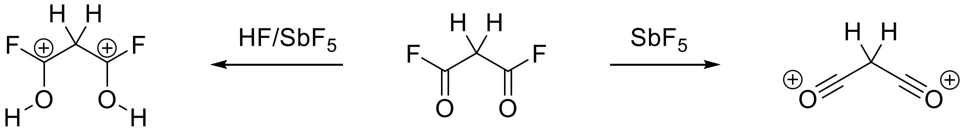

Scheme 3. Possible reactivity of malonyl difluoride with the superacidic system HF/SbF_5 or the Lewis superacid SbF_5.

3. Summary

3.1 The Reaction of Acetylenedicarboxylic Acid in Superacidic Media

The reaction of acetylenedicarboxylic acid with the hydrogen halides HCl, HBr, and HI was already described in 1882.[47] The reaction proceeds in the fuming acids to afford the respective halofumaric acids (Equation 6).[47] The corresponding reaction with hydrogen fluoride to form fluorofumaric acid has not been reported so far.

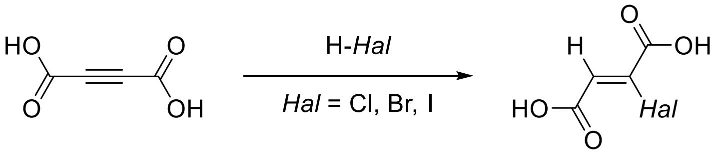

(6)

Acetylenedicarboxylic acid reacts with the binary superacids HF/*M*F_5 (*M* = As, Sb) according to Equation 7 and Equation 8.[48] Depending on the stoichiometric ratio of Lewis acid and acetylenedicarboxylic acid, the di- and monoprotonated species are obtained as the salts $[C_4H_4O_4][MF_6]$ and $[C_4H_3O_4][MF_6]$, respectively. The addition of hydrogen fluoride to the C≡C triple bond was not observed under the investigated reaction conditions.

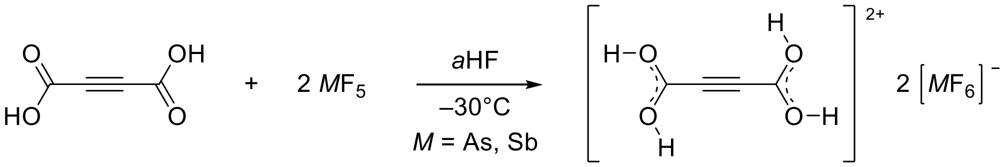

(7)

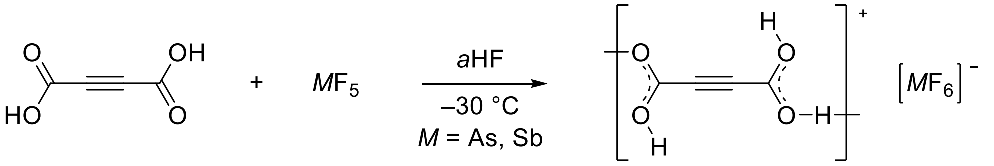

(8)

The mono- and diprotonation of acetylenedicarboxylic acid was confirmed by single-crystal X-ray structure analyses. Interestingly, the C≡C triple bond in the cations of the salts $[C_4H_3O_4][SbF_6]$ and $[C_4H_4O_4][SbF_6]$ is unaffected by the protonation compared to acetylenedicarboxylic acid.

Quantum chemical calculations of the neutral compound $C_4H_2O_4$ and the dication $C_4H_4O_4^{2+}$ were performed to study the electron distribution in these compounds. Figure 1 shows the calculated structures of $C_4H_2O_4$ and $C_4H_4O_4^{2+}$ together with NPA atomic charges. The charge of the central carbon atoms C2 and C3 is only slightly increased upon diprotonation. Thus, the *O*,*O*-diprotonation of acetylenedicarboxylic acid does not lead to sufficient electrophilic activation of the C≡C triple bond to allow an addition reaction of HF from the solvent.

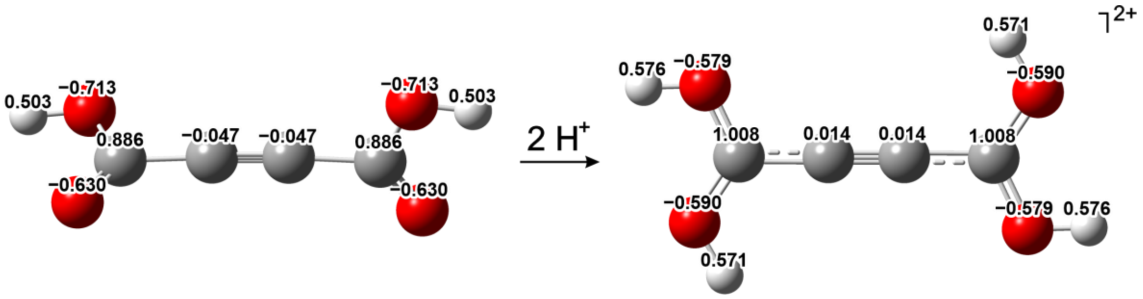

Figure 1. Calculated structures of acetylenedicarboxylic acid and its diprotonated species $C_4H_4O_4^{2+}$ together with NPA atomic charges on the respective atoms. The NPA charges are given in a.u.

In the salts of monoprotonated acetylenedicarboxylic acid ($[C_4H_3O_4][AsF_6]$, $[C_4H_3O_4][SbF_6]$) the cation is better described as twofold hemiprotonated and forms polycationic chains in the crystal structure via short O···H···O hydrogen bonds (Figure 2). The exact position of the proton is indeterminate by single-crystal X-Ray diffraction and can only be assumed to be on the inversion center in the middle of the O···O trajectory.

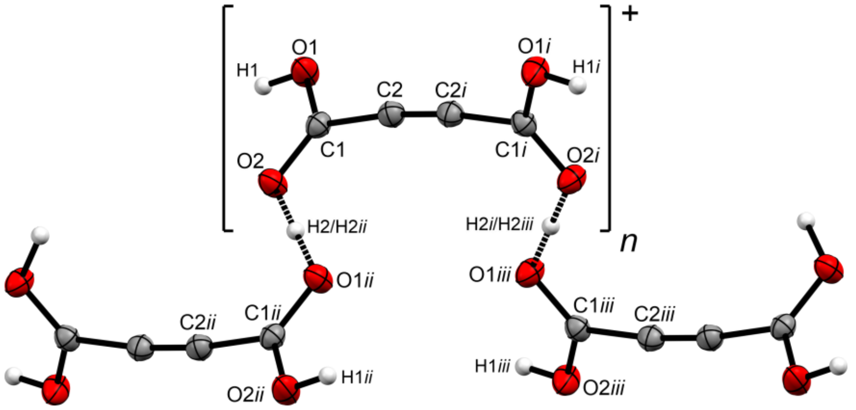

Figure 2. Twofold hemiprotonated cation chain from the crystal structure of monoprotonated acetylenedicarboxylic acid $[C_4H_3O_4][MF_6]$ (M = As, Sb). (50% probability displacement ellipsoids). Symmetry codes: *i* = 0.5−x,y,2−z; *ii* = 0.5−x,0.5−y,1.5−z; *iii* = x,0.5−y,0.5+z. Hydrogen bonds are drawn as dashed lines.

Comparable short and symmetrical hydrogen bonds, which are often found in hemiprotonated cations, have been discussed in the literature as short, strong, low-barrier (SSLB) hydrogen bonds.[49–54] The main characteristics of such hydrogen bonds are a similarly acidic donor and acceptor atom, a short donor-acceptor distance (<2.5 Å), and a low or no energy barrier at the symmetric position of the proton between the two acceptor atoms.[51] Quantum chemical calculations were performed to examine if the twofold hemiprotonation in monoprotonated acetylenedicarboxylic acid fits into the concept of SSLB hydrogen bonds. To simulate the polycationic chain, a sesquiprotonated dimer was employed for the calculations, as shown in Figure 3. A first-order saddle point with one imaginary frequency was found for the symmetrical structure when the proton is situated exactly in the middle of the O···O trajectory. This indicates a transition state (TS) between the actual minimum structures. These minimum structures were found upon a slight displacement of the proton out of the inversion center. This leads to the assumption that the position of the proton on the O···O trajectory can be described by a flat bottom energy well (Figure 3) with a small energy barrier between the two actual minima M1 and M2. This observation is in good agreement with the results from the crystal structure, as well as the concept of SSLB hydrogen bonds from the literature.[51]

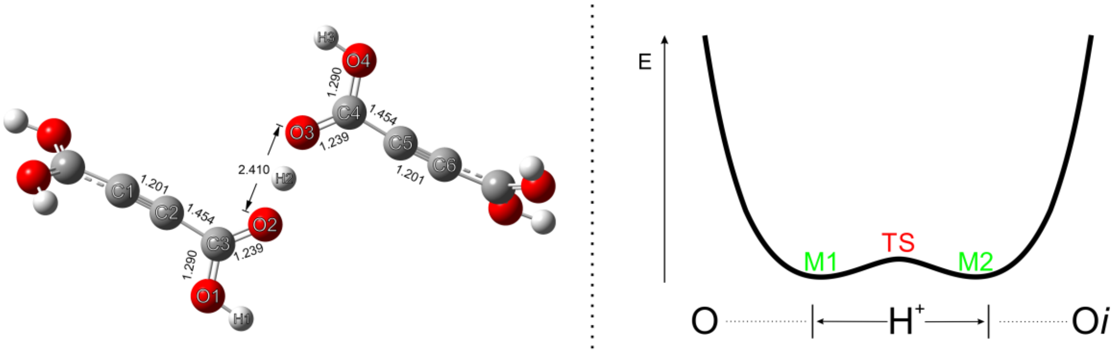

Geometry of the transition state TS

Position of the bridging proton H2

Figure 3. Left: Calculated structure of the sesquiprotonated dimer $[(C_4H_3O_4)\cdots H\cdots(C_4H_3O_4)]^{3+}$ at the first-order saddle point. Right: Schematic illustration of the flat bottom energy well typical for short, strong, low-barrier hydrogen bonds.[51]

3.2 Elusive and Highly Acidic Sulfur(IV)-Oxo Cations

3.2.1 Formation of the $FS(OH)_2^+$ Cation

Sulfur dioxide reacts with the binary superacidic system HF/SbF_5 under the formation of the salt $[FS(OH)_2][SbF_6]$.[13] The reported mechanism for this reaction is shown in Equations 9 to 11.[13] To initiate the reaction, the reaction mixture is warmed up to −25 °C for the formation of the complex $SO_2{\cdot}SbF_5$. Subsequently, the addition of HF and a further reaction in the superacid leads to the salt $[FS(OH)_2][SbF_6]$. Especially the addition of HF to the complex $SO_2{\cdot}SbF_5$ is interesting in the sense that sulfur dioxide itself does not show this reactivity towards HF.[55,56]

$$SO_2 + 2\,HF + SbF_5 \xrightarrow{-90\ ^\circ C} [H_2F]^+[SbF_6]^- + SO_2 \qquad (9)$$

$$[H_2F]^+[SbF_6]^- + SO_2 \xrightarrow{-25\ ^\circ C} SO_2{\cdot}SbF_5 + 2\,HF \qquad (10)$$

$$SO_2{\cdot}SbF_5 + 2\,HF \rightleftharpoons [FS(OH)_2]^+[SbF_6]^- \qquad (11)$$

The reported mechanism for the formation of $[FS(OH)_2][SbF_6]$ from the reaction of $SO_2{\cdot}SbF_5$ with *a*HF was verified by NMR spectroscopy (Figure 4). During the warming process of the reaction mixture in the NMR spectrometer, signal **B** is immediately detected at around 29 ppm in the ^{19}F NMR spectrum.

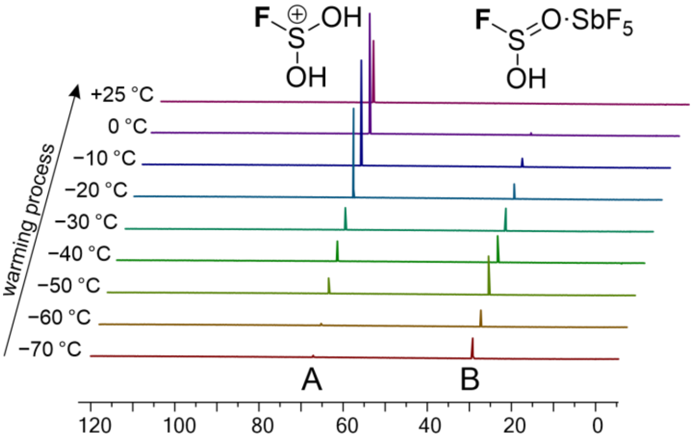

Figure 4. ^{19}F-NMR spectra of the reaction of $SO_2 \cdot SbF_5$ in *a*HF from −70 °C to 25 °C.

This signal is assigned to a complex of fluorosulfinic acid with SbF_5, which is the product of the addition reaction of HF to $SO_2 \cdot SbF_5$ (Scheme 4). By further warming of the reaction mixture, signal **B** disappears and only a second ^{19}F NMR signal of $FS(OH)_2^+$ (**A**) at around 70 ppm is observed up to room temperature. The stability of $FS(OH)_2^+$ in *a*HF solution up to room temperature is surprising since the isolated salt $[FS(OH)_2][SbF_6]$ already decomposes at around −70°C.

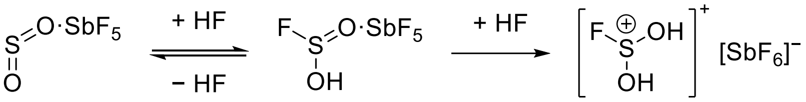

Scheme 4. Formation of $FS(OH)_2^+$ from $SO_2 \cdot SbF_5$.

The cation $FS(OH)_2^+$ was fully characterized by low-temperature Raman and IR spectroscopy as the salts $[FS(OH)_2][SbF_6]$ and $[FS(OH)_2][AsF_6]$. Additionally, a single-crystal X-ray structure analysis of $[FS(OH)_2][SbF_6]$ was performed. The quality of the crystal of this work afforded better X-Ray diffraction data than the reported crystal structure,[13] revealing a significant difference in the S−O and S−F bond lengths in the cation (Figure 5). Overall the reported results of KORNATH are confirmed and extended in detail by the results from this work.[13]

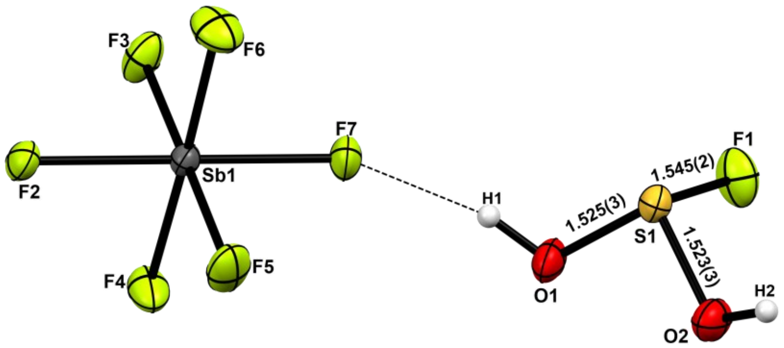

Figure 5. Formula unit of $[FS(OH)_2][SbF_6]$ with selected bond lengths in Å (50% probability displacement ellipsoids).

The described results raise the question if the complex $SO_2{\cdot}SbF_5$ is necessary for the formation of the $FS(OH)_2^+$ cation according to Equation 11, or if a protonation of SO_2 in the superacidic system HF/SbF_5, followed by HF addition leads to the same product according to Equation 12.

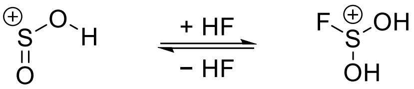

(12)

This was examined by adding stoichiometric amounts of SO_2 to the premixed superacid HF/SbF_5. The mixture was kept below −70 °C during the reaction to prevent the formation of $SO_2{\cdot}SbF_5$.[13] The obtained product was identified as $[FS(OH)_2][SbF_6]$. This indicates that SO_2 is protonated to a certain degree in the superacidic system HF/SbF_5 but it is not obtained as product because the intermediately formed SO_2H^+ reacts with the solvent *a*HF to form $FS(OH)_2^+$ according to Equation 12. The described synthesis of $FS(OH)_2^+$ was attempted with the weaker Lewis acids BF_3 and GeF_4 instead of SbF_5, but no products were obtained from these reactions.

To gain a deeper understanding of the addition of HF to the SO_2 moiety in these reactions, quantum chemical calculations were performed. The calculated molecular electrostatic potentials (MEP) mapped on the isodensity surfaces of SO_2, $SO_2{\cdot}BF_3$, $SO_2{\cdot}SbF_5$, and SO_2H^+ are shown in Figure 6, respectively. The MEP of SO_2H^+ was simulated by the ion pair $SO_2H^+{\cdots}F^-$. A background point charge (PC, charge = +1) was added next to the F^- ion to lower its basicity and simultaneously keep the overall charge of the calculated species at zero. The calculated species $[SO_2H^+F^-]_{PC}$ reproduces the calculated species $[SO_2H \cdot FH]^+$ very well and additionally allows a direct comparison of the electrostatic potentials of the SO_2 moiety in the different species.

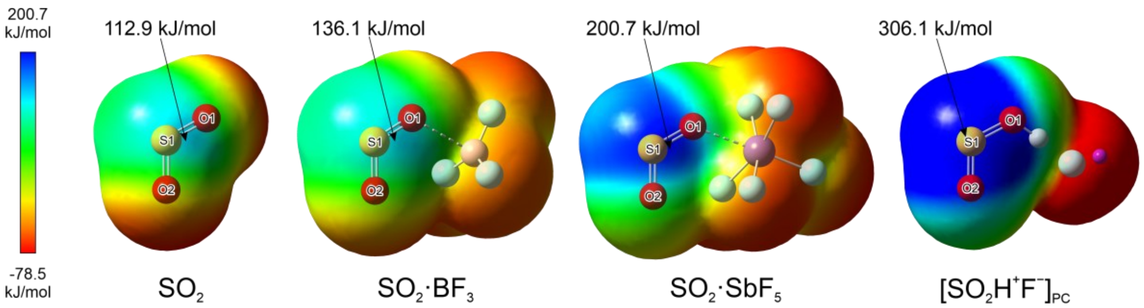

Figure 6. Molecular electrostatic potentials mapped on the isodensity surface of the respective calculated SO_2 species with the most positive points on the MEP surfaces. The mapped MEPs are illustrated in a color range of −78.5 kJ/mol (red) to 200.7 kJ/mol (blue). The color range of the MEP corresponds to the energy range of the MEP of $SO_2 \cdot SbF_5$. The positive background point charge (PC, charge = +1) of $[SO_2H^+F^-]_{PC}$ is illustrated as a purple dummy atom.

The SO_2 moiety becomes increasingly positively polarized upon interaction with increasingly strong Lewis acids. The greatest decrease in electron density is observed at the sulfur atom. Therefore, the SO_2 moiety is activated by the Lewis acid for electrophilic attacks. The highest electrophilic activation of the SO_2 moiety is observed in protonated SO_2.

From the calculations and the experimental results, it is concluded that the addition of HF to the SO_2 moiety and the formation of a stable compound is only observed when the SO_2 moiety is activated by strong Lewis acids. Therefore, at least the strong Lewis acid AsF_5 is needed for the reaction with HF and the stabilization as a salt of $FS(OH)_2^+$. Furthermore, the electron-deficient SO_2H^+ cation is expected to react with the solvent *a*HF to form $FS(OH)_2^+$ according to Equation 12. The reason why protonated SO_2 is not obtained as the product from the reaction of SO_2 with HF/SbF_5 is not the insufficient acidity of the superacid, but rather the high reactivity of the SO_2H^+ cation towards the solvent *a*HF.

3.2.2 Isolation of Protonated Sulfur Dioxide

The results on the formation of $FS(OH)_2^+$ were applied to investigate if the equilibrium of Equation 13 can be shifted to the side of protonated SO_2 by choosing appropriate conditions. This would provide a route to isolate protonated SO_2 by HF elimination from $FS(OH)_2^+$, according to Equation 13. The reaction was investigated for the H and D isotopologues.

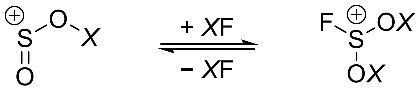

(13)

X = D, H

The elimination of XF (X = D, H) from $FS(OX)_2^+$ is achieved by redissolving the salt $[FS(OX_2)][SbF_6]$ in SO_2 at −40 °C. The solution is kept at −40 °C for several days, and subsequent removal of the volatile components *in vacuo* affords the salt $[(SO_2)_2X][Sb_2F_{11}]$ as product. The reaction proceeds according to Equation 14. Monoprotonated SO_2 is obtained by redissolving the salt $[FS(OX_2)][SbF_6]$ in 1,1,1,2-tetrafluoroethane (R-134a) at −40 °C. The solution is kept at −40 °C for several days, and subsequent removal of the volatile components *in vacuo* affords the salt $[SO_2X][Sb_2F_{11}]$ as the product. The reaction proceeds according to Equation 15.

$$2\,[\mathrm{FS(O}X)_2][\mathrm{SbF}_6] \xrightarrow[\mathrm{SO}_2]{-40\,^\circ\mathrm{C}} [(\mathrm{SO}_2)_2X][\mathrm{Sb}_2\mathrm{F}_{11}] + 3\,X\mathrm{F} \qquad (14)$$

$$X = \mathrm{D, H}$$

$$2\,[\mathrm{FS(O}X)_2][\mathrm{SbF}_6] \xrightarrow[\mathrm{R\text{-}134a}]{-40\,^\circ\mathrm{C}} [\mathrm{OSO}X][\mathrm{Sb}_2\mathrm{F}_{11}] + 3\,X\mathrm{F} + \mathrm{SO}_2 \qquad (15)$$

$$X = \mathrm{D, H}$$

The salt $[(SO_2)_2X][Sb_2F_{11}]$ which can be described as hemiprotonated SO_2, was characterized by Raman spectroscopy and by a single-crystal structure analysis of $[(SO_2)_2H][Sb_2F_{11}]$. Monoprotonated SO_2 was characterized as the salt $[SO_2D][Sb_2F_{11}]$ by Raman spectroscopy and by single-crystal structure analysis. The cations $(SO_2)_2H^+$ and SO_2D^+ are compared in Figure 7 along with bond angles and distances.

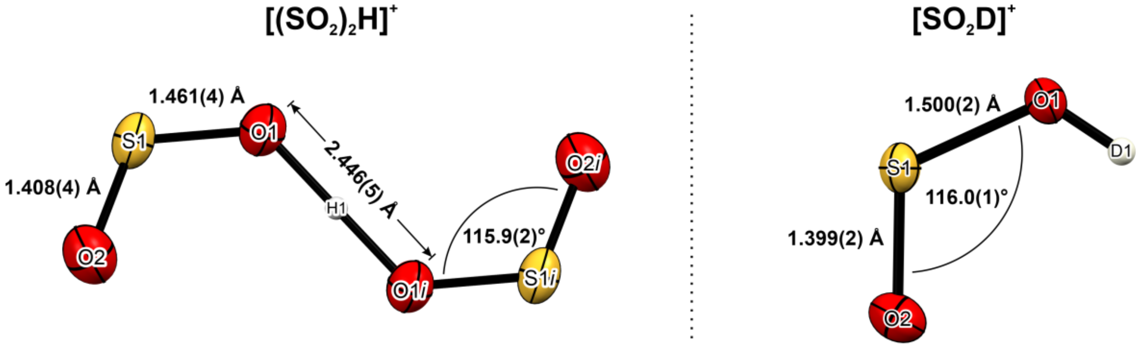

Figure 7. Structures of the cations of the salts $[(SO_2)_2H][Sb_2F_{11}]$ and $[SO_2D][Sb_2F_{11}]$ along with bond angles and distances. Symmetry code: *i* = −x,−y,1−z.

The acidity of $(SO_2)_2H^+$ was indirectly investigated by Reed *et al*. They attempted to measure the acidity of the carborane acids $H(CHB_{11}Cl_{11})$, $H(CHB_{11}H_5Cl_6)$, $H(CHB_{11}H_5Br_6)$, and $H(CHB_{11}H_5I_6)$ in liquid SO_2 solution via the mesityl oxide method by Fărcaşiu and Ghenciu.[57,58] For this method mesityl oxide was reacted with a superacidic medium (Equation 16) and a ^{13}C NMR spectrum of the solution was measured.[57]

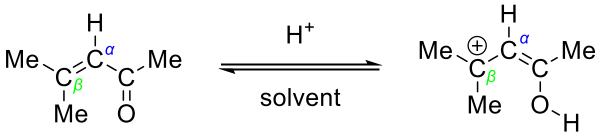

(16)

The ^{13}C NMR chemical shift difference ($\Delta\delta$) of the α- and β-carbons of mesityl oxide and its protonated species is larger the further the equilibrium is shifted to the right side of Equation 16.[57]

The acidity of the superacidic medium is deduced by correlating and comparing its $\Delta\delta$ value with H_0 values.[57,58] The carborane/SO_2 solutions showed larger $\Delta\delta$ values than the pure Brønsted superacids FSO_3H and CF_3SO_3H, which classifies them as superacidic.[58] Interestingly, the investigated carborane acids exhibit approximately the same $\Delta\delta$ value in SO_2 solution even though differing acidities were expected for the different carborane acids.[58] Under consideration that all of the investigated carborane acids protonate SO_2 to form the $(SO_2)_2H^+$ cation in solution, this observation is not surprising.[17,19,20] The $(SO_2)_2H^+$ cation is assumably the protonating species in carborane/SO_2 solutions, according to the leveling effect.[18–20] Therefore, the $\Delta\delta$ value of carborane/SO_2 solutions is a measurement of the acidity of protonated SO_2 rather than the acidity of the carborane acids. Consequently, a solution of $[(SO_2)_2H][Sb_2F_{11}]$ in liquid SO_2 is a superacidic medium as well. This agrees with the calculations of KROSSING *et al.* concerning a unified pH scale.[59] During the preparation of this thesis, the inhere presented superacidic medium $(SO_2)_2H^+/SO_2$ was used by VIRMANI to synthesize and isolate the to-date simplest carbon-centered vicinal dication, diprotonated 2,3-butanedione, which was inaccessible with the system HF/SbF_5.[60] The reaction is shown in Equation 17 without anions for simplification.[60]

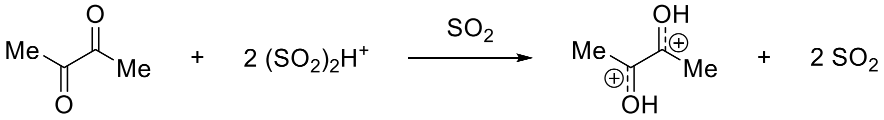

(17)

3.2.3 Isolation of Protonated Thionyl Fluoride

The successful isolation of protonated SO_2 was an impetus for the isolation of protonated species of even less basic molecules. A related, yet less basic molecule to SO_2 is SOF_2.[61] A protonation of SOF_2 has not been reported so far. However, BROWNSTEIN briefly investigated the complex $SOF_2{\cdot}SbF_5$ in *a*HF solutions.[62] NMR spectroscopic studies show, that the complex is not stable in *a*HF and reacts under the release of SOF_2.[62] The reaction was repeated in this work by dissolving the complex $SOF_2{\cdot}SbF_5$ in *a*HF according to Equation 18.

$$2\ SOF_2{\cdot}SbF_5 \xrightarrow[-78\ ^\circ C]{a\mathrm{HF}} [H_{n+1}F_n][Sb_2F_{11}] \quad + \quad 2\ SOF_2\uparrow \qquad (18)$$

After removing all volatile components *in vacuo*, only fluoronium salts of the formula $[H_{n+1}F_n][Sb_2F_{11}]$ were obtained as the product. The same result is observed when SOF_2 is reacted with the premixed binary superacidic system HF/SbF_5. This indicates that the isolation of protonated SOF_2 is at least hindered by the solvent *a*HF. To circumvent *a*HF as the solvent, R-134a was used instead and HF was applied in a stoichiometric ratio. The idea was to formally cleave the complex with HF according to Equation 19.

$$SOF_2{\cdot}Sb_2F_{10} \quad + \quad HF \quad \xrightarrow{\text{R-134a}} \quad SOF_2H^+ \quad + \quad Sb_2F_{11}^- \qquad (19)$$

First SOF_2 was reacted with two equivalents of SbF_5 in R-134a. The formation of a 1:2 complex of SOF_2:SbF_5 ($SOF_2{\cdot}Sb_2F_{10}$) in SO_2ClF was reported by GILLESPIE.[63] Subsequently, an equimolar amount of HF with respect to SOF_2 was condensed into the reaction mixture. A mixed salt of hemi- and monoprotonated thionyl fluoride ($[SOF_2H][(SOF_2)_2H][Sb_2F_{11}]_2$) was obtained as the product after removing all volatile components *in vacuo*. The salt was characterized by Raman and IR spectroscopy, and by a single-crystal X-ray structure analysis. The vibrational spectra indicate that the mixed salt is obtained as the bulk material from the reaction. The formula unit of $[SOF_2H][(SOF_2)_2H][Sb_2F_{11}]_2$ is depicted in Figure 8.

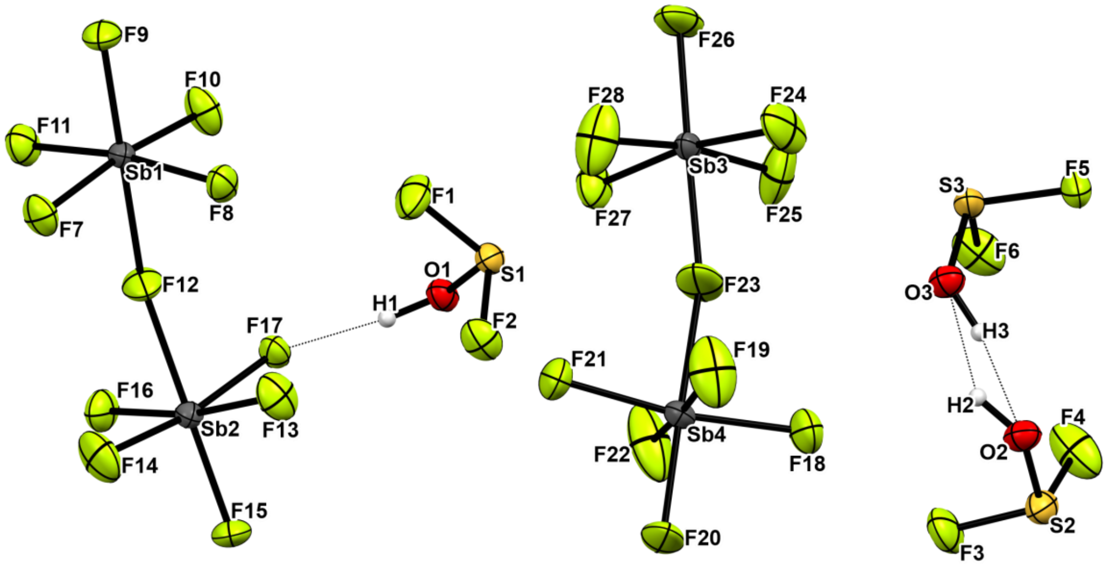

Figure 8. Formula unit of $[SOF_2H][(SOF_2)_2H][Sb_2F_{11}]_2$ (50% probability displacement ellipsoids). The protons H2 and H3 have a site occupancy factor of 0.5. Hydrogen bonds are drawn as dashed lines.

These findings lead to the assumption that protonation of SOF_2 is still present in the superacidic medium HF/SbF_5. However, the equilibrium (Equation 20) is certainly not shifted entirely towards the protonated species, as usually observed for more basic compounds in HF/SbF_5.

$$[H_{n+1}F_n][Sb_2F_{11}] \quad + \quad SOF_2 \quad \xrightleftharpoons{a\text{HF}} \quad [SOF_2H][Sb_2F_{11}] \quad + \quad n\ \text{HF} \qquad (20)$$

On the contrary, when the volatile components of this reaction mixture are removed *in vacuo*, the equilibrium is shifted to the side of the fluoronium salts due to the high volatility of SOF_2. Therefore, as solid products only fluoronium salts instead of protonated SOF_2 are obtained, when the reaction is performed in the solvent *a*HF. Changing the solvent from *a*HF to R-134a has a great influence on this equilibrium, allowing the isolation of $[SOF_2H][(SOF_2)_2H][Sb_2F_{11}]_2$. The

$(SOF_2)_2H^+$ cation proves the presence of "free" SOF_2 during the reaction, which indicates that Equation 20 is still applicable for the solvent R-134a. Overall, the observed results are summarized by Equation 21.

$$3\,SOF_2\cdot Sb_2F_{10} \quad + \quad 4\,HF \quad \xrightarrow[-70°C]{\text{R-134a}} \quad [SOF_2H][(SOF_2)_2H][Sb_2F_{11}]_2 \quad + \quad [H_2F][Sb_2F_{11}] \qquad (21)$$

Since the proton affinity of SOF_2 (659.8 kJ/mol)[64] is even lower than that of SO_2 (672.3 kJ/mol),[65] it was interesting to see if the isolated salt $[SOF_2H][(SOF_2)_2H][Sb_2F_{11}]_2$ could protonate SO_2 directly. Therefore, $[SOF_2H][(SOF_2)_2H][Sb_2F_{11}]_2$ was dissolved in liquid SO_2, and subsequently, all volatile components were removed *in vacuo*. The obtained product was identified as the salt of hemiprotonated SO_2 ($[(SO_2)_2H][Sb_2F_{11}]$) by Raman spectroscopy, which underlines the extremely high acidity of protonated thionyl fluoride. The reaction proceeds according to Equation 22.

$$[SOF_2H][(SOF_2)_2H][Sb_2F_{11}]_2 \quad \xrightarrow[-70°C]{SO_2} \quad 2\,[(SO_2)_2H][Sb_2F_{11}] \quad + \quad 3\,SOF_2 \qquad (22)$$

3.3 Isolation and Characterization of Cations Based on Malonyl Difluoride

3.3.1 Protonation of Malonyl Difluoride in Superacidic Media

The characterization of malonyl difluoride by gas-phase electron diffraction (GED) and gas-phase IR spectroscopy was reported by OBERHAMMER *et al.*[66] In the gas phase, malonyl difluoride exists exclusively as the diketo species $FOC{-}CH_2{-}COF$.[66] Therefore, malonyl difluoride was thoroughly investigated in the condensed phase by a single-crystal X-ray structure analysis, vibrational spectroscopy, and NMR spectroscopy in this work. Identical to its gas-phase structure, malonyl difluoride exists exclusively as diketo species in the solid state and in liquid *a*HF solution. Evidence of an enol-species was not found under the investigated conditions. The two independent formula units of the crystal structure of malonyl difluoride are shown in Figure 9.

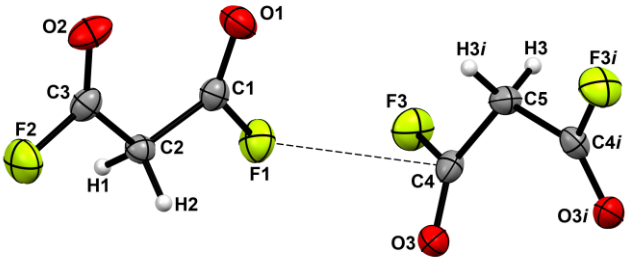

Figure 9. Two independent formula units of crystalline malonyl difluoride with 50% probability displacement ellipsoids. Symmetry code: *i* = 1−x,y,1−z. Contact is drawn as a dashed line.

Malonyl difluoride reacts with the superacidic system XF/SbF$_5$ (X = D, H) according to Equations 23-26.

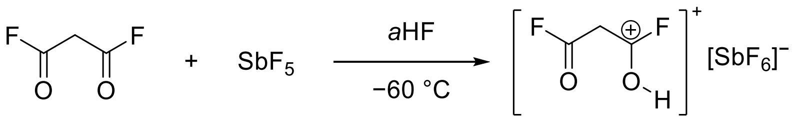

(23)

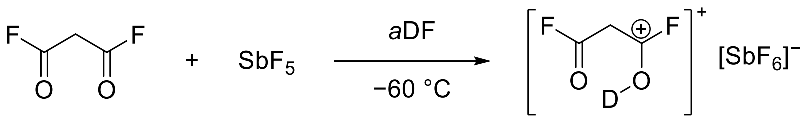

(24)

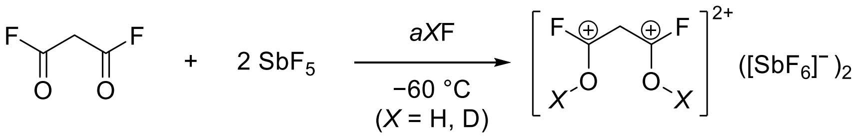

(25)

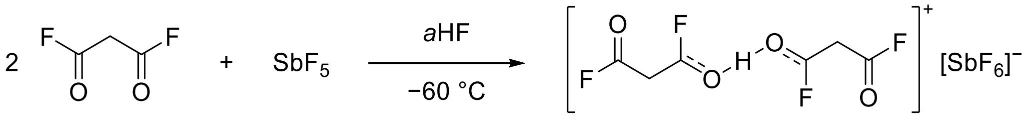

(26)

The salts of monoprotonated ([FOC−CH$_2$−C(OH)F][SbF$_6$], [FOC−CH$_2$−C(OD)F][SbF$_6$]), diprotonated ([F(HO)C−CH$_2$−C(OH)F][SbF$_6$]$_2$), and hemiprotonated ([(FOC−CH$_2$−COF)$_2$H][SbF$_6$]) malonyl difluoride were characterized by single-crystal X-ray structure analyses and low-temperature Raman spectroscopy, respectively. Additionally, low-temperature IR spectra of the two monoprotonated isotopologues were measured. The cations of the crystal structures of hemi- and diprotonated malonyl difluoride are shown in Figure 10.

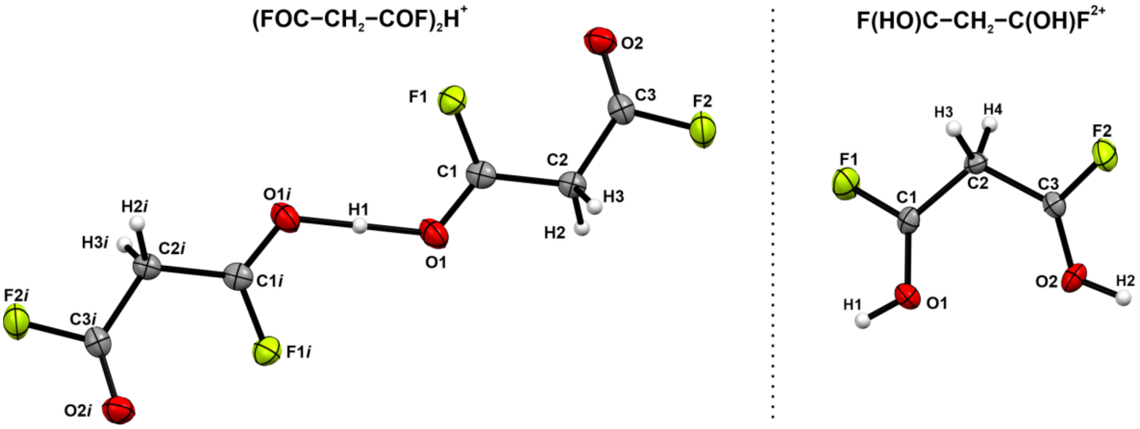

Figure 10. Left: Cation of hemiprotonated malonyl difluoride ($[(FOC{-}CH_2{-}COF)_2H][SbF_6]$) with 50% probability displacement ellipsoids. Symmetry code: *i* = 1−x,2−y,1−z. Right: Cation of diprotonated malonyl difluoride ($[F(HO)C{-}CH_2{-}C(OH)F][SbF_6]_2$) with 50% probability displacement ellipsoids.

Interestingly, in the solid state, the structures of the two monoprotonated isotopologues $FOC{-}CH_2{-}C(OH)F^+$ and $FOC{-}CH_2{-}C(OD)F^+$ differ in the positioning of the acidic proton and deuterium, respectively. This affects the geometrical parameters of the two cations in the crystal structure, which also has an effect on the vibrational spectra of the respective salts. In the literature, this rare phenomenon is described as isotopic polymorphism.[67–73] It is based on small energetic changes depending on the isotope which is involved in the hydrogen bonding.[68,74–76] The formula units of the salts $[FOC{-}CH_2{-}C(OH)F][SbF_6]$ and $[FOC{-}CH_2{-}C(OD)F][SbF_6]$ are depicted in Figure 11.

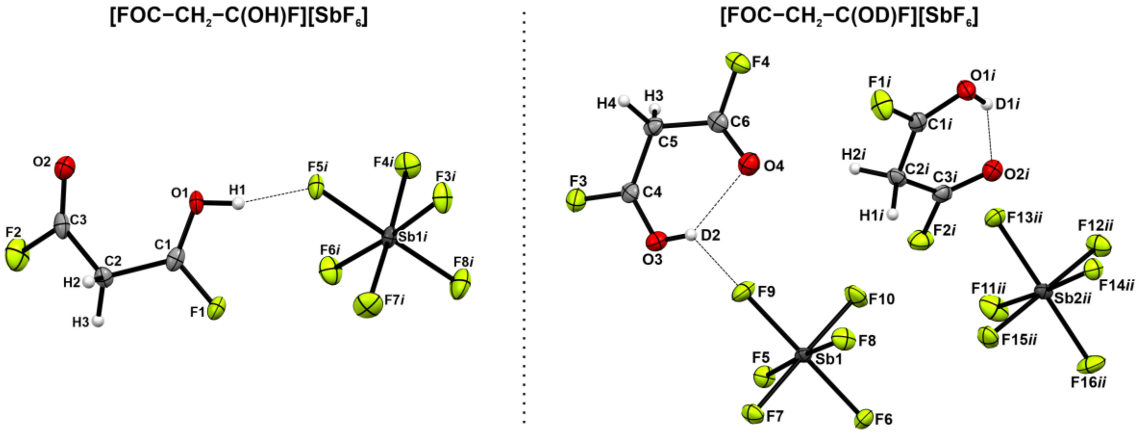

Figure 11. Left: Formula unit of monoprotonated malonyl difluoride with 50% probability displacement ellipsoids. Symmetry code: *i* = −1+x,y,z. Right: Two formula units of the deuterium isotopologue of monoprotonated malonyl difluoride with 50% probability displacement ellipsoids. Symmetry codes: *i* = 1+x,y,z; *ii* = x,y,1+z. Hydrogen bonds are drawn as dashed lines.

The electron distribution in the $F(HO)C{-}CH_2{-}C(OH)F^{2+}$ dication was addressed by quantum chemical calculations. These calculations aimed to find out whether $F(HO)C{-}CH_2{-}C(OH)F^{2+}$ is a 1,3-dication superelectrophile. The mapped molecular electrostatic potential (MEP) of the

$F(HO)C{-}CH_2{-}C(OH)F^{2+}$ dication is shown in Figure 12 together with the NPA charges of the respective atoms. From the MEP and NPA charges it is evident, that the positive charge is localized on the carbon atoms of the dication. Thus, $F(HO)C{-}CH_2{-}C(OH)F^{2+}$ is classified as 1,3-dicationic gitonic superelectrophile.[26] This finding is further supported by the results from the crystal structure. Figure 12 shows the Hirshfeld surface of the $F(HO)C{-}CH_2{-}C(OH)F^{2+}$ cation together with contacting fluorine atoms from the SbF_6^- anions. Three C···F contacts below the sum of the Van-der-Waals (VDW) radii (3.17 Å)[77] are found in the solid state structure between SbF_6^- anions and the carbenium centers (C1, C3) of $F(HO)C{-}CH_2{-}C(OH)F^{2+}$. The position of the contacting fluorine atoms in the crystal structure agrees very well with the calculated positive electrostatic potential of the dication.

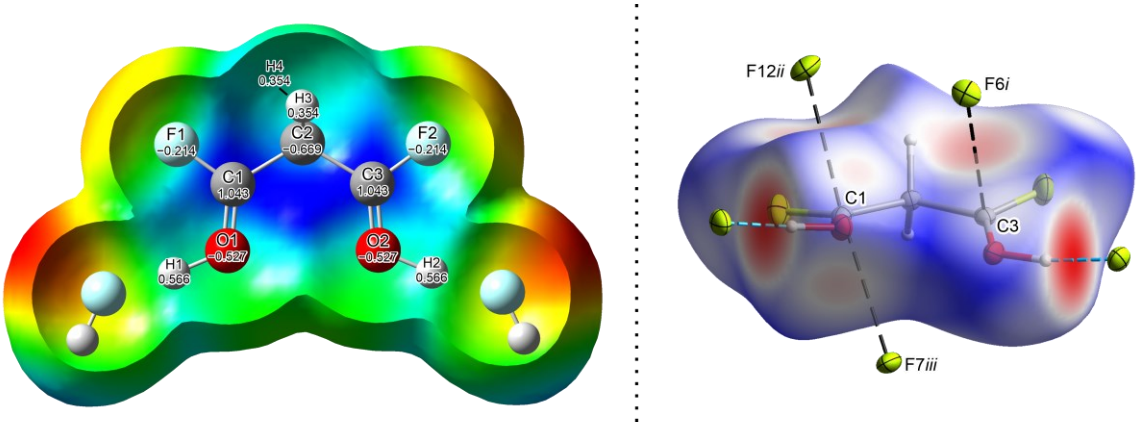

Figure 12. Left: Mapped MEP on the isodensity surface of the calculated $[F(HO)C{-}CH_2{-}C(OH)F \cdot 2HF]^{2+}$ cation, illustrated in a color range from 0.22 a.u. (red) to 0.35 a.u. (blue). The NPA charges are given in *e*. Right: Hirshfeld surface of the $F(HO)C{-}CH_2{-}C(OH)F^{2+}$ cation from the crystal structure of $[F(HO)C{-}CH_2{-}C(OH)F][SbF_6]_2$. Color coding of the Hirshfeld surface: white (distance equals VDW), blue (distance exceeds VDW distance), red (distance is smaller than VDW distance). Symmetry codes: *i* = 2−x,1−y,1−z; *ii* = 2−x,−0.5+y,1.5−z; *iii* = 1−x,1−y,1−z.

3.3.2 Isolation of Acylium Cations Based on the Malonyl Backbone

Since the reaction of malonyl difluoride with the binary superacidic system HF/SbF_5 only led to the protonation of the starting material, a different solvent was chosen to allow the formation and isolation of acylium cations. Malonyl difluoride reacts with SbF_5 in the solvent R-134a according to Equation 27. Even with a high excess of SbF_5, a diacylium cation, as described by OLAH, was not observed.[26,44]

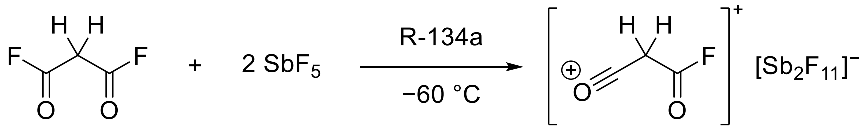

(27)

The monoacylium cation $FOC{-}CH_2{-}CO^+$ was characterized by low-temperature vibrational spectroscopy and NMR spectroscopy. Additionally, a single-crystal X-ray structure analysis of the salt $[FOC-CH_2-CO]_4[SbF_6][Sb_2F_{11}]_3\cdot SO_2$ was performed, which was obtained upon recrystallization of $[FOC-CH_2-CO][Sb_2F_{11}]$ in SO_2/SO_2ClF. The formula unit of this crystal structure is shown in Figure 13.

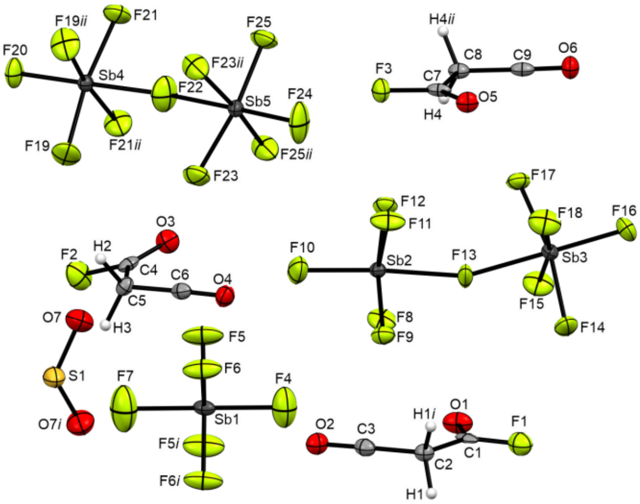

Figure 13. Formula unit of $[FOC-CH_2-CO]_4[SbF_6][Sb_2F_{11}]_3\cdot SO_2$. 50% probability displacement ellipsoids. Symmetry codes: *i* = x,−y,z; *ii* = x,1−y,z.

During longer recrystallizations of $[FOC-CH_2-CO][Sb_2F_{11}]$ in R-134a or SO_2ClF, a reaction of the starting material is observed. The starting material completely reacts over several days in solution to form the salt $[F(HO)C{=}CH-CO][Sb_2F_{11}]$. The considered reaction mechanisms are shown in Scheme 5.

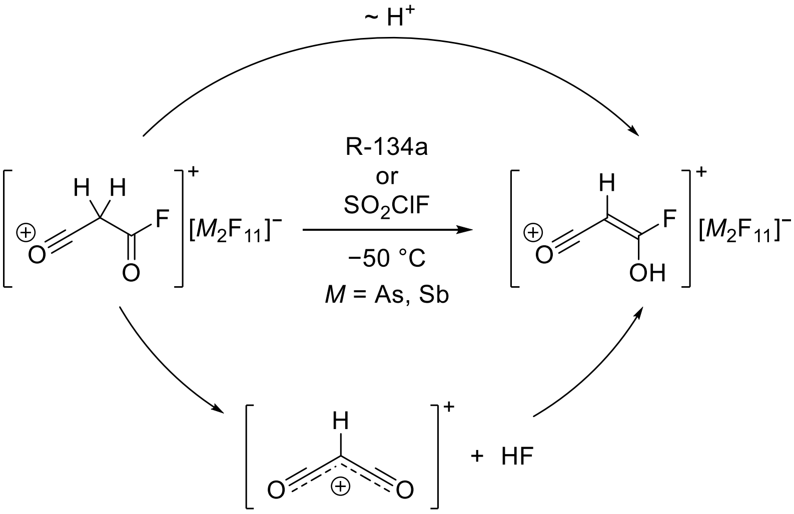

Scheme 5. Formation of the monoacylium cation $F(HO)C{=}CH-CO^+$.

The salts $[F(HO)C{=}CH-CO][M_2F_{11}]$ (M = As, Sb) were characterized by low-temperature Raman spectra and single-crystal X-ray structure analyses. The structure of the cation $F(HO)C{=}CH-CO^+$

is shown in Figure 14 along with bond lengths and bond angles. F(HO)C=CH−CO$^+$ is the enol tautomer to the keto tautomer FOC−CH$_2$−CO$^+$. Interestingly, the enol species is the favored tautomer for this cation. As explained in Chapter 3.3.1, acyl fluorides highly favor the keto tautomer.[66] This makes the F(HO)C=CH−CO$^+$ cation, the first isolated compound with a 1-fluoro-1-en-1-ol moiety. Furthermore, a second reaction pathway was considered for the formation of F(HO)C=CH−CO$^+$ (Scheme 5). An HF elimination reaction from the cation FOC−CH$_2$−CO$^+$ leads to the intermediate $C_3O_2H^+$ which reacts back with the released HF to form F(HO)C=CH−CO$^+$.

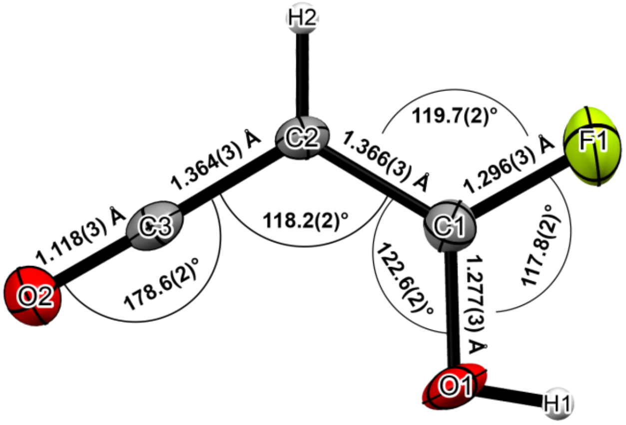

Figure 14. Structure of the cation of the salt [F(HO)C=CH−CO][As_2F_{11}]·with bond lengths and angles. 50% probability displacement ellipsoids.

The intermediately formed cation $C_3O_2H^+$ is of high interest, as it is the monoprotonated species of carbon suboxide. To remove the formed HF from the reaction mixture (Equation 28), the reactivity of the complex $SO_2{\cdot}SbF_2$ towards HF is utilized in this step (Equation 29). This prevents the formation of the F(HO)C=CH−CO$^+$ cation and enables the formation of $C_3O_2H^+$.

$$\text{FOC−CH}_2\text{−CO}^+ \longrightarrow C_3O_2H^+ + HF \tag{28}$$

$$SO_2{\cdot}SbF_5 + 2\,HF \longrightarrow [FS(OH)_2][SbF_6] \tag{29}$$

Contrary to the expected salt [FS(OH)$_2$][SbF$_6$], the formation of a different by-product is observed, which is identified as a protonated fluorosulfinic acid ester of malonyl fluoride, according to Equation 30. The salt [C_3O_2H][Sb_2F_{11}] is isolated by recrystallization of the mixture in R-134a.

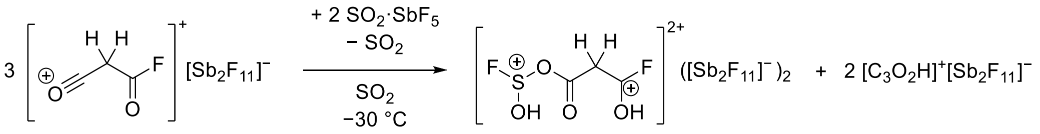

(30)

The salt [C_3O_2H][Sb_2F_{11}] was characterized by low-temperature Raman and IR spectroscopy, a single crystal X-ray structure analysis, and additionally by NMR spectroscopy of a solution in liquid SO_2. The structure of the cation $C_3O_2H^+$ is shown in Figure 15 along with bond lengths and bond angles. The structure of the cation is well comparable with the structures of the isoelectronic cations $OCNCO^+$ and N_5^+, which are reported in the literature.[78–80]

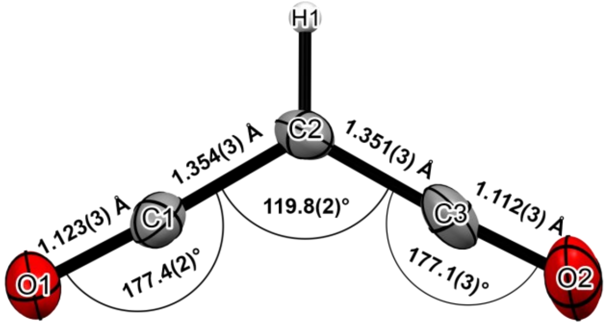

Figure 15. Structure of the cation of the salt $[C_3O_2H][As_2F_{11}]$·with bond lengths and angles. 50% probability displacement ellipsoids.

The three acylium cations $FOC{-}CH_2{-}CO^+$, $F(HO)C{=}CH{-}CO^+$, and $C_3O_2H^+$ readily react with HF when the respective salts are dissolved in liquid *a*HF at low temperatures. The reactions proceed with a formal HF addition to the C≡O and C=C bonds. The obtained product is in all cases monoprotonated malonyl difluoride according to Equations 31-33.

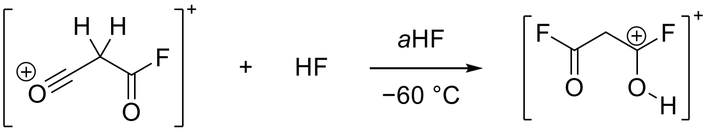

(31)

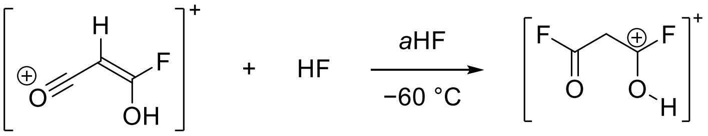

(32)

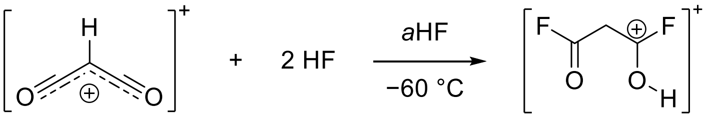

(33)

Since the electronic structure of the cations $F(HO)C{=}CH{-}CO^+$ and $C_3O_2H^+$ is not trivial, quantum chemical calculations were performed to find the most suitable Lewis structures to describe them. Therefore, a natural bond orbital (NBO) analysis, followed by a natural resonance theory (NRT) analysis was performed. The three highest weighted Lewis resonance structures of the two cations are depicted in Scheme 6 and Scheme 7, respectively.

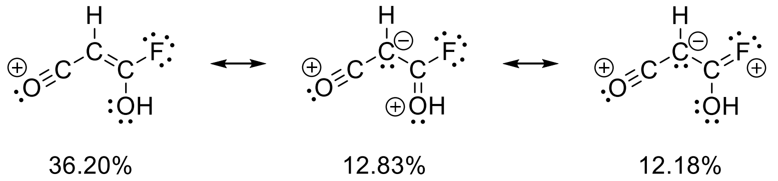

Scheme 6. Leading Lewis resonance structures of F(HO)C=CH−CO$^+$ with their weightings from the NRT analysis.

For F(HO)C=CH−CO$^+$ the highest weighted Lewis structure supports the experimental results to describe the cation as enol species with an adjected acylium group. In addition, the delocalization of the positive charge becomes evident, which explains the higher stability of F(HO)C=CH−CO$^+$ compared to FOC−CH$_2$−CO$^+$.

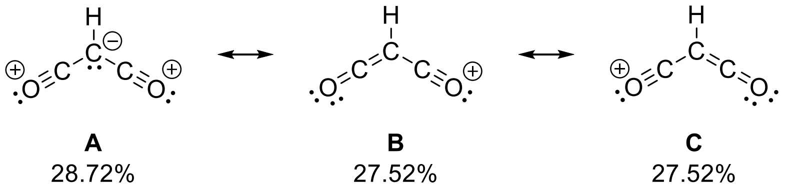

Scheme 7. Leading Lewis resonance structures of $C_3O_2H^+$ with their weightings from the NRT analysis.

The electronic structure of $C_3O_2H^+$ is more complex and difficult to describe with a single Lewis structure. The three leading Lewis resonance structures have approximately equal weightings, which indicates a high delocalization of the positive charge. The leading Lewis resonance structure **A** is best described as diacylium methanide with a lone pair on the central carbon atom and two attached acylium groups. The Lewis resonance structures **B** and **C** are degenerate and are best described as acylium ketene. The experimental results from the crystal structure and the ^{13}C NMR chemical shifts of [C_3O_2H][Sb_2F_{11}] are well comparable with the respective data for ketene and acylium ions in the literature.[81–86] The leading Lewis resonance structure **A** of $C_3O_2H^+$ appears unintuitive at first sight, due to the lone pair and negative formal charge on the central carbon atom. However, several arguments are made for this particular Lewis structure. For example, the calculated natural population analysis (NPA) charge of the central carbon atom is negative, as shown in Figure 16. Furthermore, the mapped molecular electrostatic potential (MEP) of the $C_3O_2H^+$ cation reveals that the highest electron deficiencies are situated around the acylium groups instead of the central carbon atom. Based on these findings it is argued that the Lewis resonance structure **A** best describes the experimental and theoretical results which were found for the $C_3O_2H^+$ cation.

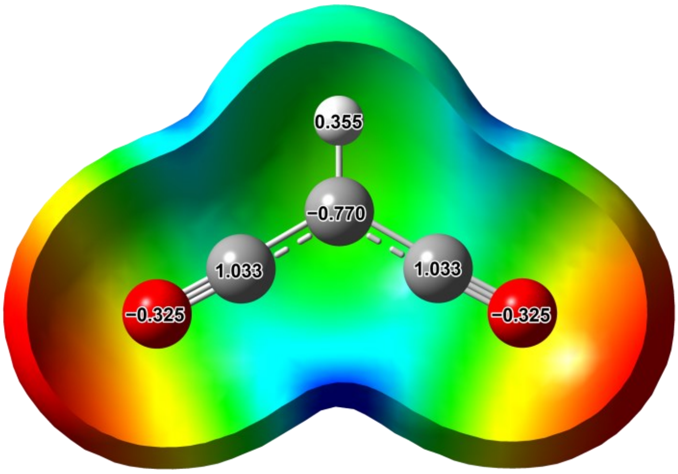

Figure 16. Molecular electrostatic potential (MEP) mapped on the electron density isosurface of the $C_3O_2H^+$ cation along with NPA charges of the respective atoms. The mapped MEP is illustrated in a color range from 0.135 a.u. (red) to 0.255 a.u. (blue). The NPA charges are given in *e*.

4. Conclusion

The reactivity of acetylenedicarboxylic acid was investigated in the binary superacidic systems HF/MF_5 (M = As, Sb). Mono- and diprotonated acetylenedicarboxylic acid were successfully isolated. A reaction of acetylenedicarboxylic acid or its protonated species with the solvent *a*HF to form fluorofumaric acid was not observed under the investigated conditions. The monoprotonated species is better described as twofold hemiprotonated acetylenedicarboxylic acid in the solid state. Quantum chemical calculations show that the short hydrogen bonds of the hemiprotonation are well comparable with short, strong, low-barrier hydrogen bonds from the literature.

The formation of the $FS(OH)_2^+$ cation in the superacidic system HF/MF_5 (M = As, Sb) was investigated by NMR spectroscopy. The cation is formed via a stepwise HF addition to the complex $SO_2\cdot SbF_5$. However, $FS(OH)_2^+$ is also observed as the only product if SO_2 is added to the premixed superacid. Based on this finding it is assumed that SO_2 is protonated in the superacidic system HF/SbF_5 but the highly electrophilic SO_2H^+ cation reacts with the solvent *a*HF to form $FS(OH)_2^+$. This is supported by quantum chemical calculations showing the electrophilic activation of the SO_2 moiety by various strong Lewis acids. The salt $[FS(OH)_2][SbF_6]$ is thermodynamically unstable toward the elimination of HF. This was exploited to prepare salts of hemi- and monoprotonated SO_2. The obtained salts were characterized by Raman spectroscopy and single-crystal X-Ray structure analysis. This synthesis allowed the clarification of the solid-state structure of protonated SO_2.

Protonated SOF_2 is not obtained as the product from the reaction of SOF_2 with the superacidic system HF/SbF_5. To isolate protonated SOF_2 the solvent R-134a was used to react $SOF_2\cdot Sb_2F_{10}$ with stoichiometric amounts of HF at low temperatures. The salt $[SOF_2H][(SOF_2)_2H][Sb_2F_{11}]_2$ is obtained as the product and was characterized by vibrational spectroscopy and single-crystal structure analysis. The high acidity of protonated SOF_2 is underlined by a direct protonation of SO_2 with the salt $[SOF_2H][(SOF_2)_2H][Sb_2F_{11}]_2$.

The structure of malonyl difluoride was investigated in the solid state as well as its basicity in HF/SbF_5. The salts of hemi-, mono, and diprotonated malonyl difluoride were isolated for the first time and characterized by vibrational and NMR spectroscopy, as well as single-crystal X-Ray structure analyses. The monoprotonated species is a rare example of H/D isotopic polymorphism leading to different solid-state structures for the H and D isotopologues. Diprotonated malonyl difluoride is a highly electron-deficient, gitonic 1,3-superelectrophile. In addition, malonyl difluoride was used for the synthesis of acylium cations. The keto-enol tautomeric monoacylium cations $FOC{-}CH_2{-}CO^+$ (keto) and $F(HO)C{=}CH{-}CO^+$ (enol) are described in the solid state for the first time. The salt $[FOC{-}CH_2{-}CO][Sb_2F_{11}]$ is used for a further reaction to prepare the salt $[C_3O_2H][Sb_2F_{11}]$. The cation $C_3O_2H^+$ is the monoprotonated species of carbon suboxide and is isolated in the condensed phase for the first time. The cation was thoroughly characterized by vibrational and NMR spectroscopy, as well as a single-crystal structure analysis. Experimental and theoretical results elucidate its unique structure.

In conclusion, the solvent *a*HF can be a limiting factor in reactions with the binary superacidic system HF/SbF_5. Despite HF being a poor nucleophile, highly reactive cations react with the solvent *a*HF, so their isolation from this solvent is not accessible. Furthermore, the basicity of the solvent *a*HF, although very low, is a limiting factor in the isolation of protonated species of volatile and weakly basic molecules. In this thesis, synthetic and preparational approaches are presented to gain access to several compounds, which were characterized in the condensed phase for the first time. The findings can be transferred to similar compounds to circumvent the limits of the superacidic system HF/SbF_5 concerning the synthesis and isolation of previously inaccessible cations.

5. References

[1] N. F. Hall, J. B. Conant, *J. Am. Chem. Soc.* **1927**, *49*, 3047.

[2] R. J. Gillespie, T. E. Peel in *Advances in Physical Organic Chemistry*, Elsevier, **1971**, S. 1–24.

[3] G. A. Olah, G. K. Surya Prakash, Á. Molnár, J. Sommer, *Superacid Chemistry*, John Wiley & Sons, Inc, Hoboken, NJ, USA, **2009**.

[4] L. P. Hammett, A. J. Deyrup, *J. Am. Chem. Soc.* **1932**, *54*, 2721.

[5] R. J. Gillespie, J. Liang, *J. Am. Chem. Soc.* **1988**, *110*, 6053.

[6] T. A. O’Donnell in *Advanced Inorganic Fluorides*, Elsevier, **2000**, S. 329–366.

[7] G. A. Olah, *A life of magic chemistry*. *Autobiographical reflections of a Nobel Prize winner*, John Wiley, New York, NY, Weinheim, **2001**.

[8] R. Minkwitz, S. Schneider, *Angew. Chem.* **1999**, *111*, 229.

[9] R. Minkwitz, R. Seelbinder, R. Schöbel, *Angew. Chem., Int. Ed.* **2002**, *41*, 111.

[10] M. Schickinger, T. Saal, F. Zischka, J. Axhausen, K. Stierstorfer, Y. Morgenstern, A. J. Kornath, *ChemistrySelect* **2018**, *3*, 12396.

[11] R. Seelbinder, N. R. Goetz, J. Weber, R. Minkwitz, A. J. Kornath, *Chem. - Eur. J.* **2010**, *16*, 1026.

[12] P. J. de Rege, J. A. Gladysz, I. T. Horvath, *Science* **1997**, *276*, 776.

[13] A. Kornath, R. Seelbinder, R. Minkwitz, *Angew. Chem., Int. Ed.* **2005**, *44*, 973.

[14] H. F. T. Klare, M. Oestreich, *J. Am. Chem. Soc.* **2021**, *143*, 15490.

[15] E. S. Stoyanov, S. E. Malykhin, *Phys. Chem. Chem. Phys.* **2016**, *18*, 4871.

[16] E. S. Stoyanov, I. V. Stoyanova, *Phys. Chem. Chem. Phys.* **2017**, *19*, 32733.

[17] E. S. Stoyanov, I. V. Stoyanova, *Angew. Chem., Int. Ed. Engl.* **2018**, *57*, 4516.

[18] M. Juhasz, S. Hoffmann, E. Stoyanov, K.-C. Kim, C. A. Reed, *Angew. Chem., Int. Ed. Engl.* **2004**, *43*, 5352.

[19] S. Cummings, H. P. Hratchian, C. A. Reed, *Angew. Chem., Int. Ed. Engl.* **2016**, *55*, 1382.

[20] C. A. Reed, *Chem. Commun. (Cambridge, U. K.)* **2005**, 1669.

[21] S. Thibaudeau, H. Carreyre, A. Mingot in *Modern Synthesis Processes and Reactivity of Fluorinated Compounds*, Elsevier, **2017**, S. 349–388.

[22] F. Liu, A. Martin-Mingot, M.-P. Jouannetaud, F. Zunino, S. Thibaudeau, *Org. Lett.* **2010**, *12*, 868.

[23] A.-C. Cantet, H. Carreyre, J.-P. Gesson, B. Renoux, M.-P. Jouannetaud, *Tetrahedron Lett.* **2006**, *47*, 5547.

[24] A.-C. Cantet, H. Carreyre, J.-P. Gesson, M.-P. Jouannetaud, B. Renoux, *J. Org. Chem.* **2008**, *73*, 2875.

[25] G. A. Olah, *Angew. Chem., Int. Ed. Engl.* **1993**, *32*, 767.

[26] G. A. Olah, D. A. Klumpp, *Superelectrophiles and Their Chemistry*, John Wiley & Sons, Inc, Hoboken, NJ, USA, **2007**.

[27] D. D. DesMarteau, *Science* **2000**, *289*, 72.

[28] K. O. Christe, J. Hegge, B. Hoge, R. Haiges, *Angew. Chem., Int. Ed.* **2007**, *46*, 6155.

[29] A. F. Baxter, J. Schaab, J. Hegge, T. Saal, M. Vasiliu, D. A. Dixon, R. Haiges, K. O. Christe, *Chem. - Eur. J.* **2018**, *24*, 16737.

[30] R. Minkwitz, S. Schneider, H. Preut, *Angew. Chem., Int. Ed. Engl.* **1998**, *37*, 494.

[31] S. Andreades, D. C. England, *J. Am. Chem. Soc.* **1961**, *83*, 4670.

[32] A. F. Baxter, J. Schaab, K. O. Christe, R. Haiges, *Angew. Chem., Int. Ed. Engl.* **2018**, *57*, 8174.

[33] G. Kloeter, K. Seppelt, *J. Am. Chem. Soc.* **1979**, *101*, 347.

[34] M. T. Nguyen, M. H. Matus, T. N. Vu, R. Haiges, K. O. Christe, D. A. Dixon, *J. Phys. Chem. A* **2008**, *112*, 1298.

[35] J. Tortajada, G. Provot, J.-P. Morizur, J.-F. Gal, P.-C. Maria, R. Flammang, Y. Govaert, *Int. J. Mass Spectrom. Ion Processes* **1995**, *141*, 241.

[36] J. B. Westmore, W. D. Buchannon, L. Plaggenborg, B. W. Wenclawiak, *J. Am. Soc. Mass Spectrom.* **1998**, *9*, 29.

[37] R. Sparrapan, M. A. Mendes, M. N. Eberlin, *J. Mass Spectrom.* **2000**, *35*, 189.

[38] M. Lang, F. Holzmeier, I. Fischer, P. Hemberger, *J. Phys. Chem. A* **2014**, *118*, 11235.

[39] J. Jin, L. Zhao, X. Wu, W. Li, Y. Liu, D. M. Andrada, M. Zhou, G. Frenking, *J. Phys. Chem. A* **2017**, *121*, 2903.

[40] O. Diels, B. Wolf, *Ber. Dtsch. Chem. Ges.* **1906**, *39*, 689.

[41] O. Diels, L. Lalin, *Ber. Dtsch. Chem. Ges.* **1908**, *41*, 3426.

[42] O. Diels, K. Hansen, *Ber. Dtsch. Chem. Ges. B* **1926**, *59*, 2555.

[43] T. Kappe, E. Ziegler, *Angew. Chem.* **1974**, *86*, 529.

[44] V. Prakash Reddy, G. K. Surya Prakash in *Advances in Physical Organic Chemistry*, Elsevier, **2009**, S. 219–260.

[45] G. A. Olah, M. B. Comisarow, *J. Am. Chem. Soc.* **1966**, *88*, 3313.

[46] D. D. Gibler, C. J. Adams, M. Fischer, A. Zalkin, N. Bartlett, *Inorg. Chem.* **1972**, *11*, 2325.

[47] E. Baudrowski, *Ber. Dtsch. Chem. Ges.* **1882**, *15*, 2694.

[48] C. Jessen, A. J. Kornath, *Eur. J. Inorg. Chem.* **2022**, e202100965.

[49] C. L. Perrin, *Science* **1994**, *266*, 1665.

[50] L. C. Remer, J. H. Jensen, *J. Phys. Chem. A* **2000**, *104*, 9266.

[51] D. Stasko, S. P. Hoffmann, K.-C. Kim, N. L. P. Fackler, A. S. Larsen, T. Drovetskaya, F. S. Tham, C. A. Reed, C. E. F. Rickard, P. D. W. Boyd et al., *J. Am. Chem. Soc.* **2002**, *124*, 13869.

[52] E. S. Stoyanov, C. A. Reed, *J. Phys. Chem. A* **2006**, *110*, 12992.

[53] S. J. Grabowski, J. M. Ugalde, *Chem. Phys. Lett.* **2010**, *493*, 37.

[54] C. A. Reed, *Acc. Chem. Res.* **2013**, *46*, 2567.

[55] F. Seel, L. Riehl, *Z. Anorg. Allg. Chem.* **1955**, *282*, 293.

[56] J. Shamir, A. Netzer, *Can. J. Chem.* **1973**, *51*, 2676.

[57] D. Fărcaşiu, A. Ghenciu, *J. Am. Chem. Soc.* **1993**, *115*, 10901.

[58] M. Juhasz, S. Hoffmann, E. Stoyanov, K.-C. Kim, C. A. Reed, *Angew. Chem., Int. Ed.* **2004**, *43*, 5352.

[59] D. Himmel, S. K. Goll, I. Leito, I. Krossing, *Angew. Chem., Int. Ed. Engl.* **2010**, *49*, 6885.

[60] A. Virmani, *In Search of Vicinal, Carbon-Centered Superelectrophiles*, Doctoral dissertation, Ludwig-Maximilians-Universität Munich, **2022**.

[61] G. de Petris, A. Cartoni, M. Rosi, V. Barone, C. Puzzarini, A. Troiani, *ChemPhysChem* **2011**, *12*, 112.

[62] S. M. Brownstein, *A Conductometric and Spectroscopic Investigation of Some Solutes in Anhydrous HF*, Doctoral dissertation, McMaster University, **1970**.

[63] P. A. W. Dean, R. J. Gillespie, *J. Am. Chem. Soc.* **1969**, *91*, 7260.

[64] F. Pepi, A. Ricci, M. Di Stefano, M. Rosi, G. D'Arcangelo, *J. Phys. Chem. A* **2002**, *106*, 9261.

[65] E. P. L. Hunter, S. G. Lias, *J. Phys. Chem. Ref. Data* **1998**, *27*, 413.

[66] A. Jin, H. G. Mack, A. Waterfeld, H. Oberhammer, *J. Am. Chem. Soc.* **1991**, *113*, 7847.

[67] S. Crawford, M. T. Kirchner, D. Bläser, R. Boese, W. I. F. David, A. Dawson, A. Gehrke, R. M. Ibberson, W. G. Marshall, S. Parsons et al., *Angew. Chem., Int. Ed. Engl.* **2009**, *48*, 755.

[68] K. Merz, A. Kupka, *Cryst. Growth Des.* **2015**, *15*, 1553.

[69] D. Mootz, M. Schilling, *J. Am. Chem. Soc.* **1992**, *114*, 7435.

[70] I. Majerz, Z. Malarski, T. Lis, *J. Mol. Struct.* **1990**, *240*, 47.

[71] B. C. K. Ip, I. G. Shenderovich, P. M. Tolstoy, J. Frydel, G. S. Denisov, G. Buntkowsky, H.-H. Limbach, *J. Phys. Chem. A* **2012**, *116*, 11370.

[72] N. P. Funnell, D. R. Allan, A. G. P. Maloney, R. I. Smith, C. J. G. Wilson, S. Parsons, *CrystEngComm* **2021**, *23*, 769.

[73] F. F. Iwasaki, Y. Saito, *Acta Crystallogr.* **1967**, *23*, 56.

[74] A. R. Ubbelohde, K. J. Gallagher, *Acta Crystallogr.* **1955**, *8*, 71.

[75] T. Steiner, *Angew. Chem., Int. Ed.* **2002**, *41*, 48.

[76] M. Ichikawa, *J. Mol. Struct.* **2000**, *552*, 63.

[77] A. Bondi, *J. Phys. Chem.* **1964**, *68*, 441.

[78] I. Bernhardi, T. Drews, K. Seppelt, *Angew. Chem., Int. Ed.* **1999**, *38*, 2232.

[79] K. O. Christe, W. W. Wilson, J. A. Sheehy, J. A. Boatz, *Angew. Chem., Int. Ed.* **1999**, *38*, 2004.

[80] A. Vij, W. W. Wilson, V. Vij, F. S. Tham, J. A. Sheehy, K. O. Christe, *J. Am. Chem. Soc.* **2001**, *123*, 6308.

[81] J. M. Le Carpentier, R. Weiss, *Acta Crystallogr., Sect. B: Struct. Crystallogr. Cryst. Chem.* **1972**, *28*, 1430.

[82] J. M. Le Carpentier, R. Weiss, *Acta Crystallogr., Sect. B: Struct. Crystallogr. Cryst. Chem.* **1972**, *28*, 1421.

[83] F. P. Boer, *J. Am. Chem. Soc.* **1968**, *90*, 6706.

[84] J. Firl, W. Runge, *Angew. Chem., Int. Ed.* **1973**, *12*, 668.

[85] S. J. Atkinson, R. Noble-Eddy, S. L. Masters, *J. Phys. Chem. A* **2016**, *120*, 2041.

[86] M. C. Bayer, N. Greither, C. Jessen, A. Nitzer, A. J. Kornath, *Eur. J. Inorg. Chem.* **2022**, *2022*.

6. Appendix

This appendix includes a list of publications and conference contributions, as well as the manuscripts, supporting information, and cover pictures that have been or will be published in the scope of this dissertation. The first manuscript has been peer-reviewed and published in a scientific journal. The other four manuscripts are currently in the process of being published. The manuscripts are organized thematically and align with the summary in this thesis, except for the content of chapter 3.2 *Elusive and Highly Acidic Sulfur(IV)-Oxo Cations*, which is summarized in two manuscripts.

6.1 List of Publications and Conference Contributions

6.1.1 Publications and Manuscripts

1. C. Jessen, A. J. Kornath, *Syntheses and Structures of Protonated Acetylenedicarboxylic Acid*, *Eur. J. Inorg. Chem.* **2022**, e202100965.
   DOI: 10.1002/ejic.202100965, Cover DOI: 10.1002/ejic.202200054
2. C. Jessen, A. J. Kornath, *Synthesis and Structure of Protonated Sulfur Dioxide*, publication in preparation.
3. C. Jessen, H. Illner, F. Zischka, A. Nitzer, A. Virmani, A. J. Kornath, *Characterization of Two Cationic Siblings: The Fluorodihydroxy- and Difluorohydroxysulfonium Cations Are Put to the Acid Test*, publication in preparation.
4. C. Jessen, D. Hollenwäger, A. J. Kornath, *A Neutron Makes the Difference - Structures of Malonyl Difluoride and its Protonated Species in Condensed Media*, publication in preparation.
5. C. Jessen, D. Hollenwäger, F. Zischka, A. J. Kornath, *Acylium Cations of Malonyl Difluoride: Synthesis and Characterization of the $C_3O_2H^+$ Cation*, publication in preparation.

6.1.2 Publications not Included in this Thesis

1. M. C. Bayer, C. Jessen, A. Kornath, *Preparation and Characterization of Protonated Fumaric Acid*, *Z. Anorg. Allg. Chem.* **2020**, *646*, 333-339.
   DOI: 10.1002/zaac.202000091

2. S. Beck, M. Raljic, C. Jessen, and A. J. Kornath, *Diprotonated Parabanic Acid: A vicinal or 1,3-dication?*, *Eur. J. Org. Chem.* **2020**, 4521–4527.
   DOI: 10.1002/ejoc.202000656

3. S. Beck, M. Feller, L. Spies, K. J. Dietrich, C. Jessen, K. Stierstorfer, and A. J. Kornath, *Protonation of γ-Butyrolactone and γ-Butyrolactam*, *ChemistryOpen* **2021**, *10*, 8–15.
   DOI: 10.1002/open.202000220

4. M. C. Bayer, C. Jessen, and A. J. Kornath, *Structure and Properties of Fumaryldifluoride*, *Z. Anorg. Allg. Chem.* **2021**, *647*, 258-265.
   DOI: 10.1002/zaac.202000248

5. S. Beck, C. Jessen, A. J. Kornath, *Protonated Ethylene Carbonate: A Highly Resonance-Stabilized Cation*, *ChemistryOpen* **2021**, *10*, 1160–1165.
   DOI: 10.1002/open.202100229

6. S. Beck, C. Jessen, A. J. Kornath, *Ring Opening and Closure Reactions of β-Propiolactone in the Superacids HF/MF$_5$ (M=Sb, As)*, *Eur. J. Org. Chem.* **2021**, 6628–6635.
   DOI: 10.1002/ejoc.202101351

7. A. Nitzer, M. Regnat, C. Jessen, A. J. Kornath, *Third Time is a Charm – Protonating Tricarboxybenzenes*, *Eur. J. Org. Chem.* **2022**, e202101488.
   DOI: 10.1002/ejoc.202101488

8. A. Nitzer, R. Hübsch, C. Jessen, A. J. Kornath, *Two Room-temperature-stable Trications – Triprotonated Triamino- and Tricyanobenzene*, *ChemistryOpen* **2022**, *11*, e202200049.
   DOI: 10.1002/open.202200049

9. S. Beck, V. Rück, L.-V. Pietsch, C. Jessen, A. J. Kornath, *Ring Opening Reactions of β-Propiolactam in Superacidic Media*, *Chem. Eur. J.* **2022**, *28*, e202104086.
   DOI: 10.1002/chem.202104086

10. S. Steiner, C. Jessen, A. J. Kornath, *Synthesis and Structural Investigation of Protonated Haloacetyl Fluorides*, *Z. Anorg. Allg. Chem.* **2022**, *648*, e202200060.
    DOI: 10.1002/zaac.202200060

11. A. Virmani, M. Pfeiffer, C. Jessen, Y. Morgenstern, A. J. Kornath, *Protonation of Pyruvic Acid – Synthesis of a plain Superelectrophile*, *Z. Anorg. Allg. Chem.* **2022**, *648*, e202200005
    DOI: 10.1002/zaac.202200005

12. M. C. Bayer, C. Kremser, C. Jessen, A. Nitzer, A. J. Kornath, *Strengthening of the C-F Bond in Fumaryl Fluoride with Superacids*, *Chem. Eur. J.* **2022**, *28*, e202104422.
    DOI: 10.1002/chem.202104422

13. M. C. Bayer, N. Greither, C. Jessen, A. Nitzer, A. J. Kornath, *Intermediates in Friedel-Crafts Acylation of Fumaryl Halides, Eur. J. Inorg. Chem.* **2022**, e202200391
DOI: 10.1002/ejic.202200391

6.1.3 Conference Contributions

1. Poster Presentation
C. Jessen, D. Hollenwäger, A. J. Kornath, *Protonation of Malonyl Difluoride*, 19th European Symposium on Fluorine Chemistry, Warsaw (Poland), August 25–31, **2019**.

2. Oral Presentation
C. Jessen, Hannah Illner, D. Hollenwäger, A. J. Kornath, *Circumventing the Limits of HF/SbF_5 – Synthesis and Isolation of Small Protonated Molecules*, 20th European Symposium on Fluorine Chemistry, Berlin (Germany), August 15–19, **2022**.

EurJIC

European Journal of Inorganic Chemistry

Chemistry Europe

European Chemical Societies Publishing

Cover Feature:

C. Jessen and A. J. Kornath

Syntheses and Structures of Protonated Acetylenedicarboxylic Acid

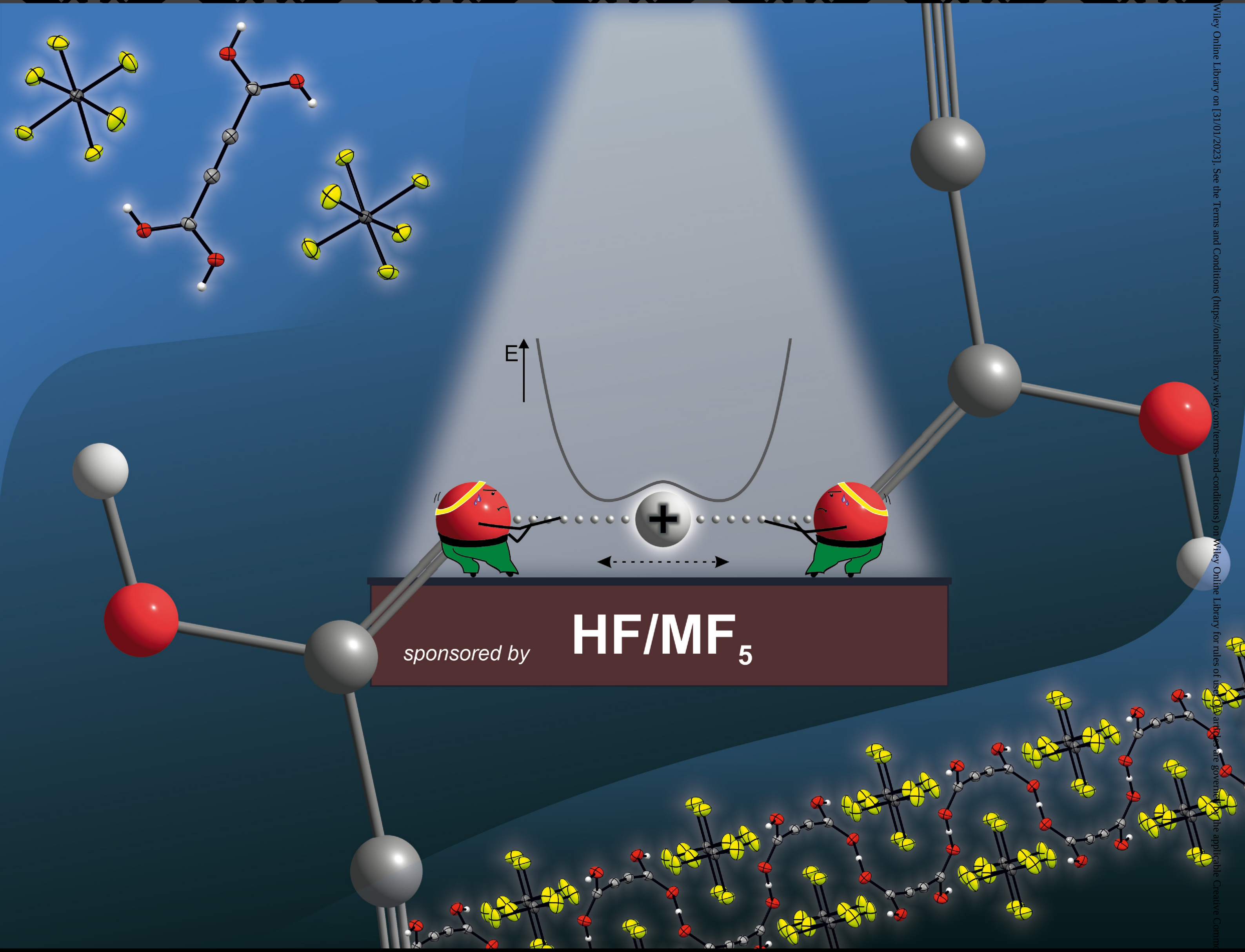

6/2022

WILEY-VCH

EurJIC
European Journal of Inorganic Chemistry

Research Article
doi.org/10.1002/ejic.202100965

Chemistry Europe
European Chemical Societies Publishing

www.eurjic.org

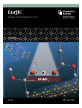

Syntheses and Structures of Protonated Acetylenedicarboxylic Acid

Christoph Jessen[a] and Andreas J. Kornath*[a]

Acetylenedicarboxylic acid ($C_4H_2O_4$) was protonated in the binary superacidic systems HF/MF_5 (M = As, Sb). Depending on the stoichiometric ratio of Lewis acid and acetylenedicarboxylic acid mono- and diprotonated acetylenedicarboxylic acid was obtained. The salts of diprotonated acetylenedicarboxylic acid were characterized by vibrational spectroscopy and in case of $[C_4H_4O_4][SbF_6]_2$ by a single-crystal X-ray structure analysis. The salt crystallizes in the monoclinic space group $C2/c$ with four formula units per unit cell. Furthermore, salts of monoprotonated acetylenedicarboxylic acid were synthesized and characterized by single-crystal X-ray structure analysis. The salts $[C_4H_3O_4][AsF_6]$ and $[C_4H_3O_4][SbF_6]$ crystallize in the monoclinic space group $C2/c$ with four formula units per unit cell. The monoprotonation is better described as a twofold hemiprotonation of acetylenedicarboxylic acid. The experimental results are discussed together with quantum chemical calculations.

Introduction

The acetylenedicarboxylic moiety is a widely applied structure motif in synthetic chemistry. It is commonly used as a dienophile and dipolarophile in cycloaddition reactions, or as Michael acceptor.[1] The acetylenedicarboxylate anion is deployed as ligand for coordination polymers or as building block for metal-organic frameworks (MOFs).[2] Its simplest form - acetylenedicarboxylic acid – was first described by *Bandrowski* in 1877. Since then, the acidic compound ($pK_{a1} = 1.75$; $pK_{a2} = 4.40$) and its corresponding anions have been thoroughly characterized. However, to the best of our knowledge the basicity of acetylenedicarboxylic acid has not been reported yet. This prompted us to investigate the behavior of acetylenedicarboxylic acid in superacid media.

Results and Discussion

Syntheses

Acetylenedicarboxylic acid was reacted in the binary superacidic systems XF/MF_5 (X = H, D; M = As, Sb) as shown in equation (1) and equation (2). Both reactions were performed in a two-step synthesis. First, the superacidic system (HF/AsF_5 or HF/SbF_5) was formed by homogenization of the Lewis acid with an excess of anhydrous hydrogen fluoride at −30 °C. After freezing the superacidic system at −196 °C, acetylenedicarboxylic acid was added under inert gas atmosphere. Then the mixture was warmed to −30 °C, where the protonation reaction took place. After the removal of excess *a*HF at −78 °C *in vacuo* the yellowish salts $[C_4H_4O_4][AsF_6]_2$ (**1**), $[C_4H_4O_4][SbF_6]_2$ (**2**) and the colorless salts $[C_4H_3O_4][AsF_6]$ (**3**), $[C_4H_3O_4][SbF_6]$ (**4**) were obtained. The salts of the diprotonated acetylenedicarboxylic acid (**1**) and (**2**) are stable up −10 °C, while the salts of the twofold hemiprotonated acetylenedicarboxylic acid (**3**) and (**4**) are stable up to 15 °C.

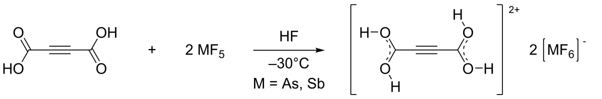

(1)

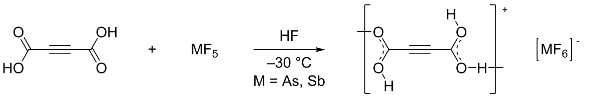

(2)

The corresponding deuterated salts $[C_4D_4O_4][AsF_6]_2$ (**5**) and $[C_4D_4O_4][SbF_6]_2$ (**6**) are obtained by changing the superacidic system from HF/MF_5 to DF/MF_5 (M = As, Sb). Due to large excess of *a*DF (100 : 1), a deuteration of approximately 98 % was achieved.

Crystal Structure of $[C_4H_4O_4][SbF_6]_2$

The salt $[C_4H_4O_4][SbF_6]_2$ (**2**) crystallizes in the monoclinic space group $C2/c$ with four formula units per unit cell. The formula unit is illustrated in Figure 1 and a summary of the geometric parameters is listed in Table 1. In the crystal packing of the starting material, acetylenedicarboxylic acid forms linear chains which are connected by disordered hydrogen bonds. Therefore, the C–O distances are equally long and in the range between regular C–O and C=O bond lengths.[3] Even though diprotonation breaks the $C_4H_2O_4$ chains apart, only small changes in its geometrical parameters are observed when $C_4H_2O_4$ is compared to (**2**). Due to the diprotonation an elongation of the C=O

---

[a] *C. Jessen, Prof. Dr. A. J. Kornath*
Department Chemie, Ludwig-Maximilians-Universität München
Butenandtstr. 5–13(D), 81377 München, Germany
E-mail: andreas.kornath@cup.uni-muenchen.de

Supporting information for this article is available on the WWW under https://doi.org/10.1002/ejic.202100965

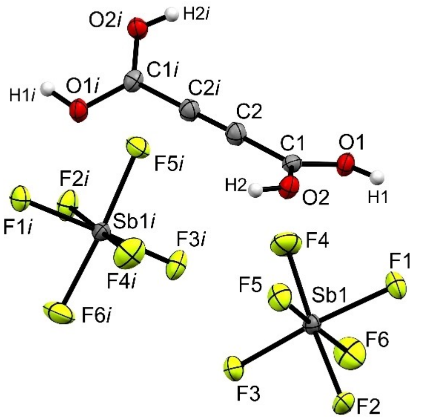

Figure 1. Formula unit of (**2**) (50% probability displacement ellipsoids). Symmetry code: $i = 1-x, y, 0.5-z$.

Table 1. Selected bond lengths and angles of acetylenedicarboxylic acid, $[C_4H_4O_4][SbF_6]_2$ **(2)** and $[C_4H_3O_4][SbF_6]$ **(4)**.

Bond lengths [Å]	$C_4H_2O_4$[5]	$[C_4H_4O_4][SbF_6]_2$	$[C_4H_3O_4][SbF_6]$
C1–C2 (C–C)	1.454(1)	1.442(4)	1.446(2)
C2–C2*i* (C≡C)	1.188(1)	1.180(5)	1.188(3)
C1–O1	1.262(1)	1.261(3)	1.282(2)
C1–O2	1.245(1)	1.264(3)	1.237(2)
Bond angles [°]			
O1–C1–O2	126.0(1)	121.2(2)	123.1(1)
O1–C1–C2	116.8(1)	116.0(2)	116.2(1)
O2–C1–C2	117.2(1)	122.8(2)	120.7(1)
C1–C2–C2*i*	177.7(1)	178.9(4)	172.9(1)
Angle of torsion [°]			
O1–C1–C2–C2*i*		142(10)	−165(1)
O2–C1–C2–C2*i*		−39(10)	14(1)
C1–C2–C2*i*–C1*i*		−146(13)	42(2)
Donor-acceptor distances [Å]			
O1–H1···F2*ii*		2.544(3)	
O2–H2···F1		2.537(2)	
O2–H2···O2*iii*			2.442(2)
O1–H1···F1			2.578 (2)

bonds of 0.019 Å is observed, which leads to bond lengths of 1.261(3) (C1–O1) and 1.264(3) Å (C1–O2) in (**2**). The positive charges are stabilized within the carboxy groups. This is also observed in the structurally similar tetrahydroxydicarbenium cation $[(HO)_2CC(OH)_2]^{2+}$ with C–O bond lengths of 1.257(2) Å and 1.259(3) Å.[4] On the contrary, the C–C and C≡C bonds are not significantly affected by the diprotonation. The $[C_4H_4O_4]^{2+}$ cation does not show a planar structure with the protonated carboxy groups being twisted with respect to each other by 41.10°.

The Sb–F bond lengths of the $[SbF_6]^-$ anion range from 1.848(2) to 1.917(2) Å. The values are typical for slightly distorted $[SbF_6]^-$ anions.[6–8] The distortion from the octahedral structure is caused by hydrogen bonds with the cation, which leads to an elongation of the Sb-F1 and Sb-F2 bonds.

Vibrational Spectra of $[C_4H_4O_4][SbF_6]_2$

Selected infrared and Raman spectra of $[C_4H_4O_4][SbF_6]_2$ (**2**), $[C_4D_4O_4][SbF_6]_2$ (**6**) and the starting materials $C_4H_2O_4$ and $C_4D_2O_4$ are shown in Figure 2. Table 2 summarizes selected experimental vibrational frequencies together with calculated frequencies of the $[C_4X_4O_4\cdot 4HF]^{2+}$ cation (X=H, D). The vibrational spectra of all synthesized salts of diprotonated acetylenedicarboxylic acid and their respective D-isotopomers are illustrated in the Supporting Information (Figure S2). According to the crystal structure, the dication possesses C_2 symmetry with 30 fundamental vibrations. All of them are expected to be IR and Raman active. The assignment is based on an analysis of the Cartesian displacement vectors of the calculated vibrational modes and a comparison with the vibrations described in the literature for $C_4H_2O_4$.[9]

The O–H stretching vibrations of (**2**) are not observed in the Raman spectrum due to the poor polarizability of the OH group. However, in the vibrational spectra of $[C_4D_4O_4][SbF_6]_2$ (**6**) the O–D stretching vibrations can be observed between 2126 cm^{-1} and 2016 cm^{-1} (Ra), and as a broad band between 2015 cm^{-1} and 2083 cm^{-1} (IR). The characteristic C≡C stretching mode is observed at 2301 cm^{-1} (**1**) and 2290 cm^{-1} (**2**), respectively with blue-shifts of 60 cm^{-1} (**1**) and 49 cm^{-1} (**2**) compared to the neutral compound.[9] The diprotonation of acetylenedicarboxylic acid is confirmed by the shifts of the CO stretching modes. The C=O stretching vibrations of $C_4H_2O_4$ at 1697 cm^{-1} and 1659 cm^{-1} are red-shifted in the diprotonated species (1644 cm^{-1} (**1**), 1645 cm^{-1} (**2**) (Ra) and 1634 cm^{-1} (**1**), 1632 cm^{-1} (**2**) (IR)).

The intense Raman lines at 1533 cm^{-1} (**1**) and 1529 cm^{-1} (**2**), respectively can be assigned to the other C–O stretching vibrations. Compared to the neutral compound, these ν(C–O)

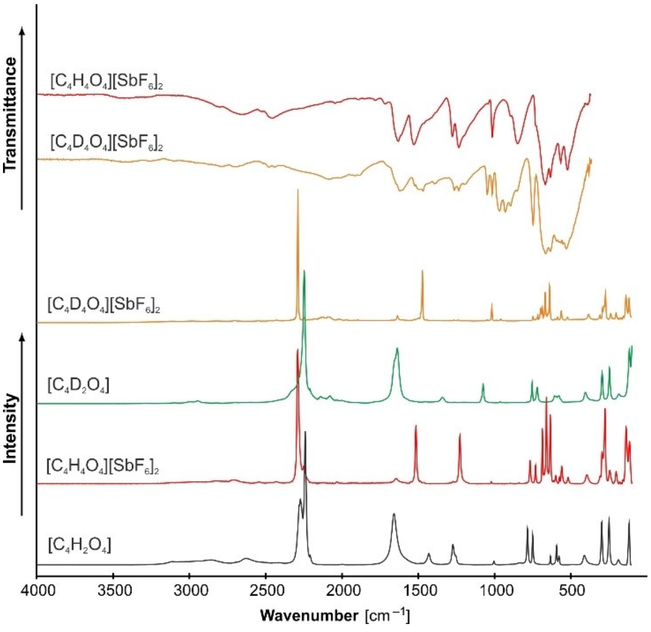

Figure 2. Low-temperature Raman and IR spectra of $[C_4X_4O_4][SbF_6]_2$ (X=H, D) (**2**, **6**), $C_4H_2O_4$ and $C_4D_2O_4$.

Table 2. Selected experimental vibrational frequencies [cm^{-1}] of $[C_4X_4O_4][SbF_6]_2$ (X = H, D) and calculated vibrational frequencies [cm^{-1}] of $[C_4X_4O_4\cdot 4HF]^{2+}$.

$[C_4H_4O_4][SbF_6]_2$ (**2**) exp.[a]		$[C_4D_4O_4][SbF_6]_2$ (**6**) exp.[a]		$[C_4H_4O_4\cdot 4\ HF]^{2+}$ calc.[b,c]	$[C_4D_4O_4\cdot 4\ HF]^{2+}$ calc.[b,c]	Assignment[d]
IR	Raman	IR	Raman	IR/Raman	IR/Raman	
2299 vw	2290 (100)		2290 (100)	2297 (0/517)	2301 (100/488)	ν(C≡C)
1632 m	1645 (4)	1626 m	1633 (6)	1654 (238/7)	1640 (570/4)	ν_s(CO)
	1592 (1)	1605 m	1604 (3)	1654 (594/4)	1639 (277/7)	ν_{as}(CO)
1529 m	1549 (2)	1518 m	1528 (3)	1521 (986/2)	1487 (996/2)	ν_{as}(CO)
	1516 (44)	1475 m	1478 (35)	1503 (78/69)	1462 (18/95)	ν_s(CO)
1277 m	1273 (2)	1016 w	1018 (12)	1247 (320/0)	1000 (59/10)	δ(COX)
1234 m		968 m	989 (2)	1234 (287/1)	946 (142/0)	δ(COX)
	1227 (36)	949 m	959 (3)	1228 (133/29)	929 (11/3)	δ(COX)
	1227 (36)	930 m	936 (2)	1228 (133/29)	910 (180/1)	δ(COX)

[a] Abbreviations for IR intensities: vs = very strong, s = strong, m = medium, w = weak. [b] Calculated on the M06/aug-cc-pVTZ level of theory. Scaling factor: 0.965. [c] IR intensities in km/mol; Raman intensities in Å^4/u. [d] X = H, D.

vibrations are blue-shifted by 110 cm^{-1} (**1**) and 90 cm^{-1} (**2**), respectively. Furthermore, four δ(COH) vibrations are observed between 1277 cm^{-1} (IR, (**2**)) and 1227 cm^{-1} (Ra, (**2**)). As expected, the corresponding δ(COD) vibrations are red-shifted and are observed between 1018 cm^{-1} (Ra, (**6**)) and 930 cm^{-1} (IR, (**6**)). In both compounds, more than the expected vibrations for anions with ideal octahedral symmetry are detected. This indicates a distortion of the $[AsF_6]^-$ and $[SbF_6]^-$ anions which is in accordance with the data from the crystal structure.

Crystal Structure of Monoprotonated Acetylenedicarboxylic Acid $[C_4H_3O_4][MF_6]$ (M=As, Sb)

The salts $[C_4H_3O_4][MF_6]$ (M = As, Sb) crystallize in the monoclinic space group $C2/c$ with four formula units per unit cell. The crystal structures of (**3**) and (**4**) are isomorphous. Since the geometric parameters of the cation in the two crystal structures do not differ significantly, only the crystal structure of $[C_4H_3O_4][SbF_6]$ (**4**) is discussed in the following part. The formula unit is illustrated in Figure 3 and the selected geometric parameters are listed in Table 1.

The formula unit of the $[AsF_6]^-$ salt (**3**) is depicted in Figure S1 and the geometric parameters of (**3**) and (**4**) are compared in Table S1 in the Supporting Information. On the one hand, the bond lengths of the carbon backbone of (**4**) are not affected by monoprotonation and are comparable to the starting material and $[C_4H_4O_4][SbF_6]_2$ (**2**). On the other hand, the bond lengths in the carboxy group change significantly. The C–O bond lengths of 1.282(2) Å (C1–O1) and 1.237(2) Å (C1–O2) differ by 0.045 Å. Therefore, there is a significant difference between the C–O bond lengths in **3** and **4** in contrast to the diprotonated species **2**, which shows no difference within the estimated standard deviations. This indicates that the positive charge is not equally distributed within the carboxy group as it is in $[C_4H_4O_4][SbF_6]_2$ (**2**). The bond angles in the $[C_4H_3O_4]^+$ cation are between the bond angles of the neutral compound and (**2**). The C1-C2-C2i bond angle with 172.9(1)° is surprisingly small for an sp-hybridized carbon atom, which results in a bent structure of the carbon scaffold. However, similar and even smaller angles along the carbon chain are well known for the acetylenedicarboxyl moiety.[5] In the $[SbF_6]^-$ anion the Sb–F bond lengths range from 1.851(2) to 1.891(1) Å, which are typical values for slightly distorted $[SbF_6]^-$ anions.[6–8] The distortion from the octahedral structure is due to hydrogen bonding towards the cation.

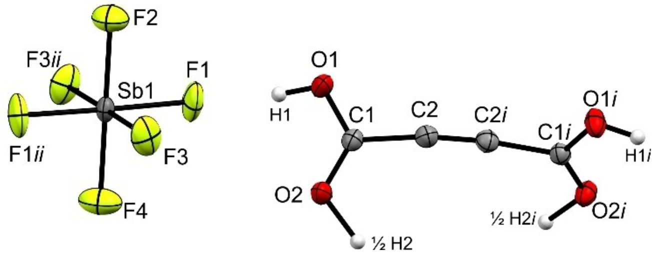

Figure 3. Formula unit of **4** (50% probability displacement ellipsoids). Symmetry codes: $I = -x, y, -0.5-z$; $ii = 1-x, y, 1.5-z$.

The cations in the crystal structure of (**4**) consist of hemiprotonated polycationic chains instead of the monoprotonated species $[C_4H_3O_4][MF_6]$. Therefore, the formally monoprotonated acetylenedicarboxylic acid is better described as twofold hemiprotonated acetylenedicarboxylic acid. A similar structure of polycationic chains with twofold hemiprotonated molecules is observed in monoprotonated p-benzoquinone and fumaric acid.[10,11] When formally monoprotonated acetylenedicarboxylic acid (**4**) is compared to monoprotonated oxalic acid, there is an interesting difference in the crystal packing. Oxalic acid shows a clear monoprotonation in its crystal structure, even though it also builds cationic chains via hydrogen bonds (Figure 4). A comparison to the C–O bond lengths in monoprotonated oxalic acid indicates that there is a significant difference between the monoprotonation and the twofold hemiprotonation. However, it should be noted, that the hemiprotonation could indicate an alternating situation between a protonation in one direction or the other. Therefore, the C–O bond lengths in (**4**), involved in the O···H···O hydrogen bonds are expected to be between the corresponding C–O bond lengths of monoprotonated oxalic acid. Indeed, this is observed and shown in Figure 4.

Figure 5 shows the difference electron density map of $[C_4H_3O_4][SbF_6]$ (**4**) in the plane of the two bridged carboxyl groups.

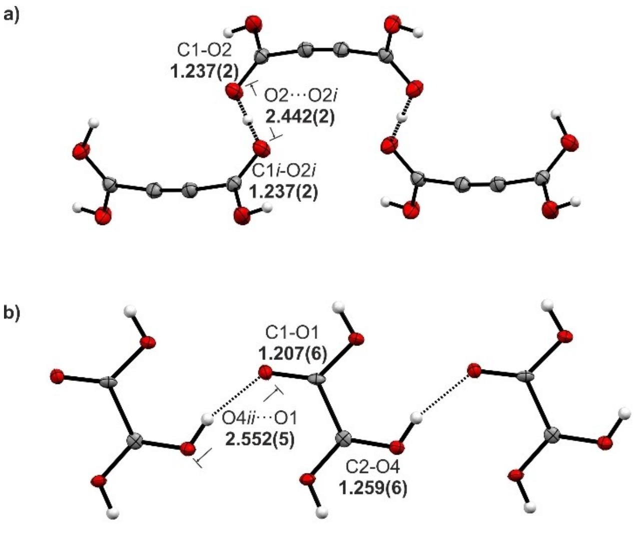

Figure 4. C–O bond lengths and O···O distances in the cationic chains of a) $[C_4H_3O_4][SbF_6]$ (**4**) and b) monoprotonated oxalic acid.[4] Bond lengths are given in Å. Symmetry codes: *I* = 0.5 − x, 0.5 − y, 1.5 − z; *ii* = x, 1.5 − y, 0.5 + z.

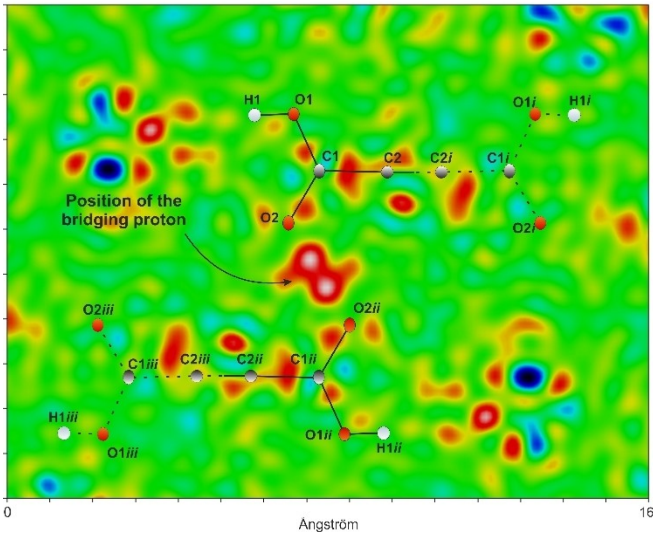

Figure 5. Difference electron density map of the $[C_4H_3O_4]^+$ cation in (**4**) without the bridging proton in the plane of the two bridged carboxyl groups.

Since the exact position of the proton is indeterminate by single-crystal X-Ray analysis, its position is assumed to be between O2 and O2*i*. For crystallographic site symmetry, the structure was successfully refined with the proton located on the inversion center. As the difference electron density map suggests, a twofold disorder with a 50 % proton occupation might be present in the crystal structure. Nevertheless, a strong hydrogen bond O2···H···O2*i* with a very short donor-acceptor distance of 2.442(2) Å is present in the crystal structure. The donor-acceptor distance is considerably shorter than the sum of the Van der Waals radii (3.00 Å).[12] Similarly short O···(H)···O distances are observed in the $(H_5O_2^+)$-cation.[13,14] Other comparable hydrogen bonds are described in the literature and are referred to as short, strong, low-barrier (SSLB) hydrogen bonds.[15,16]

Quantum chemical calculations

Quantum chemical calculations were performed on the M06/aug-cc-pVTZ level of theory with the Gaussian program package. To simulate the strong hydrogen bonds, observed in the crystal structure, four hydrogen fluoride molecules were added to the gas phase structure of the $[C_4H_4O_4]^{2+}$ cation.[4,17] Figure 6 shows the experimental and calculated structure of the $[C_4H_4O_4]^{2+}$ moiety in the $[C_4H_4O_4 \cdot 4HF]^{2+}$ cation with bond lengths and angles.

The calculated gas phase structure is in good agreement with the structure observed in the crystal structure. Also the experimental vibrational frequencies are better represented by the calculated HF solvated cation than by the naked $[C_4H_4O_4]^{2+}$ cation. The calculation of the gas phase structure of the monoprotonated cation is more complex. Due to the twofold hemiprotonation, the $[C_4H_3O_4]^+$ cation possesses C_2 symmetry in the crystal structure of (**3**) and (**4**). However, the gas phase structure of the naked $[C_4H_3O_4]^+$ cation possesses C_1 symmetry and describes the geometrical parameters of the $[C_4H_3O_4]^+$ cation only poorly. To address this issue in the calculation, two HF molecules were added to simulate anion-cation contacts and two formaldehyde molecules were added to simulate the interactions of the cationic chain in the solid state (Figure 7). This approach has already been successfully applied to simulate hydrogen bonding and is in good accordance with the data from the crystal structures (**3**) and (**4**).[11,18]

Comparing the crystal and calculated gas phase structures, it stands out that the carbon scaffold is not changed significantly by the degree of protonation. Therefore, it is interesting to compare the protonated species of this work with anionic species of acetylenedicarboxylic acid from the literature.

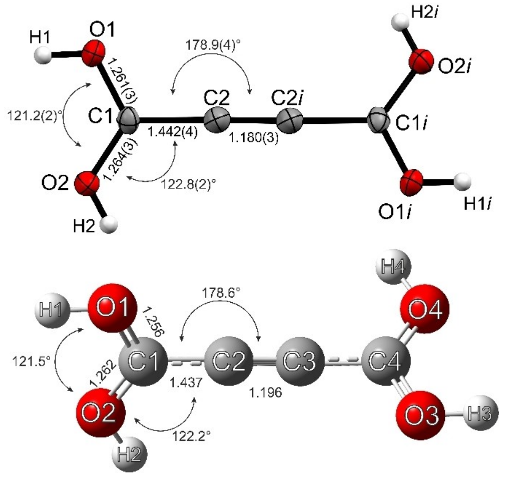

Figure 6. Experimental (top) and calculated (bottom) cationic structures of $[C_4H_4O_4 \cdot 4HF]^{2+}$. The HF molecules are omitted in the depiction of the calculated structure for clarification. Bond lengths are given in Å. Symmetry code: *i* = 1-*x*, *y*, 0.5-*z*.

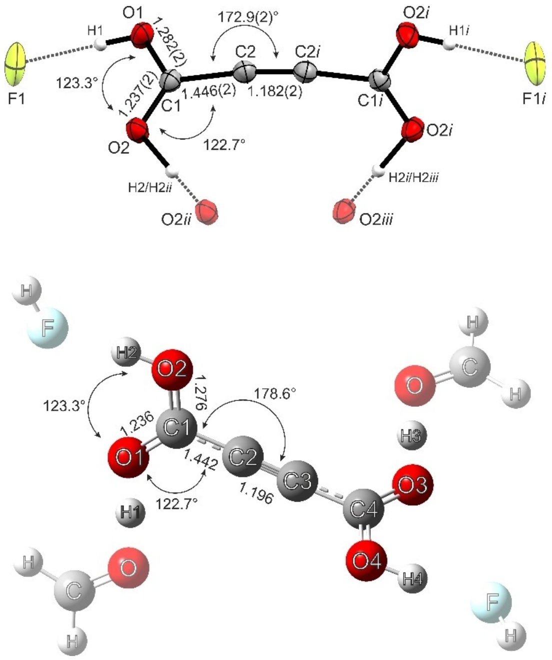

Figure 7. Experimental (top) and calculated (bottom) cationic structures of $[C_4H_4O_4\cdot 2CH_2O\cdot\cdot 2HF]^{2+}$. The intermolecular contacts, HF and formaldehyde molecules, are displayed transparently for clarification. Bond lengths are given in Å. Symmetry code: *i* = −*x*, *y*, −0.5−*z*; *ii* = 0.5−*x*, 0.5−*y*,−*z*; *iii* = −0.5 +*x*, 0.5−*y*, −0.5+z.

Table 3 summarizes the bond lengths of $[NH_4]_2[C_4O_4]$,[19] K-$[C_4HO_4]$,[20] $C_4H_2O_4$,[5] (**2**) and (**4**). The C≡C bond length is not significantly affected by the charge of the acetylenedicarboxylic moiety. However, the C–C single bond length decreases from the dianion to the dication. Interestingly, the C–O bond lengths of the monoanion and monocation differ significantly from the compounds with even charge (−2, 0, +2). Furthermore, the anions in $K[C_4HO_4]$ build infinite chains with very short O⋅⋅⋅H⋅⋅⋅O*i* hydrogen bonds (2.446(3) Å).[20] This prompted us to further investigate the hydrogen bonding in twofold hemiprotonated acetylenedicarboxylic acid $[C_4H_3O_4][MF_6]$ (*M* = As, Sb).

The above-mentioned term of short, strong, low-barrier (SSLB) hydrogen bonds describes a special case of hydrogen bonding, in which the proton is located at a variable position between two similarly acidic acceptor atoms. The main properties of these hydrogen bonds are an unusually short O⋅⋅⋅O distance of <2.5 Å and a low or no energy barrier at the symmetric position of the proton between the two acceptor atoms.

Table 3. Summarized bond lengths of selected compounds containing the acetylenedicarboxylic moiety.

Charge	Compound	Bond lengths [Å]		
		C–C	C≡C	C–O
−2	$[NH_4]_2[C_4O_4]$[19]	1.479(3)	1.203(5)	1.252(2)
−1	$K[C_4HO_4]$[20]	1.466(3)	1.191(4)	1.221(3) 1.285(3)
0	$C_4H_2O_4$[5]	1.454(1)	1.188(1)	1.245(1) 1.262(1)
		1.455(1)		1.246(1) 1.259(1)
+1	$[C_4H_3O_4][SbF_6]$	1.446(2)	1.188(3)	1.237(2) 1.282(2)
+2	$[C_4H_4O_4][SbF_6]_2$	1.442(4)	1.180(5)	1.261(3) 1.264(3)

Examples of such hydrogen bonds are observed in O-protonated homodimers of benzophenone, diethyl ether, nitrobenzene or benzaldehyde.[16,21] To investigate if the short hydrogen bonding in (**3**) and (**4**) fits into the concept of SSLB hydrogen bonding, quantum chemical calculations were performed on the B3LYP/aug-cc-pVTZ level of theory. To simulate the O⋅⋅⋅H⋅⋅⋅O*i* hydrogen bond in the polycations of (**3**) and (**4**), the calculated structure with two HF and two CH_2O molecules (Figure 7) is not suitable. Therefore, a second approach with a sesquiprotonated dimer was applied as depicted in Figure 8.

The geometry optimization leads to a first-order saddle point on the potential energy surface (TS in Figure 9). At this saddle point, the proton is situated exactly in the middle of the O⋅⋅⋅H⋅⋅⋅O trajectory. One single imaginary vibration frequency is calculated for the structure at this saddle point, which refers to the transition state of the proton transfer. The bond lengths and the O⋅⋅⋅O distance (2.410 Å) in the calculated structure are comparable to the results from the crystal structures (**3**, **4**). Further optimization of the structure with the same O⋅⋅⋅O distance of 2.410 Å then leads to two equivalent energetic

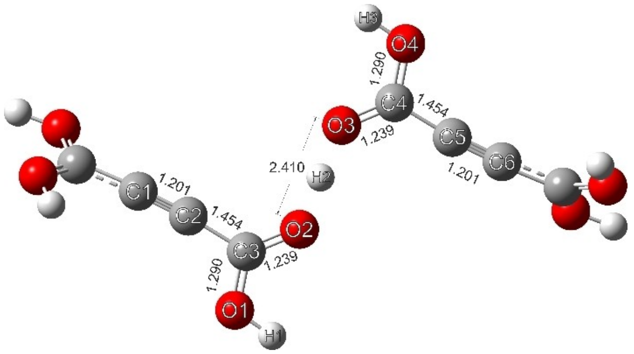

Figure 8. Optimized gas phase structure of the $[(C_4H_3O_4)\cdots H\cdots(C_4H_3O_4)]^{3+}$ cation at the transition state of the proton transfer (first-order saddle point on the potential energy surface). Bond lengths are given in Å.

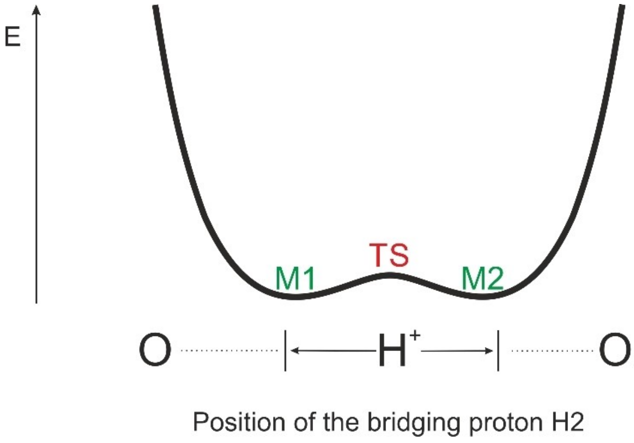

Figure 9. Schematic illustration of the flat bottom energy well typical for short, strong, low-barrier hydrogen bonds.[16,22]

minima with the bridging proton being situated slightly outside the central position (M1 and M2 in Figure 9) (Figure S6 Supporting Information). This is consistent with the results of the crystal structure, where the highest electron densities between the O···O*i* atoms are located slightly outside the inversion center (Figure 5). Furthermore, the energy difference between the transition state and the minima is the barrier height of the proton transfer, which is low (1.2 kJ/mol). This indicates an intermediate position of the proton along the O···H···O trajectory, which imposes a small asymmetry since there are two minima that are not located exactly in the middle.

All in all, the experimental and theoretical data for the hemiprotonated hydrogen bond are consistent with the concept of SSLB hydrogen bonding.[16,23] However, this topic has only been reported for proton-bound homodimers so far. Twofold hemiprotonated acetylenedicarboxylic acid shows a polycationic structure which is connected via short, strong hydrogen bonding with indeterminate positioning of the protons.

Conclusion

The reaction of acetylenedicarboxylic acid in the superacidic media HF/AsF_5 and HF/SbF_5 was investigated. The salts of diprotonated $[C_4H_4O_4][MF_6]_2$ (M=As, Sb) and monoprotonated $[C_4H_3O_4][MF_6]$ (M = As, Sb) acetylenedicarboxylic acid were obtained, depending on the stoichiometric ratio of Lewis acid to starting material. The salts were characterized by low-temperature vibrational spectroscopy and single crystal X-Ray structure analyses. The monoprotonated acetylenedicarboxylic acid is better described as a twofold hemiprotonated species. In the crystal structure short O···H···O hydrogen bonds are present, which build polycationic chains. Furthermore, quantum chemical calculations were performed on the B3LYP/aug-cc-pVTZ level of theory and discussed in context of SSLB hydrogen bonds.

Experimental Section

Caution! Note that any contact with the described compounds should be avoided. Hydrolysis of these salts forms HF which burns skin and causes irreparable damage. Safety precautions should be taken while handling these compounds.

Apparatus and Materials

All reactions were carried out by employing standard Schlenk techniques on a stainless-steel vacuum line. The syntheses of the salts were performed using FEP/PFA-reactors with stainless-steel valves. Before each reaction, the stainless-steel vacuum line and the reactors were dried with fluorine. The obtained compounds were characterized by low temperature IR- and Raman spectroscopy and single crystal X-Ray diffraction analysis. For Raman measurements, a Bruker MultiRam FT-Raman spectrometer with Nd:YAG laser excitation ($\lambda = 1064$ nm) was used. Low temperature IR-spectroscopic investigations were carried out with a Bruker Vertex-80 V FTIR spectrometer using a cooled cell with a single-crystal CsBr plate on which small amounts of the samples were placed.[24] The single crystal X-Ray diffraction studies were performed with an Oxford XCalibur3 diffractometer equipped with a Spellman generator (voltage 50 kV, current 40 mA) and a KappaCCD detector, operating with Mo-K_α radiation ($\lambda = 0.7107$ Å). The measurements were performed at 173 K. The program CrysAlisCCD[25] and for its reduction CrysAlisRED[26] were employed for the data collection. The structures were solved utilizing SHELXS-97[27] and SHELXL-97[28] of the WINGX software package[29] and verified with the software PLATON.[30] The absorption correction was performed using the SCALE3 APSACK multiscan method.[31] Quantum chemical calculations were carried out using the software package Gaussian09.[32]

Syntheses of $[C_4X_4O_4][MF_6]_2$ (X = H, D; M = As, Sb)

Initially, the binary superacid was formed by condensing the Lewis acid AsF_5 or SbF_5 (1.0 mmol) into a FEP-reactor together with anhydrous hydrogen fluoride (*a*HF) or deuterium fluoride (*a*DF) (1 mL). Both components were then warmed up to −30 °C and homogenized. After freezing the superacidic mixture at −196 °C, acetylenedicarboxylic acid (0.5 mmol) was added to the frozen mixture under nitrogen atmosphere. For the reaction, the mixture was warmed up to −30 °C and homogenized to complete solvation of the starting material. Excess of *a*HF or *a*DF was removed within 14 h at −78 °C. All products were obtained as a yellowish crystalline solid.

Syntheses of $[C_4H_3O_4][MF_6]$ (M = As, Sb)

The Lewis acid AsF_5 or SbF_5 (0.5 mmol) was condensed in a FEP reactor vessel together with *a*HF or *a*DF (2 mL) at −196 °C. The superacid was then formed by warming up to −30 °C and homogenization of the components. After freezing the superacidic mixture at −196 °C, acetylenedicarboxylic acid (0.5 mmol) was added to the frozen mixture under nitrogen atmosphere. The reaction mixture was then warmed up to −20 °C and mixed until a clear solution was received. Excess solvent was removed at −78 °C in dynamic vacuum. All products were obtained as a yellowish crystalline solid.

Deposition Numbers 2002493 (for $[C_4H_4O_4][SbF_6]$ (**2**)), 2025068 (for $[C_4H_3O_4][AsF_6]$ (**3**)) and 2025066 (for $[C_4H_3O_4][SbF_6]$ (**4**)) contain the supplementary crystallographic data for this paper. These data are provided free of charge by the joint Cambridge Crystallographic Data Centre and Fachinformationszentrum Karlsruhe Access Structures service www.ccdc.cam.ac.uk/structures.

Acknowledgements

We are grateful to the Department of Chemistry of the Ludwig Maximilian University, Munich, the Deutsche Forschungsgemeinschaft (DFG) and the F-Select GmbH for the support of this work. Open Access funding enabled and organized by Projekt DEAL.

Conflict of Interest

The authors declare no conflict of interest.

Data Availability Statement

The data that support the findings of this study are available in the supplementary material of this article.

Keywords: Protonated acetylenedicarboxylic acid · Quantum chemical calculations · Superacidic systems · Vibrational spectroscopy · X-ray diffraction

[1] a) M. Sahoo, *Synlett* **2007**, *2007*, 2142; b) C. Neochoritis, T. Zarganes-Tzitzikas, J. Stephanidou-Stephanatou, *Synthesis* **2014**, *46*, 537.
[2] a) F. Hohn, I. Pantenburg, U. Ruschewitz, *Chem. Eur. J.* **2002**, *8*, 4536; b) I. Stein, U. Ruschewitz, *Z. Naturforsch. B* **2009**, *64*, 1093; c) T. J. M. Ma Ntep, H. Reinsch, B. Moll, E. Hastürk, S. Gökpinar, H. Breitzke, C. Schlüsener, L. Schmolke, G. Buntkowsky, C. Janiak, *Chem. Eur. J.* **2018**, *24*, 14048; d) T. J. Matemb Ma Ntep, H. Reinsch, J. Liang, C. Janiak, *Dalton Trans.* **2019**, *48*, 15849.
[3] A. F. Holleman, N. Wiberg, *Anorganische Chemie*, De Gruyter, Berlin, **2017**.
[4] M. Schickinger, T. Saal, F. Zischka, J. Axhausen, K. Stierstorfer, Y. Morgenstern, A. J. Kornath, *ChemistrySelect* **2018**, *3*, 12396.
[5] A. Delori, I. B. Hutchison, C. L. Bull, N. P. Funnell, A. J. Urquhart, I. D. H. Oswald, *Cryst. Growth Des.* **2018**, *18*, 1425.
[6] R. Minkwitz, C. Hirsch, T. Berends, *Eur. J. Inorg. Chem.* **1999**, *1999*, 2249.
[7] R. Minkwitz, S. Schneider, *Angew. Chem.* **1999**, *111*, 229.
[8] M. Schickinger, C. Jessen, Y. Morgenstern, K. Muggli, F. Zischka, A. Kornath, *Eur. J. Org. Chem.* **2018**, *2018*, 6223.
[9] J. L. Delarbre, L. Maury, L. Bardet, *J. Raman Spectrosc.* **1986**, *17*, 373.
[10] M. Schickinger, M. Siegert, Y. Morgenstern, F. Zischka, K. Stierstorfer, A. Kornath, *Z. Anorg. Allg. Chem.* **2018**, *644*, 1564.
[11] M. C. Bayer, C. Jessen, A. J. Kornath, *Z. Anorg. Allg. Chem.* **2020**.
[12] A. Bondi, *J. Phys. Chem.* **1964**, *68*, 441.
[13] R. Minkwitz, S. Schneider, A. Kornath, *Inorg. Chem.* **1998**, *37*, 4662.
[14] R. Minkwitz, C. Hirsch, *Acta Crystallogr. Sect. C* **1999**, *55*, 703.
[15] a) C. L. Perrin, *Science* **1994**, *266*, 1665; b) L. C. Remer, J. H. Jensen, *J. Phys. Chem. A* **2000**, *104*, 9266; c) C. A. Reed, *Acc. Chem. Res.* **2013**, *46*, 2567.
[16] D. Stasko, S. P. Hoffmann, K.-C. Kim, N. L. P. Fackler, A. S. Larsen, T. Drovetskaya, F. S. Tham, C. A. Reed, C. E. F. Rickard, P. D. W. Boyd et al., *J. Am. Chem. Soc.* **2002**, *124*, 13869.
[17] T. Soltner, N. R. Goetz, A. Kornath, *Eur. J. Inorg. Chem.* **2011**, *2011*, 3076.
[18] M. Schickinger, D. Cibu, F. Zischka, K. Stierstorfer, C. Jessen, A. Kornath, *Chem. Eur. J.* **2018**, *24*, 13355.
[19] I. Stein, C. Näther, U. Ruschewitz, *Solid State Sci.* **2006**, *8*, 353.
[20] I. Leban, L. Golič, J. C. Speakman, *J. Chem. Soc. Perkin Trans. 2* **1973**, 703.
[21] D. Stuart, S. D. Wetmore, M. Gerken, *Angew. Chem. Int. Ed.* **2017**, *56*, 16380.
[22] E. S. Stoyanov, C. A. Reed, *J. Phys. Chem. A* **2006**, *110*, 12992.
[23] S. J. Grabowski, J. M. Ugalde, *Chem. Phys. Lett.* **2010**, *493*, 37.
[24] L. Bayersdorfer, R. Minkwitz, J. Jander, *Z. Anorg. Allg. Chem.* **1972**, *392*, 137.
[25] CrysAlisCCD, *Version 1.171.35.11 (release 16-05-2011 CrysAlis 171.NET)*, Oxford Diffraction Ltd, UK, **2011**.
[26] CrysAlisRED, *Version 1.171.35.11 (release 16-05-2011 CrysAlis 171.NET)*, Oxford Diffraction Ltd, UK, **2011**.
[27] G. M. Sheldrick, *SHELXS-97, Program for Crystal Structure Solution*, University of Göttingen, Germany, **1997**.
[28] G. M. Sheldrick, *SHELXL-97, Program for Crystal Structure Solution*, University of Göttingen, Germany, **1997**.
[29] L. J. Farrugia, *J. Appl. Crystallogr.* **1999**, *32*, 837.
[30] A. L. Spek, *PLATON, A Multipurpose Crystallographic Tool*, Utrecht University, Utrecht, Netherlands, **1999**.
[31] *SCALE3 ABSPACK, An Oxford Diffraction Program*, Oxford Diffraction Ltd, UK, **2005**.
[32] M. J. Frisch, G. W. Trucks, H. B. Schlegel, G. E. Scuseria, M. A. Robb, J. R. Cheeseman, G. Scalmani, V. Barone, B. Mennucci, G. A. Petersson, H. Nakatsuji, M. Caricato, X. Li, H. P. Hratchian, A. F. Izmaylov, J. Bloino, G. Zheng, J. L. Sonnenberg, M. Hada, M. Ehara, K. Toyota, R. Fukuda, J. Hasegawa, M. Ishida, T. Nakajima, Y. Honda, O. Kitao, H. Nakai, T. Vreven, J. A. Montgomery, J. E. Peralta, F. Ogliaro, M. Bearpark, J. J. Heyd, E. Brothers, K. N. Kudin, V. N. Staroverov, R. Kobayashi, J. Normand, K. Raghavachari, A. Rendell, J. C. Burant, S. S. Iyengar, J. Tomasi, M. Cossi, N. Rega, J. M. Millam, M. Klene, J. E. Knox, J. B. Cross, V. Bakken, C. Adamo, J. Jaramillo, R. Gomperts, R. E. Stratmann, O. Yazyev, A. J. Austin, R. Cammi, C. Pomelli, J. W. Ochterski, R. L. Martin, K. Morokuma, V. G. Zakrzewski, G. A. Voth, P. Salvador, J. J. Dannenberg, S. Dapprich, A. D. Daniels, O. Farkas, J. B. Foresman, J. V. Ortiz, J. Cioslowski, D. J. Fox, *Gaussian09, Revision A.02*, Gaussian, Inc, Wallingford CT, **2009**.

Manuscript received: November 9, 2021
Revised manuscript received: December 13, 2021
Accepted manuscript online: December 15, 2021

European Journal of
Inorganic Chemistry

Supporting Information

Syntheses and Structures of Protonated Acetylenedicarboxylic Acid

Christoph Jessen and Andreas J. Kornath*

Supporting Information

Table S1. Selected bond lengths and angles of $[C_4H_3O_4][AsF_6]$ (**3**) and $[C_4H_3O_4][SbF_6]$ (**4**). Symmetry codes: *i* = -x, y, -0.5-z; *ii* = 1-x, y, 1.5-z.

bond lengths [Å]	$[C_4H_3O_4][AsF_6]$	$[C_4H_3O_4][SbF_6]$
C1-C2 (C–C)	1.455(4)	1.446(2)
C2-C2*i* (C≡C)	1.182(4)	1.188(3)
C1-O1	1.280(3)	1.282(2)
C1-O2	1.232(3)	1.237(2)
bond angles [°]		
O1-C1-O2	124.0(2)	123.1(1)
O1-C1-C2	115.8(2)	116.2(1)
O2-C1-C2	120.1(2)	120.7(1)
C1-C2-C2*i*	171.3(2)	172.9(1)
angle of torsion [°]		
O1-C1-C2-C2*i*	166(1)	-165(1)
O2-C1-C2-C2*i*	-13(2)	14(1)
C1-C2-C2*i*-C1*i*	-43(3)	42(2)
donor-acceptor distances [Å]		
O1-H1···F1	2.611(3)	2.578(2)
O2-H2···O2*ii*	2.444(2)	2.442(2)

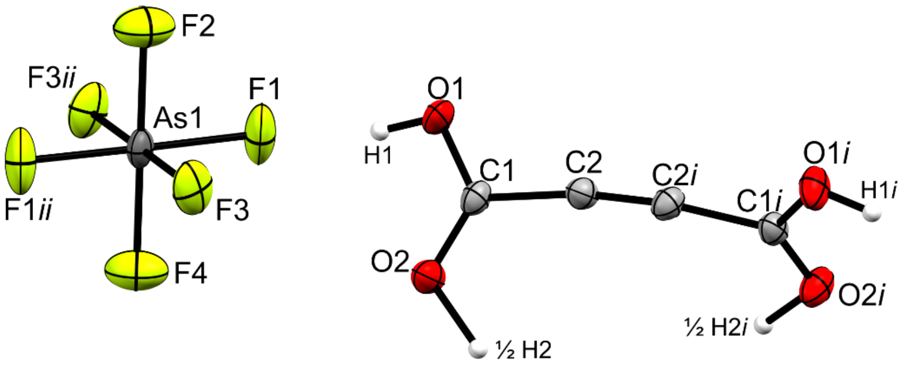

Figure S1. Formular unit of $[C_4H_3O_4][AsF_6]$ (**3**) (50% probability displacement ellipsoids). Symmetry codes: *i* = -x, y, -0.5-z; *ii* = 1-x, y, 1.5-z.

Table S2. Experimental vibrational frequencies [cm^{-1}] of $[C_4H_4O_4][MF_6]_2$ (*M*=As, Sb) and calculated vibrational frequencies [cm^{-1}] of $[C_4H_4O_4 \cdot 4\ HF]^{2+}$.

$[C_4H_4O_4][AsF_6]_2$ (**1**) exp.[a]		$[C_4H_4O_4][SbF_6]_2$ (**2**) exp.[a]		$[C_4H_4O_4 \cdot 4\ HF]^{2+}$ calc.[b,c]	Assignment		
IR	Raman	IR	Raman	IR/Raman			
				3135 (787/139)	ν_{1}	A	ν_s(OH)
				3125 (1899/55)	ν_{17}	B	ν_{as}(OH)
				2985 (312/302)	ν_{2}	A	ν_s(OH)
				2970 (5019/22)	ν_{18}	B	ν_{as}(OH)
		2798 vw					?
2731 w	2739 (4)						?
		2656 w					?
2455 w	2445 (2)	2455 w	2432 (2)				$2 \times \nu_{22}$
2285 vw	2301 (100)	2299 vw	2290 (100)	2297 (0/517)	ν_{3}	A	ν(C≡C)
	2261 (8)						?
2247 vw	2247 (5)	2044 vw	2249 (13)				ν22 + ν23
2029 vw	2031 (2)		2033 (1)				ν4 + ν13
1886 vw		1892 vw					ν4 + ν29
1844 vw		1853 vw					ν22 + ν27
1788 vw		1782 vw					?
1711 vw		1717 vw					?
1634 s	1644 (5)	1632 m	1645 (4)	1654 (238/7)	ν_{4}	A	ν_s(CO)
1614 m	1587 (3)		1592 (1)	1654 (594/4)	ν_{19}	B	ν_{as}(CO)
1533 s		1529 m	1549 (2)	1521 (986/2)	ν_{20}	B	ν_{as}(CO)
	1519 (62)		1516 (44)	1503 (78/69)	ν_{5}	A	ν_s(CO)
1423 w	1494 (4)	1464 w	1487 (2)				?
				1255 (2/1)	ν_{6}	A	δ(COH)
1261 s		1277 m	1273 (2)	1247 (320/0)	ν_{21}	B	δ(COH)
1229 s		1234 m		1234 (287/1)	ν_{22}	B	δ(COH)
	1237 (24)		1227 (36)	1228 (133/29)	ν_{7}	A	δ(COH)
	1202 (3)	1045 vw					?
1016 m		1016 m	1022 (2)	1014 (65/1)	ν_{23}	B	ν_{as}(C-C(OH)$_2$)
895 w		895 w		881 (73/0)	ν_{8}	A	δ(COH)
				879 (35/0)	ν_{24}	B	δ(COH)
		851 m	842 (1)	811 (181/0)	ν_{9}	A	δ(COH)
825 s	826 (3)			806 (97/0)	ν_{25}	B	δ(COH)
	774 (26)		768 (17)	768 (8/8)	ν_{10}	A	ν_s(C-C(OH)$_2$)
	738 (12)		732 (14)	740 (8/3)	ν_{26}	B	γ(CCO)
717 vs	723 (37)			737 (16/1)	ν_{11}	A	γ(CCO)
606 w	618 (4)		614 (2)	619 (9/1)	ν_{27}	B	δ(OCO)
	602 (8)		600 (6)	618 (0/2)	ν_{12}	A	δ(CCO)
569 s	562 (13)	567 s	576 (5)	601 (1/1)	ν_{28}	B	δ(CCO)
395 s	394 (7)	397 vw	395 (7)	307 (17/3)	ν_{13}	A	δ(OCO)
	294 (5)		308 (6)	291 (6/2)	ν_{14}	A	δ(CCC)

	256 (8)		246 (10)	253 (6/0)	ν_{29}	B	δ(CCC)
	159 (26)		158 (3)	232 (24/1)	ν_{15}	A	δ(CCC)
	134 (34)		139 (42)	130 (0/1)	ν_{30}	B	δ(CCC)
	112 (43)		116 (31)	14 (0/1)	ν_{16}	A	τ($C(OH)_2$)
Vibrations of anions MF_6^- (M=As, Sb)							
704 vs	714 (17)		687 (42)				$[AsF_6]^-$; $[SbF_6]^-$
	691 (6)	667 vs	660 (65)				$[AsF_6]^-$; $[SbF_6]^-$
663 vs	664 (74)	635 vs	635 (52)				$[AsF_6]^-$; $[SbF_6]^-$
527 s	528 (8)		560 (13)				$[AsF_6]^-$; $[SbF_6]^-$
	412 (10)	523 vs	519 (5)				$[AsF_6]^-$; $[SbF_6]^-$
388 s	375 (41)	415 vw					$[AsF_6]^-$; $[SbF_6]^-$
	367 (24)	403 vw					$[AsF_6]^-$; $[SbF_6]^-$
	307 (47)	390 vw					$[AsF_6]^-$; $[SbF_6]^-$
	225 (35)		297 (24)				$[AsF_6]^-$; $[SbF_6]^-$
			277 (57)				$[SbF_6]^-$
			203 (9)				$[SbF_6]^-$

[a] Abbrevations for IR intensities: vs = very strong, s = strong, m = medium, w = weak. [b] Calculated on the M06/aug-cc-pVTZ level of theory. Scaling factor 0.965. [c] IR intensities in km/mol; Raman intensities in Å4/m.

Table S3. Experimental vibrational frequencies [cm^{-1}] of $[C_4D_4O_4][\mathit{M}F_6]_2$ (*M*=As, Sb) and calculated vibrational frequencies [cm^{-1}] of $[C_4D_4O_4 \cdot 4\ DF]^{2+}$.

$[C_4D_4O_4][AsF_6]_2$ **(5)** exp.[a]		$[C_4D_4O_4][SbF_6]_2$ **(6)** exp.[a]		$[C_4D_4O_4 \cdot 4\ HF]^{2+}$ calc.[b,c]	Assignment		
IR	Raman	IR	Raman	IR/Raman			
	2289(100)		2290 (100)	2301 (100/488)	ν_1	A	$\nu(C{\equiv}C)$
	2249(4)		2249(6)				$C_4D_2O_4$
2200 to 1950				2289 (311/101)	ν_2	A	4 × ν(OD)
				2285 (987/26)	ν_{17}	B	
				2180 (162/127)	ν_3	A	
				2167 (2678/10)	ν_{18}	B	
1938 vw		1944 w					$\nu_6 + \nu_9$
1915 vw		1917 w					$\nu_{23} + \nu_{22}$
1890 vw		1884 w					$\nu_{23} + \nu_7$
1622 w	1636(5)	1626 m	1633(6)	1640 (570/4)	ν_{19}	B	ν_{as}(CO)
	1604(2)	1605 m	1604(3)	1639 (277/7)	ν_4	A	ν_s(CO)
1524 w	1527(3)	1518 m	1528(3)	1487 (996/2)	ν_{20}	B	ν_{as}(CO)
1470 w	1473(39)	1475 m	1478(35)	1462 (18/95)	ν_5	A	ν_s(CO)
1443 w	1444(2)	1446 w					?
1394 w		1421 w					?
1385 w		1385 w					$\nu_9 + \nu_{25}$
1263 w	1267(2)	1261 m	1263(2)				δ(COH)
1234 w	1238(2)	1230 m	1232(2)				δ(COH)
1194 w							?
1049 w	1051(2)	1049 m	1052(3)	1044 (31/1)	ν_{21}	B	ν_{as}(C-C)
1016 w	1018(12)	1016 m	1019(16)	1000 (59/10)	ν_6	A	δ(COD)
968 m	989(2)	964 s	987(2)	946 (142/0)	ν_{22}	B	δ(COD)
949 m	959(3)		957(3)	929 (11/3)	ν_7	A	δ(COD)
930 m	936(2)	933 s		910 (180/1)	ν_{23}	B	δ(COD)
897 m							?
854 m sh		866 m					?
748 s	749(5)	750 vs	752(7)	755 (21/2)	ν_{24}	B	γ(CCO_2)
	725(3)		734(15)	753 (43/1)	ν_8	A	γ(CCO_2)
	718(6)	719 vs	718(7)	698 (14/6)	ν_9	A	ν_s(C-C)
665 vs	669(23)		667(29)	637 (9/1)	ν_{25}	B	δ(COD)
				637 (6/2)	ν_{10}	A	δ(COD)
594 vs	588(4)	600 vs	589(5)	604 (2/1)	ν_{26}	B	δ(COD)
565 vs	563(9)	563 vs	564(10)	589 (8/1)	ν_{11}	A	δ(COD)
				588 (96/0)	ν_{27}	B	δ(CCO)
552 vs		552 vs		584 (46/0)	ν_{28}	B	δ(CCO)
530 vs	523(4)	527 vs	520(6)	576 (21/1)	ν_{12}	A	δ(CCO)
393 vw		388 vs		358 (37/2)	ν_{13}	A	δ(OCO)
	293(11)		288(24)	300 (18/3)	ν_{29}	B	δ(CCC)
	180(4)			283 (6/2)	ν_{14}	A	δ(CCC)

	171(3)			249 (6/0)	ν_{15}	A	δ(CCC)
	157(5)			128 (0/0)	ν_{30}	B	δ(CCC)
	140(20)		143(30)				Gitterschw.
	119(18)		121(22)	14 (0/1)	ν_{16}	A	τ($C(OD)_2$)
Vibrations of anions MF_6^- (M = As, Sb)							
		700 vs	707(16)				$[SbF_6]^-$
	698(11)	671 vs					$[AsF_6]^-$; $[SbF_6]^-$
	688(12)		692(14)				$[AsF_6]^-$; $[SbF_6]^-$
	678(6)		637(4)				$[AsF_6]^-$; $[SbF_6]^-$
	650(7)	577 vs					$[AsF_6]^-$; $[SbF_6]^-$
635 vs	640(27)	403 vs	420(8)				$[AsF_6]^-$; $[SbF_6]^-$
577 vs	604(3)		374(20)				$[AsF_6]^-$; $[SbF_6]^-$
382 vw	385(6)		363(12)				$[AsF_6]^-$; $[SbF_6]^-$
	284(13)		353(9)				$[AsF_6]^-$; $[SbF_6]^-$
	274(22)		249(5)				$[AsF_6]^-$; $[SbF_6]^-$
			225(17)				$[SbF_6]^-$

[a] Abbrevations for IR intensities: vs = very strong, s = strong, m = medium, w = weak. [b] Calculated on the M06/aug-cc-pVTZ level of theory. Scaling factor 0.965. [c] IR intensities in km/mol; Raman intensities in Å4/m.

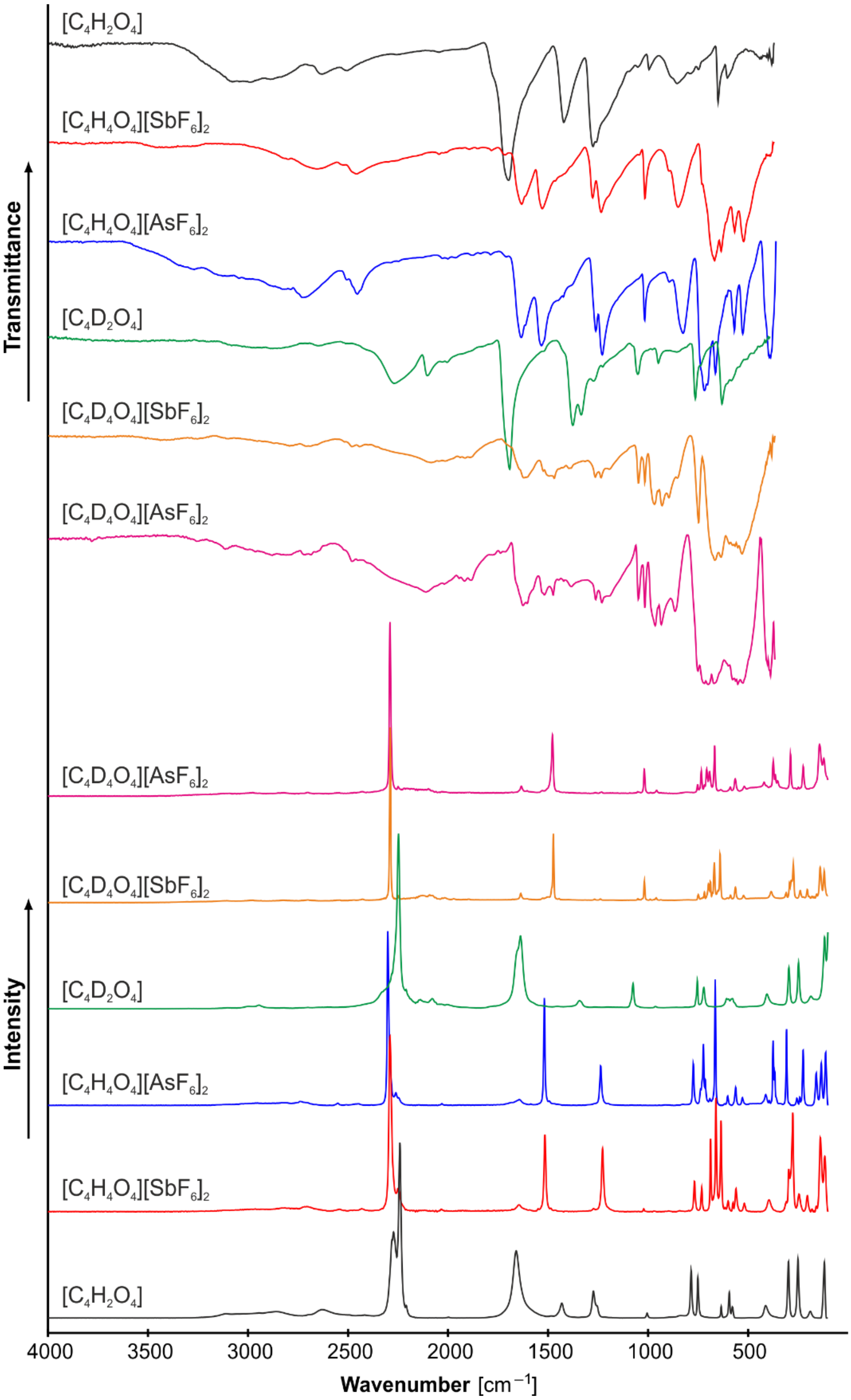

Figure S2. Low-temperature IR and Raman spectra of $[C_4X_4O_4][MF_6]_2$ (M = As, Sb) (**1**, **2**, **5**, **6**), $C_4X_2O_4$ (*X* = H, D)

Table S4. Experimental vibrational frequencies [cm^{-1}] of acetylenedicarboxylic acid and its D-isotopologue (D_2ADC).

$C_4H_2O_4$			$C_4D_2O_4$		
IR exp.[a]	Raman exp.	Assignment[b]	IR exp.[a]	Raman exp.	Assignment[b]
			2270 w	2138(5)	ν(OD)
			2104 w	2080(6)	ν(OD)
	2273(49)	1697 + 578			
	2241(100)	ν(C≡C)		2248(100)	ν(C≡C)
1697 s		ν_{as}(CO)	1691 vs		ν_{as}(CO)
	1659(38)	ν_s(CO)		1638(42)	ν_s(CO)
1421 m		ν(COH)	1377 s		ν_{as}(CO)
	1431(8)	ν(COH)	1335 m	1343(5)	ν_s(CO)
1275 s	1273(15)	δ(COH)	1273 w		δ(COH)[c]
1259 s	1256(7)	δ(COH)	1227 w		δ(COH)[c]
1051vw		?	1051 w	1075(15)	δ(COD)
995 vw	1005(3)	ν_{as}(CC)	978 vw	963(1)	δ(COD)
854 w		?	949 w		ν_{as}(CC)
791 w	785(27)	γ(CCO)	764 m	754(16)	γ(CCO)
748 vw		γ(CCO)		721(12)	γ(CCO)
	751(23)	ν_s(C-C)	631 m	607(6)	ν_s(C-C)
650 m	634(7)	δ(CCO)	584 w	598(6)	δ(CCO)
604 w	594(15)	δ(CCO)	517 vw	577(6)	δ(CCO)
	578(6)	δ(COH)			
	413(7)	δ(OCO)		406(8)	δ(OCO)
	298(32)	δ(CCC)		296(24)	δ(CCC)
	251(33)	δ(CCC)		248(27)	δ(CCC)
	189(4)	δ(CCC)		186(7)	δ(CCC)
	119(31)	Gitterschw.		118(41)	Gitterschw.

[a] Abbrevations for IR intensities: vs = very strong, s = strong, m = medium, w = weak.

[b] The assignment is based on comparison with literature and theoretical data (B3LYP/aug-cc-pVQZ).

[c] Residues of $C_4H_2O_4$

Table S5. Crystal data and structure refinement of $[C_4H_3O_4][SbF_6]_2$ (**2**), $[C_4H_3O_4][AsF_6]$ (**3**) and $[C_4H_3O_4][SbF_6]$ (**4**).

	$[C_4H_4O_4][SbF_6]_2$ (**2**)	$[C_4H_3O_4][AsF_6]$ (**3**)	$[C_4H_3O_4][SbF_6]$ (**4**)
Molecular Fomula	$C_4H_4F_{12}O_4Sb_2$	$C_4H_3AsF_6O_4$	$C_4H_3F_6O_4Sb$
Mr[g·mol^{-1}]	587.59	303.98	350.81
Crystal size [mm^3]	0.24 × 0.21 × 0.19	0.60 × 0.17 × 0.15	0.46 × 0.26 × 0.23
Crystal system	monoclinic	monoclinic	monoclinic
Space group	*C*2/*c*	*C*2/*c*	*C*2/*c*
a [Å]	10.0787(4)	8.701(1)	9.0431(6)
b [Å]	8.0601(3)	14.749(1)	14.6538(6)
b [Å]	16.1148(6)	7.790(1)	8.0169(4)
α [°]	90.00	90.00	90.00
β [°]	94.107(4)	121.908(13)	121.110(6)
γ [°]	90.00	90.00	90.00
V [Å^3]	1305.73(9)	848.6(2)	909.57(10)
Z	4	4	4
ρcalc [g·cm^{-3}]	2.989	2.379	2.562
μ [mm^{-1}]	4.300	4.104	3.125
λMoKα [Å]	0.71073	0.71073	0.71073
F(000)	1080.0	584.0	656.0
T [K]	173 K	173 K	173 K
h, k, l range	-13:6;-7:11;-22:21	-8:12;-18:21;-11:8	-13:13;-20:21;-11:11
Measured reflexes	3304	2347	4729
Unique reflexes	1751	1364	1508
Rint	0.0196	0.0320	0.0158
Parameters	109	74	75
R(F)/wR(F2)[a] (all data)	0.0246/0.0445	0.0385/0.0727	0.0166/0.0405
Weighting scheme[b]	0.0174/0.0000	0.0305/0.0000	0.0203/0.0800
S (Gof)[c]	1.058	1.003	1.087
Residual density [e·Å–3]	0.803/-0.749	0.606/-1.063	0.731/-0.624
Device	Oxford XCalibur	Oxford XCalibur	Oxford XCalibur
CCDC	2002493	2025068	2025066

[a] $R_1 = \Sigma||F_0|-|F_c||/\Sigma|F_0|$

[b] $wR_2 = [\Sigma[w(F_0^2-F_c^2)^2]/\Sigma[w(F_0)^2]]^{1/2}$; $w = [\sigma_c^2(F_0^2)+(xP)^2+yP]-1$; $P = (F_0^2+2F_c^2)/3$

[c] GoF = $\{\Sigma[w(F_o^2-F_c^2)^2]/(n-p)\}^{1/2}$ (n = number of reflections; p = total number of parameters)

Details on quantum chemical calculations

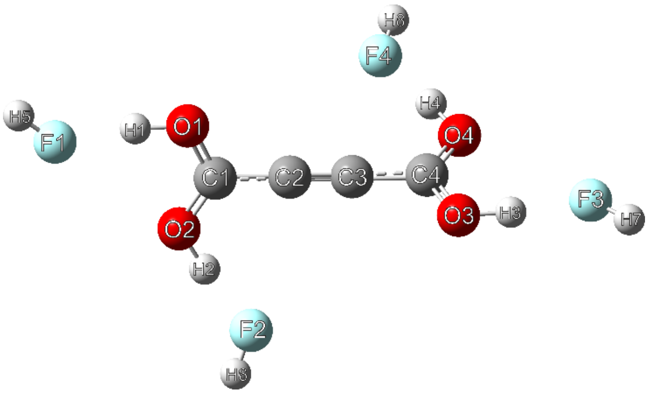

Figure S3. Optimized gas phase structure of $[C_4H_4O_4 \cdot 4HF]^{2+}$ on the M06/aug-cc-pVTZ level of theory.

Table S6. Input matrix for the structure optimization of $[C_4H_4O_4 \cdot 4HF]^{2+}$.

opt freq=raman M06/aug-cc-pvtz geom=connectivity symm=pg=c2

Symbolic Z-matrix:

Charge = 2 Multiplicity = 1

C	-0.6032	-0.00533	-0.2308
H	-3.59664	-0.80334	-1.06004
H	-2.23741	1.4794	0.97586
O	-2.73932	0.82838	0.40643
O	-2.58783	-0.83987	-1.03402
C	-2.04705	0.01076	-0.27311
C	0.60337	0.00669	-0.22957
H	3.59704	0.80257	-1.05998
H	2.23708	-1.47919	0.97643
O	2.73917	-0.82917	0.40611
O	2.58826	0.83995	-1.03339
C	2.0472	-0.01051	-0.27252
F	1.42259	-2.48861	1.86257
F	5.13642	0.6934	-1.05151
F	-1.42324	2.49049	1.86038
F	-5.13616	-0.69567	-1.05092
H	-5.7649	-1.17133	-1.54518
H	-1.78384	3.1793	2.37282
H	5.76524	1.16879	-1.54593
H	1.78281	-3.17673	2.37619

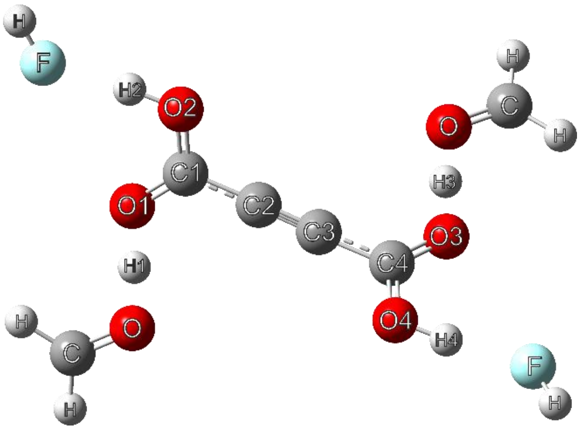

Figure S4. Optimized gas phase structure of $[C_4H_4O_4 \cdot 2CH_2O \cdot\cdot 2HF]^{2+}$ on the M06/aug-cc-pVTZ level of theory.

Table S7. Input matrix for the structure optimization of $[C_4H_4O_4 \cdot 2CH_2O \cdot\cdot 2HF]^{2+}$.

opt=tight freq=raman M06/aug-cc-pvtz geom=connectivity

Symbolic Z-matrix:

Charge = 2 Multiplicity = 1

H	-3.21766	-1.75395	-1.0826
O	-2.84816	0.2141	0.12958
C	-0.57897	-0.14933	-0.37439
O	-2.24358	-1.55621	-1.04946
C	-1.9816	-0.48353	-0.40974
H	3.21776	1.75423	-1.08199
H	2.63856	-1.24982	0.69757
O	2.8482	-0.21414	0.12967
C	0.57903	0.14943	-0.37432
O	2.24368	1.55648	-1.04895
C	1.98166	0.48364	-0.40951
F	-4.84673	-1.95868	-1.0728
F	4.84683	1.95892	-1.07205
H	-2.6386	1.24968	0.69772
O	-2.50376	2.29267	1.27352
C	-3.50285	2.89317	1.6326
O	2.50362	-2.29294	1.27313
C	3.50264	-2.8936	1.63212
H	5.37683	2.59627	-1.48409
H	-5.37669	-2.59598	-1.48496
H	-3.39223	3.84649	2.15939
H	-4.51117	2.50341	1.44194
H	3.39192	-3.84701	2.15872
H	4.511	-2.5039	1.44157

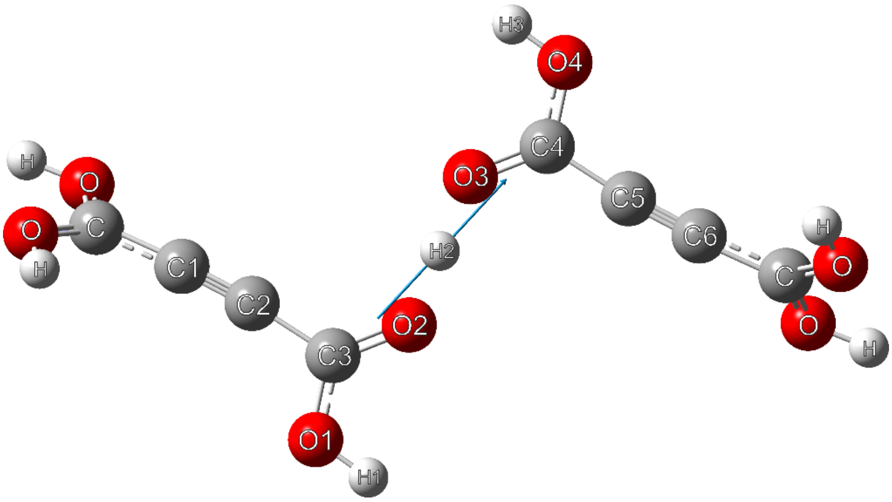

Figure S5. Maximum optimized gas phase structure of the $[(C_4H_3O_4)\cdots H\cdots(C_4H_3O_4)]^{3+}$ cation at the transition state of the proton transfer (TS in Figure 9) (First order saddle point on the potential energy surface). Calculated on the B3LYP/aug-cc-pVTZ level of theory. The displacement vector of the single imaginary frequency is shown in blue.

Table S8. Input matrix for the transition state optimization of the $[(C_4H_3O_4)\cdots H\cdots(C_4H_3O_4)]^{3+}$ cation.

```
# opt=(calcall,ts,tight) freq B3LYP/aug-cc-pvtz geom=connectivity
```

Symbolic Z-matrix:

Charge = 3 Multiplicity = 1

H	6.33193	1.43567	1.21288
O	6.08141	0.31238	-0.79654
C	3.89391	-0.18447	-0.00859
O	5.42548	1.06392	1.15295
C	5.1879	0.41472	0.09682
H	1.10691	-3.36655	-0.0903
O	-0.47648	1.10138	-0.14682
O	0.47572	-1.09567	-0.14768
C	2.83874	-0.74675	-0.06551
O	1.89543	-2.79133	-0.08221
C	1.62214	-1.5398	-0.10397
H	-6.32735	-1.44316	1.21192
H	-5.87409	0.2174	-1.58551
O	-6.08053	-0.31537	-0.79553
C	-3.89308	0.18348	-0.00839
O	-5.42153	-1.06987	1.15178
C	-5.18615	-0.41796	0.0968
H	-1.11182	3.37079	-0.08872
H	-0.00266	0.00731	-0.1451
C	-2.83895	0.7477	-0.06519
O	-1.89933	2.79409	-0.08104
C	-1.62405	1.54318	-0.10311
H	5.87297	-0.21818	-1.58746

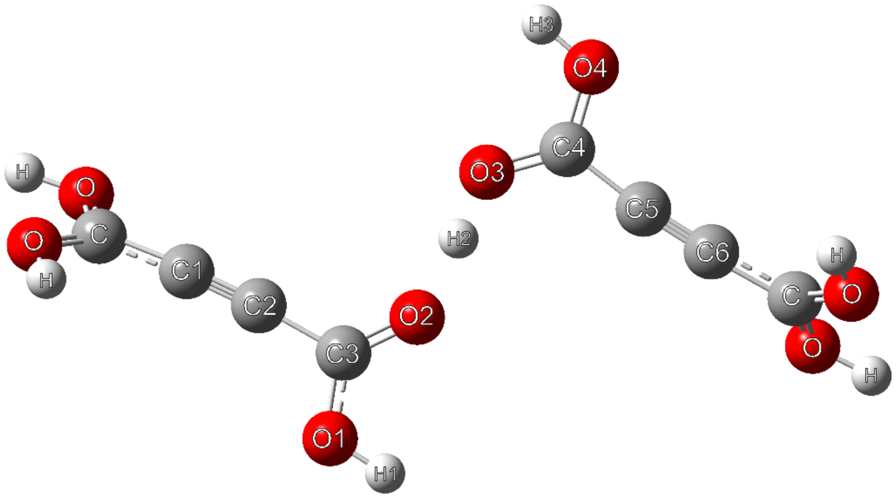

Figure S6. Optimized gas phase structure of the $[(C_4H_3O_4)\cdots H\cdots(C_4H_3O_4)]^{3+}$ cation at the minimum (M1, M2 in Figure 9) (Optimization was run with a fixed O2-O3 distance of 2.410 Å). Calculated on the B3LYP/aug-cc-pVTZ level of theory.

Table S9. Input matrix for the structure optimization of the $[(C_4H_3O_4)\cdots H\cdots(C_4H_3O_4)]^{3+}$ cation.

opt=modredundant[a] freq B3LYP/aug-cc-pvtz geom=connectivity

Symbolic Z-matrix:

Charge = 3 Multiplicity = 1

H	6.33204	1.47696	1.17946
O	6.09655	0.29564	-0.81006
C	3.89746	-0.18668	-0.0144
O	5.42389	1.10221	1.1259
C	5.18894	0.41753	0.08045
H	1.10996	-3.39304	-0.05723
O	-0.46828	1.11199	-0.13065
O	0.47228	-1.10699	-0.13065
C	2.84079	-0.75678	-0.05989
O	1.90018	-2.81598	-0.05801
C	1.62324	-1.55487	-0.08741
H	-6.33104	-1.47896	1.18246
H	-5.89519	0.25846	-1.58979
O	-6.09655	-0.29564	-0.81006
C	-3.89746	0.18668	-0.0144
O	-5.42388	-1.10221	1.1259
C	-5.19094	-0.41853	0.08045
H	-1.10796	3.39204	-0.05723
H	-0.034	0.036	-0.12964
C	-2.83979	0.75478	-0.05989
O	-1.89718	2.81298	-0.05801
C	-1.62824	1.55387	-0.08741
H	5.89319	-0.25946	-1.58779

[a] The following ModRedundant input section has been read: B 7 8 F

Synthesis and Structure of Protonated Sulfur Dioxide

Christoph Jessen,[a] Andreas J. Kornath*[a]

[a] C. Jessen, Prof. Dr. A. J. Kornath
Department of Chemistry
Ludwig-Maximilian University of Munich
Butenandtstr. 5−13, 81377 München (Germany)
E-mail: akoch@cup.uni-muenchen.de

Supporting Information for this article is given via a link at the end of the document.

Abstract: Salts of protonated sulfur dioxide were synthesized by recrystallization of $[FS(OX)_2][SbF_6]$ (X = H, D) in aprotic solvents at low temperatures. Hemiprotonated sulfur dioxide $[(SO_2)_2H][Sb_2F_{11}]$ was obtained from the solvent SO_2 and the monoprotonated sulfur dioxide $[OSOD][Sb_2F_{11}]$ by using 1,1,1,2-Tetrafluoroethane as solvent. For both compounds, single-crystals were obtained and an X-ray structure analysis was conducted. Furthermore, the salts were characterized by Raman spectroscopy and the results were discussed together with quantum chemical calculations on the M06-2X/aug-cc-pVTZ level of theory.

Sulfur dioxide is of utmost importance as a solvent in superacid chemistry, for example as the medium for reactions with "magic acid" (FSO_3H/SbF_5).[1] Also carborane acids, the strongest known Brønsted acids, are quite soluble in SO_2. *Reed et al.*[2,3] compared the acidities of different carborane acids in SO_2 solution with the mesityl oxide method[4] of Fărcaşiu. Based on their results they assumed, that the acidities of the carborane acids were leveled due to the protonation of the solvent in form of $H(SO_2)_2^+$. Later, *Stoyanov et al.* investigated the reaction of solid carborane acids with sulfur dioxide at ambient temperatures.[5] They detected hemi- and monoprotonated species of SO_2 based on subtracted infrared spectra of the condensed mixtures. Furthermore, several high-level quantum chemical calculations on protonated SO_2 have been reported, because of its relevance in astrophysics or its importance in environmental and atmospheric processes.[6,7] The site of protonation is predicted to be on one of the oxygen atoms with two almost isoenergetic forms, with the planar *cis*-form being the global energetic minimum over the planar *trans*-form.[7] Despite the effort that was taken to elucidate the properties and structure of protonated SO_2, it remained an extremely elusive cation.

The reaction of SO_2 with the superacidic system HF/SbF_5 has already been reported.[8] Sulfur dioxide undergoes HF addition and protonation under the formation of the $FS(OH)_2^+$ cation.[8] However, a protonated SO_2 molecule has not been observed under the reported reaction conditions.[8] Our idea to isolate protonated SO_2 was to use the thermally labile $FS(OH)_2^+$ cation as a precursor to synthesize protonated SO_2 by elimination of hydrogen fluoride from $FS(OH)_2^+$. First, the preparation of $FS(OH)_2^+$ was transferred from the described sapphire reactor to convenient FEP reactors. Following the reported procedure of mixing SO_2 and SbF_5 in anhydrous hydrogen fluoride (*a*HF) at elevated temperatures (−30 °C) and subsequent cooling to −70 °C or lower, yields $[FS(OH)_2][SbF_6]$ as crystalline precipitant. The pure substance is isolated by removing the excess solvent and volatile residues *in vacuo*. The extremely thermal and moisture sensitive colorless solid decomposes at −72 °C.[8] To investigate its stability in solution, a sample of neat $[FS(OH)_2][SbF_6]$ was dissolved in a small amount of SO_2 and kept at −40 °C for several days. After the precipitation of colorless crystals, the mixture was cooled to −70 °C until no further precipitation of the solid was observed. Removal of the solvent in a dynamic vacuum allowed us to perform Raman spectroscopy and single-crystal X-ray structure analysis. The formation of hemiprotonated SO_2 as $[(SO_2)_2H][Sb_2F_{11}]$ (**1**) from $[FS(OH)_2][SbF_6]$ is shown in Scheme 1. The deuterated species $[(SO_2)_2D][Sb_2F_{11}]$ (**2**) was obtained by reacting stoichiometric amounts of SO_2 and SbF_5 in *a*DF and following the same procedure as for **1** to obtain the salt $[FS(OD)_2][SbF_6]$.

To clarify the formation of hemiprotonated SO_2 from the $FS(OH)_2^+$ cation in SO_2, neat $[FS(OD)_2][SbF_6]$ was dissolved in 1,1,1,2-Tetrafluoroethane (R-134a) and kept at −40 °C for several days. After a crystalline solid precipitated, the solvent was removed in dynamic vacuum, and $[OSOD][Sb_2F_{11}]$ (**3**) was obtained as a colorless crystalline solid. This finding shows that in solution and temperatures higher than −40°C, $FS(OH)_2^+$ eliminates HF to form the cation $OSOH^+$. In the solvent SO_2, a subsequent reaction with solvent leads to the formation of the $(SO_2)_2H^+$ cation. The other important issue to clarify was the involved anion as the protonated SO_2 species never occurred as SbF_6^- salts, but solely with the $Sb_2F_{11}^-$ counteranion. Similarly, the $Sb_2F_{11}^-$ anion can stabilize the superacidic cation H_2F^+ as isolated salt $[H_2F][Sb_2F_{11}]$[9] but "$[H_2F][SbF_6]$" is unknown in the solid state. Since the starting material for the reaction is $[FS(OH)_2][SbF_6]$ no excess SbF_5 is present in the solution to form $Sb_2F_{11}^-$ anions. The only source of SbF_5 is the decomposition of the starting material. We assume that $[OSOH][SbF_6]$ occurs as an intermediate but the SbF_6^- anion can not stabilize a protonated SO_2 molecule under the described reaction condition.

This leads to the following equations (1) to (3) where $[FS(OH)_2][SbF_6]$, $[OSOH][SbF_6]$, and $[FS(OH)_2][Sb_2F_{11}]$ occur as metastable species at −40 °C (Scheme 1). As equation (5) shows $[OSOH][Sb_2F_{11}]$ is observed as a stable compound and final product. Since the compound is additionally poorly soluble in the solvent R-134a, the reaction is pulled towards that side. Finally, equation (6) shows the formation of **1** in excess SO_2, by breaking the $OSOH^+\cdots[Sb_2F_{11}]^-$ hydrogen bond.

The thermal stabilities of **1** and **3** were investigated by warming up the salts from −78 °C to 0 °C under the observation of the pressure in the vacuum line. Subsequently, the remaining solids in the FEP-reactors were analyzed by Raman spectroscopy. The absence of any vibrations of the SO_2 moiety in the remaining salts indicates the decomposition of **1** and **3** to SO_2, and fluoronium salts ($[H(HF)_n][Sb_2F_{11}]$).

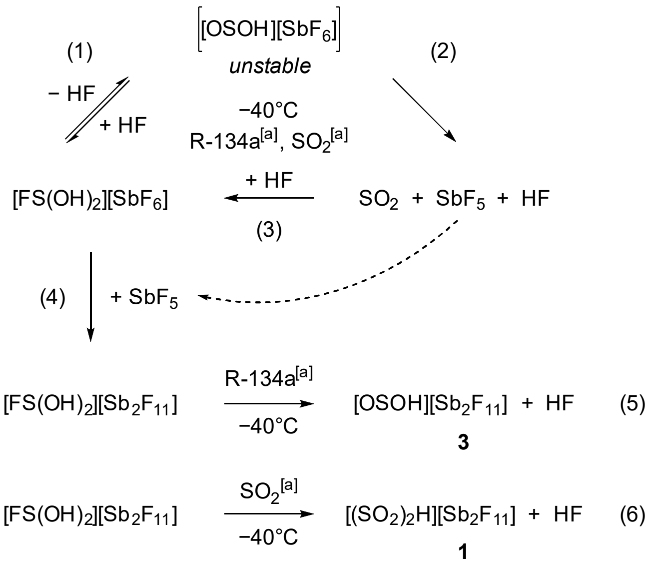

Scheme 1. Synthesis of protonated sulfur dioxide. [a]Used as a solvent in this step.

The salts decompose between −40 °C and 0 °C and at −70 °C the salts are stable for weeks under a nitrogen atmosphere. The preparation of hemi- and monoprotonated SO_2 from $[FS(OH)_2][SbF_6]$ is summarized in equations (7) and (8).

$$2\,[FS(OH)_2][SbF_6] \xrightarrow[\text{R-134a}]{-40^\circ\text{C}} [OSOH][Sb_2F_{11}] + 3\,HF + SO_2 \quad (7)$$

$$2\,[FS(OH)_2][SbF_6] \xrightarrow[SO_2]{-40^\circ\text{C}} [(SO_2)_2H][Sb_2F_{11}] + 3\,HF \quad (8)$$

The formation of hemiprotonated SO_2 is only observed in excess SO_2. In R-134a, stoichiometric amounts of SO_2, do not seem to break the $SO_2\cdots H^+\cdots[Sb_2F_{11}]^-$ hydrogen bond (equation (7)). Interestingly, the carborane acid $H(CHB_{11}Cl_{11})$ reacts similarly, forming the proton disolvate $[(SO_2)_2H][CHB_{11}Cl_{11}]$ in excess SO_2 solution, and $[OSOH][CHB_{11}Cl_{11}]$ when reacted with gaseous SO_2.[5] This highlights the low basicity and high stability of the $Sb_2F_{11}^-$ anion, allowing the isolation of protonated SO_2 species in the condensed phase.

Hemiprotonated SO_2 (**1**) crystallizes as the salt $[(SO_2)_2H][Sb_2F_{11}]$ in the triclinic space group $P\bar{1}$ with one formula unit per unit cell. The formula unit is illustrated in Figure 1. Selected bond lengths and angles are listed in Table 1. The S−O distances (1.461(4) Å, 1.408(4) Å) differ significantly from one another by 0.053 Å. In comparison, the S−O bonds in solid SO_2 are equally long with 1.4299(3) Å.[10] Due to the hemiprotonation, the S−O bond on the hemiprotonated side is significantly shortened, while the other S−O bond does not change significantly. The O−S−O bond angle in (**1**) decreases compared to SO_2 (117.16(3)°). Within the standard uncertainties, the $Sb_2F_{11}^-$ anion exhibits D_{4h}-symmetry with an inversion center on the F4 position. This high symmetry is rare for $Sb_2F_{11}^-$ anions but has been observed before in crystal structures with weak anion-cation interactions.[9,11] The Sb−F distances are in agreement with reported values.[9]

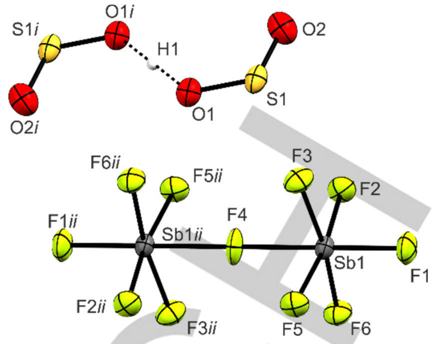

Figure 1. Formula unit of $[(SO_2)_2H][Sb_2F_{11}]$ (**1**) (50% probability displacement ellipsoids). Symmetry code: $i = -x, -y, 1-z$; $ii = 1-x, 1-y, 1-z$.

As suggested in the literature hemiprotonated SO_2 exists as a proton disolvate $(SO_2)_2H^+$.[2,3][4] The interionic contacts in the crystal structure are shown in Figure S2 in the Supporting Information. The SO_2 molecules are connected by a short hydrogen bond $O\cdots H^+\cdots O$ (2.446(5) Å) that holds the bridging proton, which is isolated from the anions. The exact position of the proton is indeterminate by single-crystal X-ray analysis. Nevertheless, the structure was successfully refined with the proton on the crystallographic inversion center. This geometry is also found for the calculated gas-phase structure of the $(SO_2)_2H^+$ cation. In addition, the cation forms three $S\cdots F$ contacts with distances between 2.656(4) Å and 2.927(3) Å, which are below the sum of the van-der-Waals (VDW) radii (3.27 Å).[12] The interionic contacts are shown on the Hirshfeld surface of the cation in Figure 3.

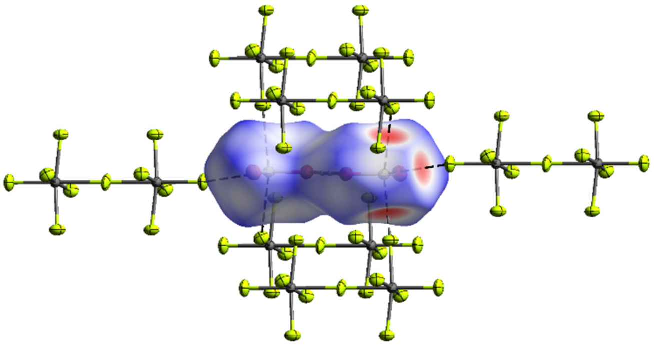

Figure 2. Interatomic contacts and Hirshfeld surface of the $(SO_2)_2H^+$ cation in **1** (mapped with d_{norm})[13,14]. Color coding of the Hirshfeld surface: white (distance *d* equals VDW), blue (*d* exceeds VDW distance), red (*d* is smaller than VDW distance).

Monoprotonated SO_2 (**3**) crystallizes in the triclinic space group $P\bar{1}$ with two formula units per unit cell. The formula unit is illustrated in Figure 3. Selected bond lengths and angles are listed in Table 1.

Due to the monoprotonation, the difference of the S−O distances (1.500(2) Å, 1.399(2) Å) increases to 0.101 Å. The O−S−O bond angle 116.0(1)° is the same as in **1**. The $Sb_2F_{11}^-$ anion is slightly angled around the bridging fluorine with an Sb−F−Sb angle of 175.7(1)°. The Sb−F distances agree with values from the literature.[15]

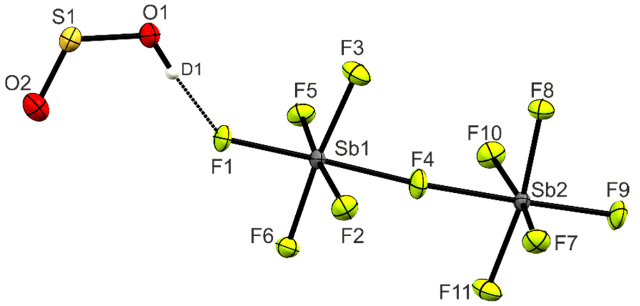

Figure 3. Formula unit of $[OSOD][Sb_2F_{11}]$ (**3**) (50% probability displacement ellipsoids).

Table 1. Selected bond lengths and angles of $[(SO_2)_2H][Sb_2F_{11}]$ (**1**), $[OSOD][Sb_2F_{11}]$ (**3**), and selected compounds from the literature.

Compound	S−O bond lengths [Å]		Bond angle [°]
	S1−O1	S1−O2	O1−S1−O2
$[(SO_2)_2H][Sb_2F_{11}]$ a)	1.461(4)	1.408(4)	115.9(2)
$[OSOD][Sb_2F_{11}]$ a)	1.500(2)	1.399(2)	116.0(1)
$OSO\text{-}SbF_5$[16]	1.469(4)	1.402(4)	115.7(3)
$[OSOCH_3][AsF_6]$[17]	1.505(5)	1.397(5)	114.9(3)
$[OSOCH_3][Sb_2F_{11}]$[18]	1.491(10)	1.379(10)	114.7(6)
SO_2 (solid)[19]	1.4299(3)	1.4299(3)	117.16(3)

a) This work.

In the crystal packing of **3**, the cation forms an O−D···F hydrogen bond to the anion with a donor-acceptor distance of 2.526(3) Å. Furthermore, three S···F contacts are formed with distances between 2.584(2) Å and 2.788(2) Å (Figure S4, Supporting Information). Overall the interionic S···F contacts in monoprotonated SO_2 are stronger than in hemiprotonated SO_2. The interionic contacts are shown on the Hirshfeld surface of the $OSOD^+$ cation in Figure 4. The coordination sphere of the cations in **1** and **3** is well comparable.

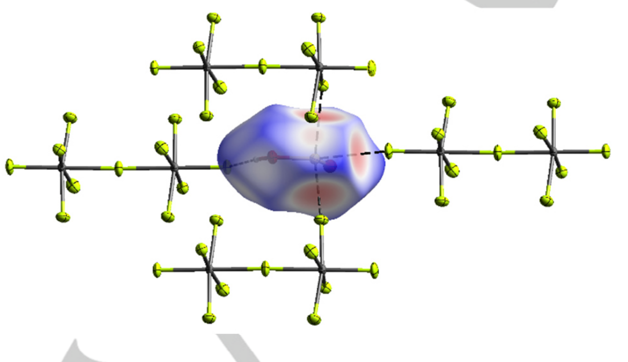

Figure 4. Interatomic contacts and Hirshfeld surface of the $OSOD^+$ cation in **3** (mapped with d_{norm})[13,14]. Color coding of the Hirshfeld surface: white (distance *d* equals VDW), blue (*d* exceeds VDW distance), red (*d* is smaller than VDW distance).

The bond lengths and angles of the cations $(SO_2)_2H^+$ (**1**) and $OSOD^+$ (**3**) are compared to similar structures from the literature in Table 1. The monoprotonation of SO_2 has a comparable effect on the S−O bond lengths as its methylation. As in $[OSOCH_3][AsF_6]$[17] the S−O bond, which is bonded to the lewis acid (H^+, CH_3^+), is significantly elongated compared to SO_2, while the other S−O bond is shortened. The hemiprotonation affects the S−O distances less than the monoprotonation. The S−O distances in **1** are well comparable with respective distances in the reported complex $OSO{-}SbF_5$.[16]

Raman spectroscopy was used in addition to single-crystal X-ray diffraction to investigate the influence of the protonation on the S−O bonds in **1** and **3** (Figure 5). Table 2 lists the observed vibrational frequencies of the cations together with calculated vibrational frequencies and their assignments. Details on the calculated structures are reported in the Supporting Information, as well as a complete list of the observed and calculated vibrational frequencies. Figure 5 illustrated the low-temperature Raman spectra of **1**, **2**, and **3** together with solid amorphous sulfur dioxide.

The $(SO_2)_2H^+$ cation possesses C_{2h} symmetry. For the cation 15 fundamental vibrations ($\Gamma_{vib}(C_{2h}) = 5\,A_g + B_g + 3\,A_u + 6\,B_u$) are expected, as well as the rule of mutual exclusion. Therefore, six Raman active vibrations and nine IR-active vibrations are expected. Since the proton occupies the inversion center, vibrational modes including a displacement of the proton ($3\,A_u + 6\,B_u$) show no Raman activity. Therefore the vibrational frequencies of $[(SO_2)_2H][Sb_2F_{11}]$ and $[(SO_2)_2D][Sb_2F_{11}]$ are identical in the Raman spectrum and no H/D-isotopic shift is observed. The only difference is a broad line at 2292 cm^{-1}, which is assigned to the contamination of deuterated H_3O^+ ($OD_nH_{3-n}^+$).[20] Single crystals of $[H_3O][SbF_6]$ were found as contaminations in all samples of the protonated SO_2 species, probably due to the long recrystallization process.

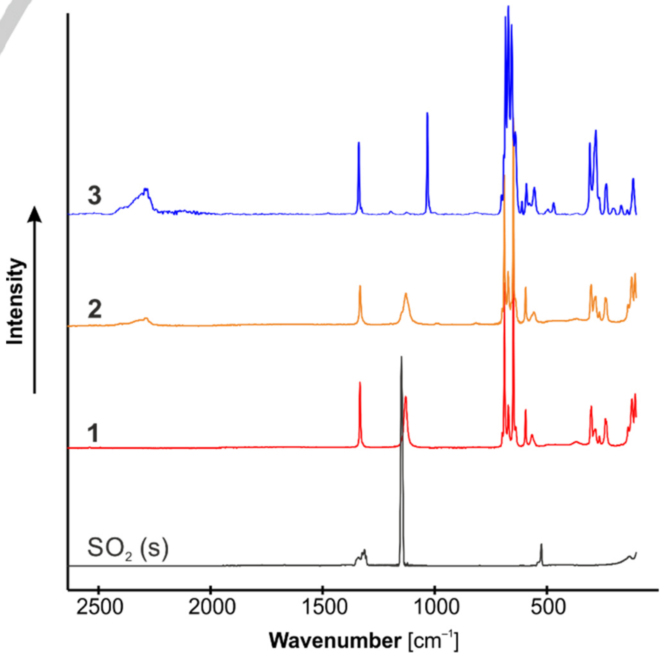

Figure 5. Low-temperature Raman spectra of $[(SO_2)_2H][Sb_2F_{11}]$ (**1**), $[(SO_2)_2D][Sb_2F_{11}]$ (**2**), $[OSOD][Sb_2F_{11}]$ (**3**) and solid amorphous sulfur dioxide.

Table 2. Selected experimental Raman frequencies [cm^{-1}] of [(SO$_2$)$_2$*X*][Sb$_2$F$_{11}$] (*X* = H, D), [OSOD][Sb$_2$F$_{11}$], [OSOCH$_3$][AsF$_6$][17], infrared frequencies of [OSOH][CHB$_{11}$Cl$_{11}$][5] and calculated vibrational frequencies [cm^{-1}] of the cations [(SO$_2$)$_2$*X*]$^+$ and [OSOD · HF]$^+$.

[(SO$_2$)$_2$*X*][Sb$_2$F$_{11}$]$^{a)}$	[(SO$_2$)$_2$*X*]$^+$ calc.$^{b), c)}$	[OSOD][Sb$_2$F$_{11}$]	[OSOD · HF]$^+$ calc.$^{b), c)}$	[OSOH]$^{+\ d), [5]}$	[OSOCH$_3$]$^{+\ d), [17]}$	Assignment
exp. Raman	IR/Raman	exp. Raman	IR/Raman	exp. IR	exp. Raman	
		2284(13)	1823(1418/43)	2700		*v*(OX)$^{a)}$
1333(32)	1355(0/26)	1338(35)	1362(121/17)	1320	1326	*v*(SO)
1129(25)	1160(0/48)	1033(49)	1047(99/18)	931	1009	*v*(SO)
566(7)	589(0/6)	591(15)	521(41/3)	583	566	*δ*(OSO)
365(3)	409(0/4)					*v*(O···*X*···O)$^{a)}$
238(14)	189(0/1)	Not observed	864(84/0)	Not observed	241	*δ*(SO*X*)$^{a)}$

a) *X* = H, D or CH$_3$ for [OSOCH$_3$][AsF$_6$]. b) Calculated on the M06-2X/aug-cc-pVTZ level of theory. Scaling factor: 0.956. c) (IR intensities in km/mol / Raman intensities in Å^4/u). d) counteranion: CHB$_{11}$Cl$_{11}^-$. e) counteranion: AsF$_6^-$.

In the Raman spectra of **1** and **2** the observed lines at 1333 cm^{-1} and 1129 cm^{-1} are assigned to the SO stretching vibrations, respectively. The Raman lines at 566 cm^{-1}, 365 cm^{-1} and are assigned to the OSO-bending vibrations in addition to the *δ*(SO*X*) vibrations at 238 cm^{-1}.

The OSOD$^+$ cation possesses C_s symmetry. For the cation six fundamental vibrations ($\Gamma_{\text{vib}}(C_s) = 5A' + 1A''$) are expected, all of which are Raman and IR-active. The SO stretching vibrations are detected at 1333 cm^{-1} and 1033 cm^{-1}, respectively. The Raman line at 591 cm^{-1} is assigned to the OSO deformation vibration.

For the Raman spectra of hemi- and monoprotonated SO$_2$, the most noticeable feature is the shifting and therefore the increasing difference (Δ*v*) between the two SO stretching vibrations. In SO$_2$ the difference between the symmetric (1148 cm^{-1}) and antisymmetric (1341 cm^{-1}) stretching vibrations amounts to 190 cm^{-1}.[21,22] In the hemiprotonated cation Δ*v* increases slightly to 204 cm^{-1}, while Δ*v* increases significantly to 305 cm^{-1} for the monoprotonated species. This fits the Δ*v* criterion for SO$_2$ complexes reported by *Shriver*, for which O-bonded SO$_2$ complexes exhibit Δ*v* > 190 cm^{-1} and S-bonded complexes Δ*v* < 190 cm^{-1}.[22] Interestingly, in **1**, **2**, and **3** only one *v*(SO) vibration is significantly redshifted compared to the neutral compound, while the other *v*(SO) vibration remains unchanged. Hence, the protonation mainly affects the SO stretching vibration with the protonated oxygen. Compared to other O-bound SO$_2$ compounds the *v*(SO) modes of **1** and **2** are well comparable with the stretching modes observed in the OSO-SbF$_5$ complex (1318 cm^{-1}, 1109/1088 cm^{-1}).[22] Like the bond lengths and angles, the frequencies of the stretching vibrations of **3** are well comparable to those of methylated SO$_2$ ([OSOCH$_3$][AsF$_6$])[17] The other vibrational frequencies observed in the Raman spectra, especially the vibrational modes of the anions are discussed in the Supporting Information.

Stoyanov et al. investigated species of protonated SO$_2$ by infrared spectroscopy.[5] The observed vibrational frequencies of the SO$_2$ moiety in [OSOH][CHB$_{11}$Cl$_{11}$] are listed in Table 2 and agree with the results from the Raman spectra of **3** in this work. The reported frequencies of the *v*(SO) vibrations (1320 cm^{-1}, 931 cm^{-1})[5] differ from the results of this work. Particularly the frequency of the *v*(SO) vibration on the protonated side in [OSOH][CHB$_{11}$Cl$_{11}$] (931 cm^{-1})[5] is red-shifted compared the respective frequency in [OSOD][Sb$_2$F$_{11}$] (1033 cm^{-1}). We attribute this finding to the extremely low basicity of the carborane anion.[23] In the reported infrared spectra of the hemiprotonated SO$_2$ species [(SO$_2$)$_2$H][CHB$_{11}$*Y*$_{11}$] (*Y* = F, Cl), the *v*(SO) and *δ*(OSO) vibrations are absent.[5] Instead, the hemiprotonation was detected based on the stretching frequencies of the O···H$^+$···O group in their work. In this work, Raman spectroscopy was used to allow the observation of the *v*(SO) and *δ*(OSO) vibrations in the (SO$_2$)$_2$H$^+$ cation.

In conclusion, we succeeded with the preparation and isolation of hemi- and monoprotonated SO$_2$ by the decomposition of the salt [FS(OH)$_2$][SbF$_6$]. The observed cations crystallize as Sb$_2$F$_{11}^-$ salts. The investigation of these salts by Raman spectroscopy gave insight into the effect of the protonation on the vibrational frequencies of the protonated SO$_2$ moiety, while the results of the single-crystal X-ray structure analyses elucidate its geometrical properties, respectively. In the case of hemiprotonated SO$_2$, Raman spectroscopy allowed the first observation of the respective *v*(SO) and *δ*(OSO) vibrational frequencies.

Acknowledgments

We are grateful to the Department of Chemistry of the Ludwig-Maximilian University, Munich, the Deutsche Forschungsgemeinschaft (DFG), and the F-Select GmbH for the support of this work.

Keywords: protonation; sulfur dioxide; single-crystal structure analysis; Raman spectroscopy, low-temperature preparation

[1] G. A. Olah, *Superacid chemistry*, Wiley, Hoboken, N.J, **2009**.

[2] C. A. Reed, *Chem. Commun.* **2005**, 1669.

[3] M. Juhasz, S. Hoffmann, E. Stoyanov, K.-C. Kim, C. A. Reed, *Angew. Chem. Int. Ed. Engl.* **2004**, *43*, 5352.

[4] D. Farcasiu, A. Ghenciu, *J. Am. Chem. Soc.* **1993**, *115*, 10901.

[5] E. S. Stoyanov, I. V. Stoyanova, *Angew. Chem. Int. Ed. Engl.* **2018**, *57*, 4516.

[6] a) D. E. Smith, B. Munson, *J. Am. Chem. Soc.* **1978**, *100*, 497; b) T. B. McMahon, P. Kebarle, *J. Am. Chem. Soc.* **1986**, *108*, 6502; c) V. Lattanzi, P. Thaddeus, M. C. McCarthy, S. Thorwirth, *J. Chem. Phys.* **2010**, *133*, 194305; d) C. Puzzarini, *Phys. Chem. Chem. Phys.* **2011**, *13*, 21319; e)

G. de Petris, A. Cartoni, M. Rosi, V. Barone, C. Puzzarini, A. Troiani, *Chemphyschem* **2011**, *12*, 112; f) D. Himmel, S. K. Goll, I. Leito, I. Krossing, *Angew. Chem. Int. Ed. Engl.* **2010**, *49*, 6885.

[7] A. J. Frank, M. Sadílek, J. G. Ferrier, F. Tureček, *J. Am. Chem. Soc.* **1997**, *119*, 12343.

[8] A. Kornath, R. Seelbinder, R. Minkwitz, *Angew. Chem. Int. Ed. Engl.* **2005**, *44*, 973.

[9] D. Mootz, K. Bartmann, *Angew. Chem. Int. Ed. Engl.* **1988**, *27*, 391.

[10] B. Post, R. S. Schwartz, I. Fankuchen.

[11] a) I. H. Sham, B. O. Patrick, B. von Ahsen, S. von Ahsen, H. Willner, R. C. Thompson, F. Aubke, *Solid State Sci.* **2002**, *4*, 1457; b) H. Willner, J. Schaebs, G. Hwang, F. Mistry, R. Jones, J. Trotter, F. Aubke, *J. Am. Chem. Soc.* **1992**, *114*, 8972; c) B. von Ahsen, C. Bach, M. Berkei, M. Köckerling, H. Willner, G. Hägele, F. Aubke, *Inorg. Chem.* **2003**, *42*, 3801.

[12] A. Bondi, *J. Phys. Chem.* **1964**, *68*, 441.

[13] S.K. Wolff, D.J. Grimwood, J.J. McKinnon, M.J. Turner, D. Jayatilaka, M.A. Spackman, *CrystalExplorer 17.5, Revision: f4e298a*, University of Western Australia, **2017**.

[14] M. A. Spackman, D. Jayatilaka, *CrystEngComm* **2009**, *11*, 19.

[15] a) J. F. Lehmann, G. J. Schrobilgen, K. O. Christe, A. Kornath, R. J. Suontamo, *Inorg. Chem*. **2004**, *43*, 6905; b) C. G. Davies, R. J. Gillespie, P. R. Ireland, J. M. Sowa, *Can. J. Chem.* **1974**, *52*, 2048.

[16] R. Minkwitz, W. Molsbeck, H. Preut, *Z. Naturforsch. B* **1989**, *44*, 1581.

[17] R. Minkwitz, D. Bernstein, H. Preut, W. Sawodny, H. Hrtner, *Z. Anorg. Allg. Chem.* **1991**, *606*, 157.

[18] R. J. Gillespie, F. G. Riddell, D. R. Slim, *J. Am. Chem. Soc.* **1976**, *98*, 8069.

[19] a) B. Post, R. S. Schwartz, I. Fankuchen, *Acta Crystallogr.* **1952**, *5*, 372; b) S. Grabowsky, P. Luger, J. Buschmann, T. Schneider, T. Schirmeister, A. N. Sobolev, D. Jayatilaka, *Angew. Chem. Int. Ed. Engl.* **2012**, *51*, 6776.

[20] K. O. Christe, P. Charpin, E. Soulie, R. Bougon, J. Fawcett, D. R. Russell, *Inorg. Chem.* **1984**, *23*, 3756.

[21] A. Anderson, R. Savoie, *Can. J. Chem.* **1965**, *43*, 2271.

[22] D. M. Byler, D. F. Shriver, *Inorg. Chem.* **1976**, *15*, 32.

[23] C. A. Reed, *Acc. Chem. Res.* **1998**, *31*, 133.

Entry for the Table of Contents

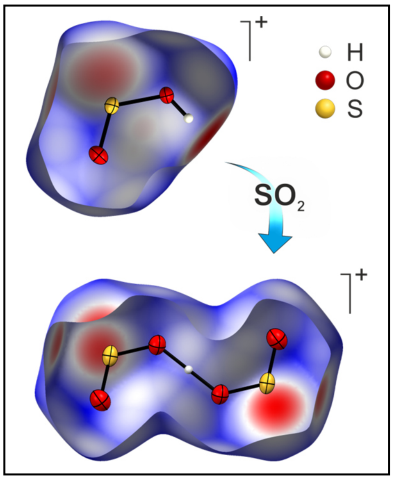

Hemi- and monoprotonated SO_2 cations have been isolated as $Sb_2F_{11}^-$ salts. The preparation of the salts was achieved by recrystallization of $[FS(OH)_2][SbF_6]$ in weakly basic, aprotic solvents at low temperatures. The elusive structures of both cationic species have been investigated by X-ray structure analysis and Raman spectroscopy.

Supporting Information
©Wiley-VCH 2019
69451 Weinheim, Germany

Synthesis and Structure of Protonated Sulfur Dioxide

Christoph Jessen, Andreas J. Kornath*

Table of Contents

1. **Experimental Procedures** 3
2. **Crystallographic Data** 4
3. **Quantum Chemical Calculations** 9
4. **Vibrational Data** 10
5. **References** 13

1. Experimental Procedures

Apparatus and materials

All reactions were carried out by employing standard Schlenk techniques on a stainless-steel vacuum line. The syntheses of the salts were performed by using FEP/PFA-reactors with a stainless-steel valve. Before each reaction, the stainless-steel vacuum line and the reactors were dried with fluorine. The obtained compounds were characterized by low-temperature Raman spectroscopy and single crystal X-Ray diffraction study. For Raman measurements a Bruker MultiRam FT-Raman spectrometer with Nd:YAG laser excitation (λ = 1064 nm) was used. The single-crystal X-ray diffraction studies were performed with an Oxford XCalibur3 diffractometer equipped with a Spellman generator (voltage 50 kV, current 40 mA) and a KappaCCD detector, operating with Mo-K_α radiation (λ = 0.7107 Å) The measurements were performed at 161 K ($[(SO_2)_2H][Sb_2F_{11}]$ (**1**)) and 115 K ($[OSOD][Sb_2F_{11}]$ (**3**)). The program CrysAlisPro 1.171.38.46 (Rigaku OD, 2015)[1] were employed for the data collection and reduction. The structures were solved utilizing SHELXT[2] and SHELXL-2018/3[3] of the WINGX software package.[4] The structures were checked using the software PLATON.[5] The absorption correction was performed using the SCALE3 ABSPACK multiscan method.[6] Quantum chemical calculations were carried out using the software package Gaussian09.[7]

Caution! Note that any contact with the described compounds should be avoided. Hydrolysis of these salts forms HF which burns skin and causes irreparable damage. Safety precautions should be taken while handling these compounds.

Syntheses of $[FS(OX)_2][SbF_6]$ (X = H, D)

Antimony pentafluoride (1.25 mmol) was condensed in an FEP reactor vessel together with sulfur dioxide (1.25 mmol) and anhydrous HF (*a*HF) or *a*DF (0.5 mL) at −196 °C. The reaction mixture was then warmed up to −30 °C and homogenised to complete solvation. The reaction mixture was kept at −70 °C for 24 h until $[FS(OX)_2][SbF_6]$ (X = H, D) crystallizes as colourless needles. Excess solvent or starting materials were removed at −78 °C in dynamic vacuum. The products were obtained as colourless crystalline solids that decompose at ca. −72 °C under dry nitrogen atmosphere as reported.[8]

Syntheses of $[(SO_2)_2X][Sb_2F_{11}]$ (X = H, D) and $[OSOD][Sb_2F_{11}]$

In an FEP reactor vessel, the neat salts of $[FS(OX)_2][SbF_6]$ (X = H, D) were cooled to −196 °C and the solvent (SO_2 (0.5 mL) or R-134a (2 mL)) was added by condensation. The mixture was then warmed up to −30 °C and homogenized until a clear solution was received. The solution was kept at −40 °C for several days until a colourless crystalline precipitant was formed and then kept at −70 °C to crystallize most of the remaining solved product. In the case of $[(SO_2)_2X][Sb_2F_{11}]$ (X = H, D) excess sulfur dioxide was removed at −70 °C in dynamic vacuum. The product was obtained as a colourless solid. In the case of $[OSOD][Sb_2F_{11}]$ excess R-134a was removed at −78 °C in dynamic vacuum and the product was obtained as a colourless solid.

2. Crystallographic Data

Table S1. Bond lengths and angles of $[(SO_2)_2H][Sb_2F_{11}]$ (**1**) and $[OSOD][Sb_2F_{11}]$ (**3**).

$[(SO_2)_2H][Sb_2F_{11}]$				$[OSOD][Sb_2F_{11}]$			
bond lengths [Å]		bond angles [°]		bond lengths [Å]		bond angles [°]	
S1-O1	1.461(3)	O2-S1-O1	115.9(2)	S1 -O1	1.500(2)	O2-S1-O1	116.0(1)
S1-O2	1.408(4)	F1-Sb1-F5	94.4(1)	S1 -O2	1.399(2)	F11-Sb2-F9	95.5(1)
Sb1-F1	1.843(3)	F1-Sb1-F6	94.5(1)	Sb2-F11	1.849(2)	F11-Sb2-F7	91.6(1)
Sb1-F2	1.862(3)	F5-Sb1-F6	91.7(1)	Sb2-F9	1.850(2)	F9-Sb2-F7	95.7(1)
Sb1-F3	1.860(3)	F1-Sb1-F3	94.6(1)	Sb2-F7	1.857(2)	F11-Sb2-F10	90.1(1)
Sb1-F4	2.0170(4)	F5-Sb1-F3	89.5(1)	Sb2-F10	1.866(2)	F9-Sb2-F10	94.9(1)
Sb1-F5	1.851(3)	F6-Sb1-F3	170.5(1)	Sb2-F8	1.871(2)	F7-Sb2-F10	169.1(1)
Sb1-F6	1.856(2)	F1-Sb1-F2	94.3(1)	Sb2-F4	2.030(2)	F11-Sb2-F8	170.6(1)
		F5-Sb1-F2	171.3(1)	Sb1-F3	1.850(2)	F9-Sb2-F8	93.9(1)
		F6-Sb1-F2	88.6(1)	Sb1-F5	1.852(2)	F7-Sb2-F8	87.70(1)
		F3-Sb1-F2	88.8(1)	Sb1-F2	1.854(2)	F10-Sb2-F8	88.9(1)
		F1-Sb1-F4	179.8(1)	Sb1-F6	1.855(2)	F11-Sb2-F4	85.9(1)
		F5-Sb1-F4	85.7(1)	Sb1-F1	1.887(2)	F9-Sb2-F4	178.5(1)
		F6-Sb1-F4	85.5(1)	Sb1-F4	2.014(2)	F7-Sb2-F4	84.7(1)
		F3-Sb1-F4	85.2(1)			F10-Sb2-F4	84.7(1)
		F2-Sb1-F4	85.6(1)			F8-Sb2-F4	84.7(1)
		Sb1-F4-Sb1	180			F3-Sb1-F5	91.0(1)
						F3-Sb1-F2	89.5(1)
						F5-Sb1-F2	172.7(1)
						F3-Sb1-F6	174.3(1)
						F5-Sb1-F6	88.7(1)
						F2-Sb1-F6	90.1(1)
						F3-Sb1-F1	93.3(1)
						F5-Sb1-F1	94.0(1)
						F2-Sb1-F1	93.3(1)
						F6-Sb1-F1	92.4(1)
						F3-Sb1-F4	88.0(1)
						F5-Sb1-F4	86.4(1)
						F2-Sb1-F4	86.3(1)
						F6-Sb1-F4	86.3(1)
						F1-Sb1-F4	178.7(1)
						Sb1-F4-Sb2	175.7(1)

Hemiprotonation

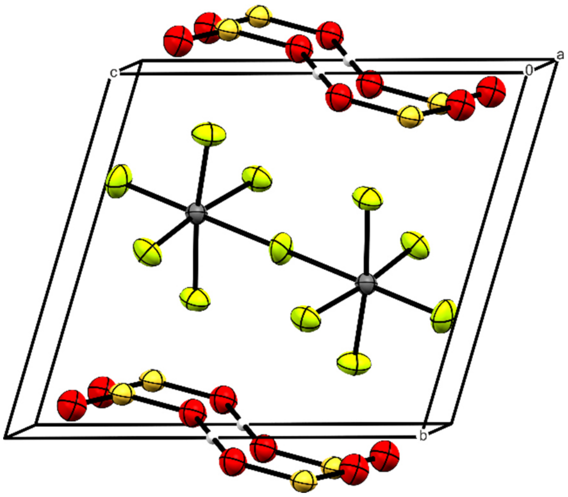

Figure S1. Crystal packing of [$(SO_2)_2H$][Sb_2F_{11}] (**1**) (50% probability displacement ellipsoids).

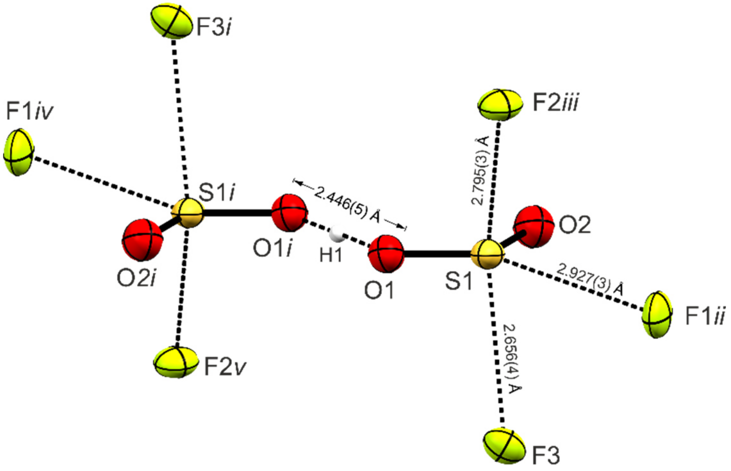

Figure S2. $(SO_2)_2H^+$ cation and selected interionic contacts (50% probability displacement ellipsoids). Symmetry code: *i* = −x, −y, 1−z; *ii* = 1−x, −y, 2−z; *iii* = x, −1+y, z; *iv* = −1+x, y, −1+z; *v* = −x,1−y,1−z

Monoprotonation

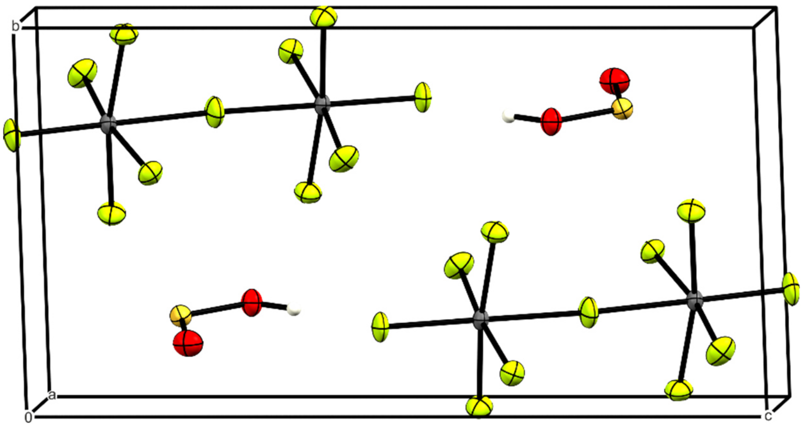

Figure S3. Crystal packing of [OSOD][Sb_2F_{11}] (**3**) (50% probability displacement ellipsoids)

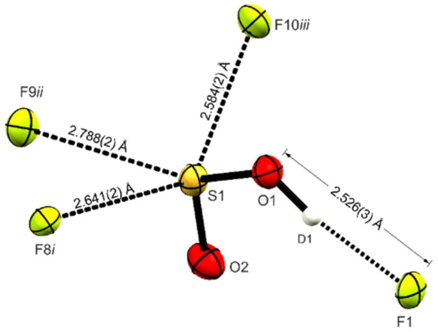

Figure S4. OSOD$^+$ cation and selected interionic contacts (50% probability displacement ellipsoids). Symmetry code: *i* = 1−x, 1−y, 1−z; *ii* = −1+x, y, −1+z; *iii* = 1−x, −y, 1−z.

Hirshfeld analysis

Hirshfeld surface analysis was conducted with the CrystalExplorer software[9]. In Figure S6, the Hirshfeld fingerprint plots of the cations in **1** and **3** are shown. For the hemiprotonation, the Hirshfeld surface was calculated for the asymmetric unit only, to also gain information about the hydrogen bond. The different contacts and their percentage of all contacts are noted in the respective diagrams. The fingerprint plots show how similar the surroundings of the cations are in the crystal structures of **1** and **3**.

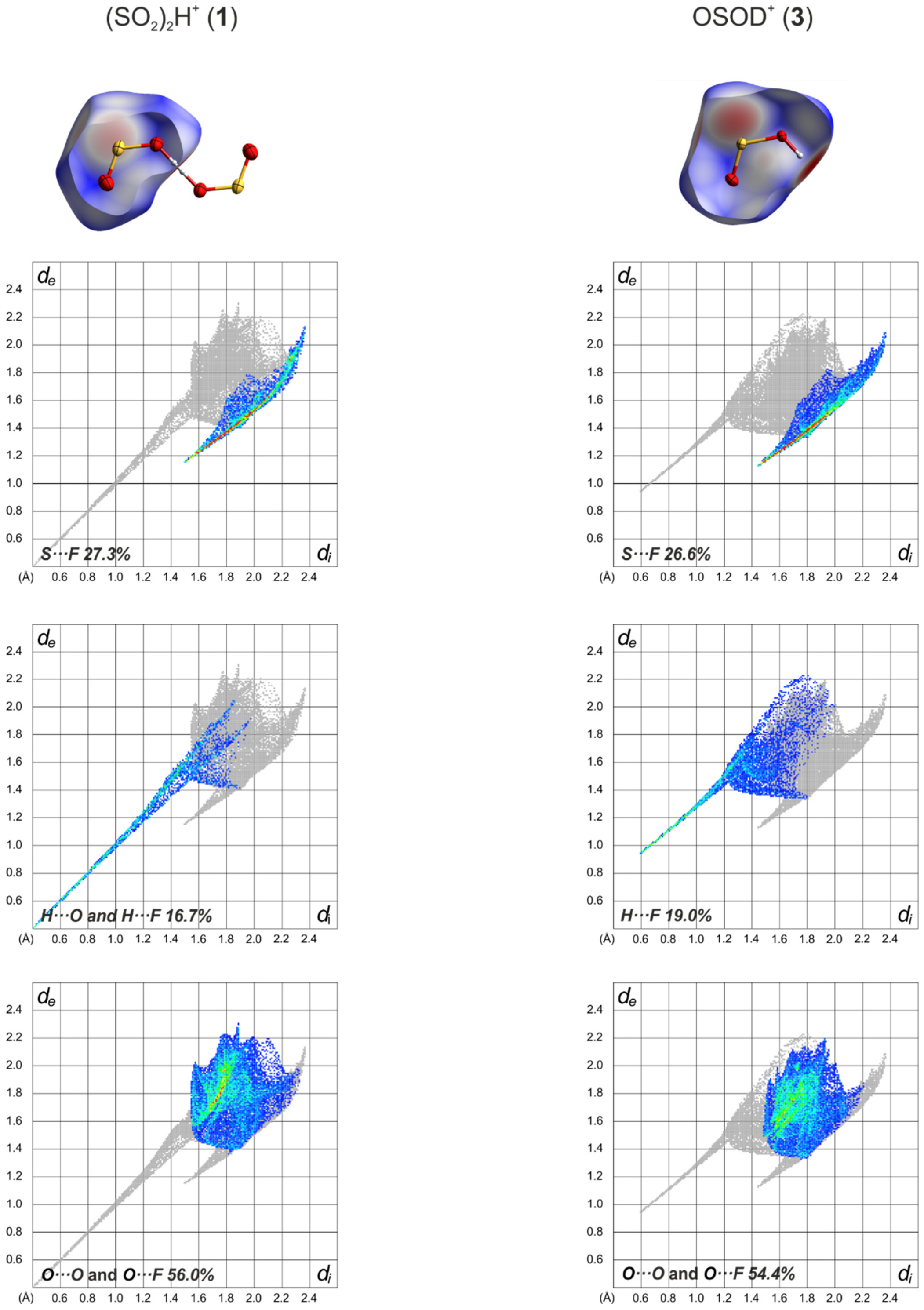

Figure S5. Fingerprint plots of the cations in the crystal structure of **1** and **3.**

Table S2. Crystal data and structure refinement of [$(SO_2)_2H$][Sb_2F_{11}] (**1**) and [OSOD][Sb_2F_{11}] (**3**).

	[$(SO_2)_2H$][Sb_2F_{11}] (**1**)	[OSOD][Sb_2F_{11}] (**3**)
Molecular Fomula	$F_{11}HO_4S_2Sb_2$	$DF_{11}O_2SSb_2$
Mr[g·mol^{-1}]	581.63	518.57
Crystal size [mm^3]	0.16 × 0.14 × 0.10	0.17 × 0.13 × 0.07
Crystal system	triclinic	triclinic
Space group	$P\bar{1}$	$P\bar{1}$
a [Å]	5.1600(9)	5.1101(2)
b [Å]	7.4554(9)	7.1158(3)
b [Å]	8.6052(11)	13.6092(7)
α [°]	71.456(11)	90.256(4)
β [°]	76.278(13)	96.366(4)
γ [°]	85.393(12)	94.751(3)
V [Å^3]	304.89(8)	490.08(4)
Z	1	2
ρcalc [g·cm^{-3}]	3.168	3.514
μ [mm^{-1}]	4.920	5.878
λMoKα [Å]	0.71073	0.71073
F(000)	266.0	468.0
T [K]	161 K	115 K
h, k, l range	-7:7,-8:10,12:11	-7:7,-10:9,-19:19
Measured reflexes	3076	5329
Unique reflexes	1866	3168
Rint	0.0353	0.0221
Parameters	89	149
R(F)/wR(F2)[a] (all data)	0.0429/0.0711	0.0285/0.0461
Weighting scheme[b]	0.0168/0.0000	0.0152/0.0000
S (Gof)[c]	1.079	1.066
Residual density [e·Å−3]	1.658/-1.536	0.854/-0.962
Device	Oxford XCalibur	Oxford XCalibur
CCDC	2073880	2073884

[a] $R_1 = \Sigma||F_0|-|F_c||/\Sigma|F_0|$.

[b] $wR_2 = [\Sigma[w(F_0^2-F_c^2)^2]/\Sigma[w(F_0)^2]]^{1/2}$; $w = [\sigma_c^2(F_0^2)+(xP)^2+yP]-1$; $P = (F_0^2+2F_c^2)/3$.

[c] GoF = $\{\Sigma[w(F_o^2-F_c^2)^2]/(n-p)\}^{1/2}$ (n = number of reflections; p = total number of parameters).

3. Quantum Chemical Calculations

All quantum chemical calculations were carried out with the Gaussian program package on the M06-2X/aug-cc-pVTZ level of theory. The structural parameters of the optimized gas-phase structures were compared to the X-Ray data. For the $OSOD^+$ cation an additional HF molecule was added to the calculation to simulate the strong hydrogen bond. For both cations, the bond lengths of the calculated structures differ from the bond lengths in the crystal structure but are appreciable for vibrational analysis. Cartesian coordinates and energies of the calculated global minima structures follow, as well as figures of the calculated gas-phase structures with bond lengths and angles.

$(SO_2)_2H^+$

Energy (M06-2X/aug-cc-pVTZ): -1097.533339 Hartree

O	-0.811794	2.725267	0.000000
S	0.557910	2.353790	0.000000
O	0.811794	0.893133	0.000000
O	-0.811794	-0.893133	0.000000
S	-0.557910	-2.353790	0.000000
O	0.811794	-2.725267	0.000000
H	0.000000	0.000000	0.000000

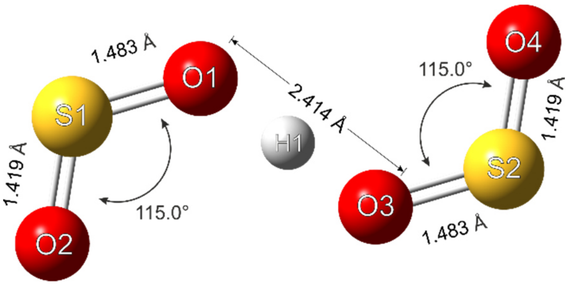

Figure S6. Calculated gas-phase structure of the $(SO_2)_2H^+$ cation.

$(SO_2)_2D^+$

Energy (M06-2X/aug-cc-pVTZ): -1097.533339 Hartree

O	-0.811794	2.725267	0.000000
S	0.557910	2.353790	0.000000
O	0.811794	0.893133	0.000000
O	-0.811794	-0.893133	0.000000
S	-0.557910	-2.353790	0.000000
O	0.811794	-2.725267	0.000000
D	0.000000	0.000000	0.000000

$[OSOD \cdot HF]^+$

Energy (M06-X/aug-cc-pVTZ): -649.354788 Hartree

F	-2.286078	0.292623	0.000107
S	1.143658	-0.240803	-0.000056
O	1.011696	1.166548	-0.000020
O	-0.167931	-0.986006	-0.000000
D	-1.074494	-0.487181	0.000053
H	-3.170498	-0.004306	0.000134

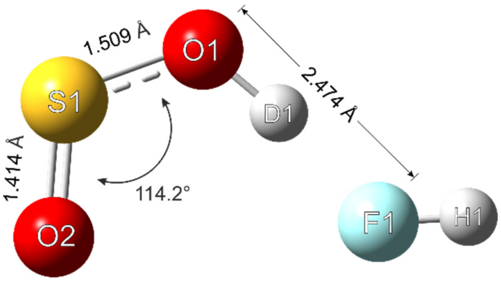

Figure S7. Calculated gas-phase structure of the $[OSOD \cdot HF]^+$ cation.

4. Vibrational Data

Table S3 lists all observed frequencies of $[(SO_2)_2H][Sb_2F_{11}]$ (**1**) and $[(SO_2)_2D][Sb_2F_{11}]$ (**2**), and frequencies of the calculated cations $(SO_2)_2X^+$. Table S4 lists all observed frequencies of $[OSOD][Sb_2F_{11}]$ (**3**) and frequencies of the calculated cation $[OSOD \cdot HF]^+$. For the $[OSOD \cdot HF]^+$ cation the vibrational modes, which are associated with the added HF molecule, are omitted in the list for clarification.

Hemiprotonation

The $(SO_2)_2H^+$ cation possesses $C2_h$ symmetry. For the cation 15 fundamental vibrations ($5A_g + 1B_g + 3A_u + 6B_u$) are expected, as well as rule of mutual exclusion. Therefore, six Raman active vibrations and nine IR-active vibrations are expected. Apart from the observed vibrations, that are discussed in the main paper, six vibrations are observed that are assigned to the $Sb_2F_{11}^-$ anion. In the crystal structure, the $Sb_2F_{11}^-$ anion possesses ideal D_{4h}-symmetry, which is confirmed by the Raman spectra of (**1**) and (**2**). This structure is rare for the $Sb_2F_{11}^-$ anion since the fluorine bridge angle is deformable and highly dependent on the crystal packing.[10,11] However, several examples of crystal structures with D_{4h} $Sb_2F_{11}^-$ anions have been reported[12]. The observed vibrational frequencies in this work agree with vibrations overserved in Raman spectra of $[Au(CO)_2][Sb_2F_{11}]$ and $[Rh(CO)_4][Sb_2F_{11}]$.[10,13,14] The observed frequencies, which are assigned to $[OD_nH_{3-n}][SbF_6]$ stem from contamination with water. For **1** the O−H vibrations are not observed in the Raman spectrum due to their poor polarizability. For **2** water contaminations result in the formation of $[OD_nH_{3-n}][SbF_6]$. The ν(O−D) vibrations of deuterated H_3O^+ are observed in the Raman spectrum at 2292 cm^{-1}.[15]

Table S3. Experimental vibrational frequencies [cm^{-1}] of $[(SO_2)_2X][Sb_2F_{11}]$ (X = H, D) (**1, 2**) and calculated vibrational frequencies [cm^{-1}] of $(SO_2)_2X^+$.

$[(SO_2)_2H][Sb_2F_{11}]$	$[(SO_2)_2D][Sb_2F_{11}]$	$(SO_2)_2H^+$ calc.[a,b]	$(SO_2)_2D^+$ calc.[a,b]	Assignment		
exp. Raman	exp. Raman	IR/Raman	IR/Raman			
	2292(5)					$[OD_nH_{3-n}][SbF_6]$[15]
		1389(351/0)	1362(225/0)	ν_{10}	B_u	$\nu_{as}(SO)$
1333(32)	1333(20)	1358(0/26)	1358(0/26)	ν_1	A_g	$\nu_s(SO)$
		1253(47/0)	924(112/0)	ν_{11}	B_u	$\nu(O\cdots X\cdots O)$[c]
1129(25)	1128(16)	1160(0/48)	1160(0/48)	ν_2	A_g	$\nu_s(SO)$
		1140(86/0)	1102(125/0)	ν_{12}	B_u	$\nu_{as}(SO)$
		1125(115/0)	814(64/0)	ν_7	A_u	$\delta(O\cdots X\cdots O)$[c]
566(7)	566(6)	589(0/6)	589(0/6)	ν_3	A_g	δ(OSO)
		571(7481/0)	422(3724/0)	ν_{13}	B_u	$\delta(O\cdots X\cdots O)$[c]
		493(176/0)	488(517/0)	ν_{14}	B_u	δ(OSO)
365(3)	368(4)	409(0/4)	409(0/4)	ν_4	A_g	$\nu(O\cdots X\cdots O)$[c]
238(14)	238(14)	189(0/1)	189(0/1)	ν_6	B_g	δ(SOH)
		121(21/0)	119(21/0)	ν_8	A_u	$\delta(O\cdots X\cdots O)$[c]
		83(0/1)	83(0/1)	ν_5	A_g	$\delta(SOX)$
		38(49/0)	37(48/0)	ν_{15}	B_u	$\delta(SOX)$
		31(1/0)	30(1/0)	ν_9	A_u	skeletal torsion
Vibrations of the anion $Sb_2F_{11}^-$ (D_{4h})[10,13,14] and the contamination $[OD_nH_{3-n}][SbF_6]$ [15]						
698(8)	698(9)					$Sb_2F_{11}^-$
688(79)	689(73)					$Sb_2F_{11}^-$
671(21)	672(27)					$[OD_nH_{3-n}][SbF_6]$ [15]
648(100)	649(100)					$Sb_2F_{11}^-$
638(11)	639(14)					$[OD_nH_{3-n}][SbF_6]$ [15]
594(19)	594(20)					$Sb_2F_{11}^-$
301(20)	301(21)					$Sb_2F_{11}^-$
283(10)	281(15)					$[OD_nH_{3-n}][SbF_6]$ [15]
264(6)	264(7)					$Sb_2F_{11}^-$

[a] Calculated on the M06-2X/aug-cc-pVTZ level of theory. Scaling factor: 0.956. [b] IR intensities in km/mol; Raman intensities in Å^4/u. [c] X = H, D.

Monoprotonation

The $[OSOD]^+$ cation possesses C_s symmetry. For the cation 6 fundamental vibrations (5*A′* + 1*A″*) are expected, of which all are Raman and IR-active.

Table S4. Experimental vibrational frequencies [cm^{-1}] of $[OSOD][Sb_2F_{11}]$ (**3**) and calculated vibrational frequencies [cm^{-1}] of $[OSOD \cdot HF]^+$.

$[OSOD][Sb_2F_{11}]$ exp. Raman	$[OSOD \cdot HF]^+$ calc.[a,b] IR/Raman	Assignment		
2284(13)	1823(1418/43)	ν_1	*A′*	ν(OD)
1338(35)	1362(121/17)	ν_2	*A′*	ν(SO)
1197(2)				?
1033(49)	1047(99/18)	ν_3	*A′*	ν(SO)
	864(84/0)	ν_4	*A′*	δ(SOD)
	641(65/0)	ν_6	*A″*	δ(SOD)
591(15)	521(41/3)	ν_5	*A′*	δ(OSO)
Vibrations of the anion $Sb_2F_{11}^-$ and the contamination $[OD_nH_{3-n}][SbF_6]$ [15]				
702(10)				$Sb_2F_{11}^-$
690(29)				$Sb_2F_{11}^-$
684(95)				$Sb_2F_{11}^-$
671(100)				$[OD_nH_{3-n}][SbF_6]$ [15]
657(91)				$Sb_2F_{11}^-$
640(40)				$[OD_nH_{3-n}][SbF_6]$ [15]
610(7)				$Sb_2F_{11}^-$
577(6)				$Sb_2F_{11}^-$
555(13)				$Sb_2F_{11}^-$
495(3)				$Sb_2F_{11}^-$
469(6)				$Sb_2F_{11}^-$
307(35)				$Sb_2F_{11}^-$
280(41)				$[OD_nH_{3-n}][SbF_6]$ [15]
266(9)				$Sb_2F_{11}^-$
234(15)				$Sb_2F_{11}^-$
204(3)				$Sb_2F_{11}^-$

[a] Calculated on the M06-2X/aug-cc-pVTZ level of theory. Scaling factor: 0.956. [b] IR intensities in km/mol; Raman intensities in Å^4/u.

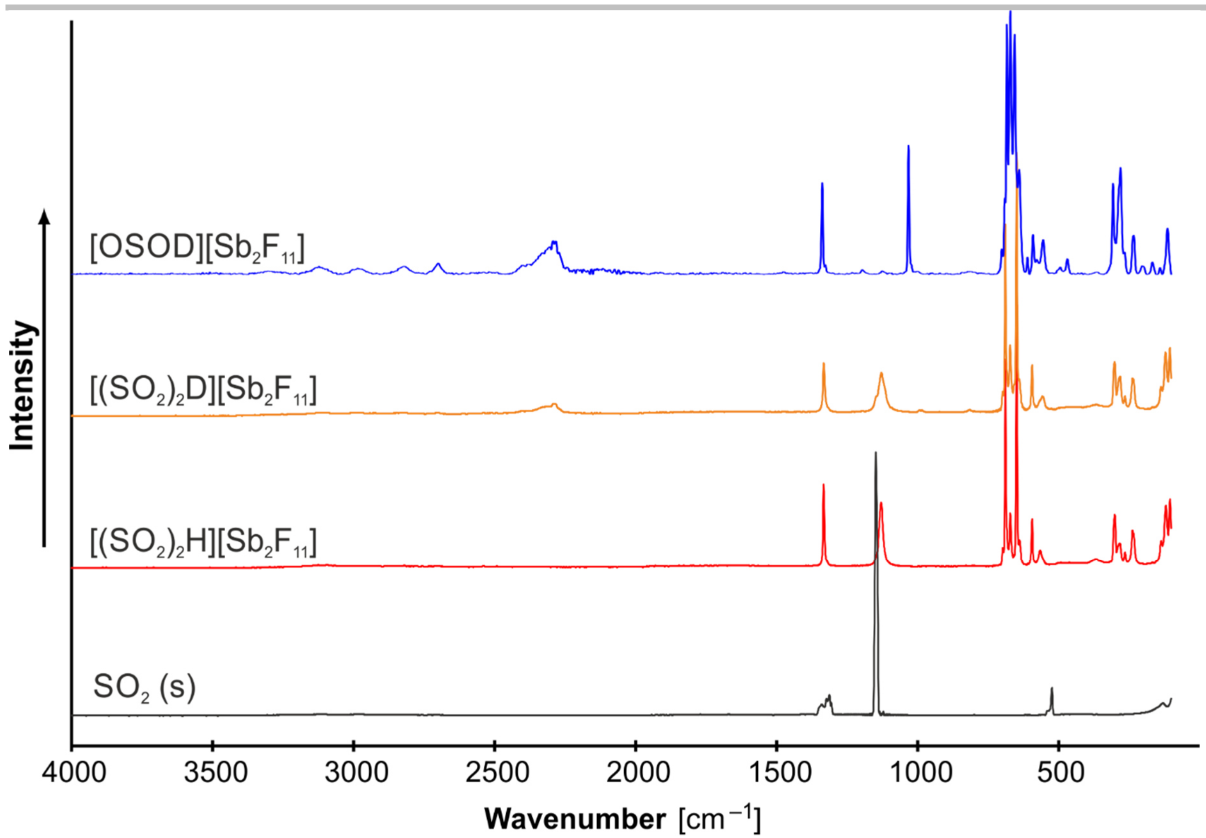

Figure S8. Low-temperature Raman spectra of **1**, **2**, **3** and solid amorphous sulfur dioxide.

5. References

[1] Rigaku Oxford Diffraction, CrysAlisPro Software System, *Version 1.171.38.46*, Rigaku Corporation,Oxford, UK, **2015**.

[2] G. M. Sheldrick, *Acta crystallographica. Section A, Foundations and advances* **2015**, *71*, 3.

[3] G. M. Sheldrick, *Acta crystallographica. Section C, Structural chemistry* **2015**, *71*, 3.

[4] L. J. Farrugia, *J. Appl. Crystallogr.* **1999**, *32*, 837.

[5] A. L. Spek, *J. Appl. Crystallogr.* **2003**, *36*, 7.

[6] *SCALE3 ABSPACK, An Oxford Diffraction Program*, Oxford Diffraction Ltd, UK, **2005**.

[7] M. J. Frisch, G. W. Trucks, H. B. Schlegel, G. E. Scuseria, M. A. Robb, J. R. Cheeseman, G. Scalmani, V. Barone, B. Mennucci, G. A. Petersson, H. Nakatsuji, M. Caricato, X. Li, H. P. Hratchian, A. F. Izmaylov, J. Bloino, G. Zheng, J. L. Sonnenberg, M. Hada, M. Ehara, K. Toyota, R. Fukuda, J. Hasegawa, M. Ishida, T. Nakajima, Y. Honda, O. Kitao, H. Nakai, T. Vreven, J. A. Montgomery, J. E. Peralta, F. Ogliaro, M. Bearpark, J. J. Heyd, E. Brothers, K. N. Kudin, V. N. Staroverov, R. Kobayashi, J. Normand, K. Raghavachari, A. Rendell, J. C. Burant, S. S. Iyengar, J. Tomasi, M. Cossi, N. Rega, J. M. Millam, M. Klene, J. E. Knox, J. B. Cross, V. Bakken, C. Adamo, J. Jaramillo, R. Gomperts, R. E. Stratmann, O. Yazyev, A. J. Austin, R. Cammi, C. Pomelli, J. W. Ochterski, R. L. Martin, K. Morokuma, V. G. Zakrzewski, G. A. Voth, P. Salvador, J. J. Dannenberg, S. Dapprich, A. D. Daniels, O. Farkas, J. B. Foresman, J. V. Ortiz, J. Cioslowski, D. J. Fox, *Gaussian09, Revision A.02*, Gaussian, Inc, Wallingford CT, **2009**.

[8] A. Kornath, R. Seelbinder, R. Minkwitz, *Angew. Chem. Int. Ed. Engl.* **2005**, *44*, 973.

[9] a) S.K. Wolff, D.J. Grimwood, J.J. McKinnon, M.J. Turner, D. Jayatilaka, M.A. Spackman, *CrystalExplorer 17.5, Revision: f4e298a*, University of Western Australia, **2017**; b) M. A. Spackman, D. Jayatilaka, *CrystEngComm* **2009**, *11*, 19.

[10] I. H. Sham, B. O. Patrick, B. von Ahsen, S. von Ahsen, H. Willner, R. C. Thompson, F. Aubke, *Solid State Sci.* **2002**, *4*, 1457.

[11] J. F. Lehmann, G. J. Schrobilgen, K. O. Christe, A. Kornath, R. J. Suontamo, *Inorg. Chem.* **2004**, *43*, 6905.

[12] a) D. Mootz, K. Bartmann, *Angew. Chem. Int. Ed. Engl.* **1988**, *27*, 391; b) H. Willner, F. Aubke, *Chem. Eur. J.* **2003**, *9*, 1668.

[13] B. von Ahsen, C. Bach, M. Berkei, M. Köckerling, H. Willner, G. Hägele, F. Aubke, *Inorg. Chem.* **2003**, *42*, 3801.

[14] H. Willner, J. Schaebs, G. Hwang, F. Mistry, R. Jones, J. Trotter, F. Aubke, *J. Am. Chem. Soc.* **1992**, *114*, 8972.

[15] K. O. Christe, P. Charpin, E. Soulie, R. Bougon, J. Fawcett, D. R. Russell, *Inorg. Chem.* **1984**, *23*, 3756.

Characterization of Two Cationic Siblings: The Fluorodihydroxy- and Difluorohydroxysulfonium Cations Are Put to the Acid Test

Christoph Jessen,[a] Hannah Illner[a], Florian Zischka[a], Alexander Nitzer[a], Alan Virmani[a] and Andreas J. Kornath*[a]

[a] C. Jessen, H. Illner, F. Zischka, A. Nitzer, A. Virmani, Prof. Dr. A. J. Kornath
Department Chemie
Ludwig-Maximilians-Universität München
Butenandtstr. 5–13, 81377 München, Germany
E-mail: andreas.kornath@cup.uni-muenchen.de

Supporting information for this article is given via a link at the end of the document.

Abstract: Reacting sulfur dioxide or trifluoromethanesulfonyl fluoride with the binary superacids HF/MF_5 leads to the formation of $[FS(OH)_2][MF_6]$ (X = H, D; M = As, Sb). The isolation of the pure salts allowed a detailed vibrational characterization by low-temperature infrared and Raman spectroscopy. An NMR spectroscopic investigation of the reaction of the complex $SO_2{\cdot}SbF_5$ in anhydrous hydrogen fluoride (aHF) revealed a stepwise addition of HF. The intermediate complex $FS(OH)O{\cdot}SbF_5$ was observed by ^{1}H- and ^{19}F-NMR spectroscopy. The reaction of $FS(OH)O{\cdot}SbF_5$ with HF was transferred to the isoelectronic complex $SOF_2{\cdot}SbF_5$. By reacting $SOF_2{\cdot}SbF_5$ with stoichiometric amounts of HF in 1,1,1,2-tetrafluoroethane (R134a), mono- and hemiprotonated thionyl fluoride was obtained as mixed salt $[SOF_2H][(SOF_2)_2H][Sb_2F_{11}]_2$. The salt was characterized by low-temperature IR and Raman spectroscopy as well as single-crystal X-ray structure analysis. Furthermore, the crystal structure of $SOF_2{\cdot}SbF_5$ was determined. Dissolving the salt $[SOF_2H][(SOF_2)_2H][Sb_2F_{11}]_2$ in SO_2 leads to the protonation of the solvent to afford hemiprotonated SO_2 $[(SO_2)_2H][Sb_2F_{11}]$. The results raise the question of whether the popular superacid solvent SO_2 is not protonated in HF/SbF_5 and whether SO_2H^+ reacts with HF to form $FS(OH)_2^+$. This question is addressed by quantum chemical calculations on the electrophilicity of the sulfur atom in $SO_2{\cdot}$LA (Lewis acid) complexes.

Introduction

Many sulfur oxo compounds and their fluorinated derivatives are known for their low basicity. This characteristic makes compounds such as SO_2, SOF_2, SO_2ClF, SO_2F_2, or CH_3SO_2F suitable for use under highly acidic reaction conditions. Especially SO_2 and SO_2ClF were used as solvents for reactions in superacid media and investigation of carbocations by Olah and co-workers.[1] The basicity of these compounds towards strong Lewis acids has been thoroughly investigated.[2,3–7] The order of decreasing basicity toward AsF_5 and SbF_5 is $CH_3SO_2F > SO_2 > SOF_2 > SO_2ClF > SO_2F_2$.[6,7] For SO_2, SOF_2, SO_2ClF methylation[8] and for SO_2 even protonation is reported.[9] Another compound of interest in this regard is trifluoromethanesulfonyl fluoride, which is the acid fluoride of the Brønsted superacid CF_3SO_3H. The protonation of the superacids CF_3SO_3H and FSO_3H was achieved in the stronger superacidic system HF/SbF_5.[10] This gave rise to the question if a protonation of CF_3SO_2F is possible in HF/SbF_5.

Experimental

In the attempt to protonate CF_3SO_2F in HF/MF_5 (M = As, Sb), MF_6^--salts of the fluorodihydroxysulfonium cation ($FS(OH)_2^+$) were obtained instead.[11] As reported CF_3SO_2F is catalytically decomposed by SbF_5 and leads to the release of CF_4 and SO_2 (Equation (1)).[12] When the reaction is performed in aHF the released SO_2 then reacts with HF/MF_5 to form the colorless salts $[FS(OH)_2][MF_6]$ which were obtained after the removal of excess *aHF* and CF_4 (Equation (3)). The reaction of SO_2 in the superacidic system HF/SbF_5 was already performed in sapphire reactors by *Kornath et al.* (Equation (2)).[11] In previous work, (*Synthesis and Structure of Protonated Sulfur Dioxide* (C. Jessen, A. J. Kornath, work in preparation)), we have shown that performing this reaction in FEP reactors significantly eased the handling of the highly temperature-sensitive $[FS(OH)_2][MF_6]$ salts. This allows the isolation of amounts of $[FS(OH)_2][MF_6]$, suitable for Raman and infrared spectroscopic measurements of the pure compound, as well as NMR spectroscopy in *aHF* for detailed characterization of the compound. It also motivated us to elucidate the reaction path of SO_2 to $FS(OH)_2^+$.

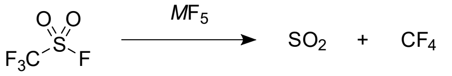

(1)

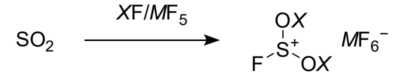

(2)

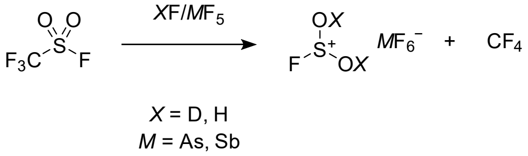

(3)

Formation of the cation $FS(OH)_2^+$

SO_2 or CF_3SO_2F reacted with the binary superacidic systems HF/MF_5 (M = As, Sb) according to Equation (2) and Equation (3). The reactions were carried out between –60 °C to 20 °C by mixing the components to complete dissolution. Cooling the solutions to −78 °C resulted in the precipitation of crystalline colorless solids, as reported in the literature.[11] The solvent and volatile residues were removed overnight at −78 °C *in vacuo* to afford

$[FS(OH)_2][MF_6]$ (**1**, **2**) as colorless solids. The deuterated salts $[FS(OD)_2][MF_6]$ (**3**, **4**) were obtained by changing the solvent and reactant from aHF to aDF (Equation (2), (3)). Additionally, we were interested to see if the reaction would also proceed with weaker Lewis acids such as BF_3 or GeF_4 to form $[FS(OH)_2][BF_4]$ or $[FS(OH)_2]_2[GeF_6]$. However, the mixtures were completely removed in the dynamic vacuum at −78 °C without affording any solid products.

From Equation (2) it is not obvious how the reaction of the starting materials to $[FS(OH)_2][MF_6]$ proceeds. As the crucial step for the reaction, *Kornath et al* reported the formation of the adduct $SO_2{\cdot}SbF_5$ with the subsequent addition of HF (Scheme 1; (Equation (4), (5)).[11] Protonation in the excess superacid leads to the final compound as shown in Equation (6).[11]

$$SO_2 + 2\,HF + SbF_5 \xrightarrow{-90\ °C} [H_2F]^+[SbF_6]^- + SO_2 \qquad (4)$$

$$[H_2F]^+[SbF_6]^- + SO_2 \xrightarrow{-25\ °C} SO_2SbF_5 + 2\,HF \qquad (5)$$

$$SO_2SbF_5 + 2\,HF \rightleftharpoons [FS(OH)_2]^+[SbF_6]^- \qquad (6)$$

Scheme 1. Formation of $[FS(OH)_2][SbF_6]$ as reported by *Kornath et al*.[11]

To elucidate the reaction of $SO_2{\cdot}SbF_5$ with HF, NMR spectroscopy was conducted. The adduct $SO_2{\cdot}SbF_5$ was prepared as described in the literature.[3,4] A standard NMR glass tube was equipped with a sealed 4 mm FEP-inliner containing $SO_2{\cdot}SbF_5$ and aHF. The reactants were kept separated in the NMR tube at −196 °C until immediately before the NMR measurement at −70 °C. The reaction was observed by ^{1}H- and ^{19}F-NMR spectroscopy by warming the mixture from −70 °C to ambient temperatures in steps of 10 °C. A detailed description of this experiment is found in the Supporting Information. Figure 1 shows a stack of the measured ^{19}F-NMR spectra from −70 °C to 25 °C. The stack of the complete spectra is shown in Figure S10 and the observed ^{1}H- and ^{19}F-shifts are listed in Table S8. In the ^{1}H NMR spectra, only one signal is observed between 10.10 ppm and 10.16 ppm (Figure S9). In the ^{19}F NMR spectra, two different signals are observed, which are assigned to the reaction product $[FS(OH)_2][SbF_6]$ (**1**) and the intermediate complex $FS(OH)O{\cdot}SbF_5$ (**5**).

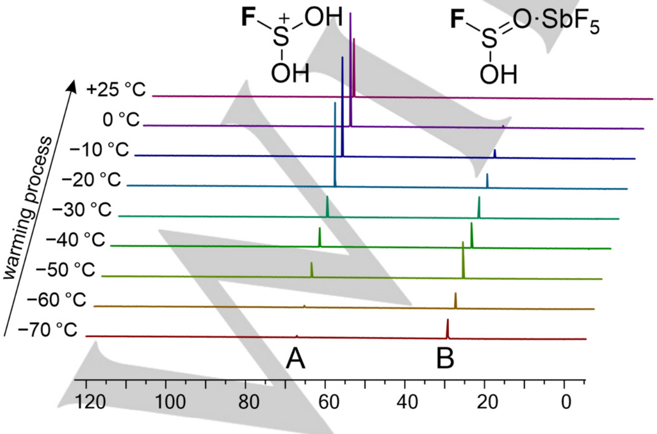

Figure 1. 19F-NMR spectra of the reaction of SO2·SbF5 in aHF from −70 °C to 25 °C.

For the first measurement at −70 °C, one signal is observed at 29.20 ppm (**B**), with traces of a second signal (**A**) at 67.10 ppm. With increasing temperature, signal **A** increases and signal **B** decreases until at ambient temperatures only signal **A** is observed at 69.51 ppm. The assignment of signal **A** was done by repeating the reaction in an FEP reactor up to ambient temperatures and subsequently removing all volatile components at −78 °C on a vacuum line. The resulting solid was identified as $[FS(OH)_2][SbF_6]$ (**1**) by Raman spectroscopy, which will be discussed later. Interestingly, the $FS(OH)_2^+$ cation exhibits surprisingly high thermal stability in aHF solution, in contrast to the thermally labile $[FS(OH)_2][MF_6]$ solids, which decompose at around −70°C. The NMR measurement was repeated for $[FS(OH)_2][SbF_6]$ at ambient temperatures and higher concentrations and the respective spectra are shown in Figure S12. For the second species that is observed in the ^{19}F-NMR spectra between 29.20 ppm and 29.78 ppm (**B**) from −70 °C to 0 °C, two options were considered. The first option considered was free fluorosulfinic acid (FSOOH). However, besides being bound in fluorosulfite esters,[13] molecular fluorosulfinic acid has not been observed to our knowledge.[14] To exclude FSOOH as an option for signal **B**, another NMR measurement as described before was employed with freshly prepared $[Cs][FSO_2]$[14,15] in aHF. ^{19}F NMR spectra of the solution were measured at −70 °C, −40 °C, and 0 °C. Except for the solvent signal (HF), no other ^{19}F signal is observable in the NMR spectra at those temperatures, as shown in Figure S14.[16] This leads to the conclusion that the fluorosulfite anion (FSO_2^-) is protonated by HF and the formed FSOOH immediately decomposes to HF and SO_2 (Equation (7)). Therefore, we can exclude that signal **B** derives from free fluorosulfinic acid.

$$[Cs][FSO_2] \overset{HF}{\rightleftharpoons} CsF + [FSOOH]^{\ddagger} \longrightarrow CsF + HF + SO_2 \qquad (7)$$

The other option considered for the ^{19}F signal **B** is the complex $FS(OH)O{\cdot}SbF_5$. This compound is the formal product of the addition of one HF molecule to the adduct $SO_2{\cdot}SbF_5$. *Olah et al.* observed a comparable complex $FS(OMe)O{\cdot}SbF_5$ when reacting methyl fluorosulfite with SbF_5 in SO_2.[17] The ^{19}F NMR spectrum of $FS(OMe)O{\cdot}SbF_5$ showed a ^{19}F NMR signal at 28.1 ppm in SO_2.[17] From these results, we extend Equation (6) by an additional step which was already considered by *Kornath et al.* (Equation (8)).[11]

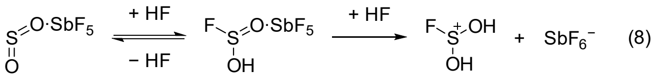

$$O{=}S{=}O{\cdot}SbF_5 \underset{-\,HF}{\overset{+\,HF}{\rightleftharpoons}} FS(OH){=}O{\cdot}SbF_5 \xrightarrow{+\,HF} [FS(OH)_2]^+ + SbF_6^- \qquad (8)$$

Attempting to isolate the complex $FS(OH)O{\cdot}SbF_5$ (**5**) from the solvents HF, SO_2, or 1,1,1,2-tetrafluoroethane (R134a) at temperatures from −85 °C to −40 °C was unsuccessful. After all attempts, the obtained solids were identified as $SO_2{\cdot}SbF_5$, $[FS(OH)_2][SbF_6]$, or mixtures of both by Raman spectroscopy. However, a quantum chemical calculation of the complex on the MP2/aug-cc-pVTZ level of theory afforded three minimum energy structures. The structures are shown in the theoretical section of the Supporting Information (Figure S15). The intermediate species $FS(OH)O{\cdot}SbF_5$ fills the gap in the reaction pathway shown in Equation (8). However, to understand the reaction of SO_2 with HF/MF_5 forming $FS(OH)_2^+$ in detail, the last reaction step (Equation 8) needs further investigation. Either a protonation of the FS(OH)O-moiety by the excess superacid as reported[11] or a direct cleavage of the O−Sb bond by HF is plausible. Since the isolation of the $FS(OH)O\cdot SbF_5$ complex was unsuccessful, a comparable compound was needed to further investigate this last reaction step.

Formation of protonated thionyl fluoride

We decided to transfer the reaction to the isoelectronic adduct $SOF_2\cdot SbF_5$ which is an isolatable solid.[5] It is described that $SOF_2\cdot SbF_5$ is not stable when dissolved in HF and reacts with the release of SOF_2.[18] To verify this, freshly prepared $SOF_2\cdot SbF_5$[3,19] was reacted in aHF at −78°C. After removing the solvent and volatile residues *in vacuo* at −78 °C, a colorless solid was obtained (Equation (9), Scheme 2). The solid was identified as a fluoronium salt ($[H_{n+1}F_n][Sb_2F_{11}]$) by Raman spectroscopy with no evidence of a remaining SOF_2 species.[20] This suggests that SOF_2 is protonated in the binary superacid HF/SbF_5 to yield "$[SOF_2H][SbF_6]$". Or at least the low basicity of SOF_2 allows an equilibrium in aHF where SOF_2 is not fully protonated (Equation (10)). Since SOF_2 has an even lower proton affinity than SO_2 (SOF_2: 659.8 kJ/mol[21], SO_2: 672.3 kJ/mol[22]) this result is not surprising.

$$2\,SOF_2\cdot SbF_5 \xrightarrow[-78\ ^\circ C]{aHF} [H_{n+1}F_n][Sb_2F_{11}] + 2\,SOF_2\uparrow \qquad (9)$$

$$[H_{n+1}F_n][Sb_2F_{11}] + SOF_2 \xrightleftharpoons{aHF} [SOF_2H][Sb_2F_{11}] + n\,HF \qquad (10)$$

Scheme 2. The reaction of SbF_5/SOF_2 in aHF based on the observed products.

The reaction was repeated using R-134a as the solvent to exclude any influence of the solvent aHF and explicitly investigate the reaction of stoichiometric amounts of $SOF_2\cdot SbF_5$ with HF. In an FEP reactor, SbF_5 and SOF_2 were mixed in R-134a at −40 °C to a complete solution to form $SOF_2\cdot SbF_5$. The mixture was frozen at −196 °C and stoichiometric amounts of HF (respective to SOF_2) were condensed into the reactor. The components were thoroughly mixed at −70 °C, and precipitation of a colorless solid was observed. After removing the solvent and volatile residues *in vacuo* at −78 °C, a colorless solid was obtained. The product was identified as a mixed salt of mono- and hemiprotonated thionyl fluoride with the counter anion $Sb_2F_{11}^-$ ($[SOF_2H][(SOF_2)_2H][Sb_2F_{11}]_2$ (**6**)). The reactions in the solvent R-134a are summarized in Scheme 3.

$$SOF_2\cdot SbF_5 + SbF_5 + HF \xrightarrow[-70\ ^\circ C]{R\text{-}134a} [SOF_2H][Sb_2F_{11}] \qquad (11)$$

$$[SOF_2H][Sb_2F_{11}] + SOF_2 \xrightarrow[-70\ ^\circ C]{R\text{-}134a} [(SOF_2)_2H][Sb_2F_{11}] \qquad (12)$$

Scheme 3. The reaction of SbF_5/SOF_2 with HF in R-134a based on the observed products.

When the reaction is performed in aHF the equilibrium shown in Equation (10) seems to be not completely shifted to the right side, due to the low basicity of SOF_2. When the solvent is removed *in vacuo* from the reaction mixture, the more volatile SOF_2 is removed more rapidly as shown in Equation (9). As a result, the equilibrium shifts completely to the left side, leaving the fluoronium salt as the product instead of protonated SOF_2. Changing the solvent from aHF to R-134a affects this equilibrium, allowing the isolation of protonated SOF_2 as described in Equation (11). However, hemiprotonated SOF_2 is also found as a product. Therefore, free SOF_2 is present in the reaction to react with the SOF_2H^+ cation forming $(SOF_2)_2H^+$ (Equation (12)). We conclude that in R-134a solution Equation (10) is still applicable to a certain extent as a source of SOF_2. Unfortunately, these results still do not quite answer the original question of how the complexes $FS(OH)O\cdot SbF_5$ and $SOF_2\cdot SbF_5$ are cleaved by HF to form the protonated species and $Sb_xF_{5x+1}^-$ anions.

Since the basicity of SOF_2 is expected to be lower than that of SO_2 we were interested if SOF_2H^+ would protonate SO_2 in solution. So far, only the solid carborane superacids $H(CHB_{11}Cl_{11})$ and $H(CHB_{11}F_{11})$ are proven to protonate SO_2.[9] Salt **6** was dissolved in SO_2 at −70 °C. Then the solvent and volatile residues were removed *in vacuo* to yield hemiprotonated SO_2 ($[(SO_2)_2H][Sb_2F_{11}]$) as a solid product identified by Raman spectroscopy (*Synthesis and Structure of Protonated Sulfur Dioxide* (C. Jessen, A. J. Kornath, work in preparation)). Therefore, $[SOF_2H][(SOF_2)_2H][Sb_2F_{11}]_2$ (**6**) is acidic enough to protonate SO_2 in solution.

Results and Discussion

Vibrational spectroscopy

$[FS(OX)_2][MF_6]$

Raman spectra of $[FS(OX)_2][SbF_6]$ (X = D, H) were reported by *Kornath et al.* in a sapphire reactor in the presence of the solvent *aHF*.[11] In this work, we succeeded in performing Raman and IR spectroscopic measurements of the pure salts $[FS(OX)_2][MF_6]$ (X = D, H; M = As, Sb). This allowed a detailed vibrational characterization of the $FS(OX)_2^+$ cation. The experimentally observed vibrational frequencies of the $FS(OX)_2^+$ cation together with the theoretical frequencies of the calculated $[FS(OX)_2\cdot 2HF]^+$ cation are listed in Table 1. A list of all observed frequencies in the vibrational spectra of the salts and structural details of the calculated $[FS(OX)_2\cdot 2HF]^+$ cation are found in the Supporting Information. Low-temperature Raman and IR spectra of **1**, **2,** and **3** are depicted in Figure 2. The $FS(OX)_2^+$ cation possesses C_s symmetry. Twelve fundamental vibrations are expected for the cation, all of which exhibit infrared and Raman activity. The vibrational modes were assigned by comparison with the calculated frequencies of $[FS(OX)_2\cdot 2HF]^+$ and the assignment from the literature.[11] The OX stretching vibrations are best observed in the deuterated compounds **3** and **4** as broad bands in the IR spectra at 2160 cm^{-1}, 2220 cm^{-1}, and broad lines in the Raman spectra at 2222 cm^{-1}, 2264 cm^{-1}, respectively. The SOH deformation vibrations of **1** and **2** are only observed in the IR spectra between 1190 cm^{-1} and 1138 $^{cm-1}$. In contrast, the δ(SOD) vibrations are also observed in the Raman spectra redshifted to 892 cm^{-1} (**3**) and 890 cm^{-1} (**4**), respectively. The most characteristic in the vibrational spectra are the SO and SF stretching vibrations. The symmetrical and antisymmetrical v(SO) vibrations are observed as intense lines and bands in all spectra between 1001 cm^{-1} and 965 cm^{-1}. In the literature the SO stretching vibrations were assigned to Raman lines observed between 1273 cm^{-1} and 910 cm^{-1}.[11] Considering that these spectra were measured in the presence of the solvent, it is plausible that the additional SO stretching vibrations in these spectra can be assigned to the $FS(OH)O\cdot SbF_5$ complex or protonated SO_2 species (*Synthesis and Structure of Protonated Sulfur Dioxide* (C. Jessen, A. J. Kornath, work in preparation)). The SF stretching mode is observed in all spectra from 828 cm^{-1} to 824 cm^{-1} (**1**, **2**) and from 816 cm^{-1} to 812 cm^{-1} (**3**, **4**). The bands and lines at lower frequencies are assigned to the remaining deformation vibrations (Table 1). The SbF_6^- and AsF_6^- anions exhibit more than the five expected vibrations for an ideal O_h symmetry. This indicates that the anions are distorted from the ideal octahedral symmetry which is in accordance with the data from the crystal structure in the literature[11].

$[SOF_2H][(SOF_2)_2H][Sb_2F_{11}]_2$

For protonated thionyl fluoride (**6**) a detailed vibrational characterization was not possible due to the occurrence of the two cations SOF_2H^+ and $(SOF_2)_2H^+$ in the bulk material. However, a comparison with the vibrational spectra of SOF_2 and $SOF_2{\cdot}SbF_5$ and with the calculated vibrational frequencies of the cationic species allowed a tentative assignment. Selected experimental vibrational frequencies of **6** and theoretical vibrational frequencies of the calculated $[SOF_2H \cdot HF]^+$ and $[(SOF_2)_2H]^+$ cations are listed in Table 2. Additional details of the structures of the calculated cations and a list of all observed vibrational frequencies of **6** are found in the Supporting Information. Figure 3 shows the low-temperature vibrational spectra of **6**, $SOF_2{\cdot}SbF_5$, and solid amorphous SOF_2.

The cation of monoprotonated SOF_2 (SOF_2H^+) possesses C_s symmetry. Nine IR and Raman active fundamental vibrations are expected for SOF_2H^+. The calculated gas-phase structure of $[(SOF_2)_2H]^+$ possesses C_{2h} symmetry. For the cation 21 fundamental vibrations are expected, of which 13 are IR active and eight are Raman active, due to the rule of mutual exclusion. However, in the crystal structure, the symmetry of $(SOF_2)_2H^+$ is reduced to C_2 as described later. With C_2 symmetry, all 21 fundamental vibrations are expected to be Raman and IR active.

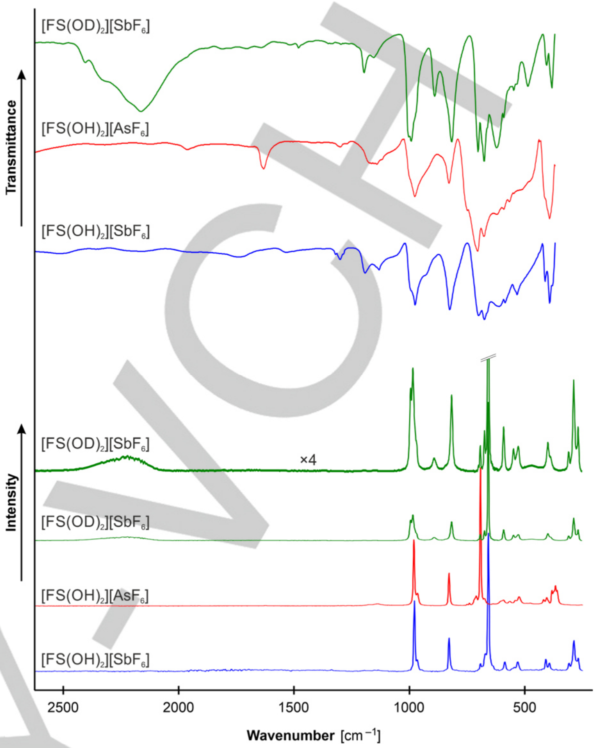

Figure 2. Low-temperature IR and Raman spectra of $[FS(OX)_2][MF_6]$ (X = H, D; M = As, Sb). The upper spectrum of $[FS(OD)_2][SbF_6]$ (**3**) is expanded fourfold for visualization.

Table 1. Experimental vibrational frequencies [cm^{-1}] of the $FS(OX)_2^+$ cation in $[FS(OX)_2][MF_6]$ (X = H, D; M = As, Sb) and calculated vibrational frequencies [cm^{-1}] of $[FS(OX)_2 \cdot 2HF]^+$.

$[FS(OH)_2][SbF_6]$ (**1**), experimental[a]		$[FS(OH)_2][AsF_6]$ (**2**), experimental[a]		$[FS(OH)_2 \cdot 2HF]^+$ calc.[b], [c]	$[FS(OD)_2][SbF_6]$ (**3**), experimental[a]		$[FS(OD)_2][AsF_6]$ (**4**), experimental[a]		$[FS(OD)_2 \cdot 2HF]^+$ calc.[b], [c]	Assignment
IR	Raman	IR	Raman	IR/Raman	IR	Raman	IR	Raman	IR/Raman	
3342(m, br)		3155(s, br)		3185(367/214)	2160(s, br)	2222(3)	2220(m, br)	2264(4)	2329(189/100)	$\nu_s(OX)$
				3143(2947/32)					2291(1499/17)	$\nu_{as}(OX)$
1190(m)		1166(w)		1227(192/0)	887(m)	892(2)	885(m)	890(3)	893(65/4)	$\delta(SOX)$
1128(m)		1138(w)		1187(18/3)	832(sh)	840(1)	834(sh)		860(67/0)	$\delta(SOX)$
990(sh)	979(51)	993(sh)	981(48)	978(255/4)	999(s)	993(15)	1001(sh)	992(21)	994(159/12)	$\nu_s(SO)$
972(s)	966(9)	974(m)	965(9)	973(72/17)	987(s)	983(19)	989(s)	985(27)	986(175/5)	$\nu_{as}(SO)$
824(s)	828(24)	825(m)	828(24)	860(201/7)	812(s)	816(14)	812(s)	814(14)	849(147/9)	$\nu(SF)$
				629(128/0)	482(m)		473(w)		452(47/0)	$\omega(SOX)$
	545(3)	546(m)	541(4)	576(5/0)					426(8/0)	$\omega(SOX)$
530(s)	530(7)		524(7)	527(15/2)	544(m)	548(4)	542(w)	550(6)	510(17/2)	$\omega(FSO_2)$
409(m)	409(9)	410(sh)	418(5)	399(104/1)	401(w)	398(5)	399(m)	395(4)	394(138/1)	$\delta(OSO)$
390(s)	393(6)	390(s)	405(6)	373(24/1)	378(m)	388(4)	370(w)	379(11)	362(26/1)	$\delta(FSO)$

[a] Abbreviations for IR intensities: vs = very strong, s = strong, m = medium, w = weak, sh = shoulder. Experimental Raman intensities are relative to a scale of 1 to 100. [b] Calculated on the M06-2X/aug-cc-pVTZ level of theory. Scaling factor: 0.956. [c] IR intensities in km/mol; Raman intensities in $Å^4$/u.

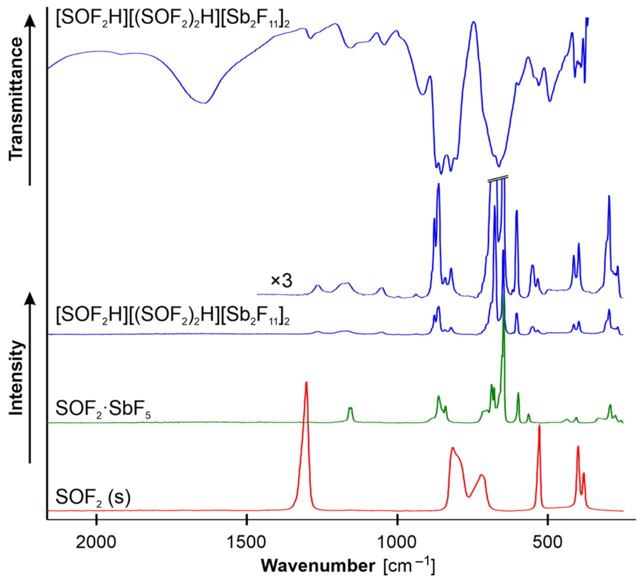

Figure 3. Low-temperature infrared and Raman spectra of **6**, $SOF_2{\cdot}SbF_5$ and solid amorphous SOF_2 (−196 °C). The IR and upper Raman spectrum of **6** are expanded for better visualization.

Table 2. Selected experimental vibrational frequencies [cm^{-1}] of $[SOF_2H][(SOF_2)_2H][Sb_2F_{11}]_2$ (**6**) and calculated vibrational frequencies [cm^{-1}] of $[SOF_2H \cdot HF]^+$ and $[(SOF_2)_2H]^+$.

$[SOF_2H][(SOF_2)_2H][Sb_2F_{11}]_2$ (**6**), experimental[a]		$[SOF_2H \cdot HF]^+$ calc.[b], [c]	$[(SOF_2)_2H]^+$ calc.[b], [c]	Assignment
IR	Raman	IR/Raman	IR/Raman	
1637(w)				ν(O···H···O)
1288(vw)	1266(3)	1218(49/4)	1315(367/0)	δ(SOH)
	1181(3)		1215(322/0)	ν(SO)
1151(vw)	1167(3)		1207(0/23)	
1041(vw)	1050(2)	1060(273/4)		
	938(1)		940(1311/0)	ν(SF)
916(w)		898(75/10)		
870(w)	877(15)	886(218/4)		
854(w)	863(22)		880(0/16)	
	842(4)		850(332/0)	
822(w)	821(6)		845(0/9)	

[a] Abbreviations for IR intensities: w = weak, vw = very weak. Experimental Raman intensities are relative to a scale of 1 to 100. [b] Calculated on the M06-2X/aug-cc-pVTZ level of theory. Scaling factor: 0.956. [c] IR intensities in km/mol; Raman intensities in Å^4/u.

The successful protonation of thionyl fluoride is proven by IR and Raman spectra. The OH stretching vibrations are not observed in the Raman spectrum due to the poor polarizability of the hydroxyl group. In the IR spectrum, a very strong band is observed at 3240 cm^{-1}. However, for this band we cannot exclude OH stretching vibrations of H_2O due to the measurement method.

Another broad band in the IR spectrum is observed at 1637 cm^{-1}. Reed and Stoyanov investigated the IR spectra of proton disolvates (L−H$^+$−L) like $(OEt_2)_2H^+$, $(acetone)_2H^+$, and $(SO_2)_2H^+$.[9,23] The proton disolvates exhibit a characteristic broad band in the respective IR spectra around 1600 cm^{-1}. The observed band at 1637 cm^{-1} agrees well with the disolvates in the literature and is therefore assigned to the ν(O···H$^+$···O) vibration of $(SOF_2)_2H^+$ (**6**). Stronger evidence for the protonation is the redshift of the intense SO stretching vibration compared to the neutral compound SOF_2 (literature value: 1307.5 cm^{-1})[24]. The calculated frequencies for the ν(SO) vibrations of $[(SOF_2)_2H]^+$ and $[SOF_2H \cdot HF]^+$ are between 1215 cm^{-1} and 1060 cm^{-1}. For the experimental frequencies, the lines at 1181 cm^{-1}, 1167 cm^{-1}, 1050 cm^{-1} (Ra), and bands at 1151 cm^{-1}, and 1041 cm^{-1} (IR) agree well with the calculated frequencies. Here, the observed stretching vibrations of hemi- and monoprotonated SO_2 serve as a reference (*Synthesis and Structure of Protonated Sulfur Dioxide* (C. Jessen, A. J. Kornath, work in preparation)). The frequencies of the ν(SO) vibrations of hemiprotonated SO_2 are comparable with the respective Lewis-acid adduct $SO_2{\cdot}SbF_5$, while the ν(SO) (protonated side) of the monoprotonated species is further red-shifted (*Synthesis and Structure of Protonated Sulfur Dioxide* (C. Jessen, A. J. Kornath, work in preparation)). The SO stretching vibration of $SOF_2{\cdot}SbF_5$ is observed at 1159 cm^{-1}.[5] Consequently, for **6** we assign the ν(SO) vibrations of $(SOF_2)_2H^+$ to the frequencies 1181 cm^{-1} (Ra), 1167 cm^{-1} (Ra), and 1151 cm^{-1} (IR), which are comparable to $SOF_2{\cdot}SbF_5$. The ν(SO) vibration of SOF_2H^+ is assigned to the frequencies 1050 cm^{-1} (Ra) and 1041 cm^{-1} (IR). Due to the protonation, the ν(SO) vibration of SOF_2H^+ is blue-shifted by 258 cm^{-1} compared to SOF_2. Based on the calculations, the ν(SF) vibrations are expected to be observed between 940 cm^{-1} and 845 cm^{-1}. The vibrational spectra of **6** show several lines and bands in this region. Compared with the neutral compound SOF_2 (ν(SF): 804 cm^{-1}, 716 cm^{-1})[24] the stretching vibrations of **6** are blue-shifted and agree very well with the ν(SF) vibrations of $SOF_2{\cdot}SbF_5$ (857 cm^{-1}, 820 cm^{-1})[5]. The ν(SF) vibrations are also comparable with the respective vibrations of the isoelectronic cations $FS(OH)_2{}^+$ and $SF_3{}^+$. The reported ν(SF) vibrations of the $SF_3{}^+$ cation are observed between 964 cm^{-1} and 910 cm^{-1} in the salts $[SF_3][BF_3]$, $[SF_3][PF_6]$, $[SF_3][AsF_6]$ and $[SF_3][SbF_6]$.[25]

Crystal structures

From the earlier described reactions suitable crystals were obtained for single crystal X-ray structure analysis for the compounds $[FS(OH)_2][SbF_6]$ (**1**), $[SOF_2H][(SOF_2)_2H][Sb_2F_{11}]_2$ (**6**) and $SOF_2{\cdot}SbF_5$ (**7**). The bond lengths and angles of the cations and the SOF_2 moiety are summarized in Table 3 together with selected compounds from the literature. A complete list of the observed geometric parameters is given in the Supporting Information.

$[FS(OH)_2][SbF_6]$

The reported structure[11] of **1** is confirmed by the data from this work. The asymmetric unit is shown in Figure 4. As reported **1** crystallizes in the monoclinic space group *P*2(1)/*c* with four formula units per unit cell.[11] However, due to the higher quality of the measured crystal, the estimated standard deviations are lower in the data from this work. This elucidates that the S1−F1 (1.545(2) Å) bond is significantly longer than the S1−O1 (1.525(3) Å) and S1−O2 (1.523(3) Å) bonds, respectively. The positions of the respective atoms, already shown by considering the contacts of the cation in the crystal structure,[11] are hereby confirmed. Additional details on the crystallographic surrounding of the $FS(OH)_2^+$ cation in **1** are discussed in the Supporting Information.

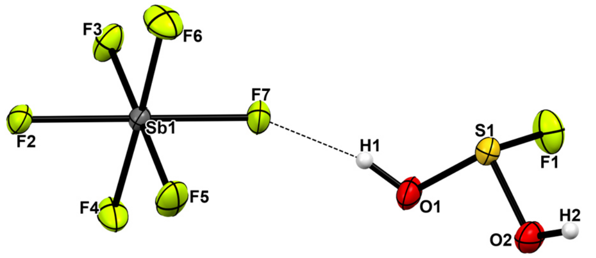

Figure 4. The asymmetric unit of $[FS(OH)_2][SbF_6]$ (**1**) (50% probability displacement ellipsoids).

Table 3. Bond lengths and angles of the cations $FS(OH)_2^+$ (**1**), SOF_2H^+ (**6**), $(SOF_2)_2H^+$ (**6**), the SOF_2 moiety in $SOF_2{\cdot}SbF_5$ (**7**) and $FS(OH)_2^+$, SOF_2, SF_3^+ from the literature. Estimated standard deviations are given in paratheses. Symmetry code: *i* = −x,0.5−y,z; *ii* = C_s; *iii* = x,0.5−y,z.

Cation/moiety	Bond lengths [Å]		Bond angles [°]	
	S−F	S−O	O−S−O/F−S−F	O−S−F
$FS(OH)_2^+$ (**1**)	S1−F1 1.545(2)	S1−O1 1.525(3)	O1−S1−O2 97.3(2)	O1−S1−F1 99.1(1)
		S1−O2 1.523(3)		O2−S1−F1 100.0(2)
$FS(OH)_2^+$ [a] literature[11]	S1−F1 1.547(7)	S1−O1 1.537(7)	O1−S1−O2 98.6(4)	O1−S1−F1 99.0(4)
		S1−O2 1.522(8)		O2−S1−F1 100.1(4)
SOF_2H^+ (**6**)	S1−F1 1.534(3)	S1−O1 1.484(3)	F1−S1−F2 95.2(2)	O1−S1−F1 103.3(2)
	S1−F2 1.528(3)			O1−S1−F2 104.0(2)
$(SOF_2)_2H^+$ (**6**)	S2−F3 1.542(3)	S2−O2 1.449(3)	F3−S2−F4 93.9(2)	O2−S2−F3 105.3(2)
	S2−F4 1.538(3)			O2−S2−F4 104.3(2)
	S3−F5 1.540(3)	S3−O3 1.458(3)	F5−S3−F6 94.0(2)	O3−S3−F5 104.6(2)
	S3−F6 1.536(4)			O3−S3−F6 103.4(2)
$SOF_2{\cdot}SbF_5$ (**7**)	S1−F1 1.538(3)	S1−O1 1.459(5)	F1−S1−F1*i* 95.4(3)	O1−S1−F1 103.8(2)
SOF_2 [c] literature[26]	S1−F1 1.583(3)	S1−O1 1.420(3)	F1−S1−F1*ii* 92.2(3)	O1−S1−F1 106.2(2)
SF_3^+ [b] literature[27]	S1−F1 1.495(2)		F1−S1−F1*iii* 97.62(7)	
	S1−F1 1.499(2)		F1−S1−F2 97.39(12)	

[a] from $[FS(OH)_2][SbF_6]$[11]. [b] from $[SF_3][BF_4]$[27]. [c] from gas electron diffraction of SOF_2[26].

$[SOF_2H][(SOF_2)_2H][Sb_2F_{11}]_2$

The salt $[SOF_2H][(SOF_2)_2H][Sb_2F_{11}]_2$ (**6**) crystallizes in the triclinic space group $P\bar{1}$ with two formula units per unit cell. Figure 5 shows the asymmetric unit of **6**. The position of the oxygen atoms was solved by consideration of short contacts with surrounding atoms and the distance to the respective sulfur atom. Since one bond length in every cation significantly differs from the two remaining bond lengths, the position of the oxygen atoms became clear. The number and position of the protons were determined by three main factors. First, since there are two $Sb_2F_{11}^-$ anions, the need for two cations is obvious. Second, there are two short interionic contacts O1⋯F17 and O2⋯O3. Third, the S−O bond lengths of the SOF_2 moieties in $[SOF_2H][(SOF_2)_2H][Sb_2F_{11}]_2$ were compared to the geometrical parameters of SOF_2. In the neutral compound, the S−O distance (1.420(3) Å) is significantly shorter compared to the respective bonds in the crystal structure of **6**.[26] This strongly indicates *O*-protonation of the SOF_2 moieties.
In the SOF_2H^+ cation the S1−O1 bond length (1.484(3) Å) is significantly elongated due to the protonation. On the other hand, the S-F bond lengths (1.534(3) Å, 1.528(3) Å) are significantly shortened compared to SOF_2 (1.583(3) Å).[26] The F−S−F bond angle (95.2(2)°) increases by 3.0°, while the O−S−F angles decrease by 2.2° and 2.9°, respectively. The elongation of the S−O bond distance agrees with the results from the vibrational analysis, wherein the SO stretching vibration of the protonated compound was observed redshifted compared to SOF_2. This is also true for the shortened S−F bonds, whose corresponding SF stretching vibrations, are observed blue-shifted in the vibrational spectra of the protonated species. The interionic contacts of the SOF_2H^+ cation are shown in Figure 6. In the crystal the SOF_2H^+ cation is connected to an anion via the strong hydrogen bond O1−H1⋯F17 (2.522(5) Å)[28]. There are three S⋯F contacts from anions towards the S1 atom with distances of 2.719(4) Å, 2.768(4) Å and 2.831(3) Å. The contacts are shorter than the sum of the van-der-Waals (VDW) radii (3.27 Å) and result in an overall distorted octahedral surrounding around the sulfur atom.[29]
The results from the crystal structures allow a comparison of the S−F bond lengths in the cations SF_3^+, SOF_2H^+, and $FS(OH)_2^+$. The relation between these cations is the successive substitution of fluorine atoms by OH groups. The S−F bond length increases appreciably from SF_3^+ to SOF_2H^+ and only slightly from SOF_2H^+ to $FS(OH)_2^+$ (Table 3).

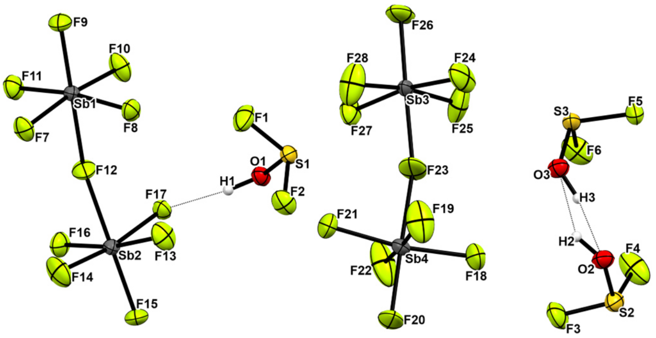

Figure 5. The asymmetric unit of $[SOF_2H][(SOF_2)_2H][Sb_2F_{11}]_2$ (**6**) (50% probability displacement ellipsoids). The protons H2 and H3 have a site occupancy factor of 0.5.

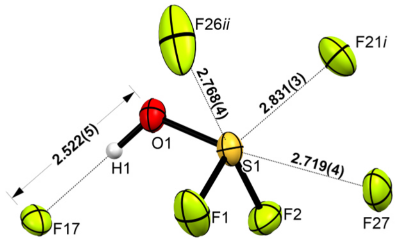

Figure 6. Interionic contacts of SOF_2H^+ (**6**) with 50% probability displacement ellipsoids. The $Sb_2F_{11}^-$ anions are reduced to the contacting fluorine atoms for better visualization. The distances are given in [Å]. Symmetry code: *i* = 1+x,y,z; *ii* = 1−x,1−y,1−z.

For the $(SOF_2)_2H^+$ cation the position of the proton during the refinement was challenging. However, the very short O2···O3 distance (2.437(3) Å) and the need for a second cation are strong indicators of its position. The short O···O distance is characteristic of hemiprotonations and was observed for hemiprotonations of diethyl ether ($[(OEt_2)_2H][CHB_{11}H_5Cl_6]$)[30] or benzaldehyde ($[(benzaldehyde)_2H][SbF_6]$)[31]. Due to the similar S−O bond lengths (S2−O2: 1.449(3) Å and S3−O3: 1.458(3) Å), the refinement as hemiprotonation best describes the structure. Since there was no appreciable electron density peak in the center of the O2···O3 trajectory, the structure was successfully refined with two half-occupied protons. The position of the protons H2 and H3 was chosen from the highest peaks between the oxygen atoms O2 and O3 in the difference electron density map. The refinement with two half-occupied protons gave a better result than the refinement with a 50% disorder of one proton. The position of the proton H2/H3 is not meaningful and was introduced for clarification only.

Within three times the standard uncertainties, the structural parameters of the two hemiprotonated SOF_2 moieties are identical. With this, the cation $(SOF_2)_2H^+$ possesses C_2 symmetry in the crystal structure when the position of the proton is ignored. The S−O bond lengths (1.449(3) Å and 1.458(3) Å) in $(SOF_2)_2H^+$ differ significantly from both the monoprotonation and the neutral compound.[26] They can be described as intermediate between neutral compound and monoprotonation. Interestingly, this is different for the S−F bond lengths of $(SOF_2)_2H^+$, which are comparable to the S−F distances of the monoprotonation but differ significantly from SOF_2. The interionic contacts of the $(SOF_2)_2H^+$ cation are shown in Figure 7. There are three S···F contacts from anions towards the S2 atom with distances of 2.786(3) Å, 2.854(4) Å, 3.218(4) Å, and three S···F contacts from anions towards the S3 atom with distances of 2.765(4) Å, 2.816(3) Å, 2.979(3) Å. Overall, the interionic contacts of the cation $(SOF_2)_2H^+$ are weaker than the interionic contacts of the monoprotonation.

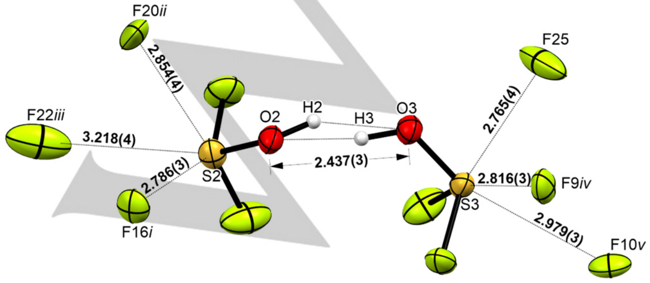

Figure 7. Interionic contacts of $(SOF_2)_2H^+$ (**6**) with 50% probability displacement ellipsoids. The $Sb_2F_{11}^-$ anions are reduced to the contacting fluorine atoms for better visualization. The distances are given in [Å]. Symmetry code: *i* = x,y,−1+z; *ii* = −x,2−y,−z; *iii* = 1−x,2−y,−z; *iv* = −x,1−y,1−z; *v* = 1−x,1−y,1−z.

$SOF_2 \cdot SbF_5$

The complex $SOF_2 \cdot SbF_5$ (**7**) crystallizes in the orthorhombic space group *Pnma* with four formula units per unit cell. The formula unit is shown in Figure 8. The crystals melt at 1 °C in nitrogen atmosphere under atmospheric pressure. The complex $SOF_2 \cdot SbF_5$ possesses C_2 symmetry. The S1−O1 bond length is 1.459(5) Å and compares well with the S−O bond lengths of $(SOF_2)_2H^+$ (**6**). The S−F bond length (1.538(3) Å) is identical to that of hemiprotonated SOF_2. The same is true for the F−S−F and O−S−F bond angles. The complexation with the strong Lewis acid SbF_5 has a similar effect on the SOF_2 moiety as the hemiprotonation (**6**).

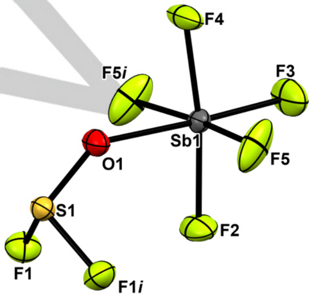

Figure 8. Formula unit of $SOF_2 \cdot SbF_5$ (**7**) (50% probability displacement ellipsoids). Symmetry code: *i* = −x,0.5−y,z.

Theoretical calculations

We successfully synthesized protonated SOF_2 with a mixture of SOF_2, HF, and SbF_5 in R-134a. In turn, SOF_2H^+ protonates SO_2, so it seems unrealistic that SO_2 itself is not protonated by the superacid HF/SbF_5. We recently reported the isolation of the salts of hemi- and monoprotonated SO_2 from recrystallization of $[FS(OH)_2][SbF_6]$ (*Synthesis and Structure of Protonated Sulfur Dioxide* (C. Jessen, A. J. Kornath, work in preparation)). During the recrystallization in SO_2 or R-134a, HF is eliminated from $FS(OH)_2^+$ to form the protonated SO_2 species. It can be assumed that this reaction is reversible in aHF (Equation (13)). Similar to the complex $SO_2 \cdot SbF_5$ which reacts in aHF with the addition of an HF molecule (Equation (8)). This raises the question if SO_2 is in fact protonated by HF/SbF_5 but the formed SO_2H^+ cations further react with the solvent aHF to form $[FS(OH)_2][SbF_6]$.

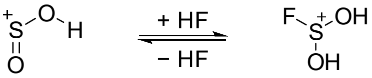

(13)

To better understand why this addition reaction proceeds in aHF, mapped molecular electrostatic potentials (MEP) were calculated for SO_2, $SO_2 \cdot BF_3$, $SO_2 \cdot SbF_5$, and $[SO_2H^+F^-]_{PC}$. Additionally, the Mulliken, ChelpG, and NPA atomic charges were calculated for the SO_2 moiety. All calculations were performed on the M06-2X/aug-cc-pVTZ level of theory. For antimony the effective core potential MWB46 was employed. The calculated structures and their mapped MEPs are shown in Figure 9.

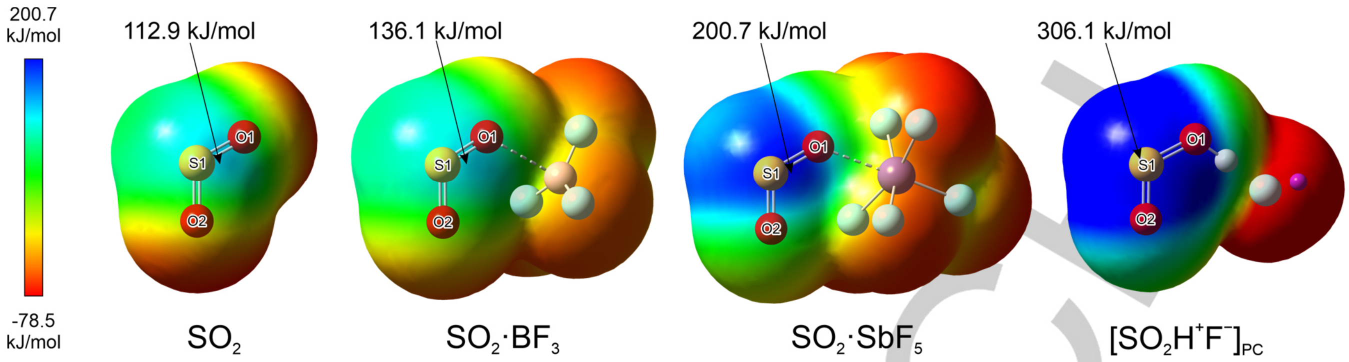

Figure 9. Molecular electrostatic potentials mapped on the isodensity surface of the respective calculated SO_2 species. The marked points are the most positive points on the MEP surfaces. The mapped MEPs are illustrated in a color range of −78.5 kJ/mol (red) to 200.7 kJ/mol (blue), with isovalue = 0.0004. The color range of the MEP surfaces was scaled to the energy range of the $SO_2\cdot SbF_5$ MEP. The positive background point charge of $[SO_2H^+F^-]_{PC}$ is illustrated as a purple dummy atom.

Table 4 summarizes the calculated atomic charges of the SO_2 moiety in the respective structures. Further details on the calculated structures are found in the Supporting Information. Since the electrostatic potential of SO_2H^+ is throughout positive due to its cationic nature, the ion pair $[SO_2H^+F^-]$ was calculated for better comparability with the other neutral SO_2-containing species in the gas phase. As expected, the optimization of $[SO_2H^+F^-]$ leads to the structure $[SO_2\cdot HF]$. To "lower the basicity" of the fluoride in the calculation, the structure of monoprotonated SO_2 from our previous work was employed $[SO_2H^{(a)}\cdot FH^{(b)}]^+$ (*Synthesis and Structure of Protonated Sulfur Dioxide* (C. Jessen, A. J. Kornath, work in preparation)). By substitution of $H^{(b)}$ for a background point charge with charge +1.0, we simulated the overall neutral ion pair $[SO_2H^+F^-]_{PC}$. The structure was optimized to a minimum, followed by a frequency calculation. The structural parameters and the calculated vibrational frequencies agreed very well with the previously found data for monoprotonated SO_2 (*Synthesis and Structure of Protonated Sulfur Dioxide* (C. Jessen, A. J. Kornath, work in preparation)).

Table 4. Calculated atomic charges (in units of e) of the SO_2 moiety in SO_2, $SO_2\cdot BF_3$, $SO_2\cdot SbF_5$, and $[SO_2H^+\cdots F^-]_{PC}$.

	SO_2	$SO_2\cdot BF_3$	$SO_2\cdot SbF_5$	$[SO_2H^+F^-]_{PC}$
S1				
Mulliken	0.982	0.897	1.050	1.099
ChelpG	0.592	0.628	0.718	0.882
NPA	1.667	1.695	1.764	1.829
O1				
Mulliken	−0.491	−0.469	−0.518	−0.251
ChelpG	−0.296	−0.300	−0.278	−0.479
NPA	−0.833	−0.868	−0.940	−0.828
O2				
Mulliken	−0.491	−0.470	−0.412	−0.353
ChelpG	−0.296	−0.287	−0.229	−0.077
NPA	−0.833	−0.810	−0.737	−0.668

The MEP surfaces show that the highest electron deficiency is located on the sulfur atom perpendicular to the O−S−O-plane. The most positive values found on the MEP surface are 112.9 kJ/mol (SO_2), 136.1 kJ/mol ($SO_2\cdot BF_3$), 200.7 kJ/mol ($SO_2\cdot SbF_5$), and 306.1 kJ/mol ($[SO_2H^+F^-]_{PC}$). The SO_2 moiety is increasingly positively polarized with the increasing strength of the adjected Lewis acid.[32] The calculated atomic charges show a similar trend. The three methods yield different total atomic charges.[33] Especially the charge on the oxygen atoms varies depending on the method. The positive charge on the sulfur atom increases for all methods.

By the complexation with Lewis acids, the SO_2 moiety becomes activated for nucleophilic attacks. The results from this work show that the $SO_2\cdot SbF_5$ complex reacts with the solvent aHF even at low temperatures with the addition of an HF molecule, followed by the reaction to $[FS(OH)_2][SbF_6]$. The mixtures with the weaker Lewis acids BF_3 or GeF_4 did not exhibit the same reactivity. The calculations strongly indicate that monoprotonated SO_2 reacts with HF to form $FS(OH)_2^+$ as described in Equation (13). Under the investigated conditions the mixtures $SO_2/HF/SbF_5$ (aHF as solvent) afforded $[FS(OH)_2][SbF_6]$ as the only product. This is true even if the superacid was formed before the addition of SO_2. We conclude, that the formation of $SO_2\cdot SbF_5$ is not necessary to afford $FS(OH)_2^+$ from HF/SbF_5 as described earlier.[11] The protonation of SO_2 by the superacid HF/SbF_5 followed by the fast reaction with the solvent aHF also leads to the formation of $FS(OH)_2^+$. Considering that *Horvath et al*. reported strong evidence for the protonation of carbon monoxide in HF/SbF_5, the protonation of SO_2 appears to be very possible.[34] In this scenario, the used solvent may play a bigger role than pure acid strength. This is supported by the isolation of protonated SOF_2 from the solvent R-134a, which was unsuccessful in aHF.

Also, the results show that the addition of SO_2 to the binary superacid HF/SbF_5, even in stoichiometric amounts (SO_2 respective to SbF_5), leads to the formation of the complex $FS(OH)O\cdot SbF_5$ and the $FS(OH)_2^+$ cation. It can be assumed that the acidity of the solution is reduced to the acidity of these compounds, which is currently unknown.

Conclusion

The formation of the $FS(OX)_2^+$ cation in the binary superacids XF/MF_5 (X = D, H; M = As, Sb) was investigated. The synthesis of these salts in FEP-reactors allowed the isolation in appreciable amounts for a detailed vibrational analysis and an X-ray single crystal structure analysis. NMR spectroscopy provided strong evidence that the reaction in aHF from $SO_2 \cdot SbF_5$ to $[FS(OH)_2][SbF_6]$ proceeds via the intermediate complex $FS(OH)O \cdot SbF_5$. Additionally, theoretical calculations were employed to investigate the electrophilicity of the sulfur atom of SO_2-Lewis acid complexes. The theoretical and experimental results show that the strong Lewis acids AsF_5, SbF_5, and H^+ allow the reaction of the SO_2-Lewis acid complex with HF. This results in the formation of $FS(OH)O \cdot SbF_5$ and subsequently the $FS(OH)_2^+$ cation. The insight about this last step enabled the transfer of the reaction to the isoelectronic complex $SOF_2 \cdot SbF_5$. Reacting the latter in R-134a with stoichiometric amounts of HF, afforded the first isolation of protonated and hemiprotonated SOF_2 as the mixed salt $[SOF_2H][(SOF_2)_2H][Sb_2F_{11}]_2$. The mixed salt was investigated and characterized by vibrational analysis and X-ray single crystal structure analysis. The results reveal the disadvantage of the solvent aHF for the protonation of molecules with very low basicity or very high electrophilicity. For the isolation of such protonated molecules, the solvent R-134a has proven to be very promising.

Experimental Section

All experimental data and procedures are found in the Supporting Information.

Deposition Numbers 2166667 ($[FS(OH)_2][SbF_6]$), 2166668 ($[SOF_2H][(SOF_2)_2H][Sb_2F_{11}]_2$) and 2166669 ($SOF_2 \cdot SbF_5$) contain the supplementary crystallographic data for this paper. These data are provided free of charge by the joint Cambridge Crystallographic Data Centre and Fachinformationszentrum Karlsruhe Access Structures service www.ccdc.cam.ac.uk/structures.

Acknowledgments

We are grateful to the Department of Chemistry of the Ludwig-Maximilian University, Munich, the Deutsche Forschungsgemeinschaft (DFG), and the F-Select GmbH for the support of this work.

Keywords: protonation; sulfur dioxide; thionyl fluoride; single-crystal structure analysis; vibrational spectroscopy

[1] G. A. Olah, *Angew. Chem. Int. Ed. Engl.* **1973**, *12*, 173.
[2] a) H. S. Booth, D. R. Martin, *J. Am. Chem. Soc.* **1942**, *64*, 2198; b) M. Brownstein, *Journal of Inorganic and Nuclear Chemistry* **1976**, *28*, 141.
[3] R. Minkwitz, W. Molsbeck, H. Preut, *Zeitschrift für Naturforschung B* **1989**, *44*, 1581.
[4] J. W. Moore, H. W. Baird, H. B. Miller, *J. Am. Chem. Soc.* **1968**, *90*, 1358.
[5] G. S. H. Chen, J. Passmore, *J. Chem. Soc., Dalton Trans.* **1979**, 1257.
[6] M. Brownstein, R. J. Gillespie, *J. Am. Chem. Soc.* **1970**, *92*, 2718.
[7] P. A. W. Dean, R. J. Gillespie, *J. Am. Chem. Soc.* **1969**, *91*, 7260.
[8] a) R. Minkwitz, D. Bernstein, H. Preut, W. Sawodny, H. Hrtner, *Z. Anorg. Allg. Chem.* **1991**, *606*, 157; b) R. J. Gillespie, F. G. Riddell, D. R. Slim, *J. Am. Chem. Soc.* **1976**, *98*, 8069; c) George A. Olah/Daniel J. Donovan/Henry C. Lin; d) J. Y. Calves, R. J. Gillespie, *J. Am. Chem. Soc.* **1977**, *99*, 1788.
[9] E. S. Stoyanov, I. V. Stoyanova, *Angew. Chem. Int. Ed. Engl.* **2018**, *57*, 4516.
[10] a) T. Soltner, N. R. Goetz, A. Kornath, *Chem. Ber.* **2011**, *2011*, 3076; b) R. Seelbinder, N. R. Goetz, J. Weber, R. Minkwitz, A. J. Kornath, *Chemistry (Weinheim an der Bergstrasse, Germany)* **2010**, *16*, 1026.
[11] A. Kornath, R. Seelbinder, R. Minkwitz, *Angew. Chem. Int. Ed. Engl.* **2005**, *44*, 973.
[12] G. A. Olah, T. OHYAMA, *Synthesis* **1976**, *1976*, 319.
[13] a) F. Seel, J. Boudier, W. Gombler, *Chem. Ber.* **1969**, *102*, 443; b) A. Zappel, *Chem. Ber.* **1961**, *94*, 873.
[14] F. Seel, L. Riehl, *Z. Anorg. Allg. Chem.* **1955**, *282*, 293.
[15] A. Kornath, F. Neumann, R. Ludwig, *Inorg. Chem.* **1997**, *36*, 5570.
[16] J. Shamir, A. Netzer, *Can. J. Chem.* **1973**, *51*, 2676.
[17] G. A. Olah, P. Schilling, J. M. Bollinger, J. Nishimura, *J. Am. Chem. Soc.* **1974**, *96*, 2221.
[18] S. M. Brownstein, *A Conductometric and Spectroscopic Investigation of Some Solutes in Anhydrous HF*, Doctoral dissertation, McMaster University, **1970**.
[19] E. E. Aynsley, R. D. Peacock, P. L. Robinson, *Chem. Ind.* **1951**, 1117.
[20] a) D. Mootz, K. Bartmann, *Angew. Chem. Int. Ed. Engl.* **1988**, *27*, 391; b) D. Mootz, K. Bartmann, *Zeitschrift für Naturforschung B* **1991**, *46*, 1659; c) B. Bonnet, C. Belin, J. Potier, Mascherpa G., *C. r. hebd. séances Acad. sci., Ser. C281* **1975**, *281*, 1011; d) B. Bonnet, G. Mascherpa, *Inorg. Chem.* **1980**, *19*, 785.
[21] F. Pepi, A. Ricci, M. Di Stefano, M. Rosi, G. D'Arcangelo, *J. Phys. Chem. A* **2002**, *106*, 9261.
[22] E. P. L. Hunter, S. G. Lias, *Journal of Physical and Chemical Reference Data* **1998**, *27*, 413.
[23] E. S. Stoyanov, C. A. Reed, *J. Phys. Chem. A* **2006**, *110*, 12992.
[24] E. L. Pace, H. V. Samuelson, *The Journal of Chemical Physics* **1966**, *44*, 3682.
[25] M. Azeem, M. Brownstein, R. J. Gillespie, *Can. J. Chem.* **1969**, *47*, 4159.
[26] I. Hargittai, F. C. Mijlhoff, *Journal of Molecular Structure* **1973**, *16*, 69.
[27] D. D. Gibler, C. J. Adams, M. Fischer, A. Zalkin, N. Bartlett, *Inorg. Chem.* **1972**, *11*, 2325.
[28] G. A. Jeffrey, *An introduction to hydrogen bonding*, Oxford Univ. Press, New York, **1997**.
[29] A. Bondi, *J. Phys. Chem.* **1964**, *68*, 441.
[30] D. Stasko, S. P. Hoffmann, K.-C. Kim, N. L. P. Fackler, A. S. Larsen, T. Drovetskaya, F. S. Tham, C. A. Reed, C. E. F. Rickard, P. D. W. Boyd et al., *J. Am. Chem. Soc.* **2002**, *124*, 13869.
[31] D. Stuart, S. D. Wetmore, M. Gerken, *Angew. Chem. Int. Ed. Engl.* **2017**, *56*, 16380.
[32] G. A. Olah, *Superacid chemistry*, Wiley, Hoboken, N.J, **2009**.
[33] F. Martin, H. Zipse, *Journal of computational chemistry* **2005**, *26*, 97.
[34] P. J. de Rege, Gladysz, Horvath, *Science (New York, N.Y.)* **1997**, *276*, 776.

Entry for the Table of Contents

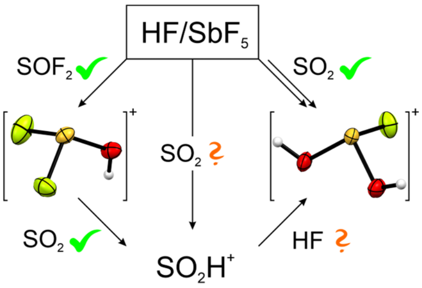

The $FS(OH)_2^+$ cation was revisited, by reacting sulfur dioxide in XF/MF_5 (X = H, D; M = As, Sb). From an observed intermediate during the reaction, a synthesis was deduced to isolate protonated thionyl fluoride for the first time. The salt $[SOF_2H][(SOF_2)_2H][Sb_2F_{11}]_2$ is acidic enough to protonate SO_2 in solution. Is SO_2 also protonated in HF/SbF$_5$ but quenched by the solvent to form $FS(OH)_2^+$?

Supporting Information

Characterization of Two Cationic Siblings. The Fluorodihydroxy- and Difluorohydroxysulfonium Cations Are Put to the Acid Test

Christoph Jessen, Hannah Illner, Florian Zischka, Alexander Nitzer, Alan Virmani and Andreas J. Kornath*

Table of Contents

1 Experimental Details 3

1.1 Apparatus and Materials 3

1.2 Computational Methods 3

1.3 Experimental Procedures 4

2 Crystallographic Data 5

2.1 $[FS(OH)_2][SbF_6]$ 6

2.2 $[SOF_2H][(SOF_2)_2H][Sb_2F_{11}]_2$ 7

2.3 $SOF_2 \cdot SbF_5$ 8

3 Vibrational Data 10

3.1 $[FS(OX)_2][MF_6]$ 10

3.2 $[SOF_2H][(SOF_2)_2H][Sb_2F_{11}]_2$ 13

4 NMR 15

5 Quantum Chemical Calculations 19

6 References 23

1 Experimental Details

Caution! Note that any contact with the described compounds should be avoided. Hydrolysis of the starting materials CF_3SO_2F, SOF_2, AsF_5, SbF_5, BF_3, GeF_4, and the synthesized salts forms HF which burns skin and causes irreparable damage. Safety precautions should be taken while handling these compounds.

1.1 Apparatus and Materials

All reactions were carried out by employing standard Schlenk techniques on a stainless steel vacuum line. The syntheses of the salts were performed using FEP/PFA reactors with stainless steel valves. Before each reaction or NMR measurement, the stainless steel vacuum line and the reactors were dried with fluorine.

For Raman measurements a Bruker MultiRam FT-Raman spectrometer with Nd:YAG laser excitation (λ = 1064 nm) was used. The measurement was performed after transferring the sample into a cooled (−196°C) glass cell under nitrogen atmosphere and subsequent evacuation of the glass cell.

Low temperature IR-spectroscopic investigations were carried out with a Bruker Vertex-80V FTIR spectrometer using a cooled cell with a single-crystal CsBr plate on which small amounts of the samples were placed.[1]

The single crystal X-Ray diffraction studies were performed with an Oxford XCalibur3 diffractometer equipped with a Spellman generator (voltage 50 kV, current 40 mA) and a KappaCCD detector, operating with Mo-Kα radiation (λ = 0.7107 Å) The measurements were performed at 173 K. The program CrysAlisPro 1.171.39.46e (Rigaku Oxford Diffraction, 2018) was employed for the data collection and reduction.[2] The structures were solved utilizing SHELXT[3] and SHELXL-2018/3[4] of the WINGX software package.[5] The structures were checked using the software PLATON.[6] The absorption correction was performed using the SCALE3 ABSPACK multiscan method.[7] Visualization was done with the software Mercury.[8] Hirshfeld surface analysis was conducted with the CrystalExplorer software[9]

NMR spectra were recorded on either a Jeol ECX400 NMR instrument or a Bruker AV400 NMR instrument. The spectrometer was externally referenced to $CFCl_3$ for ^{19}F NMR and to tetramethylsilane for ^1H NMR spectra. For visualization and evaluation, the software MestReNova Version 14.0.4 was used.[10] The spectra were recorded inside 4 mm FEP tube inliners. The NMR samples were prepared by loading a dried 4 mm FEP tube inliner with a small amount of solid ($SO_2\cdot SbF_5$ or [Cs][SO_2F]) under nitrogen atmosphere. Then the FEP tube was cooled to −196 °C and *a*HF was carefully condensed into the FEP tube at −196 °C in a way, that it froze over the solid without getting in contact with it. A sketch of this experimental procedure is illustrated in Figure S1. After the *a*HF was completely frozen, the FEP tube was evacuated, flame sealed and kept at −196 °C. Immediately before the NMR measurement, the sealed FEP tube was put in a standard glass NMR tube loaded with 0.2 mL acetone-d$_6$ as an external reference and warmed to the designated temperature. The warming process from −70 °C to 25 °C was controlled by the NMR instrument. Before every measurement at a 10 °C increment, the sample was removed from the instrument and gently shaken in the cooling stream to ensure a homogenous solution.

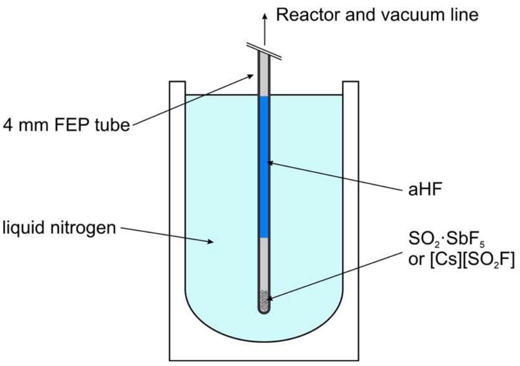

Figure S1. Part of the preparation for the NMR measurement of the reaction of $SO_2\cdot SbF_5$ or [Cs][SO_2F] in *a*HF. The FEP tube was connected to the vacuum line via a PFA reactor with a stainless steel valve.

1.2 Computational Methods

Quantum chemical calculations were carried out using the software packages Gaussian09 and Gaussian16.[11] For visualization and illustration of the calculated structures and mapped MEP surfaces the software GaussView 6 was used.[12] If not stated otherwise, all calculations were carried out on the M06-2X/aug-cc-pVTZ level of theory. For antimony, the effective core potential MWB46 was employed.

1.3 Experimental Procedures

In the following procedures applies MF_5 = SbF_5, AsF_5, and *a*XF = *a*DF, *a*HF.

[Cs][SO_2F]

[Cs][SO_2F] was prepared according to the literature.[13] After dry cesium fluoride (760 mg, 5.0 mmol) was filled into an FEP reactor, SO_2 (2 mL) was condensed into the vessel. The reactants were warmed to room temperature and thoroughly mixed for 15 min. A colorless precipitant was formed. The excess solvent was removed *in vacuo* at −78 °C. The product [Cs][SO_2F] was obtained as a colorless solid in quantitative yield.

$SO_2 \cdot SbF_5$

$SO_2 \cdot SbF_5$ was prepared according to the literature.[14] SbF_5 (1 g, 4.6 mmol) was condensed in an FEP reactor together with sulfur dioxide (2 mL). The reactants were warmed to room temperature and thoroughly mixed for 15 min. From the clear solution, the excess solvent was removed *in vacuo* at −78 °C. The product was obtained as a colorless solid.

[$FS(OX)_2$][MF_6] (similar to literature)[15][Quelle:SO2-Paper]

MF_5 (1.0 mmol) was condensed in an FEP reactor vessel together with sulfur dioxide (or CF_3SO_2F) (1.0 mmol) and aXF (0.5 mL) at −196 °C. The reaction mixture was then warmed up to −20 °C and homogenized to complete dissolution. The mixture was cooled to −78 °C and volatile components were removed overnight at −78 °C in a dynamic vacuum. The products were obtained as colorless crystalline solids. To obtain single crystals for X-ray structure analysis, the reaction mixture was slowly cooled to −70 °C and kept at that temperature overnight. Afterward, all volatile components were removed at −78 °C in a dynamic vacuum.

[$FS(OX)_2$][SbF_6] (from $SO_2 \cdot SbF_5$)

After $SO_2 \cdot SbF_5$ was filled into an FEP reactor, a twentyfold excess of aXF was condensed into the vessel. The reaction mixture was then warmed up to −20 °C and homogenized to complete dissolution. The mixture was cooled to −78 °C and volatile components were removed overnight at −78 °C in a dynamic vacuum. The products were obtained as colorless crystalline solids.

[$FS(OH)_2$][SbF_6] (from SO_2 in superacid)

SbF_5 (1.0 mmol) was condensed in an FEP reactor vessel together with *a*HF (0.5 mL) at −196 °C. To form the superacid the reactants were warmed to −40 °C and thoroughly mixed to complete dissolution. The superacid was frozen at −196 °C and SO_2 (1.0 mmol) was condensed into the reaction vessel. The reactants were warmed to −60 °C and thoroughly mixed to complete dissolution. The mixture was cooled to −78 °C and volatile components were removed overnight at −78 °C in a dynamic vacuum. The product was obtained as a colorless crystalline solid. If a larger stoichiometric amount of SbF_5 was used compared to SO_2, fluoronium salts ([$H_{n+1}F_n$][Sb_2F_{11}]) were formed as a by-product.

$SOF_2 \cdot SbF_5$

SbF_5 (0.5 mmol) was condensed into an FEP reactor vessel together with SOF_2 (0.5 mmol) and 1,1,1,2-tetrafluoroethane (R-134a) (2 mL) at −196 °C. The reactants were warmed to −40 °C and mixed to complete dissolution. Slowly cooling the mixture to −60 °C resulted in the precipitation of a colorless crystalline solid. The mixture was cooled to −78 °C and volatile components were removed at −78 °C in a dynamic vacuum. The product $SOF_2 \cdot SbF_5$ was obtained as a colorless crystalline solid.

[SOF_2H][$(SOF_2)_2H$][Sb_2F_{11}]$_2$

SbF_5 (1.0 mmol) was condensed into an FEP reactor vessel together with SOF_2 (0.5 mmol) and 1,1,1,2-tetrafluoroethane (R-134a) (2 mL) at −196 °C. The reactants were warmed to −40 °C and mixed to complete dissolution. Then the mixture was frozen at −196 °C and *a*HF (0.5 mmol) was condensed into the reaction vessel. The reactants were warmed to −70 °C and mixed for 10 min. From the reaction mixture, a colorless precipitant was formed. Removing the volatile components at −78 °C in a dynamic vacuum, afforded [SOF_2H][$(SOF_2)_2H$][Sb_2F_{11}]$_2$ as colorless solid. To obtain single crystals from the reaction mixture, the mixture was warmed up to −50 °C while gently shaking the reaction vessel. While a complete dissolution of the product was not achieved, subsequent cooling of the mixture to −70 °C allowed the growth of single crystals from the dissolved phase.

2 Crystallographic Data

Table S1. Crystal data and structure refinement of $\mathrm{[FS(OH)_2][SbF_6]}$ (**1**), $\mathrm{[SOF_2H][(SOF_2)_2H][Sb_2F_{11}]_2}$ (**6**) and $\mathrm{SOF_2{\cdot}SbF_5}$ (**7**).

	$\mathrm{[FS(OH)_2][SbF_6]}$	$\mathrm{[SOF_2H][(SOF_2)_2H][Sb_2F_{11}]_2}$	$\mathrm{SOF_2{\cdot}SbF_5}$
Molecular Formula	$\mathrm{F_7H_2O_2SSb}$	$\mathrm{F_{28}H_2O_3S_3Sb_4}$	$\mathrm{F_7OSSb}$
M_r[g·mol^{-1}]	320.83	1165.20	302.81
Crystal size [mm^3]	0.230 × 0.180 × 0.130	0.227 × 0.058 × 0.025	0.430 × 0.243 × 0.036
Crystal system	monoclinic	triclinic	orthorhombic
Space group	$P2(1)/c$	$P\overline{1}$	$Pnma$
a [Å]	5.2275(2)	5.3060(2)	13.8516(8)
b [Å]	8.2174(2)	15.1400(5)	8.0172(4)
c [Å]	16.2014(4)	16.3458(5)	5.6208(3)
α [°]	90	65.395(3)	90
β [°]	91.751(3)	85.885(3)	90
γ [°]	90	88.487(3)	90
V [Å^3]	695.63(4)	1190.79(7)	624.20(6)
Z	4	2	4
ρ_{calc} [g·cm^{-3}]	3.063	3.250	3.222
μ [mm^{-1}]	4.358	4.974	4.835
$\lambda_{MoK\alpha}$ [Å]	0.71073	0.71073	0.71073
F(000)	592.0	1060.0	552.0
T [K]	120	104	105
h, k, l range	-5:7,-11:11,-22:23	-7:7,-21:17,-23:23	-17:19,-3:11,-7:8
Measured reflexes	7053	13033	3047
Unique reflexes	2120	7264	1009
R_{int}	0.0342	0.0260	0.0334
Parameters	106	352	55
R(F)/wR(F^2)[a] (all data)	0.0282/0.0679	0.0348/0.0779	0.0365/0.0831
Weighting scheme[b]	0.0342/0.0000	0.0315/1.2636	0.0202/2.9579
S (Gof)[c]	1.046	1.019	1.205
Residual density [e·Å^{-3}]	1.257/-0.967	1.255/-1.094	1.790/-1.367
Device	Oxford XCalibur	Oxford XCalibur	Oxford XCalibur
CCDC	2166667	2166668	2166669

[a] $R_1 = \Sigma||F_0|-|F_c||/\Sigma|F_0|$.

[b] $wR_2 = [\Sigma[w(F_0^2-F_c^2)^2]/\Sigma[w(F_0)^2]]^{1/2}$; $w = [\sigma_c^2(F_0^2)+(xP)^2+yP]-1$; $P = (F_0^2+2F_c^2)/3$.

[c] GoF = $\{\Sigma[w(F_o^2-F_c^2)^2]/(n-p)\}^{1/2}$ (n = number of reflections; p = total number of parameters).

2.1 [FS(OH)$_2$][SbF$_6$]

Figure S2 shows the mapped Hirshfeld surface with d_{norm} of the FS(OH)$_2^+$ cation in **1**. Interionic contacts towards the fluorine atoms of SbF$_6^-$ anions result in a distorted octahedral geometry around the sulfur atom on one side of the cation.[15] A side view shows that the opposite side of the surface is in contact with the corresponding surface of another cation in the crystal structure (Figure S2). The shortest distances between the cations (O···O) is longer than the sum of the van-der-Waals (VDW) radii of two oxygen atoms (3.04 Å).[16] Thus, there is no interaction between the cations within their respective range of VDW radii. The cations are packed in pairs along the a-axis of the crystal structure which is shown in Figure S3.

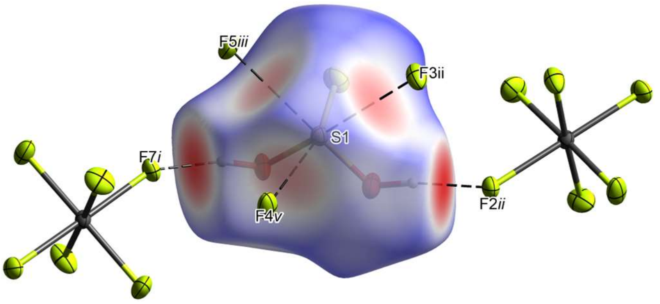

Figure S2. Hirshfeld surface and interionic contacts of the FS(OH)$_2^+$ cation in **1** mapped with d_{norm} over the range −0.7768 to 0.9452. Colour coding of the Hirshfeld surface: white (distance *d* equals VDW), blue (*d* exceeds VDW distance), red (*d* is smaller than VDW distance). For the anions of the S−F contacts, only the contacting fluorine atoms are shown for better visualization. Symmetry code: *i* = 1+x, y, z; *ii* = 1+x, 1.5−y, 0.5+z; *iii* = 1+x, y, z; *iv* = 2−x, 0.5+y, 0.5−z; *v* = 1−x, 0.5+y, 0.5−z.

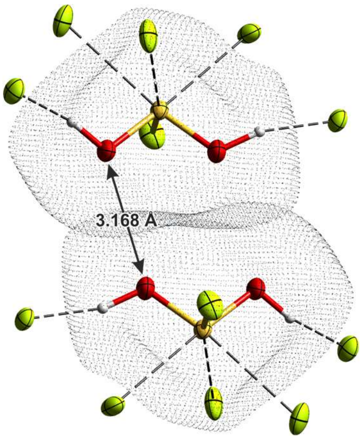

Figure S3. Shortest distance between the closely packed FS(OH)$_2^+$ cations in **1**. The Hirshfeld surfaces of the two cations are shown transparently. For surrounding SbF$_6^-$ anions, only the fluorine atoms with contacts to the cations are shown. Right: Symmetry code: *i* = 1+x, y, z; *ii* = 1+x, 1.5−y, 0.5+z; *iii* = 1+x, y, z; *iv* = 2−x, 0.5+y, 0.5−z; *v* = 1−x, 0.5+y, 0.5−z.

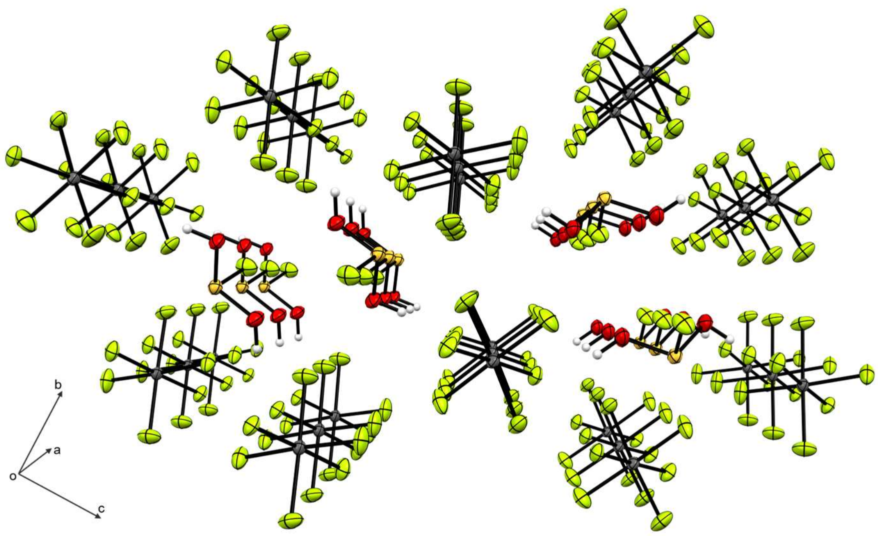

Figure S4. View along the a-axis in the crystal packing of **1**.

Table S2. Bond lengths and angles of [$FS(OH)_2$][SbF_6] (**1**).

Bond lengths [Å]		Bond angles [°]	
Sb1-F6	1.853(2)	F6-Sb1-F5	91.31(11)
Sb1-F5	1.866(2)	F6-Sb1-F4	178.32(9)
Sb1-F4	1.866(2)	F5-Sb1-F4	89.22(11)
Sb1-F3	1.871(2)	F6-Sb1-F3	91.48(10)
Sb1-F7	1.896(2)	F5-Sb1-F3	177.07(10)
Sb1-F2	1.905(2)	F4-Sb1-F3	88.02(11)
S1-O2	1.523(3)	F6-Sb1-F7	91.09(9)
S1-O1	1.525(3)	F5-Sb1-F7	90.45(10)
S1-F1	1.545(2)	F4-Sb1-F7	90.50(9)
		F3-Sb1-F7	88.59(10)
		F6-Sb1-F2	89.73(9)
		F5-Sb1-F2	90.49(10)
		F4-Sb1-F2	88.67(8)
		F3-Sb1-F2	90.43(9)
		F7-Sb1-F2	178.74(8)
		O2-S1-O1	97.29(15)
		O2-S1-F1	100.00(15)
		O1-S1-F1	99.11(13)

2.2 [SOF_2H][$(SOF_2)_2H$][Sb_2F_{11}]$_2$

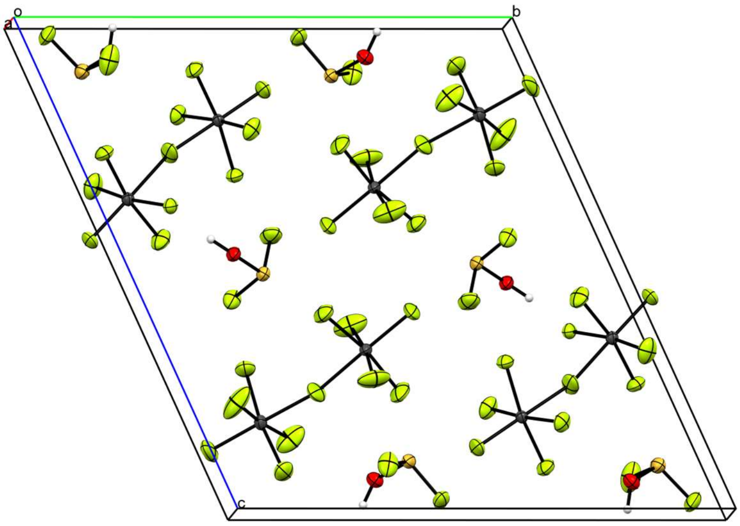

Figure S5. View on the unit cell of **6** along the a-axis.

Table S3. Bond lengths and angles of $[SOF_2H][(SOF_2)_2H][Sb_2F_{11}]_2$ (**6**).

Bond lengths [Å]		Bond angles [°]			
S1-O1	1.484(3)	O1-S1-F2	103.98(17)	F13-Sb2-F12	87.22(14)
S1-F2	1.528(3)	O1-S1-F1	103.33(19)	F15-Sb2-F12	176.63(15)
S1-F1	1.534(3)	F2-S1-F1	95.16(19)	F17-Sb2-F12	84.18(12)
S2-O2	1.449(3)	O2-S2-F4	104.26(19)	Sb2-F12-Sb1	164.25(19)
S2-F4	1.538(3)	O2-S2-F3	105.3(2)	F25-Sb3-F26	93.9(2)
S2-F3	1.542(3)	F4-S2-F3	93.87(19)	F25-Sb3-F28	171.57(19)
S3-O3	1.458(3)	O3-S3-F6	103.39(18)	F26-Sb3-F28	94.5(2)
S3-F6	1.536(4)	O3-S3-F5	104.63(18)	F25-Sb3-F24	88.34(18)
S3-F5	1.540(3)	F6-S3-F5	94.04(19)	F26-Sb3-F24	94.83(15)
Sb1-F8	1.848(3)	F8-Sb1-F7	90.17(12)	F28-Sb3-F24	91.62(18)
Sb1-F7	1.852(3)	F8-Sb1-F9	95.32(13)	F25-Sb3-F27	90.60(16)
Sb1-F9	1.855(3)	F7-Sb1-F9	95.14(14)	F26-Sb3-F27	94.91(14)
Sb1-F10	1.855(3)	F8-Sb1-F10	90.08(13)	F28-Sb3-F27	88.02(15)
Sb1-F11	1.856(3)	F7-Sb1-F10	171.70(14)	F24-Sb3-F27	170.25(14)
Sb1-F12	2.029(3)	F9-Sb1-F10	93.09(14)	F25-Sb3-F23	85.47(18)
Sb2-F16	1.840(3)	F8-Sb1-F11	170.81(13)	F26-Sb3-F23	178.91(15)
Sb2-F14	1.843(3)	F7-Sb1-F11	88.99(13)	F28-Sb3-F23	86.14(19)
Sb2-F13	1.845(3)	F9-Sb1-F11	93.87(13)	F24-Sb3-F23	84.30(15)
Sb2-F15	1.846(3)	F10-Sb1-F11	89.44(13)	F27-Sb3-F23	85.95(15)
Sb2-F17	1.899(3)	F8-Sb1-F12	85.60(13)	F19-Sb4-F22	173.2(2)
Sb2-F12	2.003(3)	F7-Sb1-F12	85.81(13)	F19-Sb4-F20	94.2(2)
Sb3-F25	1.829(4)	F9-Sb1-F12	178.67(15)	F22-Sb4-F20	92.7(2)
Sb3-F26	1.837(3)	F10-Sb1-F12	85.94(14)	F19-Sb4-F18	89.27(16)
Sb3-F28	1.844(4)	F11-Sb1-F12	85.21(13)	F22-Sb4-F18	89.86(17)
Sb3-F24	1.845(3)	F16-Sb2-F14	91.63(15)	F20-Sb4-F18	93.90(15)
Sb3-F27	1.851(3)	F16-Sb2-F13	170.13(13)	F19-Sb4-F21	90.72(17)
Sb3-F23	1.999(3)	F14-Sb2-F13	92.28(15)	F22-Sb4-F21	89.08(17)
Sb4-F19	1.831(3)	F16-Sb2-F15	93.47(13)	F20-Sb4-F21	95.04(15)
Sb4-F22	1.837(4)	F14-Sb2-F15	95.47(15)	F18-Sb4-F21	171.04(13)
Sb4-F20	1.844(3)	F13-Sb2-F15	95.18(14)	F19-Sb4-F23	86.07(19)
Sb4-F18	1.854(3)	F16-Sb2-F17	88.34(12)	F22-Sb4-F23	87.1(2)
Sb4-F21	1.855(3)	F14-Sb2-F17	170.91(14)	F20-Sb4-F23	178.98(18)
Sb4-F23	1.994(3)	F13-Sb2-F17	86.38(12)	F18-Sb4-F23	85.11(15)
		F15-Sb2-F17	93.60(13)	F21-Sb4-F23	85.95(15)
		F16-Sb2-F12	83.95(13)	Sb4-F23-Sb3	166.1(2)
		F14-Sb2-F12	86.77(15)		

2.3 $SOF_2{\cdot}SbF_5$

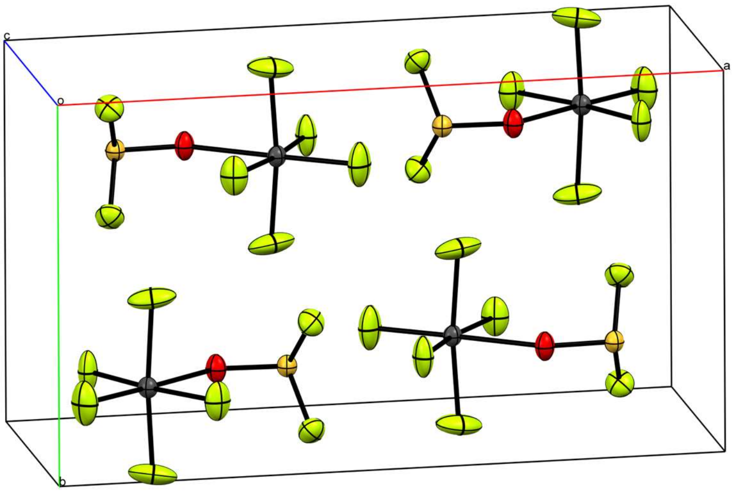

Figure S6. View on the unit cell of $SOF_2{\cdot}SbF_5$.

Table S4. Bond lengths and angles of $SOF_2 \cdot SbF_5$.

Bond lengths [Å]		Bond angles [°]		Torsion angles [°]	
Sb1-F3	1.836(5)	F3-Sb1-F2	94.9(2)	F1-S1-O1-Sb1	49.63(14)
Sb1-F2	1.843(4)	F3-Sb1-F4	94.4(2)		
Sb1-F4	1.853(4)	F2-Sb1-F4	170.73(19)		
Sb1-F5	1.858(4)	F3-Sb1-F5	94.03(12)		
Sb1-F5	1.858(4)	F2-Sb1-F5	89.61(13)		
Sb1-O1	2.093(5)	F4-Sb1-F5	89.74(12)		
S1-O1	1.459(5)	F3-Sb1-F5	94.03(12)		
S1-F1	1.538(3)	F2-Sb1-F5	89.61(13)		
S1-F1	1.538(3)	F4-Sb1-F5	89.74(12)		
		F5-Sb1-F5	171.9(3)		
		F3-Sb1-O1	177.51(19)		
		F2-Sb1-O1	87.6(2)		
		F4-Sb1-O1	83.09(18)		
		F5-Sb1-O1	85.98(12)		
		F5-Sb1-O1	85.98(12)		
		O1-S1-F1	103.84(19)		
		O1-S1-F1	103.84(19)		
		F1-S1-F1	95.4(3)		
		S1-O1-Sb1	139.7(3)		

3 Vibrational Data

3.1 [FS(O*X*)$_2$][*M*F$_6$]

Table S5. Experimental vibrational frequencies [cm^{-1}] of [FS(OH)$_2$][MF$_6$] (*M* = As, Sb) and calculated vibrational frequencies [cm^{-1}] of [FS(OH)$_2$ · 2HF]$^+$.

[FS(OH)$_2$][SbF$_6$]$_2$ (**1**) exp.[a]		[FS(OH)$_2$][AsF$_6$]$_2$ (**2**) exp.[a]		[FS(OH)$_2$ · 2HF]$^+$ calc.[b,c]	Assignment		
IR	Raman	IR	Raman	IR/Raman			
3342(m, br)		3155(s, br)		3185(367/214)	ν_1	A'	ν_s(OH)
				3143(2947/32)	ν_8	A''	ν_{as}(OH)
		1628(w)					
1298(w)		1296(vw)					
1190(m)		1166(w)		1227(192/0)	ν_2	A'	δ(SOH)
1128(m)		1138(w)		1187(18/3)	ν_9	A''	δ(SOH)
990(sh)	979(51)	993(sh)	981(48)	978(255/4)	ν_3	A'	ν_s(SO)
972(s)	966(9)	974(m)	965(9)	973(72/17)	ν_{10}	A''	ν_{as}(SO)
824(s)	828(24)	825(m)	828(24)	860(201/7)	ν_4	A'	ν(SF)
				629(128/0)	ν_5	A'	ω(SOH)
	545(3)	546(m)	541(4)	576(5/0)	ν_{11}	A''	ω(SOH)
530(s)	530(7)		524(7)	527(15/2)	ν_6	A'	ω(FSO$_2$)
409(m)	409(9)	410(sh)	418(5)	399(104/1)	ν_7	A'	δ(OSO)
390(s)	393(6)	390(s)	405(6)	373(24/1)	ν_{12}	A''	δ(FSO)
Vibrations of the anions MF_6^- (*M* = As, Sb)							
698(vs)	692(6)	746(s)	711(8)	746(s)			AsF_6^-; SbF_6^-
673(vs)	671(13)	702(vs)	692(100)	702(vs)			AsF_6^-; SbF_6^-
608(s)	658(100)	675(s)	677(6)	675(s)			AsF_6^-; SbF_6^-
582(s)	638(4)	619(s)	592(5)	619(s)			AsF_6^-; SbF_6^-
	586(7)	588(s)	383(11)	588(s)			AsF_6^-; SbF_6^-
	552(2)	565(m)	374(11)	565(m)			AsF_6^-; SbF_6^-
	308(6)		367(15)				AsF_6^-; SbF_6^-
	287(23)		360(12)				AsF_6^-; SbF_6^-

[a] Abbreviations for IR intensities: vs = very strong, s = strong, m = medium, w = weak, sh = shoulder, br = broad. Experimental Raman intensities are relative to a scale of 1 to 100. [b] Calculated on the M06-2X/aug-cc-pVTZ level of theory. Scaling factor: 0.956. [c] IR intensities in km/mol; Raman intensities in Å^4/u.

Table S6. Experimental vibrational frequencies [cm^{-1}] of $[FS(OD)_2][MF_6]$ (M = As, Sb) and calculated vibrational frequencies [cm^{-1}] of $[FS(OD)_2 \cdot 2HF]^+$.

$[FS(OD)_2][SbF_6]$ (**3**) exp.[a]		$[FS(OD)_2][AsF_6]$ (**4**) exp.[a]		$[FS(OD)_2 \cdot 2HF]^+$ calc.[b,c]	Assignment		
IR	Raman	IR	Raman	IR/Raman			
3105(m)							
2920(m)							
2401(w)							
2160(s, br)	2222(3)	2220(m, br)	2264(4)	2329(189/100)	ν_1	A'	ν_s(OD)
				2291(1499/17)	ν_8	A''	ν_{as}(OD)
		1333(w)					
1192(m)							
999(s)	993(15)	1001(sh)	992(21)	994(159/12)	ν_2	A'	ν_s(SO)
987(s)	983(19)	989(s)	985(27)	986(175/5)	ν_9	A''	ν_{as}(SO)
887(m)	892(2)	885(m)	890(3)	893(65/4)	ν_3	A'	δ(SOD)
832(sh)	840(1)	834(sh)		860(67/0)	ν_{10}	A''	δ(SOD)
812(s)	816(14)	812(s)	814(14)	849(147/9)	ν_4	A'	ν(SF)
544(m)	548(4)	542(w)	550(6)	510(17/2)	ν_5	A'	$\omega(FSO_2)$
482(m)		473(w)		452(47/0)	ν_6	A'	ω(SOD)
				426(8/0)	ν_{11}	A''	ω(SOD)
401(w)	398(5)	399(m)	395(4)	394(138/1)	ν_7	A'	δ(OSO)
378(m)	388(4)	370(w)	379(11)	362(26/1)	ν_{12}	A''	δ(FSO)
Vibrations of the anions MF_6^- (M = As, Sb)							
698(vs)	691(5)	748(m)	749(1)				AsF_6^-; SbF_6^-
673(vs)	673(7)		739(2)				AsF_6^-; SbF_6^-
	657(100)	717(s)	718(4)				AsF_6^-; SbF_6^-
617(s)		675(m)	691(100)				AsF_6^-; SbF_6^-
586(s)	590(8)	640(m)	633(1)				AsF_6^-; SbF_6^-
555(m)		592(m)	596(10)				AsF_6^-; SbF_6^-
530(m)	526(5)	527(w)	524(6)				AsF_6^-; SbF_6^-
	308(4)	409(m)	417(4)				AsF_6^-; SbF_6^-
	287(16)	390(m)					AsF_6^-; SbF_6^-
	274(4)		362(7)				AsF_6^-; SbF_6^-
	268(8)		356(9)				AsF_6^-; SbF_6^-

[a] Abbrevations for IR intensities: vs = very strong, s = strong, m = medium, w = weak, sh = shoulder, br = broad. The experimental Raman intensities are corrected to a scale of 1 to 100 [b] Calculated on the M06-2X/aug-cc-pVTZ level of theory. Scaling factor: 0.956. [c] IR intensities in km/mol; Raman intensities in Å^4/u.

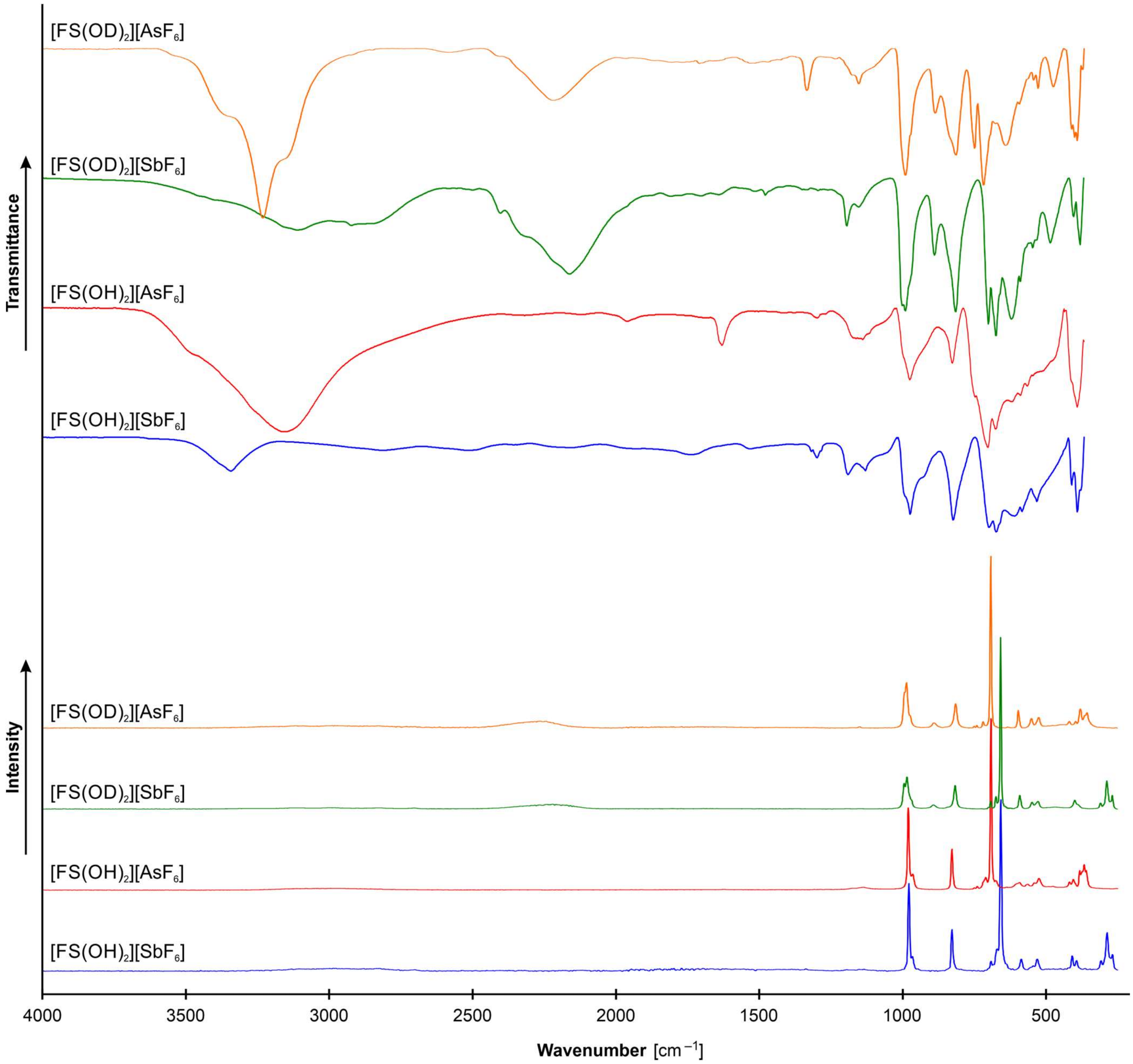

Figure S7. Low-temperature IR and Raman spectra of [FS(O*X*)$_2$][*M*F$_6$] (**1**, **2**, **3**, **4**), (*M* = As, Sb; *X* = H, D).

3.2 $[SOF_2H][(SOF_2)_2H][Sb_2F_{11}]_2$

Table S7. Tentative assignment of experimental vibrational frequencies [cm^{-1}] of $[SOF_2H][(SOF_2)_2H][Sb_2F_{11}]_2$ and calculated vibrational frequencies [cm^{-1}] of $[SOF_2H \cdot HF]^+$ and $[(SOF_2)_2H]^+$.

$[SOF_2H][(SOF_2)_2H][Sb_2F_{11}]_2$		Assignment of overlapping vibrations	$[SOF_2H \cdot HF]^+$ calc.[a,b]				$[(SOF_2)_2H]^+$ calc.[a,b]			
exp. IR	exp. Raman		IR/Raman	Assignment			IR/Raman	Assignment		
3240(vs)										
2577(vw)			2622(2416/98)	ν_1	A'	ν(OH)				
2214(vw)										
1917(vw)										
1637(w)		ν(O···H···O)								
1288(vw)							1315(367/0)	ν_1	A'	δ(SOH)
	1266(3)		1218(49/4)	ν_2	A'	δ(SOH)				
	1181(3)						1215(322/0)	ν_2	A'	ν(SO)
1151(vw)	1167(3)						1207(0/23)	ν_3	A'	ν(SO)
1117(vw)										
1099(vw)							1048(144/0)	ν_{14}	A''	ω(SOH)
1041(vw)	1050(2)		1060(273/4)	ν_3	A'	ν(SO)				
	997(1)									
916(w)	938(1)	ν(SF)					940(1311/0)	ν_4	A'	ν(SF)
	877(15)		898(75/10)	ν_4	A'	ν_s(SF)	880(0/16)	ν_5	A'	ν(SF)
870(w)	863(22)		886(218/4)	ν_7	A''	ν_{as}(SF)	850(332/0)	ν_{15}	A''	ν(SF)
854(w)	842(4)						845(0/9)	ν_{16}	A''	ν(SF)
822(w)	821(6)									
802(w)			775(92/0)	ν_8	A''	ω(OH)				
	551(6)						585(0/6)	ν_6	A'	δ(OSF)
530(vw)	534(4)		540(21/3)	ν_5	A'	$\omega(SOF_2)$				
494(w)	492(2)						535(2653/0)	ν_7	A'	δ(SOH)
457(vw)							497(2981/0)	ν_8	A'	ν(O···H···O)
438(vw)							443(0/4)	ν_9	A'	ν(O···H···O)
411(vw)	414(8)	δ(FSF), δ(OSF)					396(0/2)	ν_{17}	A''	δ(OSF)
397(vw)	397(11)		376(32/0)	ν_6	A'	δ(FSF)	382(0/1)	ν_{10}	A'	δ(FSF)
390(vw)			375(2/1)	ν_9	A''	δ(OSF)	382(10/0)	ν_{18}	A''	δ(OSF)
378(vw)							377(265/0)	ν_{11}	A'	δ(FSF)
							73(0/1)	ν_{12}	A'	δ(SOH)
							67(0/0)	ν_{19}	A''	ω(SOH)
							49(3/0)	ν_{20}	A''	$\omega(SF_2)$
							25(0/0)	ν_{21}	A''	$\omega(SF_2)$
							19(78/0)	ν_{13}	A'	ω(SOH)
Vibrations of the anion $Sb_2F_{11}^-$										
	688(25)	$Sb_2F_{11}^-$								
679(w)	677(100)	$Sb_2F_{11}^-$								
	648(66)	$Sb_2F_{11}^-$								
663(w)		$Sb_2F_{11}^-$								
	616(2)	$Sb_2F_{11}^-$								
598(vw)	604(17)	$Sb_2F_{11}^-$								
	297(20)	$Sb_2F_{11}^-$								
	285(5)	$Sb_2F_{11}^-$								
	277(5)	$Sb_2F_{11}^-$								
	268(6)	$Sb_2F_{11}^-$								

[a] Abbrevations for IR intensities: vs = very strong, s = strong, m = medium, w = weak, vw = very weak, sh = shoulder. Experimental Raman intensities are relative to a scale of 1 to 100. [b] Calculated on the M06-2X/aug-cc-pVTZ level of theory. Scaling factor 0.956. [c] IR intensities in km/mol; Raman intensities in Å^4/u.

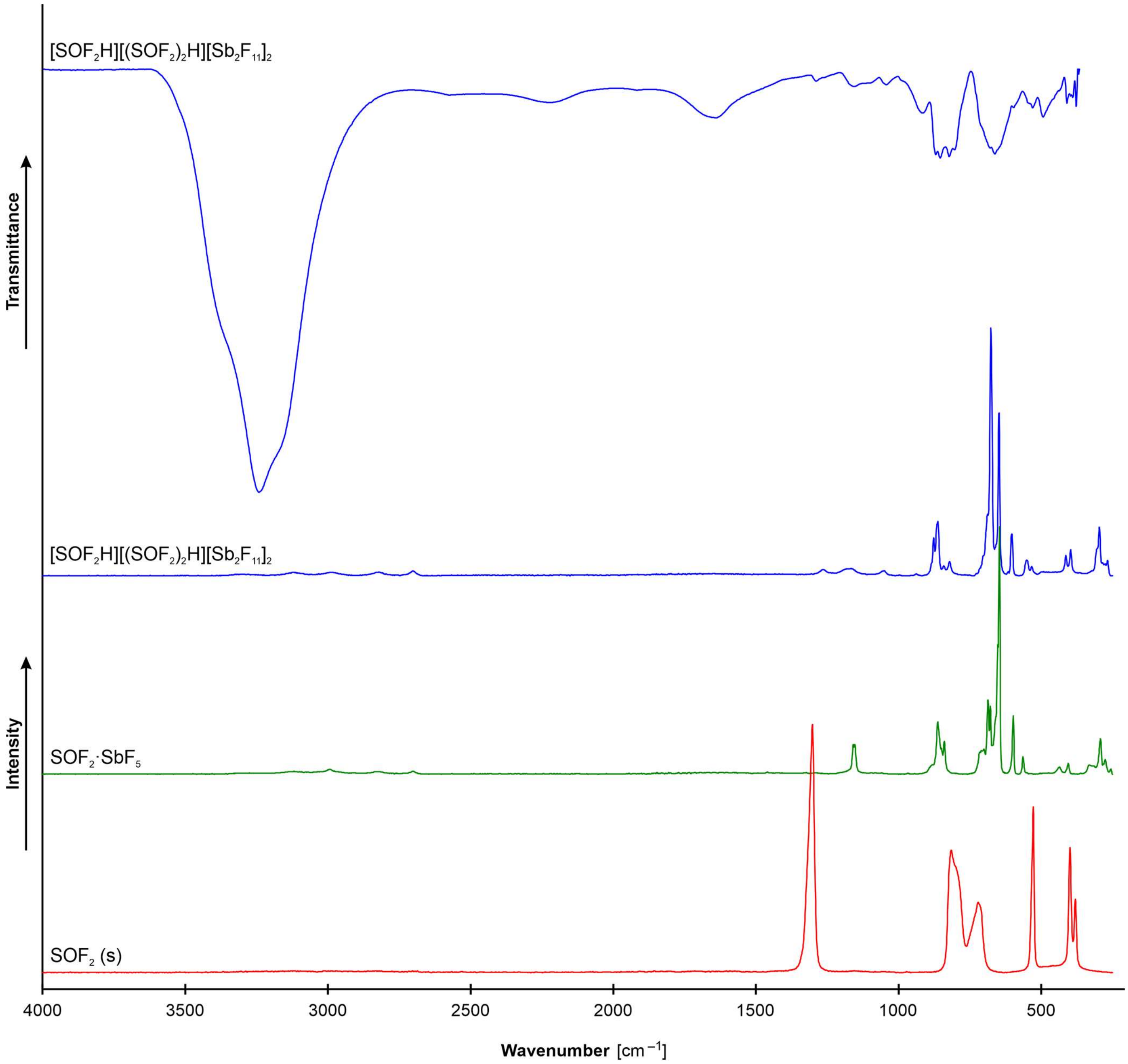

Figure S8. Low-temperature IR and Raman spectra of [SOF$_2$H][(SOF$_2$)$_2$H][Sb$_2$F$_{11}$]$_2$ (**6**) and SOF$_2$·SbF$_5$ (**7**) and solid amorphous SOF$_2$ (−196 °C).

4 NMR

Table S8. Observed ^{1}H and ^{19}F NMR chemical shifts [ppm] during the reaction of $SO_2 \cdot SbF_5$ in *a*HF from −70 °C to 25 °C

Solvent: *a*HF			
	NMR Nucleus / Assigned Species[a] (Chemical Shift δ in ppm)[b]		
Temperature	^{1}H / $[FS(O\mathbf{H})_2]^+$, $FS(O\mathbf{H})O \cdot SbF_5$	^{19}F / $[\mathbf{F}S(OH)_2]^+$	^{19}F / $\mathbf{F}S(OH)O \cdot SbF_5$
-70	10.10 (s)	67.10 (s)	29.20 (s)
-60	10.12 (s)	67.27 (s)	29.29 (s)
-50	10.12 (s)	67.41 (s)	29.41 (s)
-40	10.13 (m)	67.55 (s)	29.49 (s)
-30	10.14 (m)	67.69 (s)	29.56 (s)
-20	10.13 (m)	67.84 (s)	29.65 (s)
-10	10.13 (m)	67.97 (s)	29.71 (s)
0	10.14 (m)	68.12 (s)	29.78 (s)
+25	10.16 (m)	69.51 (s)	Not observed

[a] The observed nuclei in the assigned species are highlighted in bold characters.

[b] The multiplicity of the signal is given in parentheses.

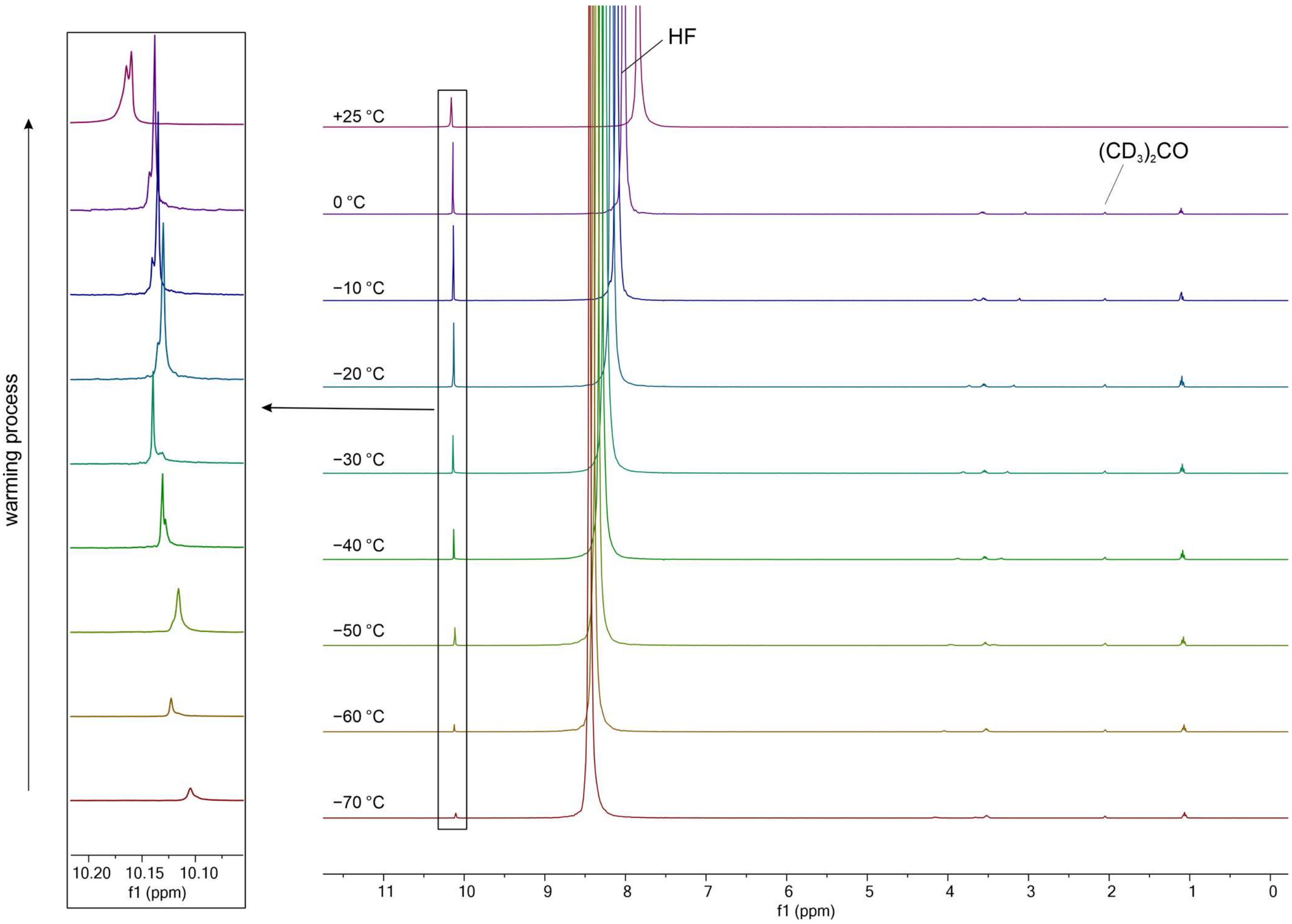

Figure S9. Stacked ^{1}H NMR spectra were measured during the warming process of the reaction of $SOF_2 \cdot SbF_5$ in *a*HF with acetone-D_6 as an external reference. The ^{1}H signals between 1.0 ppm and 4.0 ppm are due to the external reference and ethanol, which was used for cooling the sample. The spectrum at +25 °C was measured in a fresh NMR glass tube without the external reference as a comparison.

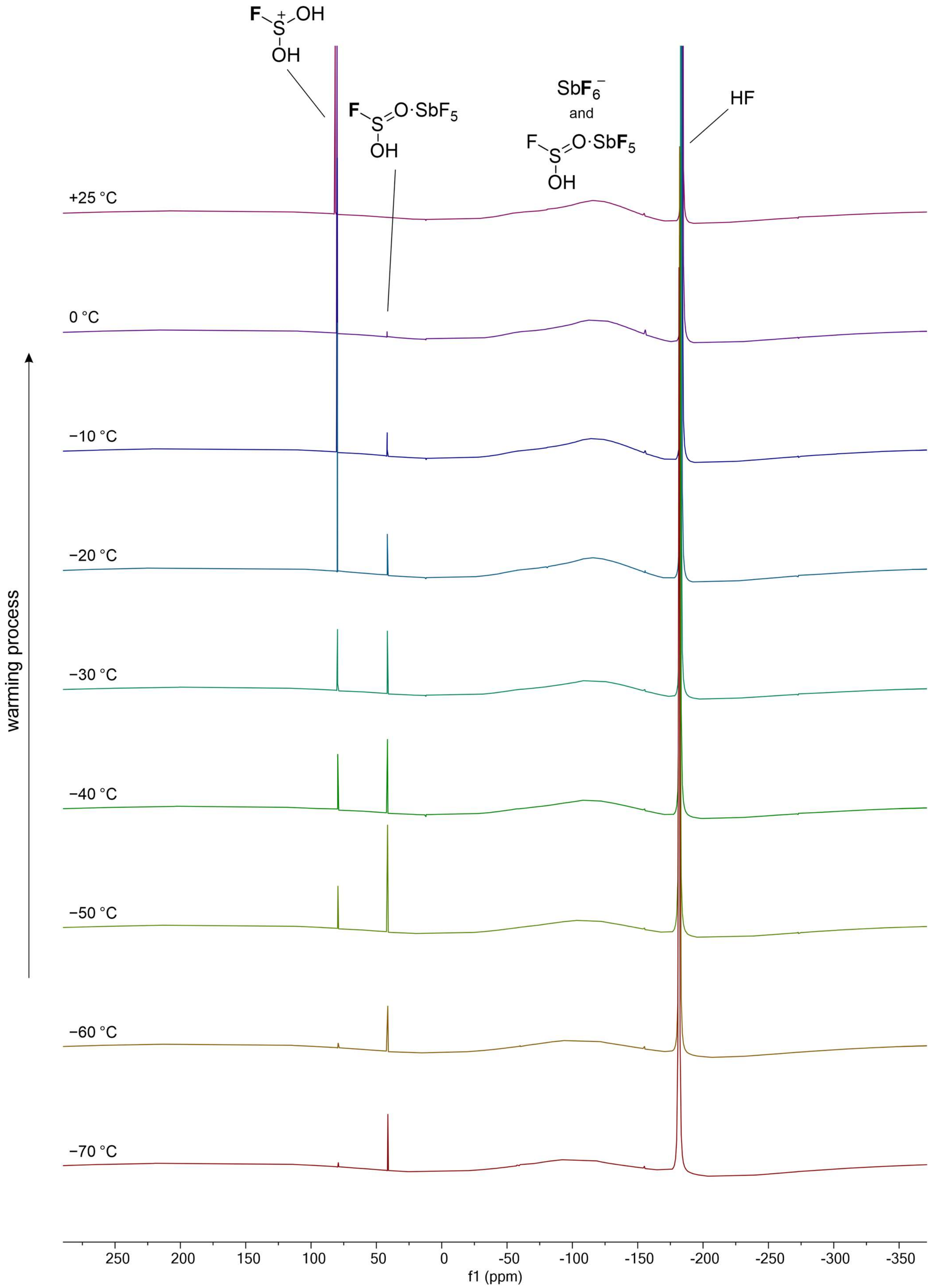

Figure S10. Stacked ^{19}F NMR spectra measured during the warming of the reaction of $SOF_2\cdot SbF_5$ (**7**) in *a*HF.

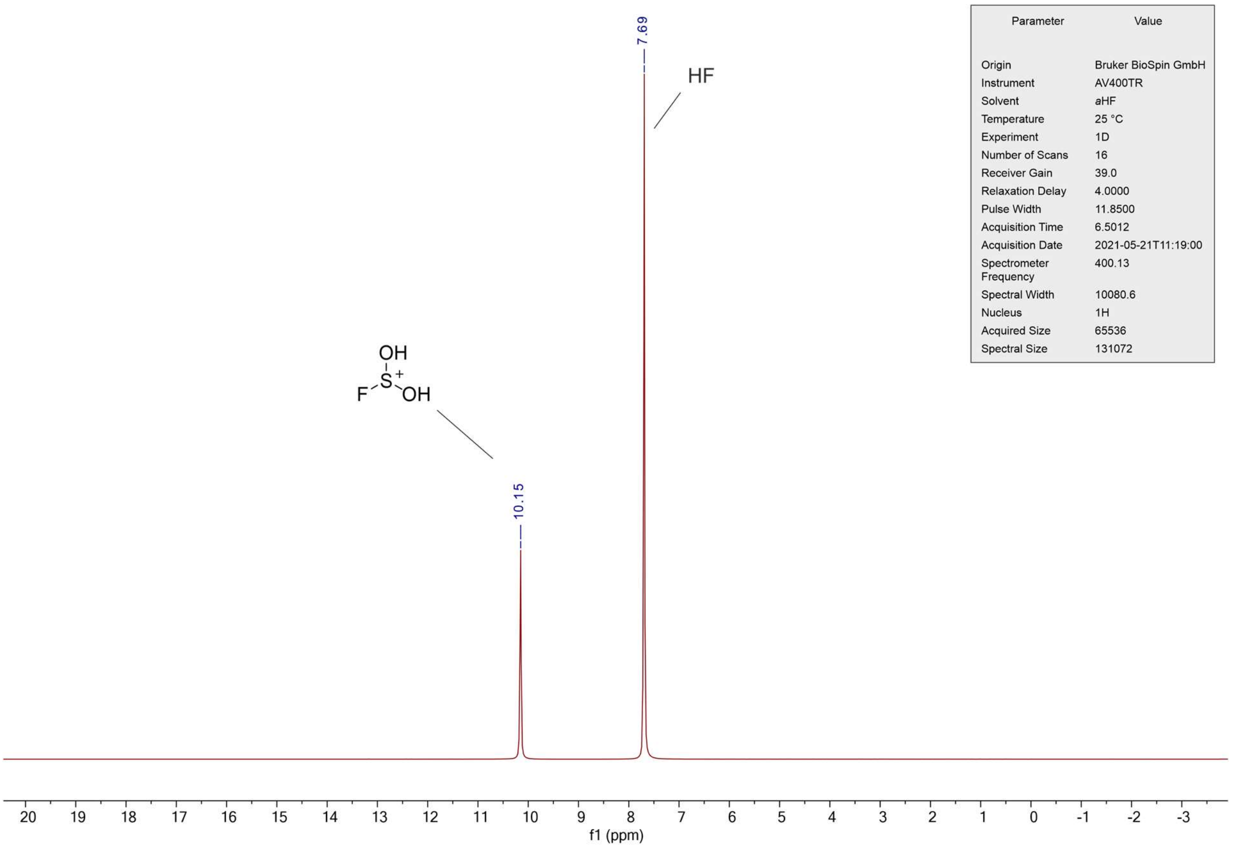

Parameter	Value
Origin	Bruker BioSpin GmbH
Instrument	AV400TR
Solvent	*a*HF
Temperature	25 °C
Experiment	1D
Number of Scans	16
Receiver Gain	39.0
Relaxation Delay	4.0000
Pulse Width	11.8500
Acquisition Time	6.5012
Acquisition Date	2021-05-21T11:19:00
Spectrometer Frequency	400.13
Spectral Width	10080.6
Nucleus	1H
Acquired Size	65536
Spectral Size	131072

Figure S11. ^{1}H NMR spectrum of [FS(OH)$_2$][SbF$_6$] in *a*HF at 25 °C. First, the spectrum was measured with acetone-D$_6$ as an external reference. Then a second measurement was done without the external reference in a fresh NMR tube for a cleaner spectrum. The chemical shifts in the spectrum above correspond to the shifts from the first spectrum, which were referenced to acetone-D$_6$.

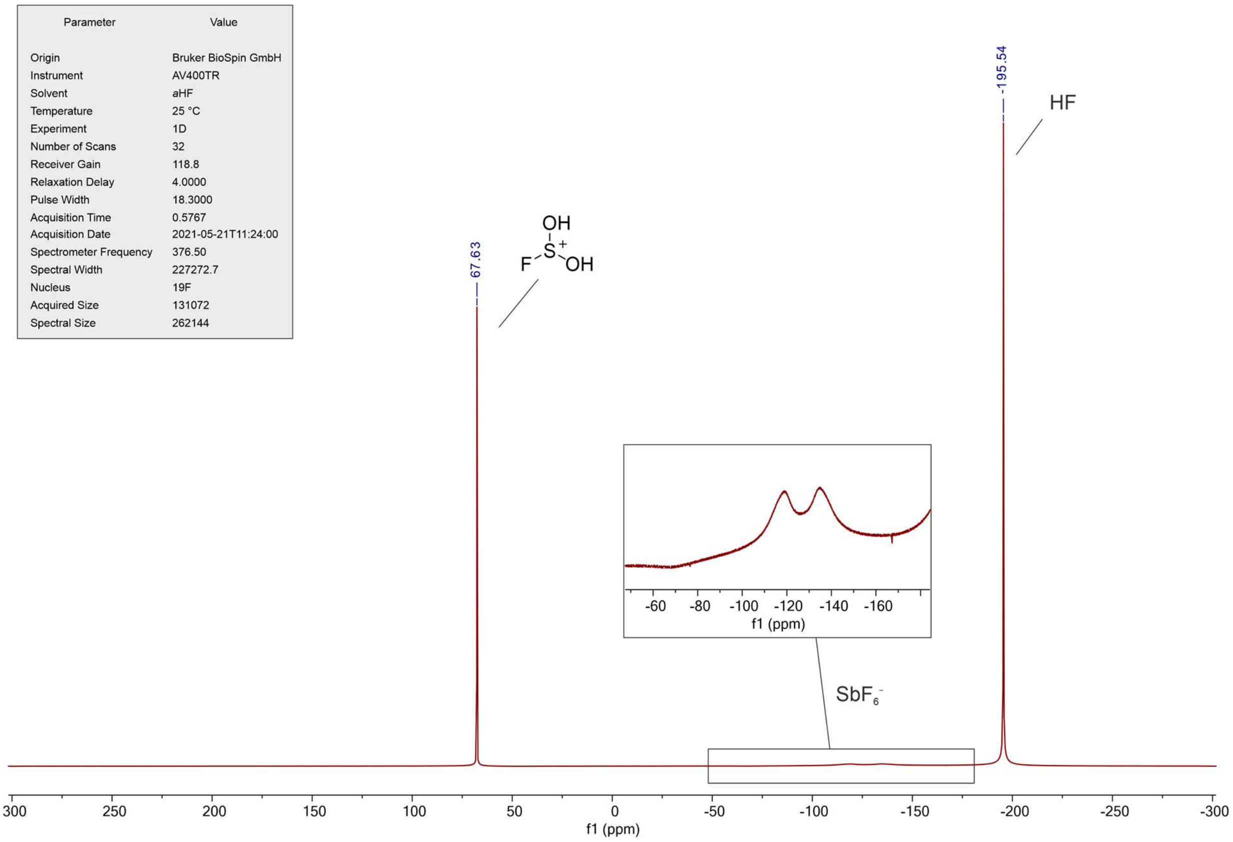

Parameter	Value
Origin	Bruker BioSpin GmbH
Instrument	AV400TR
Solvent	*a*HF
Temperature	25 °C
Experiment	1D
Number of Scans	32
Receiver Gain	118.8
Relaxation Delay	4.0000
Pulse Width	18.3000
Acquisition Time	0.5767
Acquisition Date	2021-05-21T11:24:00
Spectrometer Frequency	376.50
Spectral Width	227272.7
Nucleus	19F
Acquired Size	131072
Spectral Size	262144

Figure S12. ^{19}F NMR spectrum of [FS(OH)$_2$][SbF$_6$] in *a*HF at 25 °C.

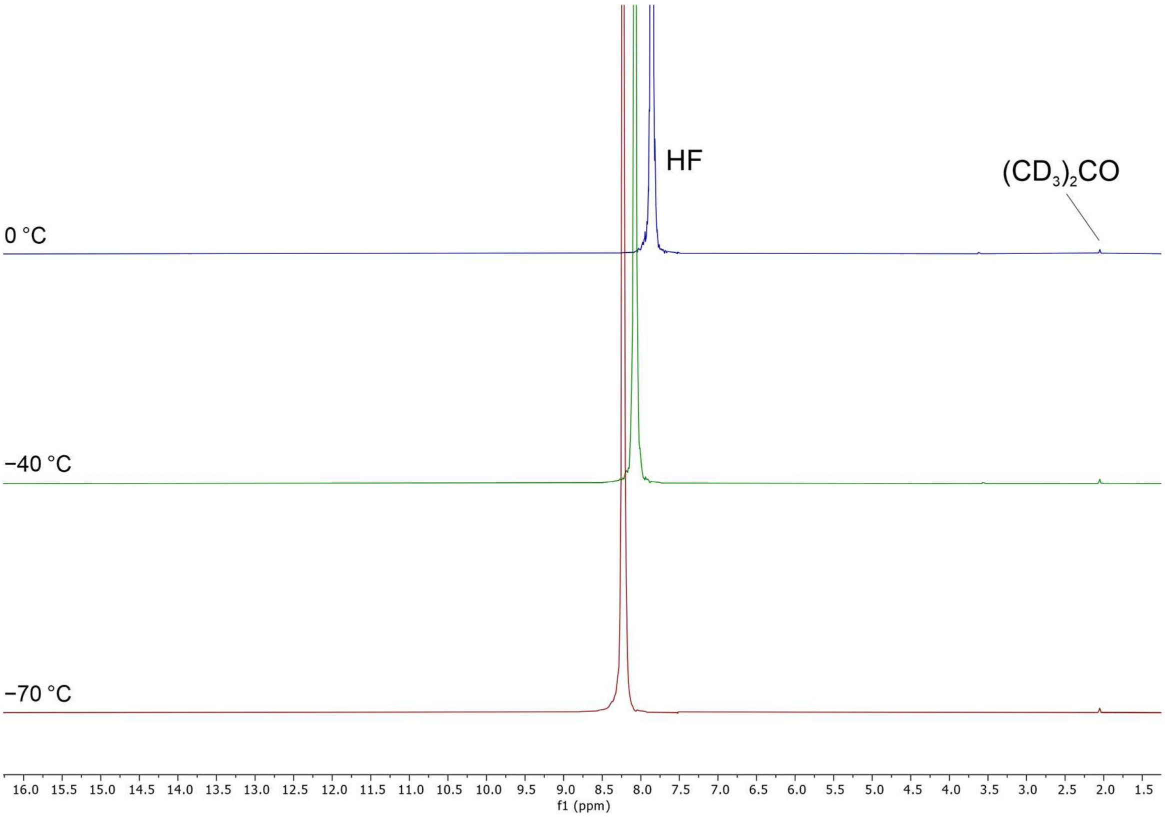

Figure S13. Stacked ^{1}H NMR spectra after the dissolution of [Cs][FSO$_2$] in *a*HF. The sample was frozen at −196 °C before the measurement. The first measurement was done immediately after warming the sample to −70 °C. The spectra at −40 °C and 0 °C were measured after warming to the respective temperature.

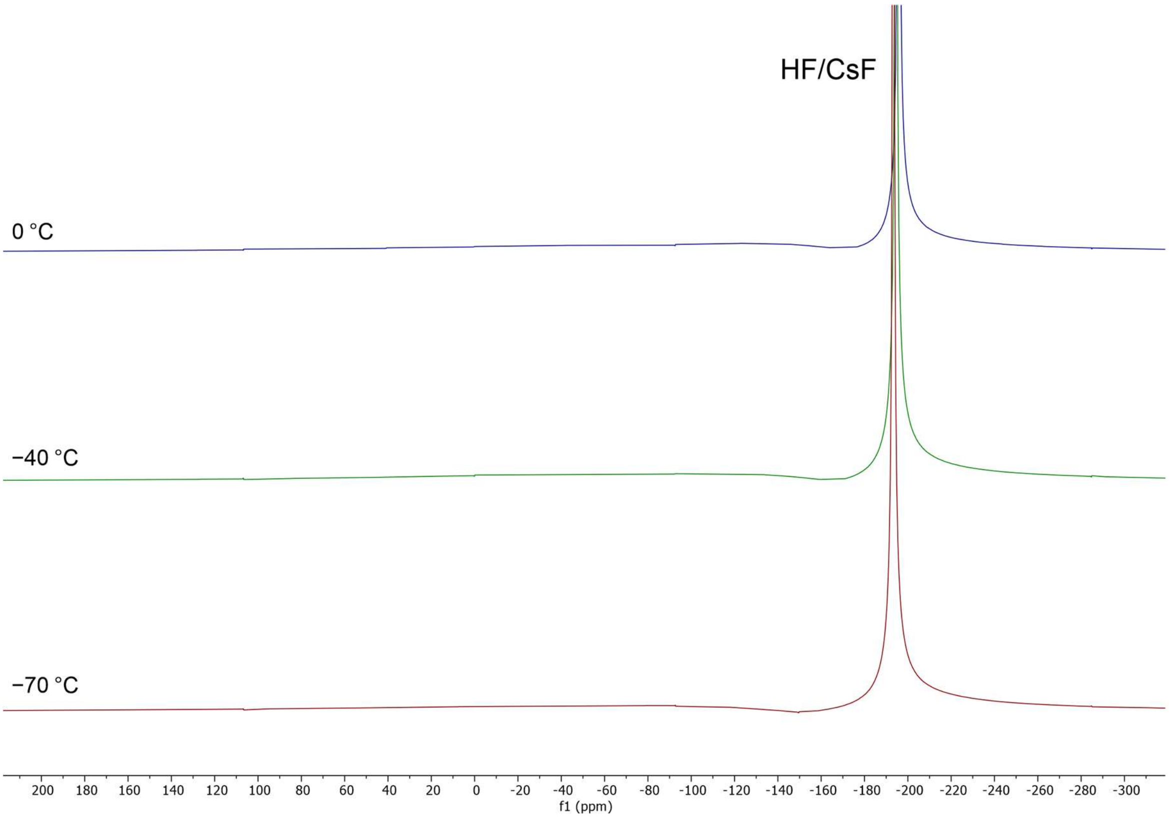

Figure S14. Stacked ^{19}F NMR spectra after the dissolution of [Cs][FSO$_2$] in *a*HF. The sample was frozen at −196 °C before the measurement. The first measurement was done immediately after warming the sample to −70 °C. The spectra at −40 °C and 0 °C were measured after warming to the respective temperature.

5 Quantum Chemical Calculations

The optimized structures are given with their cartesian coordinates x, y, z in angstrom. An illustration of the respective structures together with the calculated bond lengths in angstrom is shown next to the tables. The structure of the complex $FS(OH)O\cdot SbF_5$ was calculated on the MP2/aug-cc-pVTZ level of theory. For antimony, the effective core potential MWB46 was employed. For $FS(OH)O\cdot SbF_5$ three stationary points on the potential energy surface were found, which were confirmed as true minima by a frequency calculation. Figure S15 illustrates the three minimum structures together with their energy difference. Structure **I** was found as the global energetic minimum and is stabilized by an intramolecular hydrogen bond.

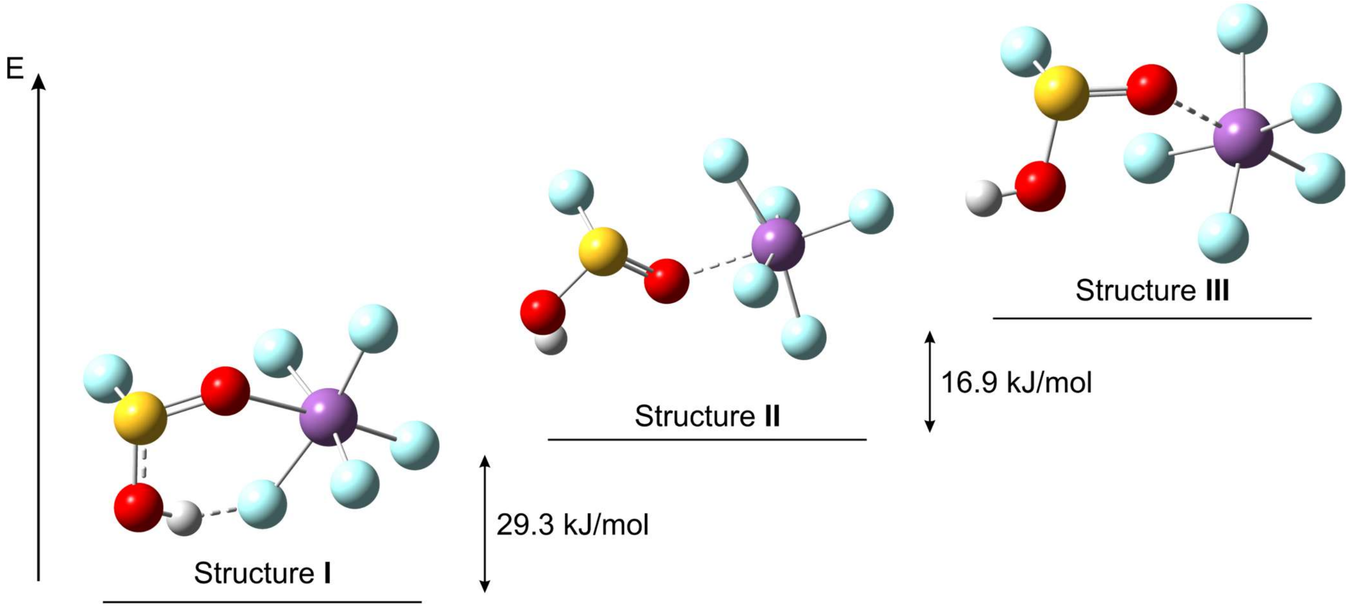

Figure S15. Calculated minimum energy geometries found for the complex $FS(OH)O\cdot SbF_5$ and their respective energy difference.

[$FS(OH)O\cdot SbF_5$] (I)

Energy (MP2/aug-cc-pVTZ): -1152.513683 Hartree

S	2.437177	-0.030497	0.530198	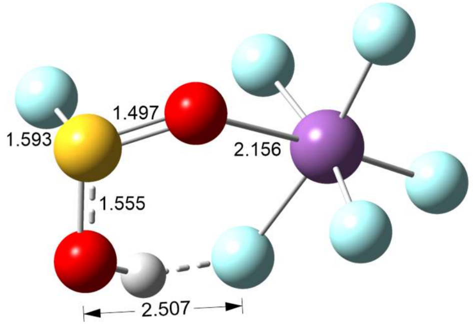
F	2.654381	-1.112858	-0.618719	
O	2.467110	1.265522	-0.328489	
O	1.024103	-0.287743	0.951082	
H	1.601440	1.344009	-0.841720	
Sb	-0.888782	-0.018772	-0.007718	
F	-2.493155	0.291571	-0.894432	
F	-0.962770	1.513005	1.066284	
F	-0.389002	-1.506305	-1.028041	
F	-1.535206	-1.094889	1.372177	
F	0.148184	1.051599	-1.256001	

$[FS(OH)O\cdot SbF_5]$ (II)

Energy (MP2/aug-cc-pVTZ): -1152.502499 Hartree

S	2.232076	-0.062343	-0.357125
F	2.773056	1.321190	0.204662
O	3.406816	-0.993210	0.141980
O	1.121546	-0.376691	0.590352
H	3.305042	-1.178824	1.095679
Sb	-0.968334	-0.005766	0.002657
F	-2.710092	0.330062	-0.557202
F	-0.113761	1.310217	-1.062331
F	-1.319416	-1.419426	1.176356
F	-0.956074	1.194044	1.439206
F	-0.547057	-1.243910	-1.353563

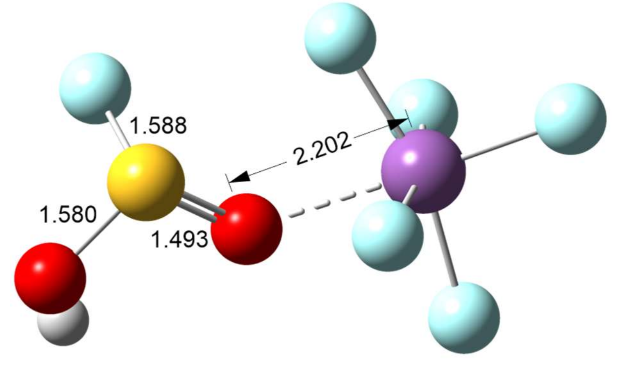

$[FS(OH)O\cdot SbF_5]$ (III)

Energy (MP2/aug-cc-pVTZ): -1152.496049 Hartree

S	2.478002	-0.029606	0.528968
F	2.673284	-1.159870	-0.572167
O	2.460409	1.232804	-0.443057
O	1.078893	-0.148115	0.961377
H	3.370995	1.520062	-0.629896
Sb	-0.920329	0.001191	-0.031253
F	-2.593677	0.123089	-0.837995
F	-0.557337	1.842788	0.030363
F	-0.845742	-1.868555	0.085064
F	-1.487220	0.074177	1.751205
F	0.099951	-0.098807	-1.610499

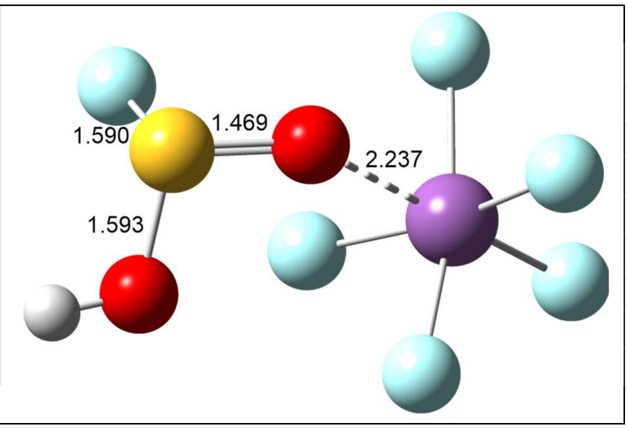

$[FS(OH)_2\cdot 2HF]^+$

Energy (M06-2X/aug-cc-pVTZ): -850.315018 Hartree

F	3.246744	-0.760684	-0.456628
S	0.000000	0.082616	-0.129353
F	0.000000	1.602619	-0.454316
O	1.155644	0.012577	0.880209
O	-1.155644	0.012577	0.880209
H	2.014617	-0.271677	0.467889
H	-2.014617	-0.271677	0.467889
F	-3.246744	-0.760684	-0.456628
H	4.160877	-0.855499	-0.320672
H	-4.160877	-0.855500	-0.320671

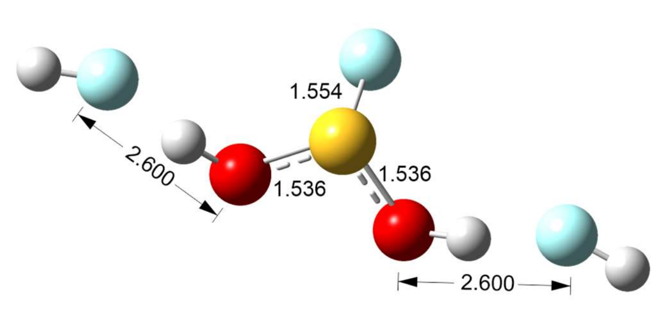

$[FS(OD)_2\cdot 2HF]^+$

Energy (M06-2X/aug-cc-pVTZ): -850.315018 Hartree

F	3.246744	-0.760684	-0.456628
S	0.000000	0.082616	-0.129353
F	0.000000	1.602619	-0.454316
O	1.155644	0.012577	0.880209
O	-1.155644	0.012577	0.880209
D	2.014617	-0.271677	0.467889
D	-2.014617	-0.271677	0.467889
F	-3.246744	-0.760684	-0.456628
H	4.160877	-0.855499	-0.320672
H	-4.160877	-0.855500	-0.320671

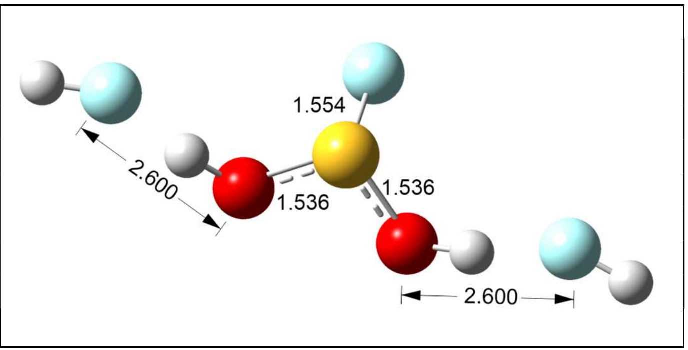

[SOF$_2$H]$^+$

Energy (M06-2X/aug-cc-pVTZ): -673.361695 Hartree

S	0.459985	0.029402	0.000000	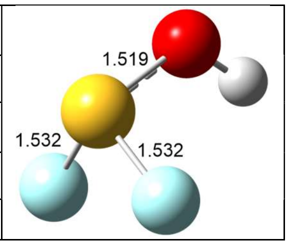
F	-0.236182	-0.718154	1.141343	
F	-0.236182	-0.718154	-1.141343	
O	-0.236182	1.379138	0.000000	
H	-1.219038	1.423238	0.000000	

[SOF$_2$H · HF]$^+$

Energy (M06-2X/aug-cc-pVTZ): -773.842614 Hartree

S	0.944310	-0.000010	0.360292	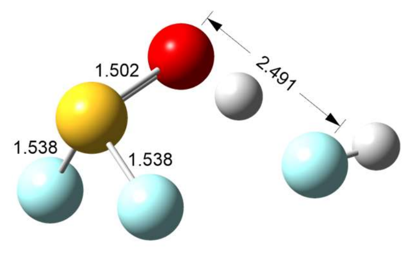
F	0.784094	-1.140969	-0.658961	
F	0.784066	1.141031	-0.658863	
O	-0.369128	-0.000058	1.088440	
H	-1.248222	-0.000038	0.560386	
F	-2.411144	0.000020	-0.337678	
H	-3.320865	-0.000068	-0.133051	

[(SOF$_2$)$_2$H]$^+$

Energy (M06-2X/aug-cc-pVTZ): -1346.507588 Hartree

S	-2.352873	-0.000006	-0.497700	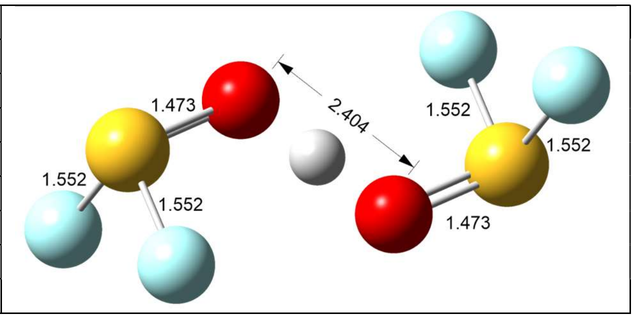
F	-2.526508	-1.142908	0.537824	
F	-2.526478	1.142946	0.537776	
O	-0.908400	-0.000030	-0.787258	
S	2.352897	-0.000002	0.497686	
F	2.526466	-1.142913	-0.537839	
F	2.526442	1.142940	-0.537805	
O	0.908436	-0.000022	0.787329	
H	0.000029	-0.000029	0.000054	

[SO$_2$]

Energy (M06-2X/aug-cc-pVTZ): -548.619552 Hartree

O	0.000000	1.230915	-0.369977	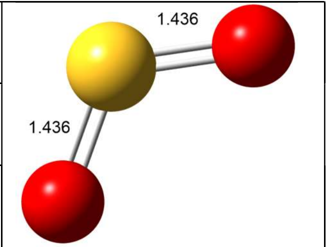
S	0.000000	0.000000	0.369977	
O	0.000000	-1.230915	-0.369977	

[SO$_2$·BF$_3$]

Energy (M06-2X/aug-cc-pVTZ): -873.230620 Hartree

S	1.897511	-0.390062	-0.003045	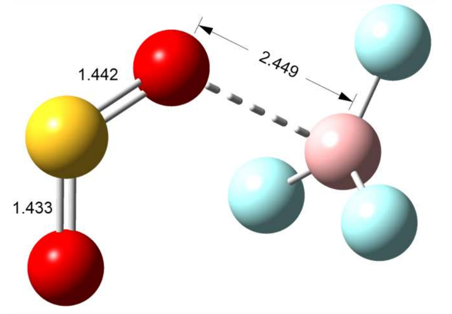
O	1.949474	1.041985	0.002750	
O	0.596176	-1.010817	0.039701	
F	-2.232469	-0.952882	-0.056837	
F	-1.320293	0.743503	1.149966	
F	-1.222006	0.782640	-1.121221	
B	-1.550492	0.166461	-0.007613	

$[SO_2\cdot SbF_5]$

Energy (M06-2X/aug-cc-pVTZ): -1053.415964 Hartree

S	2.673805	-0.428178	0.000106
O	2.826913	0.985685	-0.000089
O	1.310224	-0.960026	-0.000016
Sb	-0.728186	0.034095	-0.000014
F	-2.380297	0.874202	-0.000098
F	0.104972	1.086669	1.309368
F	-1.067044	-1.251207	-1.311677
F	-1.067155	-1.250856	1.311973
F	0.105023	1.086381	-1.309584

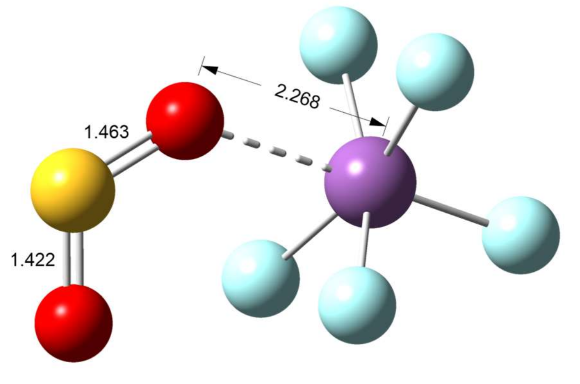

$[SO_2H\cdot HF]^+$

Energy (M06-2X/aug-cc-pVTZ): -649.354746 Hartree

F	-2.285942	0.327896	0.000107
S	1.135262	-0.247850	-0.000056
O	1.016677	1.160726	-0.000026
O	-0.183286	-0.980551	-0.000005
H	-1.083150	-0.471237	0.000047
H	-3.174701	0.044380	0.000129

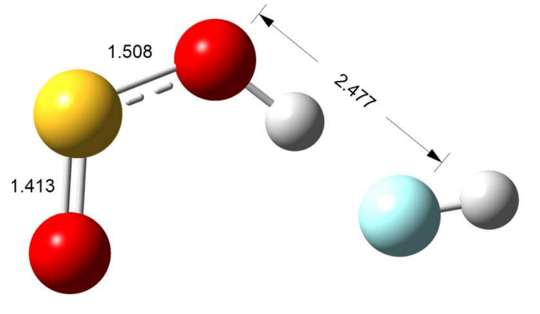

$[SO_2H^+F^-]_{PC}$

Energy (M06-2X/aug-cc-pVTZ): -649.299887 Hartree

F	-0.027955	0.000002	0.020529
S	-0.003743	0.000003	3.463929
O	1.374007	-0.000002	3.144784
O	-0.917520	0.000012	2.269383
H	-0.553541	0.000009	1.282505
PC[a]	-0.429300	0.000000	-0.828300

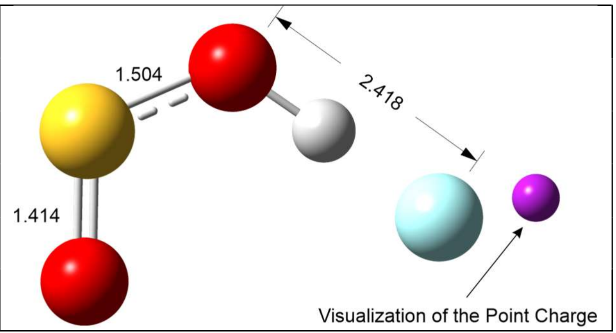

[a] Point charge with charge +1.0.

6 References

[1] L. Bayersdorfer, R. Minkwitz, J. Jander, *Z. Anorg. Allg. Chem.* **1972**, *392*, 137.

[2] Rigaku Oxford Diffraction, CrysAlisPro Software System, *Version 1.171.39.46e*, Rigaku Corporation,Oxford, UK, **2018**.

[3] G. M. Sheldrick, *Acta crystallographica. Section A, Foundations and advances* **2015**, *71*, 3.

[4] G. M. Sheldrick, *Acta crystallographica. Section C, Structural chemistry* **2015**, *71*, 3.

[5] L. J. Farrugia, *J. Appl. Crystallogr.* **1999**, *32*, 837.

[6] A. L. Spek, *J. Appl. Crystallogr.* **2003**, *36*, 7.

[7] *SCALE3 ABSPACK, An Oxford Diffraction Program*, Oxford Diffraction Ltd, UK, **2005**.

[8] C. F. Macrae, I. Sovago, S. J. Cottrell, P. T. A. Galek, P. McCabe, E. Pidcock, M. Platings, G. P. Shields, J. S. Stevens, M. Towler et al., *J. Appl. Crystallogr.* **2020**, *53*, 226.

[9] a) S.K. Wolff, D.J. Grimwood, J.J. McKinnon, M.J. Turner, D. Jayatilaka, M.A. Spackman, *CrystalExplorer 17.5, Revision: f4e298a*, University of Western Australia, **2017**; b) M. A. Spackman, D. Jayatilaka, *CrystEngComm* **2009**, *11*, 19.

[10] Mestrelab Research S.L., *MestReNova Version 14.0.0*, **2019**.

[11] a) M. J. Frisch, G. W. Trucks, H. B. Schlegel, G. E. Scuseria, M. A. Robb, J. R. Cheeseman, G. Scalmani, V. Barone, B. Mennucci, G. A. Petersson, H. Nakatsuji, M. Caricato, X. Li, H. P. Hratchian, A. F. Izmaylov, J. Bloino, G. Zheng, J. L. Sonnenberg, M. Hada, M. Ehara, K. Toyota, R. Fukuda, J. Hasegawa, M. Ishida, T. Nakajima, Y. Honda, O. Kitao, H. Nakai, T. Vreven, J. A. Montgomery, J. E. Peralta, F. Ogliaro, M. Bearpark, J. J. Heyd, E. Brothers, K. N. Kudin, V. N. Staroverov, R. Kobayashi, J. Normand, K. Raghavachari, A. Rendell, J. C. Burant, S. S. Iyengar, J. Tomasi, M. Cossi, N. Rega, J. M. Millam, M. Klene, J. E. Knox, J. B. Cross, V. Bakken, C. Adamo, J. Jaramillo, R. Gomperts, R. E. Stratmann, O. Yazyev, A. J. Austin, R. Cammi, C. Pomelli, J. W. Ochterski, R. L. Martin, K. Morokuma, V. G. Zakrzewski, G. A. Voth, P. Salvador, J. J. Dannenberg, S. Dapprich, A. D. Daniels, O. Farkas, J. B. Foresman, J. V. Ortiz, J. Cioslowski, D. J. Fox, *Gaussian09, Revision A.02*, Gaussian, Inc, Wallingford CT, **2009**; b) M. J. Frisch, G. W. Trucks, H. B. Schlegel, G. E. Scuseria, M. A. Robb, J. R. Cheeseman, G. Scalmani, V. Barone, G. A. Petersson, H. Nakatsuji et al., *Gaussian16 Revision C.01*, **2016**.

[12] Roy Dennington, Todd A. Keith, John M. Millam, *GaussView Version 6*, **2019**.

[13] a) F. Seel, L. Riehl, *Z. Anorg. Allg. Chem.* **1955**, *282*, 293; b) A. Kornath, F. Neumann, R. Ludwig, *Inorg. Chem.* **1997**, *36*, 5570.

[14] a) E. E. Aynsley, R. D. Peacock, P. L. Robinson, *Chem. Ind.* **1951**, 1117; b) R. Minkwitz, W. Molsbeck, H. Preut, *Zeitschrift für Naturforschung B* **1989**, *44*, 1581.

[15] A. Kornath, R. Seelbinder, R. Minkwitz, *Angew. Chem. Int. Ed. Engl.* **2005**, *44*, 973.

[16] A. Bondi, *J. Phys. Chem.* **1964**, *68*, 441.

A Neutron Makes the Difference - Structures of Malonyl Difluoride and its Protonated Species in Condensed Media

Christoph Jessen,[a],[b] Dirk Hollenwäger, [a] and Andreas J. Kornath*[a],[b]

[a] C. Jessen, D. Hollenwäger, Prof. Dr. A. J. Kornath
Department Chemie
Ludwig-Maximilians-Universität München
Butenandtstr. 5–13, 81377 München, Germany
E-mail: andreas.kornath@cup.uni-muenchen.de
[b] C. Jessen, Prof. Dr. A. J. Kornath
F-Select GmbH
Semmelweisstrasse 5
82152 Planegg

Supporting information for this article is given via a link at the end of the document.

Abstract: Malonyl difluoride was investigated in the condensed phase and its behavior in superacidic solutions was elucidated. The salts of hemi-, mono, and diprotonated malonyl difluoride were isolated as products, depending on the stoichiometric ratio of Lewis acid in the reaction mixture. The neutral compound, as well as the salts of the protonated species, were characterized by Raman spectroscopy, single-crystal X-Ray structure analyses, and NMR spectroscopy. The H/D isotopologues of monoprotonated malonyl difluoride exhibit different structures in their respective crystal structures. This phenomenon of H/D isotopic polymorphism is also observable by vibrational spectroscopy. Additionally, NMR spectroscopic measurements were performed to investigate the structure of monoprotonated malonyl difluoride in *a*HF solution. Quantum chemical calculations were employed to investigate the energetically favored structure of the isolated monoprotonated malonyl difluoride cation and if diprotonated malonyl difluoride is a 1,3-dicationic gitonic superelectrophile.

Introduction

The 1,3-dicarbonyl or *β*-dicarbonyl motif is ubiquitous in natural products and all fields of chemistry. It is applied for condensation reactions in organic chemistry as well as a chelating ligand in inorganic chemistry.[1,2] A prominent characteristic of *β*-dicarbonyl compounds is their keto-enol tautomerism.[2] The equilibrium between the diketo and enol forms is highly influenced by the carbonyl substituents (Equation 1).

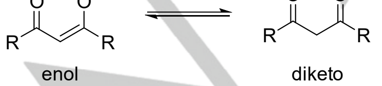

(1)

Understanding and predicting this equilibrium has been the objective of extensive theoretical and structural studies of *β*-dicarbonyl compounds.[3,4] As a result, the substituents are divided into two groups. Group **I** substituents like R = H, CH_3, CF_3, $C(CH_3)_3$ favor the enol tautomer, whereas group **II** substituents with free lone pairs like R = F, Cl, OMe, NH_2 favor the diketo structure.[3] Gas electron diffraction (GED) experiments by *Oberhammer et al.* showed that malonyl dichloride (R = Cl) and malonyl difluoride (R = F) exclusively exist in the diketo form in the gas phase.[5–8] An additional characteristic of the diketo tautomers of *β*-dicarbonyl is their conformation, meaning the relative orientation of the two C=O groups as shown in Figure 1. In the gas-phase, the three dominant conformations are the U-cis (C−C−C−O = 0°), S-gauche, and W-gauche conformations.[5–8] An additional possible conformation is the U-gauche conformation with 0° < C−C−C−O < 51° and C_2 symmetry.[8] The gas phase structure of malonyl difluoride was determined by GED to be a mixture of 90% S-gauche and 10% W-gauche.[8]

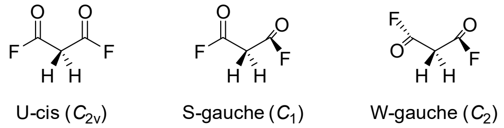

Figure 1. Conformations of malonyl difluoride in the gas phase.

Upon monoprotonation, *β*-dicarbonyl compounds also form different structures depending on the carbonyl substituents.[9] *Brouwer* investigated several *β*-dicarbonyl compounds in superacidic media by NMR spectroscopy.[9] In solution, the monoprotonation either leads to a dihydroxyallyl type cation corresponding to the protonated enol form (group **I** substituents)[9–12] or a hydroxycarbenium cation corresponding to a protonated diketo form (group **II** substituents).[9] The substituents do not influence the structure of the diprotonated species, leading to a 1,3-dicarbenium ion, respectively.[9]

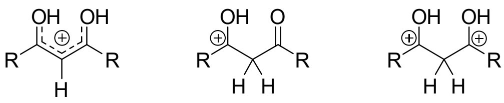

However, very little is known about the solid-state structure of protonated *β*-dicarbonyl compounds. Recently, we reported on the protonation of malonic acid in the superacidic system HF/SbF_5. The cation in the salt of monoprotonated malonic acid exhibits an intramolecular hydrogen bond, forming a six-membered ring-like structure.[13]

By combining research on the structure of neutral β-dicarbonyl and their protonated species, we were first interested in elucidating the structure of malonyl difluoride in the solid state. Subsequently, we were motivated to investigate the influence of protonation on the structure of malonyl difluoride and, in particular, to find out whether a dihydroxyallyl cation structure could form upon monoprotonation. In addition, the diprotonation of malonyl difluoride was of interest with respect to the formation of a possible 1,3-superelectrophile.

Results and Discussion

Syntheses

Malonyl difluoride (**1**) was synthesized according to *Oberhammer*.[8] Single crystals of **1** were grown from a 1,1,1,2-tetrafluoroethane solution at −70 °C. The protonation of malonyl difluoride is achieved by reacting the compound with the binary superacidic system XF/SbF$_5$ (X = D, H) in a two-step synthesis. First, the superacid is formed by mixing SbF$_5$ with *a*XF at −40 °C. Then the superacid is frozen at −196 °C to add the designated amount of malonyl difluoride. Upon warming up to −60 °C the reaction of the starting material and the superacid takes place. The reactants are thoroughly mixed to complete dissolution at −60 °C. Then volatile components are removed in a dynamic vacuum at −78 °C to afford the products as colorless salts. When *a*DF is used as solvent and reactant instead of *a*HF, the deuterated species at the site of protonation is obtained. The observed products are shown in Scheme 1. The stoichiometric amount of SbF$_5$ compared to malonyl difluoride determines the degree of protonation of the product. Application of equimolar amounts of Lewis acid and **1** leads to the salts of monoprotonated malonyl difluoride [FOC−CH$_2$−C(OH)F][SbF$_6$] (**2**) and [FOC−CH$_2$−C(OD)F][SbF$_6$] (**3**). Interestingly, the structures of the two isotopologues differ affecting the crystal structure and vibrational spectra, respectively. The diprotonated species [F(XO)C−CH$_2$−C(OX)F][SbF$_6$]$_2$ (X = H (**4**), D (**5**)) are obtained upon application of two equivalents of SbF$_5$ compared to **1**. Additionally, a salt of hemiprotonated malonyl difluoride (**6**) is isolated, when the reaction is performed with two equivalents of malonyl difluoride compared to the Lewis acid.

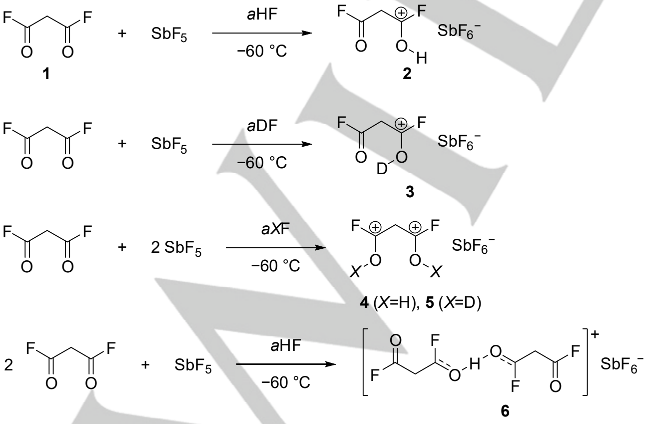

Scheme 1. Syntheses of mono- (**2**, **3**), di- (**4**, **5**), and hemiprotonated (**6**) malonyl difluoride species.

Crystal Structures

Malonyl difluoride crystallizes in the monoclinic space group C_2 with six units per unit cell. The melting point of the solid is around −32 °C. The two crystallographically independent formula units of **1** are shown in Figure 2. Selected geometrical parameters of **1** are listed in Table 1 together with reported data for malonyl difluoride from gas electron diffraction (GED) experiments.[8] Two crystallographically independent malonyl difluoride molecules are present in the unit cell. Molecule **1a** exhibits C_1 symmetry, whereas molecule **1b** occupies a special position with C_2 symmetry. In the crystal structure, malonyl difluoride shows the diketo form, which was also observed in the gas phase by *Oberhammer et al.*[8] However, the non-planar U-gauche conformation is observed for **1a** and **1b** in the solid state, which has no relevance in the gas-phase structure. The geometrical parameters of **1** agree very well with the data from the GED.[8] In structure **1a** the C1−F1 bond is slightly elongated compared to the other C−F bonds due to an intermolecular C···F contact (C4···F1: 3.022(2) Å). The COF groups in both molecules are twisted to each other, causing the non-planar structure.

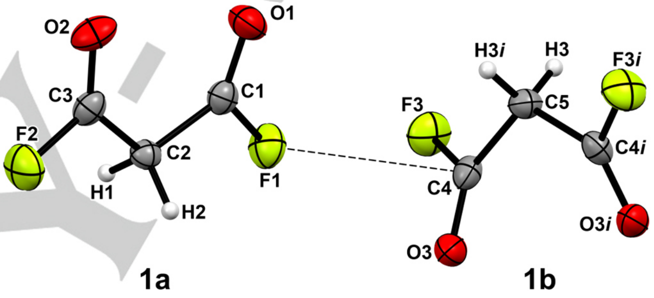

Figure 2. Two independent formula units of malonyl difluoride (**1**) consisting of the two crystallographically independent molecules **1a** and **1b** (50% probability displacement ellipsoids). Symmetry code: *i* = 1−x, y,1−z.

Monoprotonated malonyl difluoride crystallizes in two different crystal structures depending on the superacidic system of either DF/SbF$_5$ or HF/SbF$_5$. The formula units of the two crystal structures are shown in Figure 3 and Figure 5, respectively. The geometrical parameters are summarized in Table 2. From an *a*HF solution, the salt [FOC−CH$_2$−C(OH)F][SbF$_6$] (**2**) crystallizes in the orthorhombic space group $P2_12_12_1$ with four formula units per unit cell.

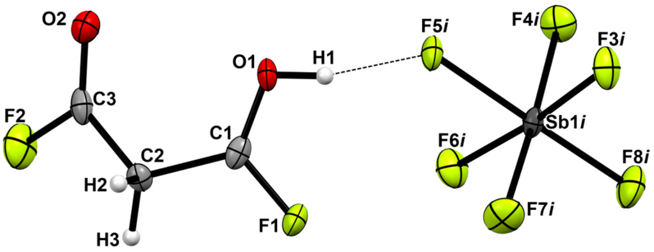

Figure 3. Formula unit of monoprotonated malonyl difluoride (**2**) with 50% probability displacement ellipsoids. Symmetry code: *i* = −1+x,y,z.

Table 1. Selected geometrical parameters of malonyl difluoride in the crystal structure **1** and the gas phase from GED experiments.[8] Symmetry code: *i* = 1−x, y,1−z.

	1a	**1b**	literature GED[8]
Symmetry	C_1	C_2	C_1
Conformation	U-gauche	U-gauche	90% S-gauche 10% W-gauche
Bond lengths [Å]			
C−C	1.486(2) (C1−C2)	1.492(2) (C4−C5)	1.502(5)
	1.492(2) (C2−C3)		
C−F	1.357(2) (C1−F1)	1.340(2) (C4−F3)	1.349(4)
	1.340(2) (C3−F2)		
C−O	1.170(2) (C1−O1)	1.172(2) (C4−O3)	1.177(3)
	1.172(2) (C3−O2)		
Bond angles [°]			
C−C−C	114.5(1) (C1−C2−C3)	112.9(2) (C4−C5−C4*i*)	110.2(10)
F−C−O	119.7(2) (F1−C1−O1)	120.1(1) (F3−C4−O3)	121.2(11)
C−C−F	109.0(1) (C2−C1−F1)	110.5(1) (C5−C4−F3)	109.7(7)
C−C−O	131.4(2) (C2−C1−O1)	129.3(2) (C5−C4−O3)	129.1(8)
Torsion angles [°]			
C−C−C−O	2.8(3) (C1−C2−C3−O2)	25.6(1) (C4−C5−C4*i*−O3*i*)	112.0(20)

The O-protonation mainly affects the protonated acyl fluoride group. Upon protonation, the C1−O1 bond length is significantly elongated to 1.218(9) Å, while the C1−F1 bond length is significantly shortened to 1.289(8) Å. This is in agreement with results from protonated acyl fluoride groups in the literature.[14,15] The bond lengths of the unprotonated acyl fluoride group and the C−C bonds do not change compared to the starting material. A noticeable characteristic of the cation of **2** is that both acyl fluoride groups are twisted out of the molecular plane. This is explained considering the interionic contacts in the crystal structure of **2** which are depicted in Figure 4. Four C···F contacts to adjacent anions below the sum of the van-der-Waals (VDW) radii (3.17 Å)[16] are observed, two of which are formed by one single fluorine atom F4*iv*. The acidic proton is involved in the short hydrogen bond O1−H1···F5*i* (2.428(5) Å), which is characterized as a strong hydrogen bond according to the classification of *Jeffrey*.[17]

Table 2. Selected geometrical parameters of $[FOC-CH_2-C(OH)F][SbF_6]$ (**2**), $[FOC-CH_2-C(OD)F][SbF_6]$ (**3**), $[F(HO)C-CH_2-C(OH)F][SbF_6]_2$ (**4**), and $[(FOC-CH_2-COF)_2H][SbF_6]$ (**6**) with estimated standard deviations in parentheses. Symmetry codes: *i* = −1+x, y, z; *ii* = −x, 2−y, 1−z; *iii* = 1−x, 2−y, 1−z; *iv* = x,y,1+z.

	2	**3a**	**4**	**6**
Bond lengths [Å]				
C1−C2	1.487(9)	1.471(3)	1.477(4)	1.477(3)
C2−C3	1.511(11)	1.488(3)	1.482(4)	1.494(3)
C1−F1	1.289(8)	1.277(3)	1.285(3)	1.298(2)
C3−F2	1.329(10)	1.324(3)	1.285(3)	1.346(2)
C1−O1	1.218(9)	1.239(3)	1.212(4)	1.214(2)
C3−O2	1.163(8)	1.188(3)	1.219(4)	1.175(2)
Bond angles [°]				
C1−C2−C3	111.9(6)	112.4(2)	115.4(2)	117.5(2)
F1−C1−O1	119.6(6)	114.8(2)	120.1(3)	119.4(2)
F2−C3−O2	121.8(10)	121.3(2)	120.0(3)	120.4(2)
C2−C1−F1	115.9(6)	116.7(2)	114.4(3)	118.1(2)
C2−C3−F2	110.4(7)	111.9(2)	113.5(3)	108.3(2)
C2−C1−O1	124.4(6)	128.4(2)	125.4(3)	122.4(2)
C2−C3−O2	127.8(10)	126.8(2)	126.4(3)	131.3(2)
Donor-acceptor distances[a] (D−*X*···A)[b] [Å]				
	2.428(5) (O1···F5*i*)	2.745(2) (O1···F14*ii*)	2.397(3) (O1···F5)	2.444(2) (O1···O1*iii*)
		2.824(2) (O1···F15*iv*)	2.377(3) (O2···F10)	
		2.625(2) (O1···O2)		

[a] Donor-acceptor distances of the hydrogen bonds in which the acidic protons are involved. [b] *X* = D, H.

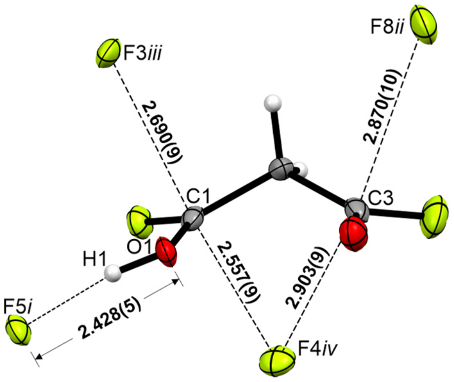

Figure 4. Interionic contacts of monoprotonated malonyl difluoride (**2**) with 50% probability displacement ellipsoids. The SbF_6^- anions are reduced to the contacting fluorine atoms for better visualization. The distances are given in [Å]. Symmetry codes: *i* = −1+x,y,z; *ii* = 1.5−x,1−y,−0.5+z; *iii* = −0.5+x,0.5−y,1−z; *iv* = −0.5+x,1.5−y,1−z.

From *a*DF the deuterated salt [FOC−CH$_2$−C(OD)F][SbF$_6$] (**3**) crystallizes in the triclinic space group $P\bar{1}$ with four formula units per unit cell. The asymmetric unit consists of two crystallographically independent FOC−CH$_2$−C(OD)F$^+$ cations (**3a**, **3b**) and SbF$_6^-$ anions (Figure 5). Since the geometrical parameters of the two cations **3a** and **3b** are equal within their estimated standard deviations, cation **3a** is discussed below. Compared to the cation in **2**, the protonation also takes place at an oxygen atom of one acyl fluoride group. However, the acidic deuterium forms an intramolecular hydrogen bond with the oxygen of the remaining acyl fluoride group. This leads to a different stabilization of the positive charge affecting the entire cation. Compared to **1**, the C1−O1 bond in **3a** is significantly elongated to 1.239(3) Å while the C1−F1 bond is significantly shortened to 1.277(3) Å. In the unprotonated acyl fluoride group, the C3−O2 bond is also slightly elongated while the C3−F2 bond is slightly shortened, respectively. Also the C1−C2 bond length is slightly shortened and measures 1.471(3) Å. The C2−C3 bond distance is unaffected by the protonation. In a direct comparison of the respective bond lengths of the cations in **3** and **2,** no significant difference is elucidated due to the high estimated standard deviations of **2**.

As mentioned above, the interionic contacts and the stabilization of the acidic proton/deuterium constitutes the most significant difference between the monoprotonated isotopologues **2** and **3**. An illustration of interionic contacts in the crystal structure of **3** is found in Figure S5 in the Supporting Information. The characteristic contacts of **3** are the intramolecular hydrogen bonds O1−D1···O2 (2.625(2) Å) and O3−D2···O4 (2.637(3) Å) (Figure 5). According to the classification of *Jeffrey*, these hydrogen bonds are considered moderate.[17] A similar structure with an intramolecular hydrogen bond was found for monoprotonated malonic acid.[13] As in monoprotonated malonic acid, the intramolecular hydrogen bonds in **3** cause a nearly planar geometry of the cations. However, the intramolecular hydrogen bond in the crystal structure of monoprotonated malonic acid is significantly shorter, forming a six-membered ring-like structure.[13] The deuterium in **3** is involved in other hydrogen bonding apart from the intramolecular interaction. Cation **3a** forms two moderate hydrogen bonds O1−D1···F14*ii* (2.745(2) Å) and O1−D1···F14*ii* (2.824(2) Å). Cation **3b** forms only one additional hydrogen bond O3−D2···F9 measuring 2.708(2) Å (Figure S5).

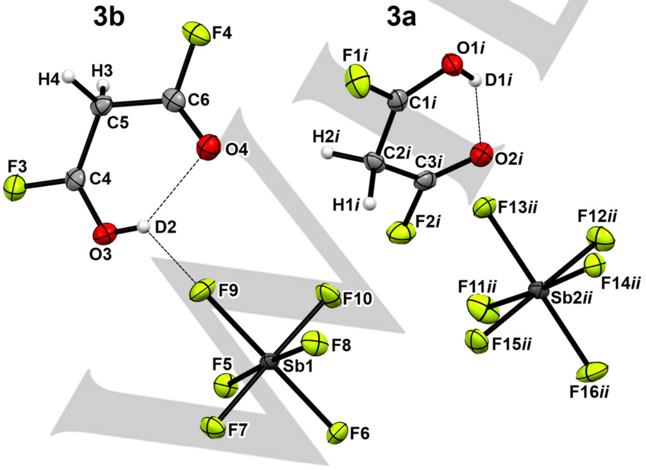

Figure 5. Formula unit of the deuterium isotopologue of monoprotonated malonyl difluoride (**3**) with 50% probability displacement ellipsoids. Symmetry codes: *i* = 1+x,y,z; *ii* = x,y,1+z.

The formation of different crystal structures upon the replacement of H for D especially in hydrogen bonds is described as the rare phenomenon of isotopic polymorphism.[18,19] It is based on small energetic changes depending on the isotope which is involved in the hydrogen bonding.[19,20] Known compounds that exhibit isotopic polymorphism include oxalic acid dihydrate,[21] trifluoroacetic acid tetrahydrate,[22] pyridine,[18] or the crystalline pentachlorophenol/4-methylpyridine complex.[23] To our knowledge, there is no example of a reported structure with a hydrogen bond that includes fluorine atoms, that exhibits H/D isotopic polymorphism.

The salt of diprotonated malonyl difluoride [F(HO)C−CH$_2$−C(OH)F][SbF$_6$]$_2$ (**4**) crystallizes in the monoclinic space group $P2_1/c$ with four formula units per unit cell. The formula unit of **4** is shown in Figure 6. Selected geometrical parameters of **4** are listed in Table 2. Interionic contacts of the cation in the crystal structure are illustrated in Figure 7.

The F(HO)C−CH$_2$−C(OH)F^{2+} cation possesses C_1 symmetry in the crystal structure with a similar U-gauche diketo conformation as malonyl difluoride, with both acidic protons oriented away from the cation. Upon diprotonation, the C−O bond lengths are elongated to 1.212(4) Å (C1−O1) and 1.219(4) Å (C3−O2), and both C−F bond lengths decrease significantly to 1.285(3) Å, respectively. The diprotonation affects the bond lengths of the protonated acyl fluoride groups similar to the monoprotonation. However, the C−O bond lengths in the diprotonated species are still surprisingly short for protonated carbonyl groups and even for protonated acyl fluoride groups.[14,15,24] This finding can be explained by the superelectrophilic character of the diprotonated species, which will be further discussed in the quantum chemical calculations section.[25] Compared to **1** the C−C bond distances are not affected by the diprotonation.

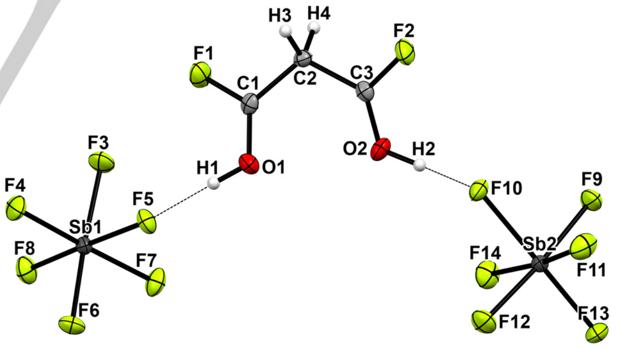

Figure 6. Formula unit of diprotonated malonyl difluoride (**4**) with 50% probability displacement ellipsoids.

As in the crystal structure of monoprotonated malonyl difluoride, the positive charges of the cation in **4** are stabilized by interionic contacts and hydrogen bonding. Four C···F contacts below the sum of the VDW radii (3.17 Å)[16] are observed, two of which are formed by a single fluorine atom. The distances of contacts measure between 2.656(4) Å and 3.063(3) Å. The formed hydrogen bonds towards SbF$_6^-$ anions are particularly interesting, since the O1−H1···F5 (2.397(3) Å) and O2−H2···F10 (2.377(3) Å) hydrogen bonds are remarkably short. These distances are significantly shorter compared to the O−H···F hydrogen bonds in **2** or other reported acyl fluorides.[14,15]

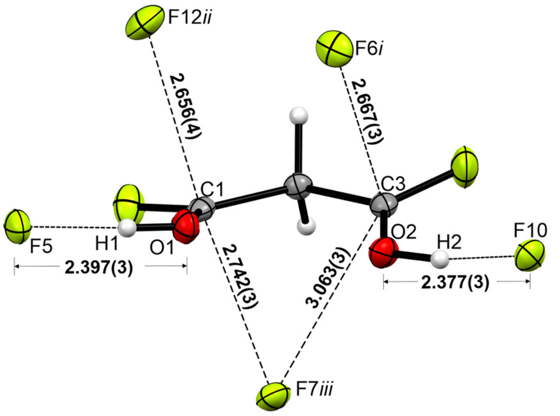

Figure 7. Interionic contacts of diprotonated malonyl difluoride (**4**) with 50% probability displacement ellipsoids. The SbF_6^- anions are reduced to the contacting fluorine atoms for better visualization The distances are given in [Å]. Symmetry code: *i* = 2−x,1−y,1−z; *ii* = 2−x,−0.5+y,1.5−z; *iii* = 1−x,1−y,1−z.

Even shorter hydrogen bonds of this type are rare and were found in different fluorides and hydrogen fluoride adducts with the shortest reported distances measuring below 2.340 Å.[26] The two short hydrogen bonds also affect the structure of the adjacent SbF_6^- anions. The fluorine atoms not involved in the hydrogen bonds show Sb−F distances between 1.8545(18) Å and 1.8672(19) Å, which is in agreement with reported bond lengths in hexafluoridoantimonates.[27] On the other side, the Sb1−F5 (1.9525(17) Å) and Sb2−F10 (1.9745(18) Å) bond lengths are extremely elongated due to strong hydrogen bonding.[28] This results in a distortion of the SbF_6^- anions from the ideal octahedral structure.

The salt of hemiprotonated malonyl difluoride $[(FOC{-}CH_2{-}COF)_2H][SbF_6]$ (**6**) crystallizes in the monoclinic space group $P2_1/c$ with two formula units per unit cell. Selected bond lengths and angles are listed in Table 2. Further details on the crystal structure of **6** are given in the Supporting Information.

Vibrational spectroscopy

Solid malonyl difluoride (**1**) and the protonated species **2**, **3**, **4**, **5**, and **6** were investigated by low-temperature Raman spectroscopy. Additionally, low-temperature IR spectra of the salts of the monoprotonated species **2** and **3** were measured. Excerpts of all measured spectra are stacked in Figure 8. The full spectra are shown in Figure S9 in the Supporting Information. Selected experimental and calculated vibrational frequencies are listed in Table 3. Lists of all observed and calculated vibrational frequencies are provided in the Supporting Information.

The species $[FOC{-}CH_2{-}COF]$, $[FOC{-}CH_2{-}C(OH)F \cdot HF]^+$, $[FOC{-}CH_2{-}C(OD)F \cdot HF]^+$, $[F(HO)C{-}CH_2{-}C(OH)F \cdot 2HF]^{2+}$, $[F(DO)C{-}CH_2{-}C(OD)F \cdot 2HF]^{2+}$, and $[(FOC{-}CH_2{-}COF)_2H]^+$ were quantum chemically calculated. The calculated structures are shown in Chapter 5 of the Supporting Information. The calculated frequencies were employed to assign the observed experimental frequencies. For better accordance of the calculated structures with the experimental structures from the X-Ray structure analysis, HF molecules were added to the gas-phase structures to simulate hydrogen bonding found in the solid state. This also improved the agreement between the calculated and experimental vibrational frequencies. The protonation of malonyl difluoride is proven by Raman and IR spectroscopy. In addition, the degrees of protonation can be distinguished by characteristic vibrational modes that are shifted or newly observed upon protonation. The vibrational spectra of the investigated salts agree well with the structures of the cationic species from the single-crystal X-Ray structure analyses.

The observed experimental vibrational frequencies of malonyl difluoride were assigned, supported by the calculated frequencies of the U-gauche conformer with C_2 symmetry, which was also found in the crystal structure of **1**. In amorphous malonyl difluoride (−196 °C), the $\nu(CH_2)$ vibrations are observed at 2963 cm^{-1} and 2935 cm^{-1} in the Raman spectrum. The CO stretching vibrations are detected at 1865 cm^{-1} and 1843 cm^{-1}. The intense line at 1372 cm^{-1} is assigned to the $\delta(CH_2)$ vibration. The CF stretching vibrations are detected at 1152 cm^{-1} and 1062 cm^{-1}. Additional lines in the same regions of the spectrum are probably caused by different conformations of malonyl difluoride in the solid state.

The cation of **6** (hemiprotonation) exhibits C_i symmetry in the crystal structure as well as the calculated structure. Therefore, the rule of mutual exclusion applies to the cation of **6**. Only the $24A_g$ modes are Raman active of the expected 51 fundamental vibrations ($\Gamma_{vib}(C_i) = 24A_g + 27A_u$). Hemiprotonated malonyl difluoride is detected mainly by two characteristic vibrations. Upon hemiprotonation, the CO stretching vibration is red-shifted to 1748 cm^{-1} in the Raman spectrum, while the CO stretching vibration of the unprotonated acyl fluoride group is not affected. The second characteristic is the blue shift of the CF stretching vibration of the hemiprotonated acyl fluoride group to 1317 cm^{-1}.

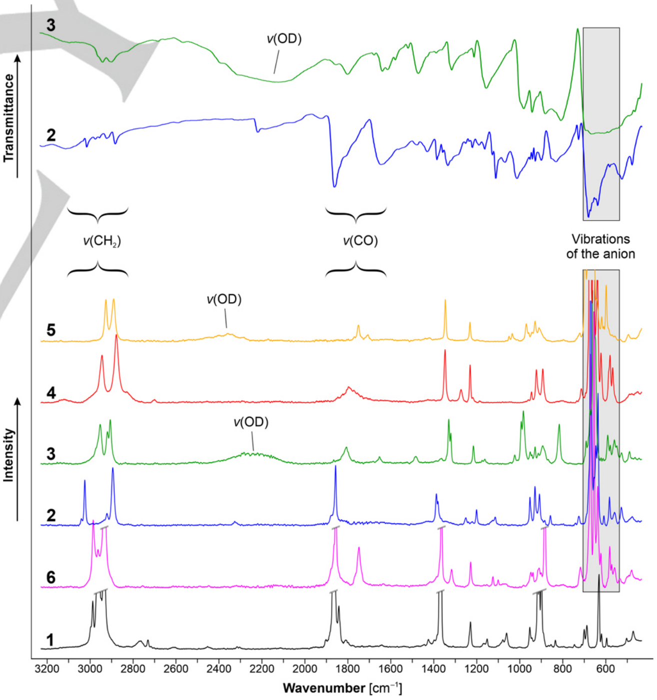

Figure 8. Stacked excerpts of low-temperature Raman spectra of **1**, **2**, **3**, **4**, **5**, **6**, and low-temperature IR spectra of **2** and **3**.

The cation of **2** (monoprotonation) exhibits C_1 symmetry in the crystal structure as well as the calculated structure. Therefore, 24 fundamental vibrations are expected for the cation, all of which are IR and Raman active. The distinctive features of the IR and Raman spectra of **2** are the shifted $\nu(CH_2)$ vibrations as well as the shifted $\nu(CO)$ and $\nu(CF)$ vibrations of the protonated acyl fluoride group. Compared to **1**, the CH_2 stretching vibrations of **2** are detected blue-shifted in the spectra at 3022 cm^{-1}/3025 cm^{-1} (IR/Raman) and red-shifted at 2889 cm^{-1}/2894 cm^{-1} (IR/Raman), respectively. The difference between the two CH_2 stretching vibrations amounts to 133 cm^{-1} (131 cm^{-1} Raman), which is a distinctive characteristic of the monoprotonation, presumably caused by solid-state effects. Even though the CO stretching vibration of the protonated acyl fluoride group is not observed in the Raman spectrum, it is detected at 1649 cm^{-1} in the IR spectrum. The same is true for the respective CF stretching vibration, which is only observed at 1479 cm^{-1} in the IR spectrum. The red shift of the ν(CO) vibration and the blue shift of the ν(CF) vibration verify the protonation and are in good agreement with the data of protonated acyl fluorides from the literature.[14,15] The shifted vibrational frequencies agree with the results from the crystal structure of **2** where the protonation caused a significant elongation of the C−O bond and a shortening of the C−F bond in the protonated acyl fluoride group.

The calculated structure of the cation $[FOC-CH_2-C(OD)F \cdot HF]^+$ with an intramolecular hydrogen bond exhibits C_s symmetry with 24 fundamental vibrations ($\Gamma_{vib}(C_s) = 16A' + 8A''$). For this cation, it is particularly interesting to see if the H/D isotopic polymorphism, that was observed for the crystal structures of **2** and **3** could also be observed by vibrational spectroscopy of the solid bulk material. The most obvious evidence for protonation in **3** is the OD stretching vibration observed as a broad band at 2127 cm^{-1} in the IR spectrum and as a broad line at 2227 cm^{-1} in the Raman spectrum. The frequencies are in good agreement with the Teller-Redlich rule for a H/D isotopic effect,[29] since the ν(OH) vibration is expected at a frequency of around 3200 cm^{-1}.[14,15] The CO stretching vibrations of **3** are detected at 1805 cm^{-1} and 1641 cm^{-1} in the IR spectrum and at 1807 cm^{-1} and 1653 cm^{-1} in the Raman spectrum, respectively. Therefore both ν(CO) vibrations are red-shifted upon protonation in DF/SbF_5 in contrast to **2** where only one ν(CO) vibration is shifted. The vibrational mode at 1641 cm^{-1}/1653 cm^{-1} (IR/Raman) agrees with the respective ν(CO) vibration in **2**. The red shift of the other ν(CO) vibration indicates a weakening of the C−O bond in the unprotonated acyl fluoride group. This is consistent with the results from the crystal structure of **3**, wherein the intramolecular O−D···O hydrogen bond significantly weakened the C−O bond of the unprotonated acyl fluoride group. We conclude, that the H/D isotopic polymorphism of salts **2** and **3** is indeed observable by vibrational spectroscopy.

The diprotonated salts **4** and **5** were also characterized by Raman spectroscopy. The calculated structures of the cations $[F(XO)C-CH_2-C(OX)F \cdot 2HF]^{2+}$ (X = D, H) exhibit C_2 symmetry with 27 fundamental vibrations ($\Gamma_{vib}(C_2) = 14A + 13B$). Due to the poor polarizability of the O−H bond, the OH stretching vibrations of **4** are not visible in the Raman spectrum. In contrast, the respective OD stretching vibrations of **5** are observed as a broad line at around 2361 cm^{-1}. Another broad line is observed at 1797 cm^{-1} in the Raman spectrum of **4**. It is assigned to one CO stretching vibration, although a superimposition of both CO stretching vibrations is also conceivable. In the spectrum of **5,** the ν(CO) vibrations are observed at 1751 cm^{-1} and 1706 cm^{-1}. Surprisingly, the ν(CO) vibrations of diprotonated malonyl difluoride cations are less red-shifted, than the respective ν(CO) vibrations of the monoprotonated species. This finding can be explained by the shorter C−O bonds of the diprotonated species due to their higher oxonium character. This was mentioned before in the crystal structure section and will be further discussed in the theoretical section (Scheme 2). The ν(CF) vibrations are observed in neither the spectrum of **4** nor **5**.

Table 3. Selected experimental vibrational frequencies of malonyl difluoride (**1**) (solid, −196 °C), $[FOC-CH_2-C(OH)F][SbF_6]$ (**2**), $[FOC-CH_2-C(OD)F][SbF_6]$ (**3**), $[F(HO)C-CH_2-C(OH)F][SbF_6]_2$ (**4**), $[F(DO)C-CH_2-C(OD)F][SbF_6]_2$ (**5**), $[(FOC-CH_2-COF)_2H][SbF_6]$ (**6**), and calculated frequencies of $[FOC-CH_2-COF]$, $[FOC-CH_2-C(OH)F \cdot HF]^+$, $[FOC-CH_2-C(OD)F \cdot HF]^+$, $[F(HO)C-CH_2-C(OH)F \cdot 2HF]^{2+}$, $[F(DO)C-CH_2-C(OD)F \cdot 2HF]^{2+}$, $[(FOC-CH_2-COF)_2H]^+$.

Mode	**1** exp.[a]	**6** (0.5×H$^+$) exp.[a]	**2** (1×H$^+$) exp.[a]		**3** (1×D$^+$) exp.[a]		**4** (2×H$^+$) exp.[a]	**5** (2×D$^+$) exp.[a]
	Raman	Raman	IR	Raman	IR	Raman	Raman	Raman
$\nu(CH_2)$	2963 (100) *[3000 (41)]*	2985 (20) *[3026 (77)]*	3022 (m) *[3022(25/37)]*	3025 (12)	2949 (m) *[2946 (39/44)]*	2953 (10)	2945 (12) *[2902 (41)]*	2926 (11) *[2902 (41)]*
$\nu(CH_2)$	2935 (52) *[2961 (110)]*	2933 (40) *[2965 (211)]*	2889 (m) *[2959 (23/100)]*	2894 (15)	2906 (m) *[2917 (53/113)]*	2906 (11)	2878 (17) *[2880 (120)]*	2891 (11) *[2880 (118)]*
$\nu(OX)$[d]	–	n.o. *[1502 (0)]*	3230 (m) *[2780 (2396/109)]*	n.o.	2127 (m, br) *[2083 (826/24)]*	2227 (2)	n.o. *[2132 (66)]*	2361 (2) *[1598 (18)]*
$\nu(CO)$	1865 (94) *[1911 (20)]*	1856 (33) *[1868 (21)]*	1865 (s) *[1869 (278/11)]*	1857 (15)	1805 (m) *[1860 (255/17)]*	1807 (4)	1797 (4) *[1733 (5)]*	1751 (4) *[1737 (9)]*
$\nu(CO)$	1843 (11) *[1872 (5)]*	1748 (13) *[1759 (27)]*	1649 (m) *[1670 (343/7)]*	n.o.	1641 (m) *[1667 (192/3)]*	1653 (2)	n.o. *[1676 (1)]*	1706 (2) *[1684 (4)]*
$\delta(CH_2)$	1372 (39) *[1373 (6)]*	1364 (28) *[1401 (5)]*	1387 (m) *[1380 (29/5)]*	1387 (8)	1319 (m) *[1322 (88/7)]*	1321 (8)	1348 (13) *[1307 (87/10)]*	1347 (11) *[1307 (74/11)]*
$\nu(CF)$	1152 (3) *[1135 (3)]*	1317 (28) *[1338 (13)]*	1479 (m) *[1467 (226/4)]*	n.o.	1473 (m) *[1451 (316/3)]*	1484 (2)	n.o. *[1491 (1)]*	n.o. *[1435 (7)]*
$\nu(CF)$	1062 (4) *[1061 (2)]*	1125 (6) *[1160 (4)]*	1190 (m) *[1162 (172/2)]*	1201 (4)	1157 (m) *[1159 (223/1)]*	n.o.	n.o. *[1435 (7)]*	n.o. *[1356 (17)]*

[a] Abbreviations for IR intensities: s = strong, m = medium, br = broad, n.o. = not observed. Experimental Raman intensities are relative to a scale of 1 to 100. [b] Calculated on the M06-2X/aug-cc-pVTZ level of theory. Scaling factor: 0.956. [c] Calculated IR intensities in km/mol; calculated Raman intensities in Å^4/u. [d] X = D, H.

NMR spectroscopy

^{1}H, ^{13}C, and ^{19}F NMR spectroscopy were employed to investigate if the described solid-state structures are also observed in *a*HF solution. Therefore, *a*HF solutions of malonyl difluoride (**1**), [FOC−CH$_2$−C(OH)F][SbF$_6$] (**2**), and [F(HO)C−CH$_2$−C(OH)F][SbF$_6$]$_2$ (**4**), were prepared and the ^{1}H, ^{13}C, and ^{19}F NMR spectra of the samples were subsequently measured at −60 °C. The observed chemical shifts are listed in Table 4 and the measured spectra are shown in the Supporting Information.

The degree of protonation of malonyl difluoride can be distinguished by NMR spectroscopy in *a*HF solution. The chemical shifts of the neutral compound agree with the reported values from the literature.[8,30] Upon protonation the ^{1}H and ^{13}C signals of the CH$_2$ group are shifted downfield. The ^{13}C signal and the ^{19}F signal of the acyl fluoride group are also shifted downfield. The chemical shift of the carbon atom proves the carbenium character of the protonated species.[9,11,12] *Brouwer* showed that the protonation of *β*-dicarbonyl compounds in superacidic media leads to different structures of the resulting cation (Figure 9).[9] While the diprotonated compounds always exhibit structure **C**, the structure of the monoprotonated cation depends on the carbonyl substituents. In diketones the dihydroxyallyl cation structure **A** was observed.[9–12] For *β*-keto esters, diesters, and diacids structure **B** was observed.[9]

Table 4. ^{1}H, ^{13}C, and ^{19}F chemical shifts of malonyl difluoride (**1**), [FOC−CH$_2$−C(OH)F][SbF$_6$] (**2**), and [F(HO)C−CH$_2$−C(OH)F][SbF$_6$]$_2$ (**4**) in *a*HF at −60 °C.

	1[a]	**2**[a] (1×H$^+$)	**4**[a] (2×H$^+$)
δ[^{1}H] C**H**$_2$	3.58 (s)	4.42 (m)	4.25 (s)
δ[^{1}H] O**H**		10.22 (m)	9.90 (m)
δ[^{13}C] **C**H$_2$	33.43 (t, *J*=59.2 Hz)	34.79 (t, *J*=49.9 Hz)	35.13 (t, *J*=47.5 Hz)
δ[^{13}C] **C**O(H$^+$)F	158.49 (dd, *J*=358.8 Hz, 14.6 Hz)	166.80 (dd, *J*=365.5 Hz, 14.0 Hz)	169.01 (dd, *J*=367.0 Hz, 13.9 Hz)
δ[^{19}F] CO(H$^+$)**F**	44.78 (s)	49.59 (s)	50.18 (s)

[a] Chemical shifts are given in ppm.

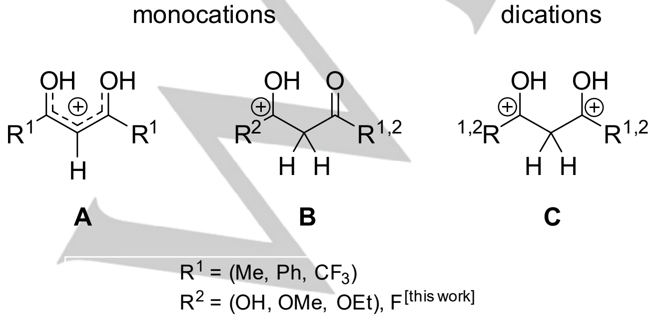

Figure 9. Structure of mono- and diprotonated *β*-dicarbonyl compounds in *a*HF solution.[9,11,12]

To investigate the structure of the [FOC−CH$_2$−C(OH)F]$^+$ cation in *a*HF solution a DEPT spectrum was measured with dichloromethane as reference (Supporting Information). It clearly shows the CH$_2$ group of the monoprotonated species. This proves that the [FOC−CH$_2$−C(OH)F]$^+$ cation exhibits the protonated diketo structure **B** in *a*HF solution. However, for the monoprotonated species **2** only one signal is observed for each respective group. Therefore, in *a*HF solution, the [FOC−CH$_2$−C(OH)F]$^+$ cation has a symmetrical equilibrium structure. This was also observed by *Brouwer* and *Olah et al.* during their investigation of similar protonated *β*-dicarbonyl compounds.[11,12] *Olah* explains this with an equilibrium due to a fast proton exchange with the solvent or between the carbonyl groups.[12]

Quantum chemical calculations

It was interesting to calculate the energetic differences between the possible monoprotonated cations. Therefore, the structures of three isomers of the monoprotonated malonyl difluoride cation were optimized on the MP2/aug-cc-pVTZ level of theory. By a subsequent vibrational analysis, the structures were found to be true minima. The minimum geometries of the three cations were then employed to calculate the respective single point energies on the CCSD(t)/aug-cc-pVTZ level of theory. The three calculated structures together with their energy differences are shown in Figure 10.

The constitutional isomer **III**, which can be described as a dihydroxyallyl cation and corresponds to the O-protonated enol form, is the energetically most favored isomer. This is surprising since this structure of monoprotonated malonyl difluoride was neither observed in the solid state nor solution. The neutral compound malonyl difluoride is exclusively observed in its diketo form. Thus, a formation of the isomer **III** upon protonation would require a proton shift, which unavoidably requires CH deprotonation. This seems highly unrealistic in the superacidic system HF/SbF$_5$ and indicates why the dihydroxyallyl cationic structure **III** is not observed for monoprotonated malonyl difluoride. This also agrees with the results for comparable monoprotonated *β*-dicarbonyl compounds from the literature.[9–12,31] Further proof that the dihydroxyallyl cationic structure is not present in the superacidic solutions is obtained from the vibrational spectra of the obtained salts. A proton exchange of the CH protons with the solvent *a*DF would lead to C-deuterated species. However, no CD stretching vibrations are evident in the vibrational spectra of the salts obtained from DF/SbF$_5$ solutions. The energy difference between the calculated structures **I** and **II** amounts to 37.9 kJ/mol. This indicates that conformer **II** with an intramolecular hydrogen bond is the expected structure for monoprotonated malonyl difluoride. However, the two conformational isomers **I** and **II** were both observed in this work. In the solid state, the cation of monoprotonated malonyl difluoride [FOC−CH$_2$−C(OH)F][SbF$_6$] (**2**) exhibits a structure that is comparable to the calculated structure of conformer **I**. In contrast, the structure of the cation in the isotopologue salt [FOC−CH$_2$−C(OD)F][SbF$_6$] (**3**) is comparable with the calculated structure of conformer **II**.

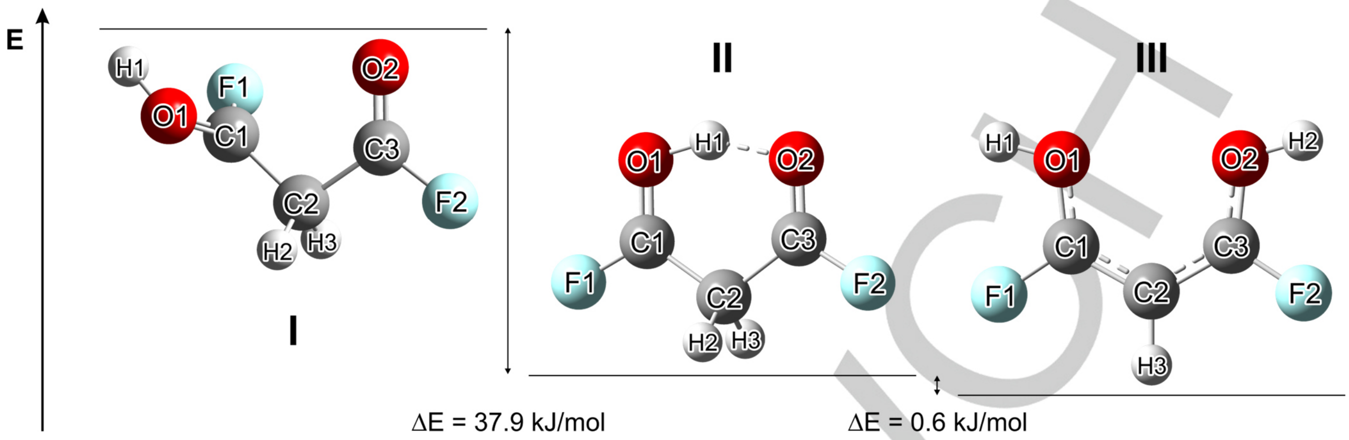

Figure 10. Quantum chemically calculated geometries (MP2/aug-cc-pVTZ) of two isomers of monoprotonated malonyl difluoride [FOC−CH_2−C(OH)F]$^+$ (**I**, **II**) and [F(HO)C−CH−C(OH)F]$^+$ (**III**) together with the energy differences of their respective single point energies (CCSD(t)/aug-cc-pVTZ//MP2/aug-cc-pVTZ).

It shows that the calculated energy differences do not necessarily allow conclusions to be made about the experimental results in the solid state, where interionic contacts are ubiquitous. This was shown in detail in the discussion of crystal structures of **2** and **3**. Those interionic contacts in the solid state overcome the energy difference between the calculated naked cations. In summary, the results from the theoretical investigations of monoprotonated malonyl difluoride are interestingly quite contrary to the experimental data found in this work. This underlines the importance of interionic contacts in the solid state.

In addition to the calculations concerning the monoprotonated species, quantum chemical calculations addressing the electron distribution in the F(HO)C−CH_2−C(OH)F^{2+} cation were performed. The hydroxycarbenium character of the F(HO)C−CH_2−C(OH)F^{2+} carbodication, was experimentally shown by the downfield shift of the ^{13}C NMR signals of the acyl fluoride carbons upon protonation. This suggests that F(HO)C−CH_2−C(OH)F^{2+} is a 1,3-dication (Scheme 2).

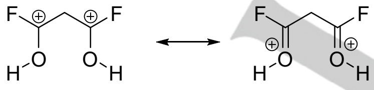

Scheme 2. Resonance Lewis structures of F(HO)C−CH_2−C(OH)F^{2+}.

The 1,3-dicationic character is also evident from the calculated mapped molecular electrostatic potential (MEP) of the dication (Figure 11). The MEP of F(HO)C−CH_2−C(OH)F^{2+} shows that the highest electron deficiency is located around the carbon atoms of the protonated acyl fluoride groups. Following the classification of *Olah*, diprotonated malonyl difluoride is a 1,3-dicationic gitonic superelectrophile.[25] However, the oxonium character of the cation should not be underestimated. As shown in Scheme 2, the hydroxycarbenium resonance structure is less favored for the diprotonated species due to the charge repulsion of the positive charges. Therefore, the oxonium character leads to a relatively short C−O bond length, in comparison to other protonated carbonyl compounds.[14,15,24]

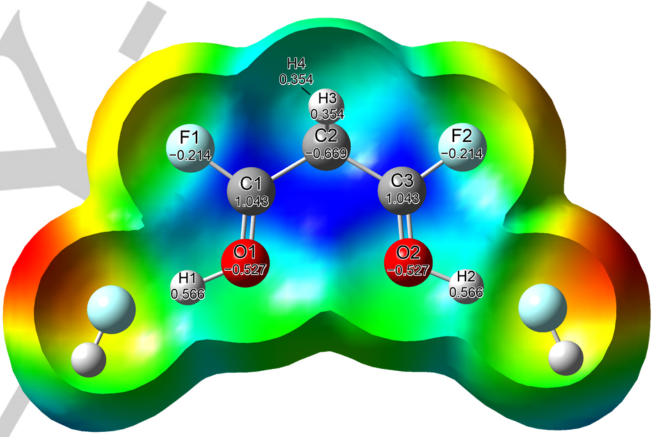

Figure 11. MEP mapped on the isodensity surface of [F(HO)C−CH_2−C(OH)F · 2HF]$^{2+}$ along with NPA charges of the respective atoms. The MEP is illustrated in a color range from 0.22 a.u. (red) to 0.35 a.u. (blue). The NPA charges are given in a.u. Calculations were performed on the M06-2X/aug-cc-pVTZ level of theory.

Conclusion

The solid-state structure of malonyl difluoride was elucidated by single crystal structure analysis. While the molecule predominantly exhibits a diketo S-gauche conformation in the gas phase, in the crystal structure a diketo U-gauche conformation with C_1 and C_2 symmetry is found.

Furthermore, malonyl difluoride was reacted with the superacidic system HF/SbF_5 for the first time. The reaction leads to salts of hemiprotonated, monoprotonated, and diprotonated malonyl difluoride depending on the stoichiometric amount of SbF_5 in the reaction mixture. The obtained salts were characterized by single-crystal X-ray structure analysis, low-temperature Raman spectroscopy, and in the case of the monoprotonated species additionally by low-temperature IR spectroscopy. Surprisingly, different structures were identified for the monoprotonated species and its deuterated isotopologue. The cation of $[FOC{-}CH_2{-}C(OD)F][SbF_6]$ carries the acidic deuterium an intramolecular hydrogen bond, which is not present in $[FOC{-}CH_2{-}C(OH)F][SbF_6]$. The structural difference between the two isotopologues in the solid state is shown by the X-ray structure analyses as well as by vibrational spectroscopy. This makes monoprotonated malonyl difluoride a rare example of H/D isotopic polymorphism. Diprotonated malonyl difluoride is a small and electron-deficient 1,3-dicationic gitonic superelectrophile, as shown by experimental results and quantum chemical calculations.

Experimental Section

All experimental data and procedures are found in the Supporting Information.

Deposition Numbers 2203671 ($FOC{-}CH_2{-}COF$), 2203673 ($[FOC{-}CH_2{-}C(OH)F][SbF_6]$), 2203674 ($[FOC{-}CH_2{-}C(OD)F][SbF_6]$), 2203675 ($[F(HO)C{-}CH_2{-}C(OH)F][SbF_6]_2$) and 2203676 ($[(FOC{-}CH_2{-}COF)_2H][SbF_6]$) contain the supplementary crystallographic data for this paper. These data are provided free of charge by the joint Cambridge Crystallographic Data Centre and Fachinformationszentrum Karlsruhe Access Structures service www.ccdc.cam.ac.uk/structures.

Acknowledgments

We are grateful to the Department of Chemistry of the Ludwig-Maximilian University, Munich, the Deutsche Forschungsgemeinschaft (DFG), and the F-Select GmbH for the support of this work.

Keywords: super acid; malonyl difluoride; protonation; single-crystal structure analysis; vibrational spectroscopy

[1] a) D. Bonne, Y. Coquerel, T. Constantieux, J. Rodriguez, *Tetrahedron: Asymmetry* **2010**, *21*, 1085; b) J. Christoffers, *Eur. J. Org. Chem.* **1998**, *1998*, 1259; c) D. Gibson, *Coord. Chem. Rev.* **1969**, *4*, 225; d) G. de Gonzalo, A. R. Alcántara, *Pharmaceuticals* **2021**, *14*; e) P. E. Hansen, *Pharmaceuticals* **2021**, *14*.

[2] J. Emsley in *Structure and Bonding*, Springer Berlin Heidelberg, Berlin, Heidelberg, **1984**, pp. 147–191.

[3] N. V. Belova, V. V. Sliznev, H. Oberhammer, G. V. Girichev, *J. Mol. Struct.* **2010**, *978*, 282.

[4] J. L. Burdett, M. T. Rogers, *J. Am. Chem. Soc.* **1964**, *86*, 2105.

[5] M. M. Schiavoni, H.-G. Mack, H. Di Loretto, C. Védova, *J. Mol. Struct.: THEOCHEM* **1996**, *364*, 189.

[6] N. Pietri, J. P. Aycard, A. Allouche, P. Verlaque, T. Chiavassa, *Spectrochim. Acta, Part A* **1995**, *51*, 1891.

[7] H.-G. Mack, H. Oberhammer, C. Védova, *J. Mol. Struct.* **1995**, *346*, 51.

[8] A. Jin, H. G. Mack, A. Waterfeld, H. Oberhammer, *J. Am. Chem. Soc.* **1991**, *113*, 7847.

[9] D. M. Brouwer, *Recl. Trav. Chim. Pays-Bas* **1968**, *87*, 225.

[10] G. A. Olah, M. Calin, *J. Am. Chem. Soc.* **1968**, *90*, 4672.

[11] D. M. Brouwer, *Chem. Commun. (London)* **1967**, 515.

[12] G. A. Olah, C. U. Pittman, *J. Am. Chem. Soc.* **1966**, *88*, 3310.

[13] M. Schickinger, F. Zischka, K. Stierstorfer, A. Kornath, *Eur. J. Org. Chem.* **2019**, *2019*, 1876.

[14] S. Steiner, C. Jessen, A. J. Kornath, *Z. Anorg. Allg. Chem.* **2022**, *648*.

[15] M. C. Bayer, C. Kremser, C. Jessen, A. Nitzer, A. J. Kornath, *Chem. - Eur. J.* **2022**, *28*, e202104422.

[16] A. Bondi, *J. Phys. Chem.* **1964**, *68*, 441.

[17] G. A. Jeffrey, *An introduction to hydrogen bonding*, Oxford Univ. Press, New York, **1997**.

[18] S. Crawford, M. T. Kirchner, D. Bläser, R. Boese, W. I. F. David, A. Dawson, A. Gehrke, R. M. Ibberson, W. G. Marshall, S. Parsons et al., *Angew. Chem., Int. Ed. Engl.* **2009**, *48*, 755.

[19] K. Merz, A. Kupka, *Cryst. Growth Des.* **2015**, *15*, 1553.

[20] a) A. R. Ubbelohde, K. J. Gallagher, *Acta Crystallogr.* **1955**, *8*, 71; b) T. Steiner, *Angew. Chem., Int. Ed.* **2002**, *41*, 48; c) M. Ichikawa, *J. Mol. Struct.* **2000**, *552*, 63.

[21] F. F. Iwasaki, Y. Saito, *Acta Crystallogr.* **1967**, *23*, 56.

[22] D. Mootz, M. Schilling, *J. Am. Chem. Soc.* **1992**, *114*, 7435.

[23] a) I. Majerz, Z. Malarski, T. Lis, *J. Mol. Struct.* **1990**, *240*, 47; b) B. C. K. Ip, I. G. Shenderovich, P. M. Tolstoy, J. Frydel, G. S. Denisov, G. Buntkowsky, H.-H. Limbach, *J. Phys. Chem. A* **2012**, *116*, 11370; c) N. P. Funnell, D. R. Allan, A. G. P. Maloney, R. I. Smith, C. J. G. Wilson, S. Parsons, *CrystEngComm* **2021**, *23*, 769.

[24] D. Stuart, S. D. Wetmore, M. Gerken, *Angew. Chem., Int. Ed. Engl.* **2017**, *56*, 16380.

[25] G. A. Olah, D. A. Klumpp, *Superelectrophiles and Their Chemistry*, John Wiley & Sons, Inc, Hoboken, NJ, USA, **2007**.

[26] a) V. V. Ghazaryan, M. Fleck, A. M. Petrosyan, *J. Cryst. Growth* **2013**, *362*, 182; b) V. S. Minkov, V. V. Ghazaryan, E. V. Boldyreva, A. M. Petrosyan, *Acta Crystallogr., Sect. C: Struct. Chem.* **2015**, *71*, 733.

[27] a) F. P. Boer, *J. Am. Chem. Soc.* **1966**, *88*, 1572; b) K. O. Christe, X. Zhang, J. A. Sheehy, R. Bau, *J. Am. Chem. Soc.* **2001**, *123*, 6338; c) Z. Mazej, E. Goreshnik, *Eur. J. Inorg. Chem.* **2022**, *2022*.

[28] C. Bour, R. Guillot, V. Gandon, *Chem. - Eur. J.* **2015**, *21*, 6066.

[29] J. Weidlein, U. Müller, K. Dehnicke, *Schwingungsspektroskopie. Eine Einführung*, Thieme, Stuttgart, **1988**.

[30] W. Althoff, M. Fild, *Z. Naturforsch., B: J. Chem. Sci.* **1973**, *28*, 98.

[31] J. W. Larsen, *J. Am. Chem. Soc.* **1970**, *92*, 5136.

Entry for the Table of Contents

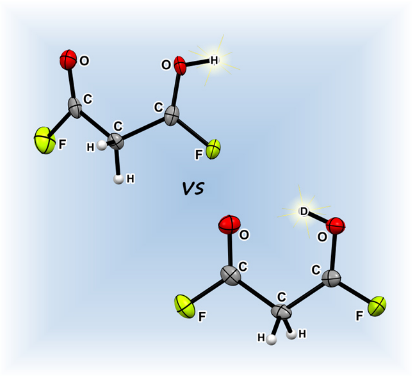

Malonyl difluoride turned out to be a versatile compound in the condensed phase, especially when investigated in the superacid medium HF/SbF_5. Not only is diprotonation of this small diacyl fluoride achieved, but also the H/D isotopologues of the monoprotonated species are rare examples of isotopic polymorphism in the solid state. Their structure is elucidated by single-crystal X-ray diffraction and their stability is fathomed by quantum-chemical calculations.

Supporting Information

A Neutron Makes the Difference - Structures of Malonyl Difluoride and its Protonated Species in Condensed Media

Christoph Jessen, Dirk Hollenwäger, and Andreas J. Kornath*

Table of Contents

1 Experimental Details 3

1.1 Apparatus and Materials 3

1.2 Computational Methods 3

1.3 Experimental Procedures 4

2 Crystallographic Data 5

2.1 $FOC{-}CH_2{-}COF$ (1) 6

2.2 $[(FOC{-}CH_2{-}COF)_2H][SbF_6]$ (6) 6

2.3 $[FOC{-}CH_2{-}C(OH)F][SbF_6]$ (2) 7

2.4 $[FOC{-}CH_2{-}C(OD)F][SbF_6]$ (3) 9

2.5 $[F(HO)C{-}CH_2{-}C(OH)F][SbF_6]_2$ (4) 10

3 Vibrational Data 12

3.1 Malonyl Difluoride 12

3.2 Hemiprotonated Malonyl Difluoride 14

3.3 Monoprotonated Malonyl Difluoride 15

3.4 Diprotonated Malonyl Difluoride 16

4 NMR 18

4.1 Malonyl Difluoride 18

4.2 Monoprotonated Malonyl difluoride 20

4.3 Diprotonated Malonyl Difluoride 23

5 Quantum Chemical Calculations 25

6 References 29

1 Experimental Details

Caution! Note that any contact with the described compounds should be avoided. Hydrolysis of malonyl difluoride, SF_4, and SbF_5 may form HF which burns skin and causes irreparable damage. Safety precautions should be taken while handling these compounds.

1.1 Apparatus and Materials

All reactions were carried out by employing standard Schlenk techniques on a stainless steel vacuum line. The syntheses of the salts were performed using FEP/PFA reactors with stainless steel valves. Before each reaction or NMR measurement, the stainless steel vacuum line and the reactors were dried with fluorine.

For Raman measurements a Bruker MultiRam FT-Raman spectrometer with Nd:YAG laser excitation (λ = 1064 nm) was used. The measurement was performed after transferring the sample into a cooled (−196°C) glass cell under nitrogen atmosphere and subsequent evacuation of the glass cell.

Low temperature IR-spectroscopic investigations were carried out with a Bruker Vertex-80V FTIR spectrometer using a cooled cell with a single-crystal CsBr plate on which small amounts of the samples were placed.[1] The Gas-phase IR-spectra were taken in a stainless steal cell with silicon windows.

The single crystal X-Ray diffraction studies were performed with an Oxford XCalibur3 diffractometer equipped with a Spellman generator (voltage 50 kV, current 40 mA) and a KappaCCD detector, operating with Mo-Kα radiation (λ = 0.7107 Å) The measurements were performed at 173 K. The program CrysAlisPro 1.171.39.46e (Rigaku Oxford Diffraction, 2018) was employed for the data collection and reduction.[2] The structures were solved utilizing SHELXT[3] and SHELXL-2018/3[4] of the WINGX software package.[5] The structures were checked using the software PLATON.[6] The absorption correction was performed using the SCALE3 ABSPACK multiscan method.[7] Visualization was done with the software Mercury.[8]

NMR spectra were recorded on either a Jeol ECX400 NMR instrument or a Bruker AV400 NMR instrument. The spectrometer was externally referenced to $CFCl_3$ for ^{19}F NMR and to tetramethylsilane for ^{1}H NMR spectra. For visualization and evaluation, the software MestReNova Version 14.0.4 was used.[9] The spectra were recorded inside 4 mm FEP tube inliners. The NMR samples were prepared by transferring the *a*HF-solution of the respective compound into a dried 4 mm FEP tube inliner under nitrogen atmosphere. Then the FEP tube was frozen at −196 °C. The FEP tube was evacuated, flame sealed and kept at −196 °C. Immediately before the NMR measurement, the sealed FEP tube was put in a standard glass NMR tube loaded with 0.2 mL acetone-d_6 as an external reference and warmed to the designated temperature.

1.2 Computational Methods

Quantum chemical calculations were carried out using the software packages Gaussian09 and Gaussian16.[10] For visualization and illustration of the calculated structures the software GaussView 6 was used.[11] If not stated otherwise, all calculations were carried out on the M06-2X/aug-cc-pVTZ level of theory.

1.3 Experimental Procedures

In the following procedures applies: *aX*F = *a*DF, *a*HF.

Malonyl difluoride (1)

Malonyl difluoride ($FOC{-}CH_2{-}COF$) was prepared according to the literature.[12] Malonyl difluoride was stored in a glass flask with a grease-free stopcock at −20 °C.

Monoprotonated malonyl difluoride (2, 3)

SbF_5 (1.0 mmol) was condensed in an FEP reactor vessel together with a*X*F (0.5 mL) at −196 °C. The reactants were warmed to −40 °C and thoroughly mixed to complete dissolution, to form the superacid. The superacid was frozen at −196 °C and malonyl difluoride (1.0 mmol) was added using a syringe under nitrogen atmosphere. The reactants were warmed to −60 °C and thoroughly mixed to complete dissolution. The mixture was cooled to −78 °C and volatile components were removed overnight at −78 °C in a dynamic vacuum. The product was obtained as a colorless solid. $[FOC{-}CH_2{-}C(OH)F][SbF_6]$ (**2**) was synthesized by using aHF as reactant and solvent. $[FOC{-}CH_2{-}C(OD)F][SbF_6]$ (**3**) was synthesized by using *a*DF as reactant and solvent.
To obtain single crystals, the reaction mixture was slowly cooled from −60 °C to −78 °C until the precipitation of crystalline solids was observed. Then volatile components were removed overnight at −78 °C.

Diprotonated malonyl difluoride (4, 5)

SbF_5 (2.0 mmol) was condensed in an FEP reactor vessel together with a*X*F (0.5 mL) at −196 °C. The reactants were warmed to −40 °C and thoroughly mixed to complete dissolution, to form the superacid. The superacid was frozen at −196 °C and malonyl difluoride (1.0 mmol) was added using a syringe under nitrogen atmosphere. The reactants were warmed to −60 °C and thoroughly mixed to complete dissolution. The mixture was cooled to −78 °C and volatile components were removed overnight at −78 °C in a dynamic vacuum. The product was obtained as a colorless solid. $[F(HO)C{-}CH_2{-}C(OH)F][SbF_6]_2$ (**4**) was synthesized by using aHF as reactant and solvent. $[F(HO)C{-}CH_2{-}C(OH)F][SbF_6]_2$ (**5**) was synthesized by using aDF as reactant and solvent.
To obtain single crystals, the reaction mixture was slowly cooled from −60 °C to −78 °C until the precipitation of crystalline solids was observed. Then volatile components were removed overnight at −78 °C.

Hemiprotonated malonyl difluoride (6)

SbF_5 (0.5 mmol) was condensed in an FEP reactor vessel together with aHF (0.5 mL) at −196 °C. The reactants were warmed to −40 °C and thoroughly mixed to complete dissolution, to form the superacid. The superacid was frozen at −196 °C and malonyl difluoride (1.0 mmol) was added using a syringe under nitrogen atmosphere. The reactants were warmed to −60 °C and thoroughly mixed to complete dissolution. The mixture was cooled to −78 °C and volatile components were removed overnight at −78 °C in a dynamic vacuum. The product was obtained as a colorless solid.
To obtain single crystals, the reaction mixture was slowly cooled from −60 °C to −70 °C until the precipitation of crystalline solids was observed. Then volatile components were removed overnight at −78 °C.

2 Crystallographic Data

Table S1. Crystal data and structure refinement of **1**, **2**, **3**, **4**, **6**.

	1	**6**	**2**	**3**	**4**
Molecular Formula	$C_3H_2F_2O_2$	$C_6H_5F_{10}O_4Sb$	$C_3H_3F_8O_2Sb$	$C_3H_2DF_8O_2Sb$	$C_3H_4F_{14}O_2Sb_2$
M_r[g·mol^{-1}]	108.05	452.85	344.8	345.81	581.56
Crystal size [mm^3]	0.551 × 0.318 × 0.144	0.550 × 0.220 × 0.190	0.270 × 0.250 × 0.150	0.305 × 0.249 × 0.063	0.300 × 0.260 × 0.210
Crystal system	monoclinic	monoclinic	orthorhombic	triclinic	monoclinic
Space group	$C2$	$P2_1/c$	$P2_12_12_1$	$P\bar{1}$	$P2_1/c$
a [Å]	19.0053(15)	5.1146(2)	5.1138(3)	7.8033(2)	7.5142(3)
b [Å]	4.7477(3)	10.5958(4)	7.7189(3)	9.9283(3)	13.8924(5)
c [Å]	6.8901(5)	11.2033(4)	20.3986(10)	10.7623(3)	11.8687(5)
α [°]	90	90	90	84.849(2)	90
β [°]	107.626(6)	91.992(3)	90	86.557(2)	91.743(3)
γ [°]	90	90	90	76.878(2)	90
V [Å^3]	592.52(8)	606.78(4)	805.19(7)	808.07(4)	1238.40(8)
Z	6	2	4	4	4
ρ_{calc} [g·cm^{-3}]	1.817	2.479	2.844	2.842	3.119
μ [mm^{-1}]	0.206	2.418	3.544	3.531	4.542
$\lambda_{MoK\alpha}$ [Å]	0.71073	0.71073	0.71073	0.71073	0.71073
F(000)	324	428	640	640	1064
T [K]	103(2)	143(2)	143(2)	100(2)	143(2)
h, k, l range	−28:27,−6:7,−10:10	−7:7,−14:15,−15:16	−6:4,−10:7,−27:21	−11:11,−14:14,−16:15	−10:10,−19:19,−16:16
Reflections collected	6099	6485	2559	9006	12858
Independent reflections	2002	2001	1830	5228	3768
R_{int}	0.0234	0.0222	0.0282	0.0171	0.0393
Parameters	108	98	129	259	197
R(F)/wR(F^2)[a] (all data)	0.0305/.0722	0.0315/0.0480	0.0391/0.0705	0.0291/0.0596	0.0391/0.0557
Weighting scheme[b]	0.0369/0.0899	0.0183/0.3342	0.0204/0.0000	0.0262/0.2141	0.0181/0.0000
S (Gof)[c]	1.039	1.058	1.026	1.077	1.014
Residual density [e·Å^{-3}]	0.266/−0.157	0.720/−0.543	0.717/−1.200	1.056/−0.633	1.548/−1.172
Device	Oxford XCalibur	Oxford XCalibur	Oxford XCalibur	Oxford XCalibur	Oxford XCalibur
CCDC	2203671	2203676	2203673	2203674	2203675

[a] $R_1 = \Sigma||F_0|-|F_c||/\Sigma|F_0|$.

[b] $wR_2 = [\Sigma[w(F_0^2-F_c^2)^2]/\Sigma[w(F_0)^2]]^{1/2}$; $w = [\sigma_c^2(F_0^2)+(xP)^2+yP]-1$; $P = (F_0^2+2F_c^2)/3$.

[c] GoF = $\{\Sigma[w(F_o^2-F_c^2)^2]/(n-p)\}^{1/2}$ (n = number of reflections; p = total number of parameters).

2.1 FOC−CH$_2$−COF (1)

Table S2. Structural parameters of FOC−CH$_2$−COF (**1**)

Bond lengths [Å]		Bond angles [°]		Torsion angles [°]	
F1−C1	1.357(2)	O2−C3−F2	120.0(2)	O3−C4−C5−C4	25.6(1)
F3−C4	1.340(2)	O2−C3−C2	131.0(2)	F3−C4−C5−C4	−157.4(1)
F2−C3	1.340(2)	F2−C3−C2	109.0(1)	O1−C1−C2−C3	0.5(2)
O3−C4	1.172(2)	O3−C4−F3	120.1(1)	F1−C1−C2−C3	−178.9(1)
O2−C3	1.172(2)	O3−C4−C5	129.3(2)	O2−C3−C2−C1	2.9(2)
O1−C1	1.170(2)	F3−C4−C5	110.5(1)	F2−C3−C2−C1	−178.0(1)
C3−C2	1.492(2)	C4−C5−C4	112.9(2)		
C4−C5	1.492(2)	O1−C1−F1	119.7(2)		
C1−C2	1.486(2)	O1−C1−C2	131.4(2)		
		F1−C1−C2	109.0(1)		
		C1−C2−C3	114.5(1)		

2.2 [(FOC−CH$_2$−COF)$_2$H][SbF$_6$] (6)

Table S3. Structural parameters of [(FOC−CH$_2$−COF)$_2$H][SbF$_6$] (**6**).

Bond lengths [Å]		Bond angles [°]		Torsion angles [°]	
Sb1−F3	1.862(1)	F3−Sb1−F3	180.00(9)	O1−C1−C2−C3	163.2(2)
Sb1−F3	1.862(1)	F3−Sb1−F5	89.04(6)	F1−C1−C2−C3	−20.7(3)
Sb1−F5	1.875(1)	F3−Sb1−F5	90.96(6)	C1−C2−C3−O2	−5.1(3)
Sb1−F5	1.875(1)	F3−Sb1−F5	90.96(6)	C1−C2−C3−F2	175.5(2)
Sb1−F4	1.876(1)	F3−Sb1−F5	89.04(6)		
Sb1−F4	1.876(1)	F5−Sb1−F5	180		
F1−C1	1.298(2)	F3−Sb1−F4	89.04(7)		
F2−C3	1.346(2)	F3−Sb1−F4	90.96(7)		
O1−C1	1.214(2)	F5−Sb1−F4	90.20(5)		
O1−H1	1.222(2)	F5−Sb1−F4	89.80(5)		
O2−C3	1.175(2)	F3−Sb1−F4	90.96(7)		
C1−C2	1.477(3)	F3−Sb1−F4	89.04(7)		
C2−C3	1.494(3)	F5−Sb1−F4	89.80(5)		
		F5−Sb1−F4	90.20(5)		
		F4−Sb1−F4	180		
		C1−O1−H1	122.0(2)		
		O1−C1−F1	119.4(2)		
		O1−C1−C2	122.4(2)		
		F1−C1−C2	118.1(2)		
		C1−C2−C3	117.5(2)		
		O2−C3−F2	120.4(2)		
		O2−C3−C2	131.3(2)		
		F2−C3−C2	108.3(2)		

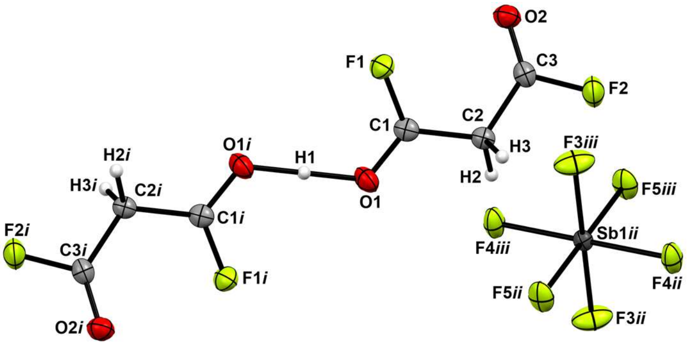

Figure S1. Formula unit of hemiprotonated malonyl difluoride (**6**) with 50% probability displacement ellipsoids. Symmetry code: *i* = 1−x,2−y,1−z; *ii* = 1.5−x,0.5+y, 0.5−z; *iii* = 0.5+x,1.5−y,−0.5+z.

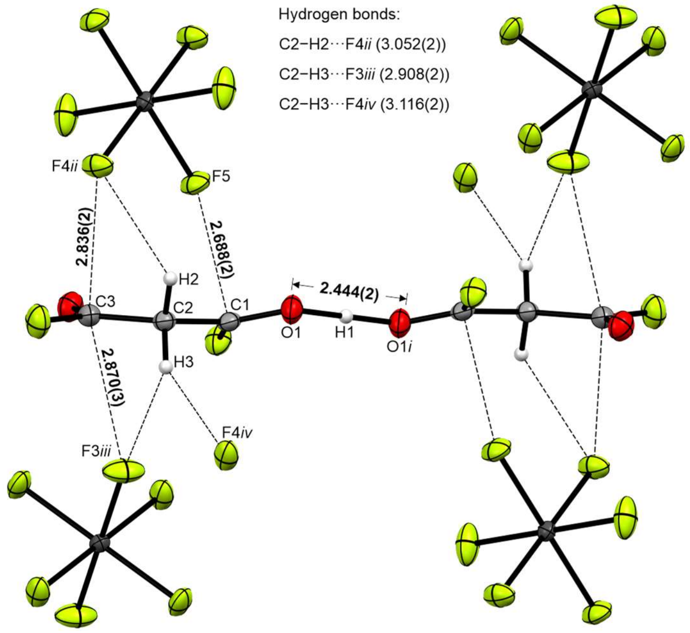

Figure S2. Interionic contacts of hemiprotonated malonyl difluoride with 50% probability displacement ellipsoids. Some of the SbF_6^- anions are reduced to the contacting fluorine atoms for better visualization. The distances are given in [Å]. Symmetry code: *i* = 1−x,2−y,1−z; *ii* = 1−x,1−y,1−z; *iii* = 0.5−x,0.5+y,0.5−z; 0.5+x,1.5−y,−0.5+z.

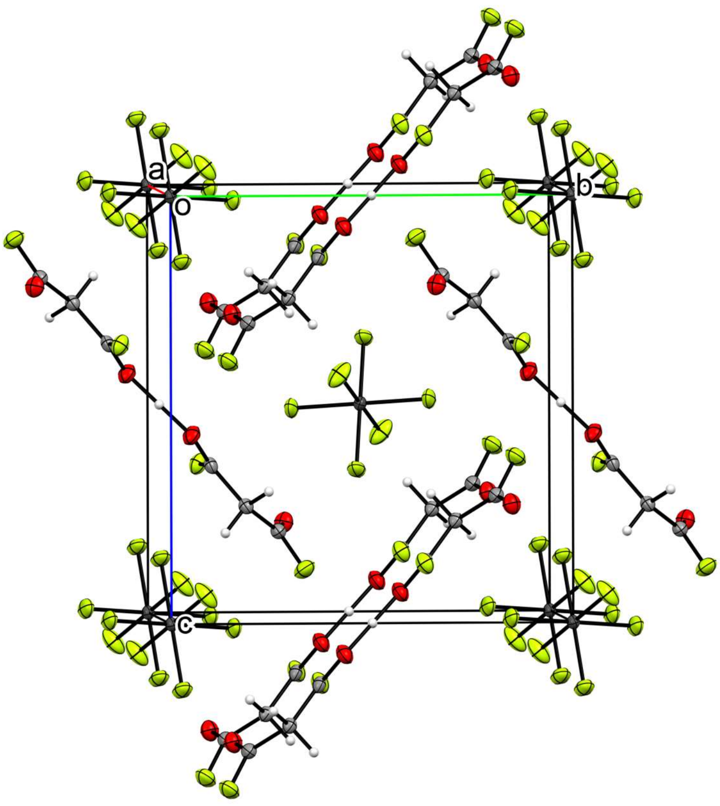

Figure S3. Crystal packing of hemiprotonated malonyl difluoride with 50% probability displacement ellipsoids.

2.3 [FOC−CH$_2$−C(OH)F][SbF$_6$] (2)

Table S4. Structural parameters of [FOC−CH$_2$−C(OH)F][SbF$_6$] (**2**).

Bond lengths [Å]		Bond angles [°]		Torsion angles [°]	
Sb1−F8	1.858(4)	F8−Sb1−F7	93.1(2)	C1−C2−C3−O2	−45.0(13)
Sb1−F7	1.860(4)	F8−Sb1−F6	92.4(2)	C1−C2−C3−F2	136.4(7)
Sb1−F6	1.863(4)	F7−Sb1−F6	91.6(2)	C3−C2−C1−O1	36.2(11)

Sb1−F3	1.866(4)	F8−Sb1−F3	92.6(2)	C3−C2−C1−F1	−146.7(7)
Sb1−F4	1.880(4)	F7−Sb1−F3	89.7(2)	C1−C2−C3−O2	−45.0(13)
Sb1−F5	1.933(4)	F6−Sb1−F3	174.8(2)		
O2−C3	1.163(8)	F8−Sb1−F4	90.0(2)		
F2−C3	1.329(10)	F7−Sb1−F4	176.8(2)		
C2−C1	1.487(9)	F6−Sb1−F4	89.2(2)		
C2−C3	1.511(11)	F3−Sb1−F4	89.3(2)		
F1−C1	1.289(8)	F8−Sb1−F5	178.9(2)		
O1−C1	1.218(9)	F7−Sb1−F5	88.0(2)		
		F6−Sb1−F5	87.8(2)		
		F3−Sb1−F5	87.3(2)		
		F4−Sb1−F5	88.9(2)		
		C1−C2−C3	111.9(6)		
		O2−C3−F2	121.8(10)		
		O2−C3−C2	127.8(10)		
		F2−C3−C2	110.4(7)		
		O1−C1−F1	119.6(6)		
		O1−C1−C2	124.4(6)		
		F1−C1−C2	115.9(6)		

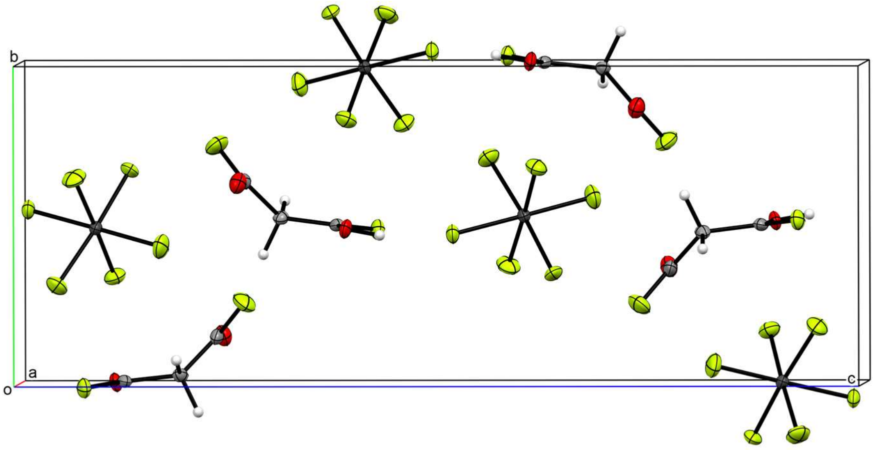

Figure S4. Crystal packing of monoprotonated malonyl difluoride with 50% probability displacement ellipsoids.

2.4 [FOC−CH$_2$−C(OD)F][SbF$_6$] (3)

Table S5. Structural parameters of [FOC−CH$_2$−C(OD)F][SbF$_6$] (**3**).

Bond lengths [Å]		Bond angles [°]		Torsion angles [°]	
F2−C3	1.324(3)	O1−C1−F1	114.8(2)	O1−C1−C2−C3	−1.1(3)
F1−C1	1.277(3)	O1−C1−C2	128.4(2)	F1−C1−C2−C3	−179.5(2)
O1−C1	1.239(3)	F1−C1−C2	116.7(2)	C1−C2−C3−O2	6.6(3)
O2−C3	1.188(3)	C1−C2−C3	112.4(2)	C1−C2−C3−F2	−174.7(2)
C1−C2	1.471(3)	O2−C3−F2	121.3(2)	O3−C4−C5−C6	1.3(3)
C2−C3	1.488(3)	O2−C3−C2	126.8(2)	F3−C4−C5−C6	−178.7(2)
F3−C4	1.270(3)	F2−C3−C2	111.9(2)	O4−C6−C5−C4	−0.7(3)
F4−C6	1.323(3)	O3−C4−F3	116.0(2)	F4−C6−C5−C4	179.8(2)
O3−C4	1.240(3)	O3−C4−C5	128.0(2)	O1−C1−C2−C3	−1.1(3)
O4−C6	1.183(3)	F3−C4−C5	116.0(2)		
C4−C5	1.475(3)	O4−C6−F4	121.3(2)		
C6−C5	1.493(3)	O4−C6−C5	126.9(2)		
Sb1−F10	1.8664(14)	F4−C6−C5	111.8(2)		
Sb1−F5	1.8691(14)	C4−C5−C6	112.8(2)		
Sb1−F9	1.8747(15)	F10−Sb1−F5	92.12(7)		
Sb1−F8	1.8778(14)	F10−Sb1−F9	90.29(7)		
Sb1−F7	1.8808(14)	F5−Sb1−F9	90.91(7)		
Sb1−F6	1.8897(14)	F10−Sb1−F8	90.33(7)		
Sb2−F16	1.8647(15)	F5−Sb1−F8	176.15(6)		
Sb2−F15	1.8698(14)	F9−Sb1−F8	92.05(7)		
Sb2−F11	1.8793(15)	F10−Sb1−F7	177.43(6)		
Sb2−F14	1.8802(13)	F5−Sb1−F7	90.36(6)		
Sb2−F12	1.8813(14)	F9−Sb1−F7	90.35(7)		
Sb2−F13	1.8846(15)	F8−Sb1−F7	87.16(7)		
		F10−Sb1−F6	89.35(7)		
		F5−Sb1−F6	88.24(6)		
		F9−Sb1−F6	179.06(6)		
		F8−Sb1−F6	88.81(6)		
		F7−Sb1−F6	90.05(6)		
		F16−Sb2−F15	90.10(7)		
		F16−Sb2−F11	91.34(8)		
		F15−Sb2−F11	91.24(7)		
		F16−Sb2−F14	91.44(7)		
		F15−Sb2−F14	90.99(6)		
		F11−Sb2−F14	176.43(7)		
		F16−Sb2−F12	89.95(7)		
		F15−Sb2−F12	179.35(6)		
		F11−Sb2−F12	88.11(7)		
		F14−Sb2−F12	89.66(6)		
		F16−Sb2−F13	179.23(7)		
		F15−Sb2−F13	90.08(7)		
		F11−Sb2−F13	87.91(7)		
		F14−Sb2−F13	89.30(6)		
		F12−Sb2−F13	89.86(7)		

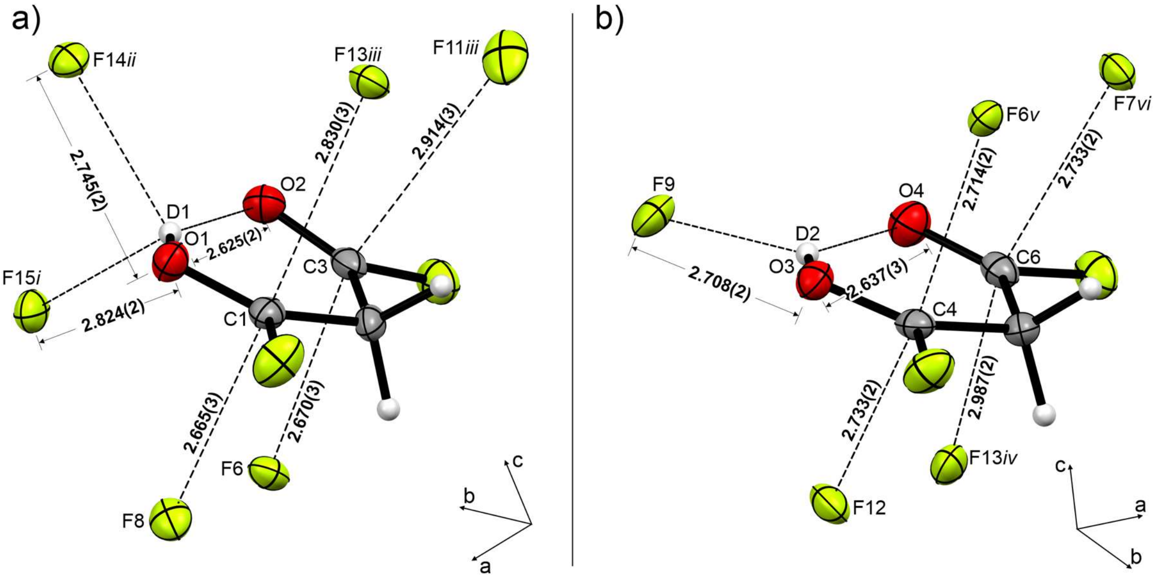

Figure S5. Interionic contacts of two cations a) and b) in the deuterium isotopologue of monoprotonated malonyl difluoride (**3**) with 50% probability displacement ellipsoids. The distances are given in [Å]. Symmetry code: *i* = x,y,1+z; *ii* = −x,2−y,1−z; *iii* = −1+x,y,1+z; *iv* = 1−x,2−y,−z; *v* = 1−x,1−y,1−z; *vi* = 1+x,y,z,1−z.

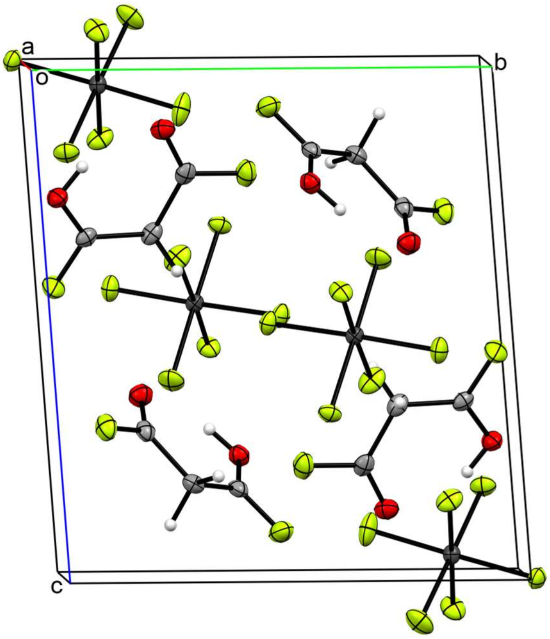

Figure S6. Crystal packing of the deuterium isotopologue of monoprotonated malonyl difluoride (**3**) with 50% probability displacement ellipsoids.

2.5 [F(HO)C−CH$_2$−C(OH)F][SbF$_6$]$_2$ (4)

Table S6. Structural parameters of [(F(HO)C−CH$_2$−C(OH)F][SbF$_6$] (**4**).

Bond lengths [Å]		Bond angles [°]		Torsion angles [°]	
Sb1−F3	1.8564(18)	F3−Sb1−F8	93.99(9)	O1−C1−C2−C3	12.2(4)
Sb1−F8	1.8566(18)	F3−Sb1−F4	89.13(10)	F1−C1−C2−C3	−170.4(2)
Sb1−F4	1.8604(18)	F8−Sb1−F4	92.72(9)	O2−C3−C2−C1	14.2(4)
Sb1−F6	1.8625(18)	F3−Sb1−F6	172.31(8)	F2−C3−C2−C1	−167.5(3)
Sb1−F7	1.8691(18)	F8−Sb1−F6	93.53(8)		
Sb1−F5	1.9525(17)	F4−Sb1−F6	88.91(9)		
Sb2−F13	1.8545(18)	F3−Sb1−F7	90.62(9)		
Sb2−F11	1.8562(19)	F8−Sb1−F7	90.39(8)		
Sb2−F14	1.8573(18)	F4−Sb1−F7	176.89(8)		
Sb2−F9	1.8641(18)	F6−Sb1−F7	90.94(9)		
Sb2−F12	1.8672(19)	F3−Sb1−F5	86.17(8)		
Sb2−F10	1.9745(18)	F8−Sb1−F5	178.18(8)		

F1−C1	1.285(3)	F4−Sb1−F5	89.10(8)
F2−C3	1.285(3)	F6−Sb1−F5	86.36(8)
O1−C1	1.212(4)	F7−Sb1−F5	87.80(8)
O2−C3	1.219(4)	F13−Sb2−F11	93.26(9)
C1−C2	1.477(4)	F13−Sb2−F14	93.95(9)
C3−C2	1.482(4)	F11−Sb2−F14	172.40(9)
		F13−Sb2−F9	93.15(8)
		F11−Sb2−F9	91.44(9)
		F14−Sb2−F9	90.55(9)
		F13−Sb2−F12	91.59(9)
		F11−Sb2−F12	88.23(9)
		F14−Sb2−F12	89.18(9)
		F9−Sb2−F12	175.26(8)
		F13−Sb2−F10	179.54(7)
		F11−Sb2−F10	87.17(8)
		F14−Sb2−F10	85.61(8)
		F9−Sb2−F10	87.00(8)
		F12−Sb2−F10	88.25(8)
		O1−C1−F1	120.1(3)
		O1−C1−C2	125.4(3)
		F1−C1−C2	114.4(3)
		O2−C3−F2	120.0(3)
		O2−C3−C2	126.4(3)
		F2−C3−C2	113.5(3)
		C1−C2−C3	115.4(2)

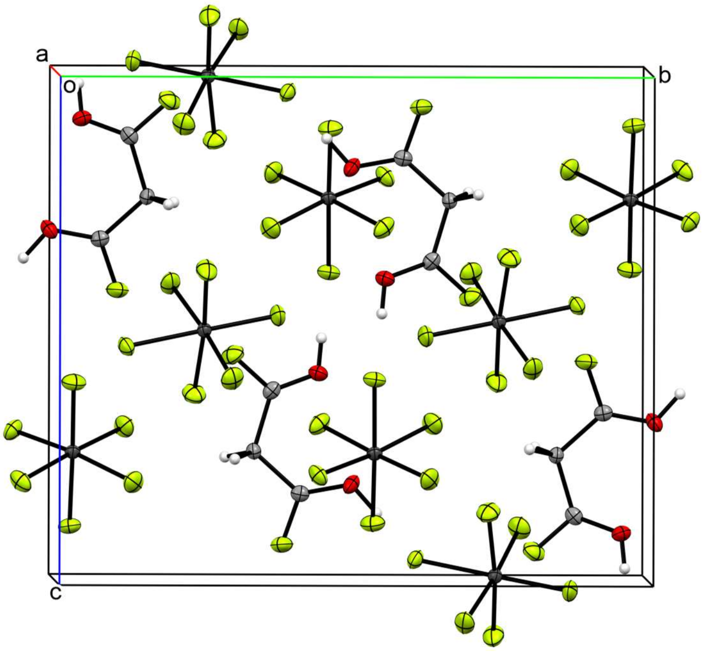

Figure S7. Crystal packing of diprotonated malonyl difluoride (**4**) with 50% probability displacement ellipsoids.

3 Vibrational Data

3.1 Malonyl Difluoride

Table S7. Experimental vibrational frequencies [cm^{-1}] of $\mathrm{FOC{-}CH_2{-}COF}$ (**1**) and calculated vibrational frequencies [cm^{-1}] of $[\mathrm{FOC{-}CH_2{-}COF}]_\mathrm{U}$ (U-gauche) and $[\mathrm{FOC{-}CH_2{-}COF}]_\mathrm{S}$ (S-gauche).

Exp. Raman[a]	Exp. Raman[a]	$[\mathrm{FOC{-}CH_2{-}COF}]_\mathrm{U}$ calc.[b,c] U-gauche (C_2)	Assignment			Exp. IR[a]	$[\mathrm{FOC{-}CH_2{-}COF}]_\mathrm{s}$ calc.[b,c] S-gauche (C_1)[12]	Assignment		
−196 °C (solid)	0 °C (liquid)	IR/Raman				25 °C (gas)	IR/Raman			
2987 (13)					?					
2963 (100)	3000 (26)	3000 (5/41)	ν_{12}	B	$\nu_\mathrm{as}(\mathrm{CH})$		3022 (3/42)	ν_1	A	$\nu(\mathrm{CH_2})$
2935 (52)	2954 (100)	2961 (4/110)	ν_1	A	$\nu_\mathrm{s}(\mathrm{CH})$		2967 (3/104)	ν_2	A	$\nu(\mathrm{CH_2})$
1865 (94)	1857 (72)	1911 (455/20)	ν_2	A	$\nu_\mathrm{s}(\mathrm{CO})$	1875 (vs)	1887 (313/20)	ν_3	A	$\nu(\mathrm{CO})$
1843 (11)		1872 (81/5)	ν_{13}	B	$\nu_\mathrm{as}(\mathrm{CO})$		1876 (291/10)	ν_4	A	$\nu(\mathrm{CO})$
1425 (3)	1405 (17)				?	1418 (w)				?
1372 (39)	1385 (11)	1373 (20/6)	ν_3	A	$\delta(\mathrm{CH_2})$	1392 (m)	1385 (32/5)	ν_5	A	$\delta(\mathrm{CH_2})$
1366 (44)		1349 (191/0)	ν_{14}	B	$\omega(\mathrm{CH_2})$	1360 (m)	1319 (152/1)	ν_6	A	$\omega(\mathrm{CH_2})$
1229 (7)	1242 (6)	1201 (11/1)	ν_4	A	$\tau(\mathrm{CH_2})$	1284 (s)	1225 (86/2)	ν_7	A	$\tau(\mathrm{CH_2})$
						1192 (s)				?
						1175 (s)				?
1152 (3)	1151 (5)	1135 (62/3)	ν_5	A	$\nu_\mathrm{s}(\mathrm{CF})$	1148 (m)	1135 (91/2)	ν_8	A	$\nu(\mathrm{CF})$
1062 (4)	1104 (5)	1061 (380/2)	ν_{15}	B	$\nu_\mathrm{as}(\mathrm{CF})$	1107 (m)	1101 (261/2)	ν_9	A	$\nu(\mathrm{CF})$
	1073 (3)				?	1086 (s)				?
954 (6)	955 (7)	930 (11/0)	ν_{16}	B	$\gamma(\mathrm{COF})$		938 (6/1)	ν_{10}	A	$\gamma(\mathrm{COF})$
917 (22)	909 (42)	894 (62/0)	ν_{17}	B	$\nu(\mathrm{CC})$	899 (w)	894 (13/5)	ν_{11}	A	$\nu(\mathrm{CC})$
909 (23)	856 (16)	893 (10/10)	ν_6	A	$\nu(\mathrm{CC})$	866 (w)	864 (41/5)	ν_{12}	A	$\nu(\mathrm{CC})$
900 (26)					?					
700 (5)	726 (24)	687 (21/3)	ν_7	A	$\delta(\mathrm{FCO})$	727 (vw)	717 (20/4)	ν_{13}	A	$\delta(\mathrm{FCO})$
687 (6)	700 (7)				?	706 (w)				?
631 (19)	628 (28)	609 (37/2)	ν_{18}	B	$\delta(\mathrm{FCO})$	631 (m)	611 (36/2)	ν_{14}	A	$\delta(\mathrm{FCO})$
596 (3)	571 (3)	578 (7/0)	ν_8	A	$\gamma(\mathrm{COF})$	569 (w)	556 (18/1)	ν_{15}	A	$\gamma(\mathrm{COF})$
502 (3)	540 (4)	490 (10/0)	ν_{19}	B	$\rho(\mathrm{CH_2})$	548 (vw)	530 (12/1)	ν_{16}	A	$\rho(\mathrm{CH_2})$
405 (3)	406 (16)	359 (0/2)	ν_9	A	$\delta(\mathrm{CCF})$		394 (0/1)	ν_{17}	A	$\delta(\mathrm{CCO})$
376 (21)	371 (28)	345 (1/1)	ν_{20}	B	$\delta(\mathrm{CCO})$		345 (1/1)	ν_{18}	A	$\delta(\mathrm{CCF})$
		175 (2/0)	ν_{10}	A	$\delta(\mathrm{CCC})$		149 (3/0)	ν_{19}	A	$\delta(\mathrm{CCC})$
		31 (0/1)	ν_{11}	A	$\tau(\mathrm{COF})$		61 (7/0)	ν_{20}	A	$\rho(\mathrm{COF})$
		24 (10/0)	ν_{21}	B	$\rho(\mathrm{COF})$		56 (1/1)	ν_{21}	A	$\tau(\mathrm{COF})$

[a] Abbreviations for IR intensities: vs = very strong, s = strong, m = medium, w = weak, vw = very weak. Experimental Raman intensities are relative to a scale of 1 to 100. [b] Calculated on the M06-2X/aug-cc-pVTZ level of theory. Scaling factor: 0.956. [c] IR intensities in km/mol; Raman intensities in Å^4/u.

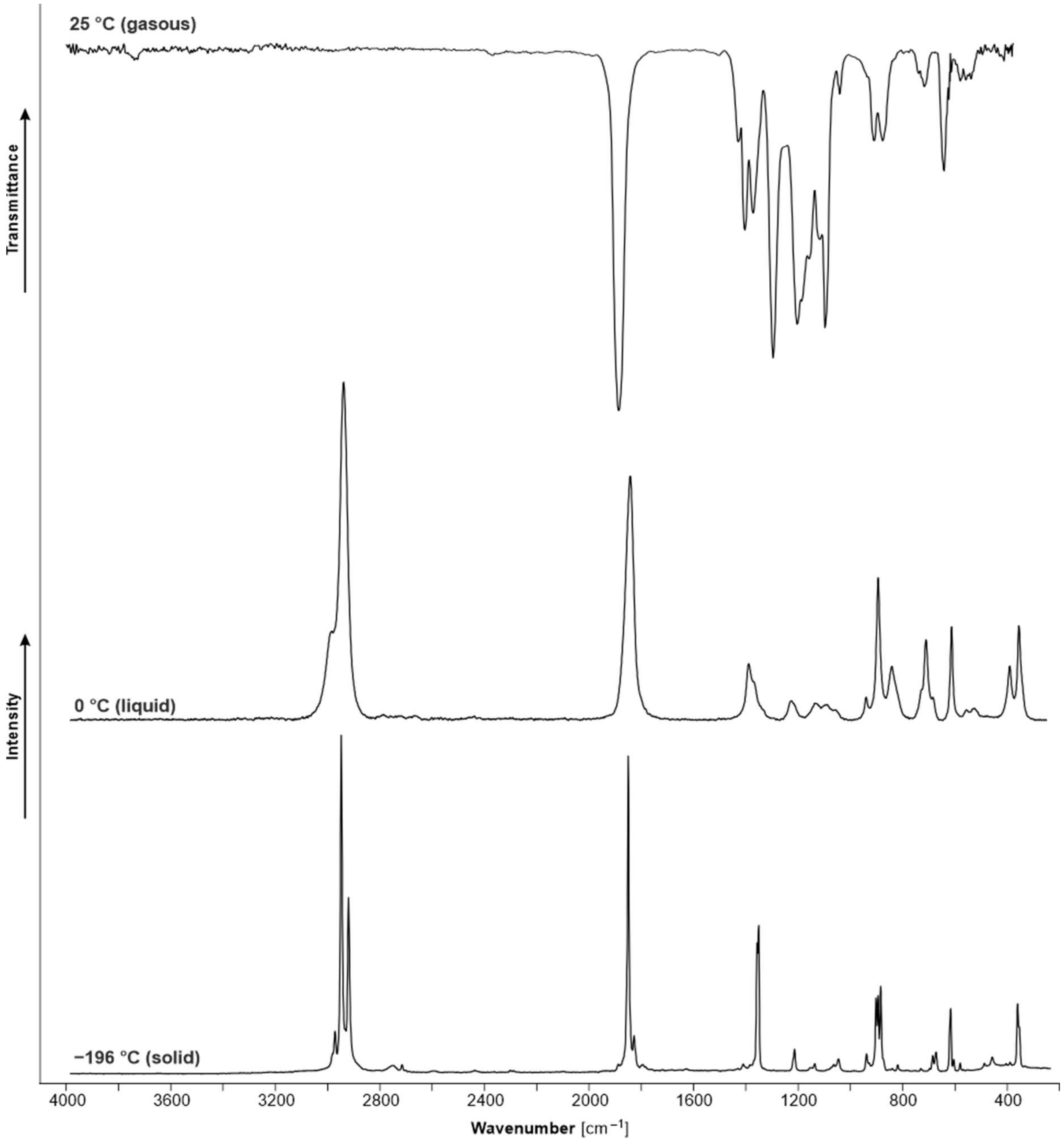

Figure S8. Raman spectra of malonyl difluoride (**1**) at −196 °C(solid), 0 °C(liquid), and gas IR spectrum of **1** at ambient temperatures.

3.2 Hemiprotonated Malonyl Difluoride

Table S8. Experimental vibrational frequencies [cm^{-1}] of [(FOC−CH$_2$−COF)$_2$H][SbF$_6$] (**6**) and calculated vibrational frequencies [cm^{-1}] of [(FOC−CH$_2$−COF)$_2$H]$^+$. Raman active vibrations are marked in bold.

[(FOC−CH$_2$−COF)$_2$H][SbF$_6$] (**6**) exp.[a] Raman	[(FOC−CH$_2$−COF)$_2$H]$^+$ calc.[b,c] IR/Raman	Assignment		
	3026 (33/0)	ν_{25}	A_u	$\nu(\mathrm{CH_2})$
2985 (20)	**3026 (0/77)**	**ν_{1}**	**A_g**	**$\nu(\mathrm{CH_2})$**
2964 (12)				
2933 (40)	**2965 (0/211)**	**ν_{2}**	**A_g**	**$\nu(\mathrm{CH_2})$**
	2965 (38/0)	ν_{26}	A_u	$\nu(\mathrm{CH_2})$
	1869 (614/0)	ν_{27}	A_u	$\nu(\mathrm{CO})$
1856 (33)	**1868 (0/21)**	**ν_{3}**	**A_g**	**$\nu(\mathrm{CO})$**
	1772 (296/0)	ν_{28}	A_u	$\nu(\mathrm{CO})$
1748 (13)	**1759 (0/27)**	**ν_{4}**	**A_g**	**$\nu(\mathrm{CO})$**
	1502 (577/0)	ν_{29}	A_u	$\nu(\mathrm{O{\cdots}H{\cdots}O})$
1364 (28)	**1401 (0/5)**	**ν_{5}**	**A_g**	**$\delta(\mathrm{CH_2})$**
	1389 (65/0)	ν_{30}	A_u	$\delta(\mathrm{CH_2})$
1317 (8)	**1338 (0/13)**	**ν_{6}**	**A_g**	**$\nu(\mathrm{CF})$**
	1308 (371/0)	ν_{31}	A_u	$\delta(\mathrm{COH})$
	1298 (273/0)	ν_{32}	A_u	$\nu(\mathrm{CF})$
1228 (9)	**1295 (0/9)**	**ν_{7}**	**A_g**	**$\omega(\mathrm{CH_2})$**
	1237 (162/0)	ν_{33}	A_u	$\delta(\mathrm{COH})$
1125 (6)	**1160 (0/4)**	**ν_{8}**	**A_g**	**$\nu(\mathrm{CF})$**
	1160 (146/0)	ν_{34}	A_u	$\nu(\mathrm{CF})$
1101 (5)	**1137 (0/6)**	**ν_{9}**	**A_g**	**$\tau(\mathrm{CH_2})$**
	1134 (173/0)	ν_{35}	A_u	$\tau(\mathrm{CH_2})$
949 (7)	**950 (0/2)**	**ν_{10}**	**A_g**	**$\delta(\mathrm{CH_2})$**
	944 (145/0)	ν_{36}	A_u	$\nu(\mathrm{O{\cdots}H{\cdots}O})$
939 (7)				?
	912 (237/0)	ν_{37}	A_u	$\nu(\mathrm{CC})$
909 (8)				?
900 (7)	**910 (0/9)**	**ν_{11}**	**A_g**	**$\nu(\mathrm{CC})$**
	894 (148/0)	ν_{38}	A_u	$\nu(\mathrm{CC})$
884 (42)	**888 (0/12)**	**ν_{12}**	**A_g**	**$\nu(\mathrm{CC})$**
718 (8)	**750 (0/12)**	**ν_{13}**	**A_g**	**$\delta(\mathrm{CCC})$**
	738 (11/0)	ν_{39}	A_u	$\delta(\mathrm{CCC})$
	702 (0/1)	**ν_{14}**	**A_g**	**$\delta(\mathrm{CCO})$**
	612 (674/0)	ν_{40}	A_u	$\delta(\mathrm{OCF})$
	575 (2803/0)	ν_{41}	A_u	$\nu(\mathrm{O{\cdots}H{\cdots}O})$
572 (10)	**569 (0/4)**	**ν_{15}**	**A_g**	**$\delta(\mathrm{OCF})$**
	553 (1017/0)	ν_{42}	A_u	$\delta(\mathrm{CCO})$
559 (10)	**547 (0/3)**	**ν_{16}**	**A_g**	**$\gamma(\mathrm{COF})$**
	521 (1412/0)	ν_{43}	A_u	$\gamma(\mathrm{COF})$
536 (7)	**518 (0/2)**	**ν_{17}**	**A_g**	**$\gamma(\mathrm{COF})$**
352 (13)	**356 (0/0)**	**ν_{18}**	**A_g**	**$\delta(\mathrm{CCF})$**
	345 (110/0)	ν_{44}	A_u	$\delta(\mathrm{CCF})$
	335 (1825/0)	ν_{45}	A_u	$\delta(\mathrm{CCO})$
267 (9)	**255 (0/2)**	**ν_{19}**	**A_g**	**$\rho(\mathrm{CH_2})$**
	184 (0/1)	**ν_{20}**	**A_g**	**$\delta(\mathrm{CCC})$**
	149 (75/0)	ν_{46}	A_u	$\delta(\mathrm{CCC})$
	111 (0/0)	**ν_{21}**	**A_g**	**$\delta(\mathrm{COH})$**
	88 (0/1)	**ν_{22}**	**A_g**	**$\tau(\mathrm{O{\cdots}H{\cdots}O})$**
	71 (66/0)	ν_{47}	A_u	$\rho(\mathrm{CH_2})$
	64 (7/0)	ν_{48}	A_u	$\delta(\mathrm{CCF})$
	56 (0/1)	**ν_{23}**	**A_g**	**$\delta(\mathrm{CCF})$**
	35 (0/1)	**ν_{24}**	**A_g**	**$\tau(\mathrm{O{\cdots}H{\cdots}O})$**
	29 (18/0)	ν_{49}	A_u	$\delta(\mathrm{COH})$
	20 (2/0)	ν_{50}	A_u	$\delta(\mathrm{O{\cdots}H{\cdots}O})$
	8 (6/0)	ν_{51}	A_u	$\tau(\mathrm{O{\cdots}H{\cdots}O})$
Vibrations of the anion $\mathrm{SbF_6^-}$				
671 (61)				$\mathrm{SbF_6^-}$
655 (100)				$\mathrm{SbF_6^-}$
638 (29)				$\mathrm{SbF_6^-}$
623 (13)				$\mathrm{SbF_6^-}$
581 (15)				$\mathrm{SbF_6^-}$
480 (10)				$\mathrm{SbF_6^-}$
375 (12)				$\mathrm{SbF_6^-}$
291 (38)				$\mathrm{SbF_6^-}$
280 (28)				$\mathrm{SbF_6^-}$

[a] The experimental Raman intensities are corrected to a scale of 1 to 100 [b] Calculated on the M06-2X/aug-cc-pVTZ level of theory. Scaling factor: 0.956. [c] IR intensities in km/mol; Raman intensities in Å^4/u.

3.3 Monoprotonated Malonyl Difluoride

Table S9. Experimental vibrational frequencies [cm^{-1}] of [FOC−CH$_2$−C(O*X*)F][SbF$_6$] (**2**, **3**) (*X* = D, H) and calculated vibrational frequencies [cm^{-1}] of [FOC−CH$_2$−C(O*X*)F · HF]$^+$.

[FOC−CH$_2$−C(OH)F][SbF$_6$] (**2**) exp.[a]		[FOC−CH$_2$−C(OH)F · HF]$^+$ calc.[b,c]	Assignment			[FOC−CH$_2$−C(OD)F][SbF$_6$] (**3**) exp.[a]		[FOC−CH$_2$−C(OD)F · HF]$^+$ calc.[b,c]	Assignment		
Raman	IR	IR/Raman				Raman	IR	IR/Raman			
	3230 (m)	2780 (2396/109)	ν_3	A	$\nu(\mathrm{OH})$	2953 (10)	2949 (m)	2946 (39/44)	ν_{17}	A''	$\nu_{as}(\mathrm{CH_2})$
	3121 (m)				H_3O^+[d][13]	2920 (8)					?
3025 (12)	3022 (m)	3022 (25/37)	ν_1	A	$\nu(\mathrm{CH_2})$	2906 (11)	2906 (m)	2917 (53/113)	ν_1	A'	$\nu_s(\mathrm{CH_2})$
	2984 (w)				(**6**)[d]	2227 (2)	2127 (m, br)	2083 (826/24)	ν_2	A'	$\nu(\mathrm{OD})$
	2962 (w)				(**1**)[d]		1859 (m)				(**1**)[d]
2922 (3)	2930 (w)				(**6**)[d]	1807 (4)	1805 (m)	1860 (255/17)	ν_3	A'	$\nu(\mathrm{CO})$
2894 (15)	2889 (m)	2959 (23/100)	ν_2	A	$\nu(\mathrm{CH_2})$		1680 (w)				?
1857 (15)	1865 (s)	1869 (278/11)	ν_4	A	$\nu(\mathrm{CO})$	1653 (2)	1641 (m)	1667 (192/3)	ν_4	A'	$\nu(\mathrm{CO})$
	1649 (m)	1670 (343/7)	ν_5	A	$\nu(\mathrm{CO})$		1618 (m)				?
	1479 (m)	1467 (226/4)	ν_6	A	$\nu(\mathrm{CF})$		1581 (w)				?
	1431 (m)				?		1522 (w)				?
1387 (8)	1387 (m)	1380 (29/5)	ν_7	A	$\delta(\mathrm{CH_2})$	1484 (2)	1473 (m)	1451 (316/3)	ν_5	A'	$\nu(\mathrm{CF})$
1381 (6)	1360 (m)				?	1331 (11)	1391 (w)	1335 (31/5)	ν_6	A'	$\omega(\mathrm{CH_2})$
	1337 (m)				?	1321 (8)	1319 (m)	1322 (88/7)	ν_7	A'	$\delta(\mathrm{CH_2})$
1251 (2)	1252 (w)	1281 (284/7)	ν_8	A	$\omega(\mathrm{CH_2})$		1246 (w)				
1239 (1)	1236 (w)				?	1216 (5)	1215 (w)	1181 (0/2)	ν_{18}	A''	$\tau(\mathrm{CH_2})$
1221 (1)	1221 (m)	1229 (58/3)	ν_9	A	$\delta(\mathrm{COH})$		1157 (m)	1159 (223/1)	ν_8	A'	$\nu(\mathrm{CF})$
1201 (4)	1190 (m)	1162 (172/2)	ν_{10}	A	$\nu(\mathrm{CF})$	993 (11)					?
	1163 (m)				?	983 (13)	984 (s)				?
	1128 (m)				?	952 (3)	943 (s)	930 (33/0)	ν_{19}	A''	$\gamma(\mathrm{COF})$
1115 (2)	1113 (s)	1137 (32/3)	ν_{11}	A	$\tau(\mathrm{CH_2})$	928 (4)		919 (2/1)	ν_9	A'	$\nu(\mathrm{CC})$
	1068 (m)				?	893 (5)	881 (s)	896 (1/8)	ν_{10}	A'	$\nu(\mathrm{CC})$
	1013 (s)				?	816 (10)	808 (s)	779 (405/7)	ν_{11}	A'	$\delta(\mathrm{COD})$
953 (7)	953 (m)	948 (97/0)	ν_{12}	A	$\delta(\mathrm{COH})$	691 (6)	690 (vs)	699 (35/0)	ν_{20}	A''	$\delta(\mathrm{COD})$
	941 (m)				?			666 (74/3)	ν_{12}	A'	$\delta(\mathrm{CCO})$
929 (10)	928 (m)	932 (41/1)	ν_{13}	A	$\delta(\mathrm{COH})$	591 (7)	608 (vs)	607 (1/0)	ν_{21}	A''	$\gamma(\mathrm{COF})$
908 (8)	899 (m)	909 (6/7)	ν_{14}	A	$\nu(\mathrm{CC})$	578 (5)	586 (vs)	601 (35/1)	ν_{13}	A'	$\delta(\mathrm{COF})$
884 (1)		873 (29/5)	ν_{15}	A	$\nu(\mathrm{CC})$		442 (s)	435 (8/0)	ν_{22}	A''	$\rho(\mathrm{CH_2})$
858 (3)	831 (m)				?	401 (8)	397 (s)	406 (152/0)	ν_{14}	A'	$\delta(\mathrm{CCF})$
725 (2)	725 (w)	732 (14/6)	ν_{16}	A	$\delta(\mathrm{CCC})$	376 (4)	374 (s)	378 (7/3)	ν_{15}	A'	$\delta(\mathrm{CCC})$
582 (7)	581 (m)	610 (21/2)	ν_{17}	A	$\delta(\mathrm{OCF})$			228 (8/0)	ν_{16}	A'	$\delta(\mathrm{CCC})$
559 (3)	569 (m)	549 (12/3)	ν_{18}	A	$\delta(\mathrm{OCF})$			112 (2/0)	ν_{23}	A''	$\tau(\mathrm{COF})$
527 (5)	523 (s)	533 (10/1)	ν_{19}	A	$\gamma(\mathrm{COF})$			73 (13/0)	ν_{24}	A''	$\rho(\mathrm{COF})$
417 (4)	417 (m)	430 (122/1)	ν_{20}	A	$\rho(\mathrm{CH_2})$						
390 (6)	392 (m)	374 (61/1)	ν_{21}	A	$\rho(\mathrm{CH_2})$						
328 (1)		340 (12/0)	ν_{22}	A	$\delta(\mathrm{CCF})$						
		153 (7/0)	ν_{23}	A	$\delta(\mathrm{CCC})$						
		68 (9/1)	ν_{24}	A	$\tau(\mathrm{COF})$						
Vibrations of the anion SbF_6^-						Vibrations of the anion SbF_6^-					
670 (100)	679 (vs)				SbF_6^-	673 (14)	665 (vs)				SbF_6^-
654 (12)	669 (vs)				SbF_6^-	658 (100)	656 (vs)				SbF_6^-
646 (20)	648 (s)				SbF_6^-		638 (vs)				SbF_6^-
636 (33)	636 (s)				SbF_6^-		621 (vs)				SbF_6^-
608 (3)					SbF_6^-	560 (6)	559 (vs)				SbF_6^-
477 (2)	476 (m)				SbF_6^-	549 (5)	544 (vs)				SbF_6^-
298 (10)					SbF_6^-	526 (3)					SbF_6^-
282 (20)					SbF_6^-	489 (3)	490 (s)				SbF_6^-
271 (13)					SbF_6^-		463 (s)				SbF_6^-
						306 (5)					SbF_6^-
						287 (28)					SbF_6^-
						268 (7)					SbF_6^-

[a] The experimental Raman intensities are corrected to a scale of 1 to 100 [b] Calculated on the M06-2X/aug-cc-pVTZ level of theory. Scaling factor: 0.956. [c] IR intensities in km/mol; Raman intensities in Å^4/u. [d] Traces of the respective compound as impurities.

3.4 Diprotonated Malonyl Difluoride

Table S10. Experimental vibrational frequencies [cm^{-1}] of $[CH_2(C(OX)F)_2][SbF_6]_2$ (**4**, **5**) (X = D, H) and calculated vibrational frequencies [cm^{-1}] of $[CH_2(C(OD)F)_2 \cdot 2HF]^{2+}$.

$[CH_2(C(OH)F)_2][SbF_6]_2$ (**4**) exp.[a]	$[CH_2(C(OH)F)_2 \cdot 2HF]^{2+}$ calc.[b,c]	Assignment			$[CH_2(C(OD)F)_2][SbF_6]_2$ (**5**) exp.[a]	$[CH_2(C(OD)F)_2 \cdot 2HF]^{2+}$ calc.[b,c]	Assignment		
Raman	IR/Raman				Raman	IR/Raman			
2945 (12)	2902 (76/41)	ν_{15}	B	$\nu_{as}(CH_2)$	2926 (11)	2902 (76/41)	ν_{15}	B	$\nu_{as}(CH_2)$
2878 (17)	2880 (83/120)	ν_{1}	A	$\nu_{s}(CH_2)$	2891 (11)	2880 (96/118)	ν_{1}	A	$\nu_{s}(CH_2)$
	2132 (1809/66)	ν_{2}	A	$\nu_{s}(OH)$	2361 (2)	1598 (842/18)	ν_{3}	A	$\nu_{s}(OD)$
	2064 (5220/33)	ν_{16}	B	$\nu_{as}(OH)$		1551 (2826/7)	ν_{17}	B	$\nu_{as}(OD)$
1797 (4)	1733 (839/5)	ν_{3}	A	$\nu_{s}(CO)$	1751 (4)	1737 (514/9)	ν_{2}	A	$\nu_{s}(CO)$
	1676 (306/1)	ν_{17}	B	$\nu_{as}(CO)$	1706 (2)	1684 (8/4)	ν_{16}	B	$\nu_{as}(CO)$
	1491 (98/1)	ν_{18}	B	$\nu_{as}(CF)$		1435 (247/7)	ν_{18}	B	$\nu_{as}(CF)$
	1435 (456/7)	ν_{4}	A	$\nu_{s}(CF)$		1356 (458/17)	ν_{4}	A	$\nu_{s}(CF)$
	1320 (1/0)	ν_{19}	B	$\delta(COH)$	1347 (11)	1307 (74/11)	ν_{5}	A	$\delta(CH_2)$
1348 (13)	1307 (87/10)	ν_{5}	A	$\delta(CH_2)$		1225 (58/0)	ν_{19}	B	$\omega(CH_2)$
1274 (3)	1276 (40/4)	ν_{6}	A	$\delta(COH)$	1231 (5)	1213 (0/2)	ν_{6}	A	$\tau(CH_2)$
1231 (10)	1214 (0/2)	ν_{7}	A	$\tau(CH_2)$	1050 (1)	1015 (4/0)	ν_{20}	B	$\delta(COD)$
1218 (1)	1204 (87/0)	ν_{20}	B	$\omega(CH_2)$	1035 (2)	1010 (60/2)	ν_{7}	A	$\delta(COD)$
	1045 (220/0)	ν_{21}	B	$\delta(COH)$	969 (5)				?
	1040 (0/0)	ν_{8}	A	$\delta(COH)$	944 (2)	929 (38/0)	ν_{21}	B	$\gamma(COF)$
923 (8)	929 (16/0)	ν_{22}	B	$\nu_{as}(CC)$	928 (5)	890 (16/0)	ν_{22}	B	$\nu_{as}(CC)$
946 (3)	929 (38/0)	ν_{23}	B	$\gamma(COF)$	910 (4)	852 (78/9)	ν_{8}	A	$\nu_{s}(CC)$
893 (9)	879 (34/9)	ν_{9}	A	$\nu_{s}(CC)$		774 (0/0)	ν_{9}	A	$\delta(COD)$
713 (4)	706 (10/1)	ν_{10}	A	$\delta(OCF)$	720 (2)	767 (101/0)	ν_{23}	B	$\delta(COD)$
	647 (22/2)	ν_{24}	B	$\delta(CCF)$	698 (37)	685 (21/1)	ν_{10}	A	$\delta(OCF)$
	630 (0/0)	ν_{11}	A	$\gamma(COF)$		632 (36/2)	ν_{24}	B	$\delta(CCF)$
424 (3)	452 (0/0)	ν_{25}	B	$\rho(CH_2)$	494 (2)	613 (0/0)	ν_{11}	A	$\gamma(COF)$
355 (2)	389 (74/0)	ν_{12}	A	$\delta(CCC)$	431 (4)	445 (0/0)	ν_{25}	B	$\rho(CH_2)$
	247 (17/1)	ν_{26}	B	$\delta(CCF)$	384 (3)	383 (63/0)	ν_{12}	A	$\delta(CCC)$
	140 (2/0)	ν_{13}	A	$\delta(CCC)$		247 (17/1)	ν_{26}	B	$\delta(CCF)$
	99 (42/1)	ν_{27}	B	$\rho(COF)$		139 (2/0)	ν_{13}	A	$\delta(CCC)$
	15 (0/0)	ν_{14}	A	$\tau(COF)$		98 (39/1)	ν_{27}	B	$\rho(COF)$
						15 (0/0)	ν_{14}	A	$\tau(COF)$
Vibrations of the anion SbF_6^-					Vibrations of the anion SbF_6^-				
675 (59)				SbF_6^-	674 (88)				SbF_6^-
657 (100)				SbF_6^-	655 (100)				SbF_6^-
639 (35)				SbF_6^-	645 (11)				SbF_6^-
623 (13)				SbF_6^-	619 (6)				SbF_6^-
579 (12)				SbF_6^-	609 (4)				SbF_6^-
567 (9)				SbF_6^-	598 (14)				SbF_6^-
325 (3)				SbF_6^-	343 (2)				SbF_6^-
307 (4)				SbF_6^-	300 (27)				SbF_6^-
297 (23)				SbF_6^-	288 (12)				SbF_6^-
292 (23)				SbF_6^-	268 (9)				SbF_6^-
282 (25)				SbF_6^-					

[a] The experimental Raman intensities are corrected to a scale of 1 to 100 [b] Calculated on the M06-2X/aug-cc-pVTZ level of theory. Scaling factor: 0.956. [c] IR intensities in km/mol; Raman intensities in Å^4/u.

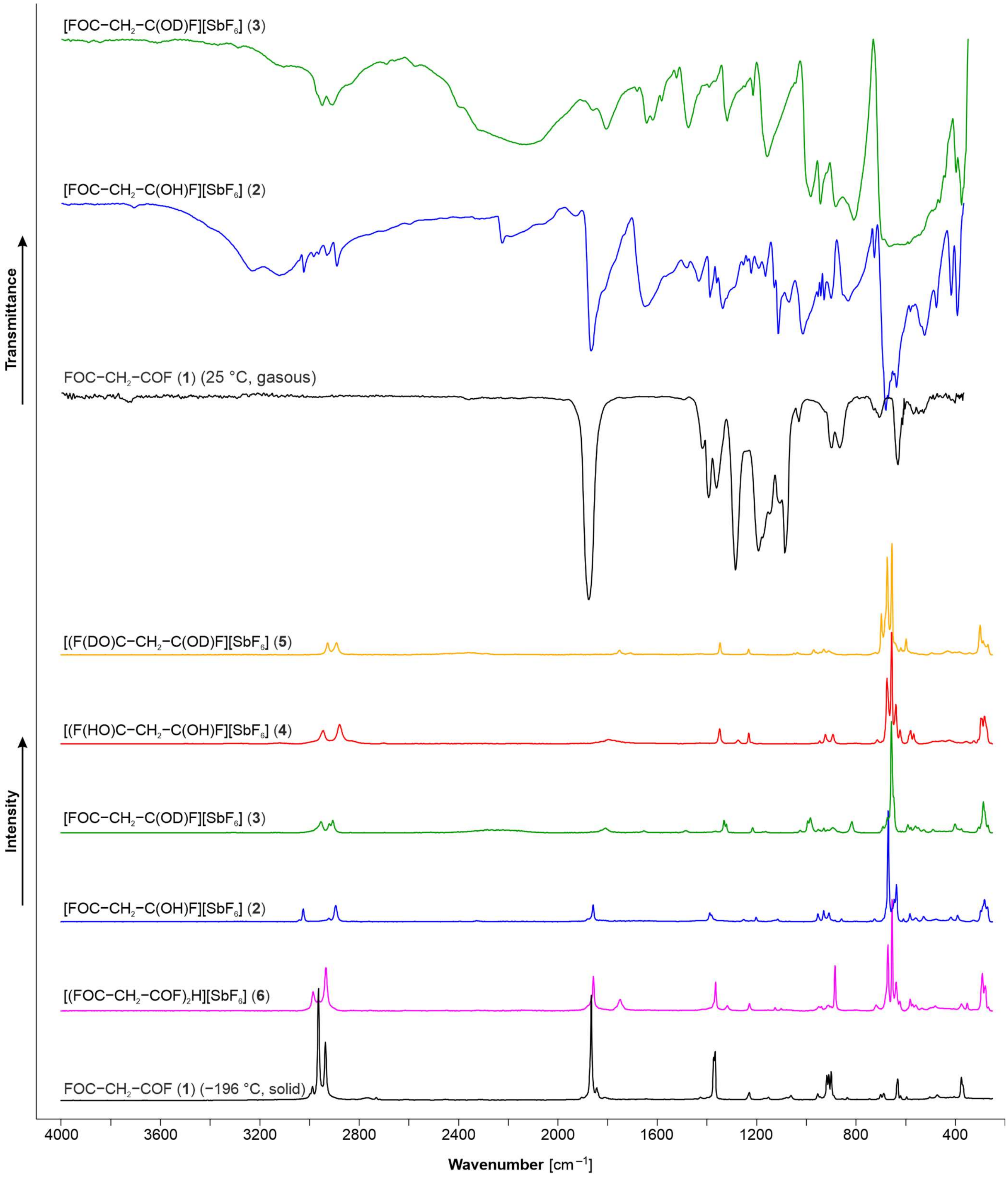

Figure S9. Low-temperature and Raman spectra of **1**, **2**, **3**, **4**, **5**, **6**, gas IR spectrum of **1**, and low-temperature IR spectra of **2** and **3**.

4 NMR

4.1 Malonyl Difluoride

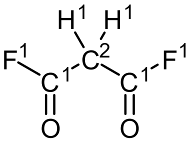

^{1}H NMR (400 MHz, *a*HF) δ [ppm] = 3.58 (s, H1).
^{13}C NMR (101 MHz, *a*HF) δ [ppm] = 158.49 (dd, J=358.8 Hz, 14.6 Hz; C1), 33.43 (t, J=59.2 Hz, C2).
^{19}F NMR (376 MHz, *a*HF) δ [ppm] = 44.78 (s, F1).

^{1}H NMR - Malonyldifluoride in *a*HF

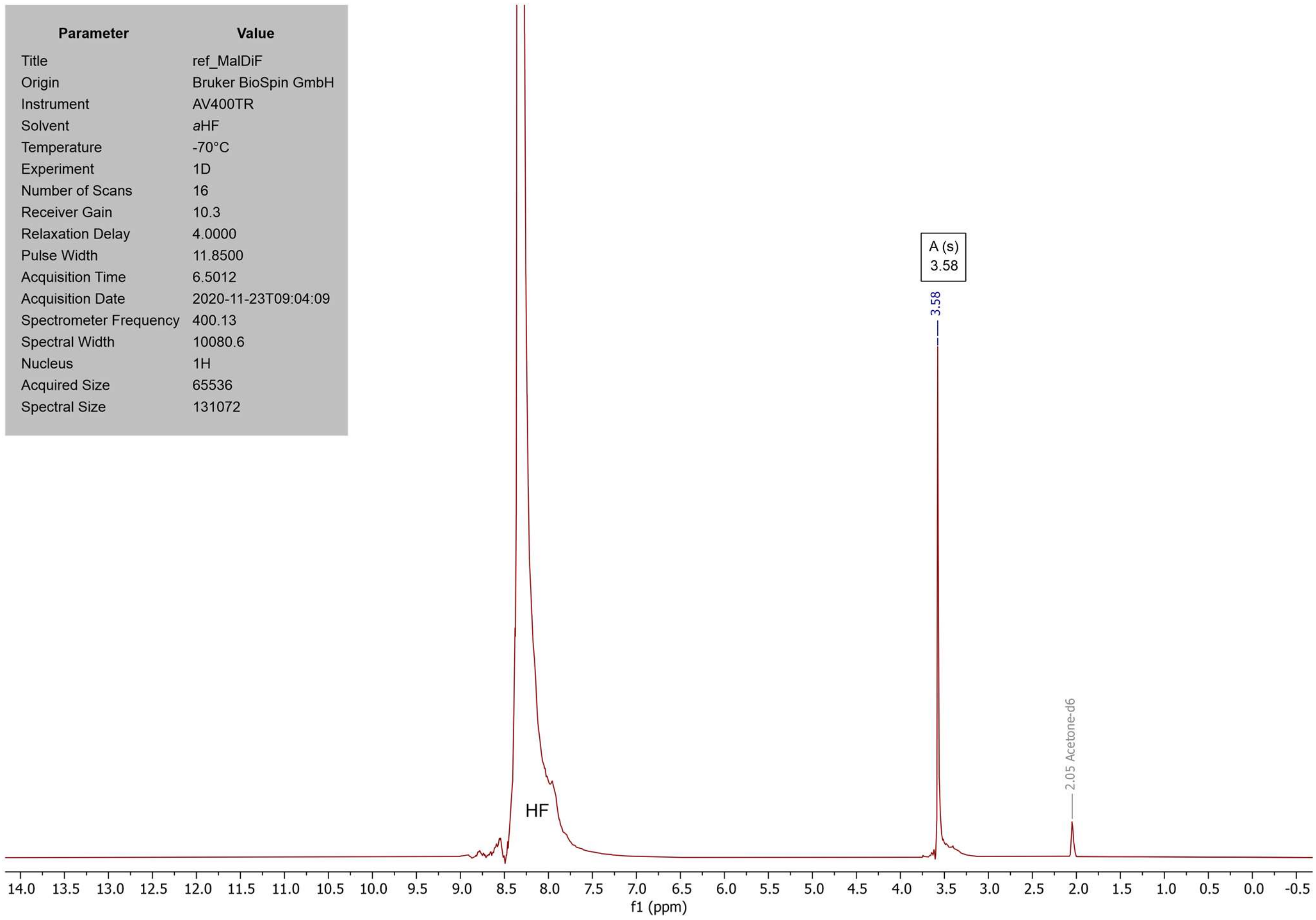

Parameter	Value
Title	ref_MalDiF
Origin	Bruker BioSpin GmbH
Instrument	AV400TR
Solvent	*a*HF
Temperature	-70°C
Experiment	1D
Number of Scans	16
Receiver Gain	10.3
Relaxation Delay	4.0000
Pulse Width	11.8500
Acquisition Time	6.5012
Acquisition Date	2020-11-23T09:04:09
Spectrometer Frequency	400.13
Spectral Width	10080.6
Nucleus	1H
Acquired Size	65536
Spectral Size	131072

^{13}C NMR - Malonyldifluoride in *a*HF

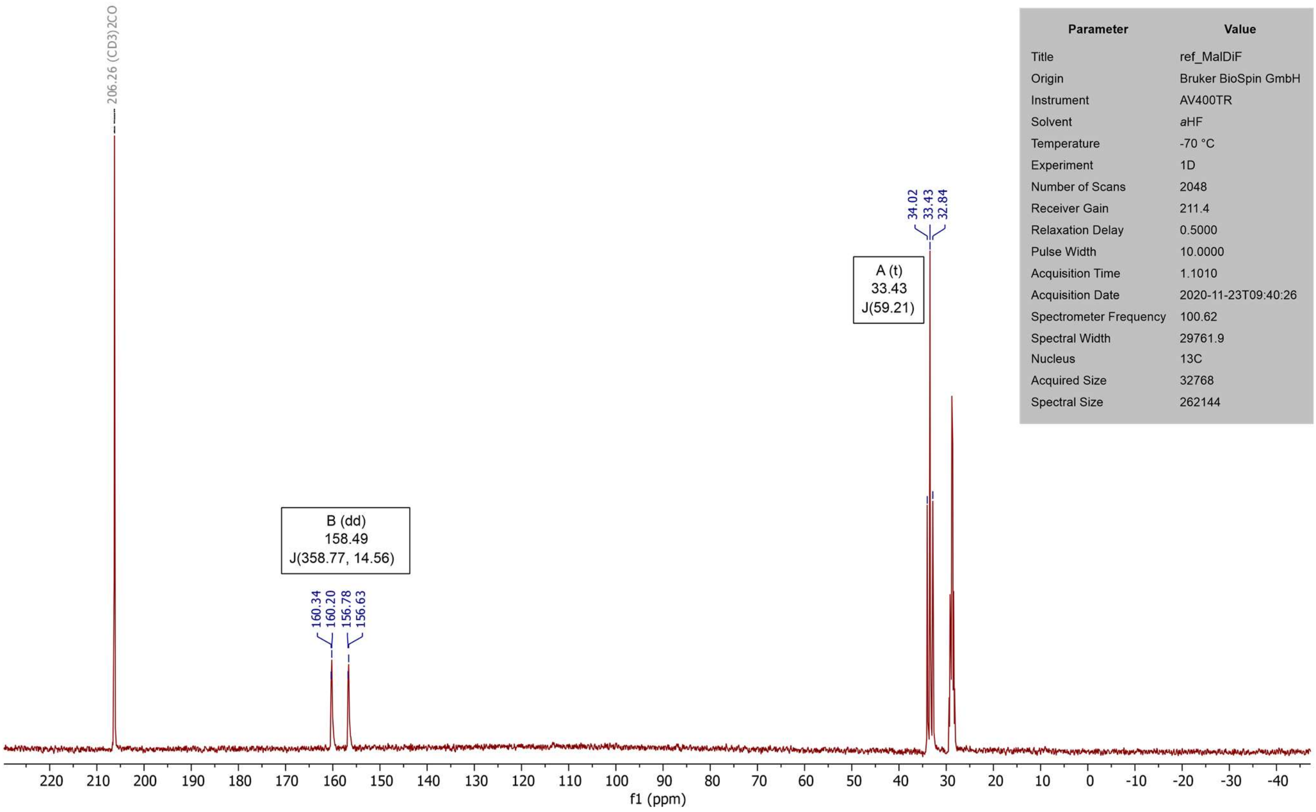

Parameter	Value
Title	ref_MalDiF
Origin	Bruker BioSpin GmbH
Instrument	AV400TR
Solvent	*a*HF
Temperature	-70 °C
Experiment	1D
Number of Scans	2048
Receiver Gain	211.4
Relaxation Delay	0.5000
Pulse Width	10.0000
Acquisition Time	1.1010
Acquisition Date	2020-11-23T09:40:26
Spectrometer Frequency	100.62
Spectral Width	29761.9
Nucleus	13C
Acquired Size	32768
Spectral Size	262144

^{19}F NMR - Malonyldifluoride in *a*HF

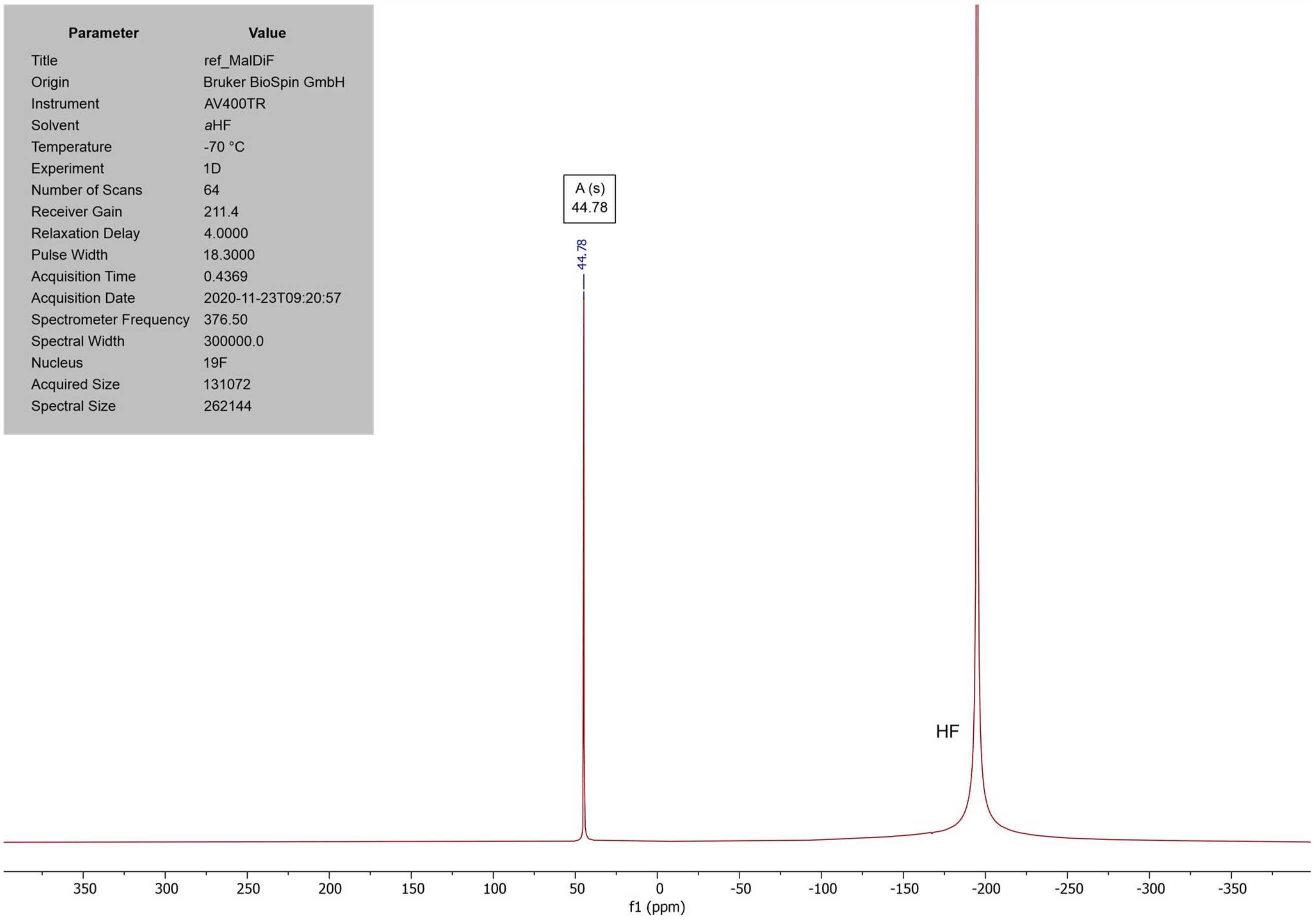

Parameter	Value
Title	ref_MalDiF
Origin	Bruker BioSpin GmbH
Instrument	AV400TR
Solvent	*a*HF
Temperature	-70 °C
Experiment	1D
Number of Scans	64
Receiver Gain	211.4
Relaxation Delay	4.0000
Pulse Width	18.3000
Acquisition Time	0.4369
Acquisition Date	2020-11-23T09:20:57
Spectrometer Frequency	376.50
Spectral Width	300000.0
Nucleus	19F
Acquired Size	131072
Spectral Size	262144

4.2 Monoprotonated Malonyl difluoride

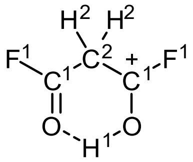

^{1}H NMR (400 MHz, *a*HF) δ [ppm] = 10.52 – 9.99 (m, H1), 4.45 – 4.40 (m, H2).
^{13}C NMR (101 MHz, *a*HF) δ [ppm] = 166.80 (dd, *J*=365.5 Hz, 14.0 Hz, C1), 34.79 (t, *J*=49.9 Hz, C2).
^{19}F NMR (376 MHz, *a*HF) δ [ppm] = 49.59 (s, F1).

^{1}H NMR - [FOC−CH$_2$−C(OH)F][SbF$_6$] (2) in *a*HF

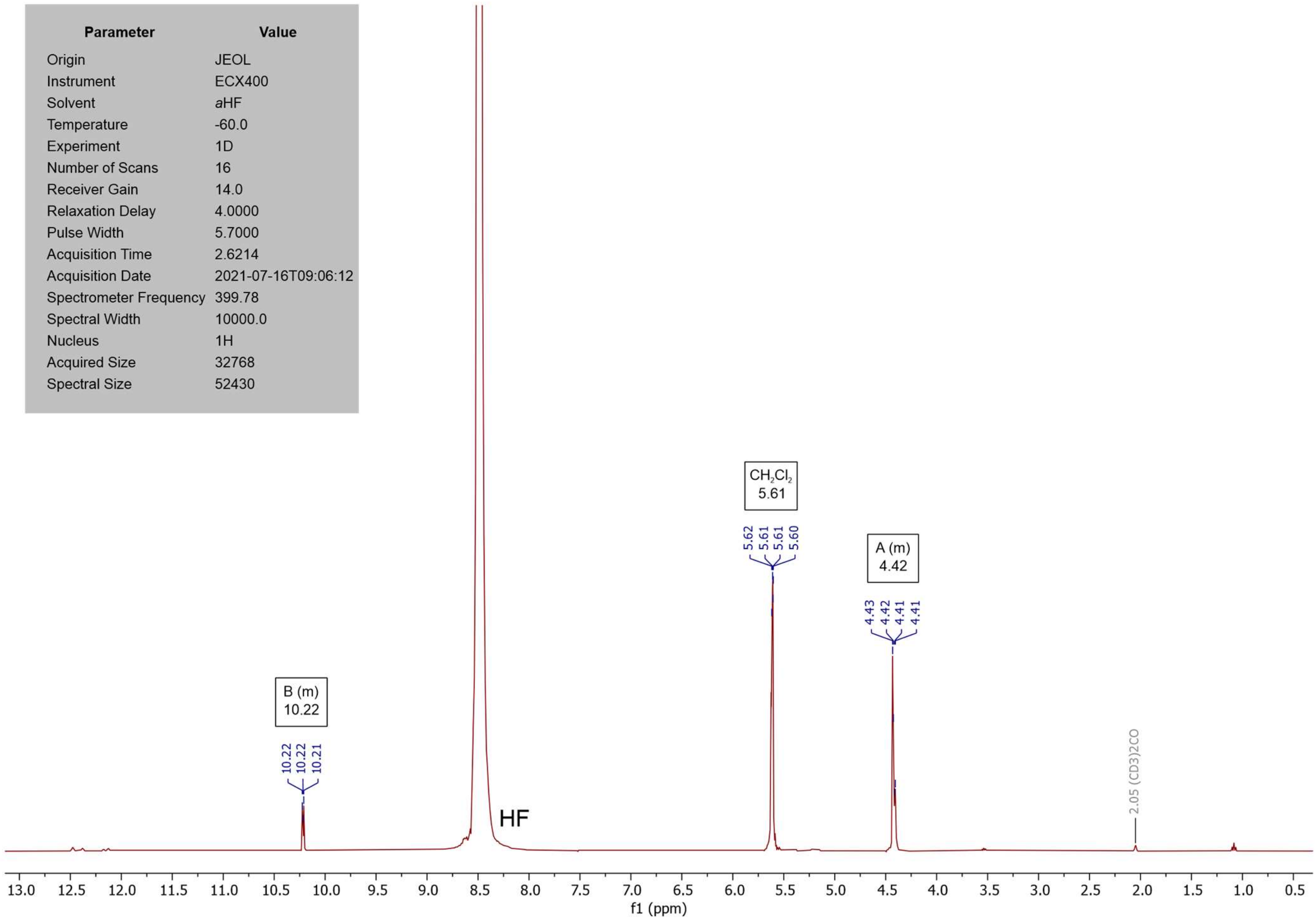

Parameter	Value
Origin	JEOL
Instrument	ECX400
Solvent	*a*HF
Temperature	-60.0
Experiment	1D
Number of Scans	16
Receiver Gain	14.0
Relaxation Delay	4.0000
Pulse Width	5.7000
Acquisition Time	2.6214
Acquisition Date	2021-07-16T09:06:12
Spectrometer Frequency	399.78
Spectral Width	10000.0
Nucleus	1H
Acquired Size	32768
Spectral Size	52430

^{13}C NMR - [FOC−CH$_2$−C(OH)F][SbF$_6$] (2) in *a*HF

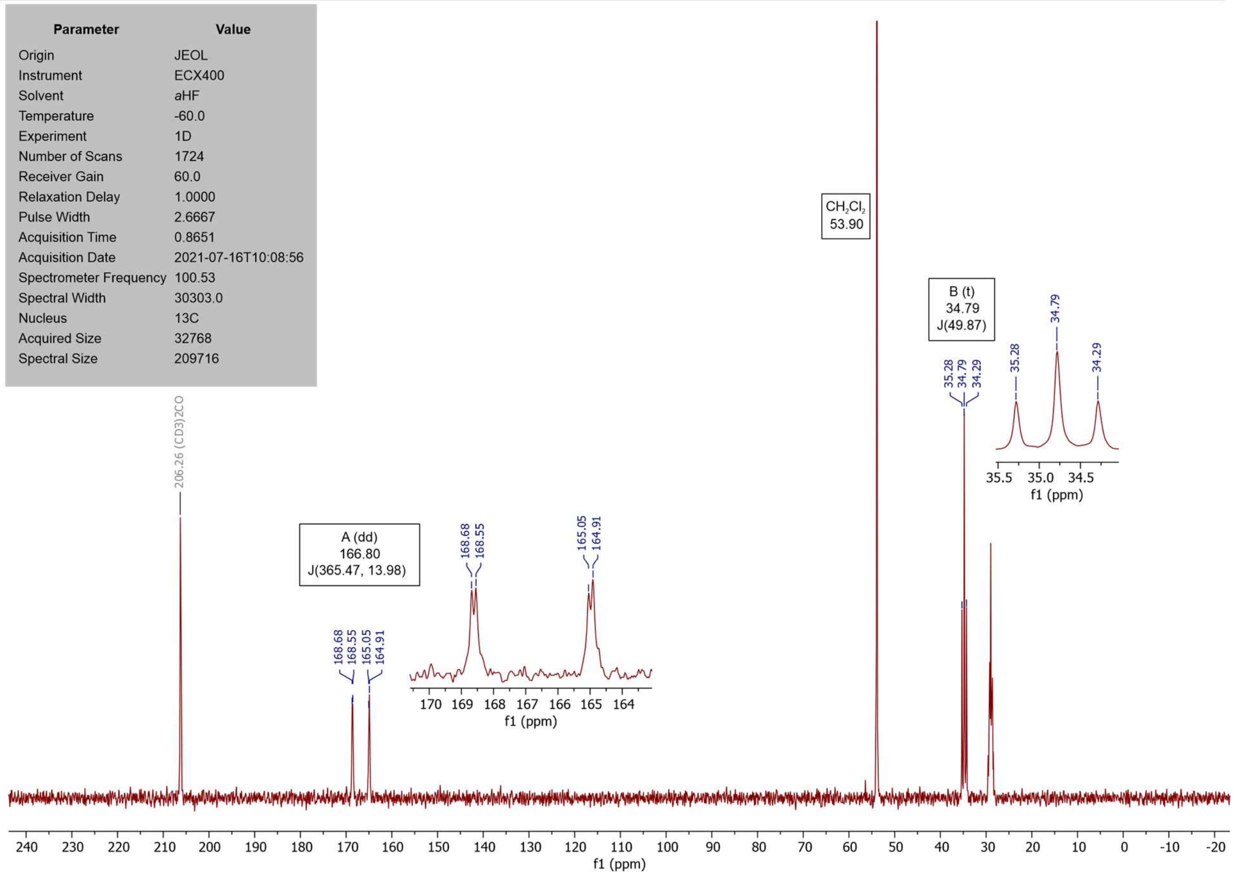

Parameter	Value
Origin	JEOL
Instrument	ECX400
Solvent	*a*HF
Temperature	-60.0
Experiment	1D
Number of Scans	1724
Receiver Gain	60.0
Relaxation Delay	1.0000
Pulse Width	2.6667
Acquisition Time	0.8651
Acquisition Date	2021-07-16T10:08:56
Spectrometer Frequency	100.53
Spectral Width	30303.0
Nucleus	13C
Acquired Size	32768
Spectral Size	209716

^{13}C{^{1}H} NMR - [FOC−CH$_2$−C(OH)F][SbF$_6$] (2) in *a*HF

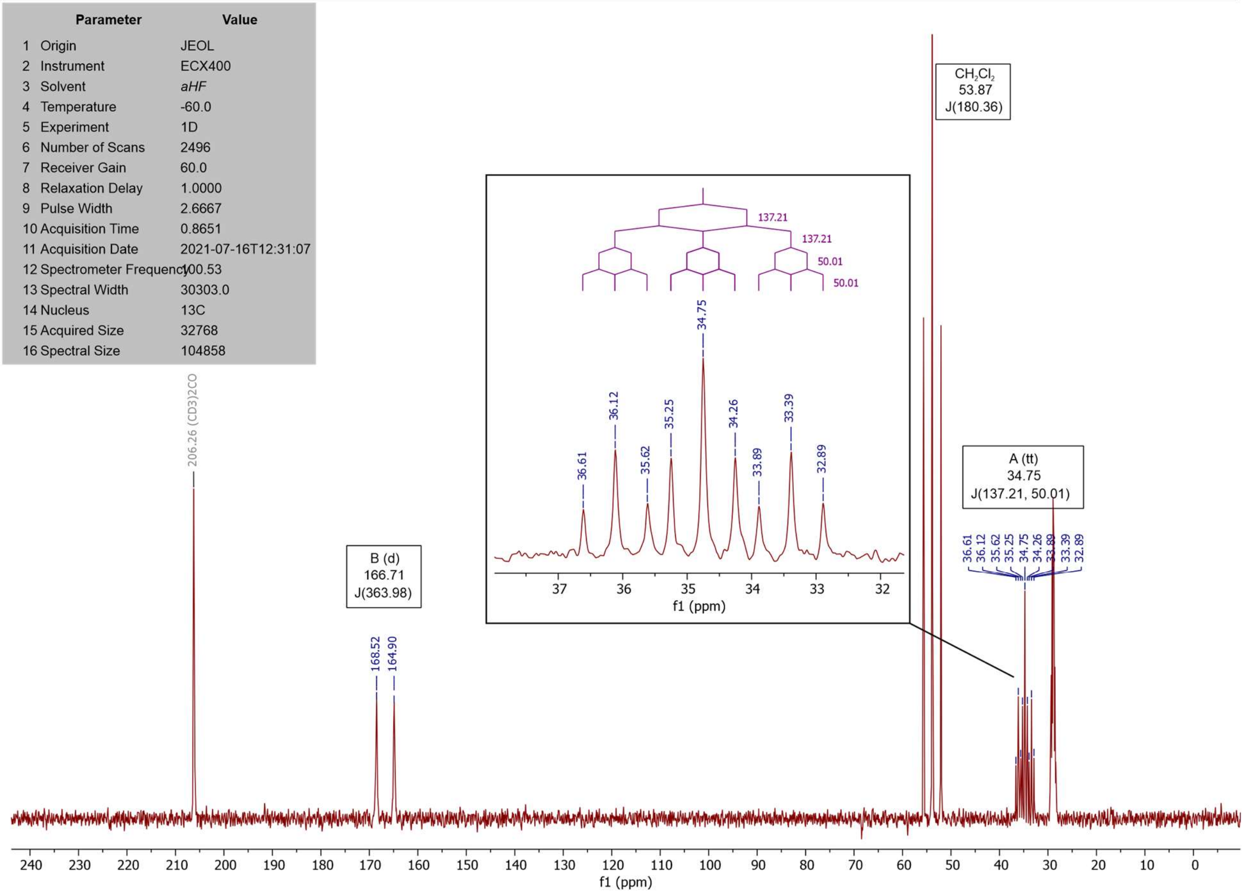

Parameter	Value
1 Origin	JEOL
2 Instrument	ECX400
3 Solvent	*aHF*
4 Temperature	-60.0
5 Experiment	1D
6 Number of Scans	2496
7 Receiver Gain	60.0
8 Relaxation Delay	1.0000
9 Pulse Width	2.6667
10 Acquisition Time	0.8651
11 Acquisition Date	2021-07-16T12:31:07
12 Spectrometer Frequency	100.53
13 Spectral Width	30303.0
14 Nucleus	13C
15 Acquired Size	32768
16 Spectral Size	104858

^{13}C NMR DEPT135 - [FOC−CH$_2$−C(OH)F][SbF$_6$] (2) in *a*HF

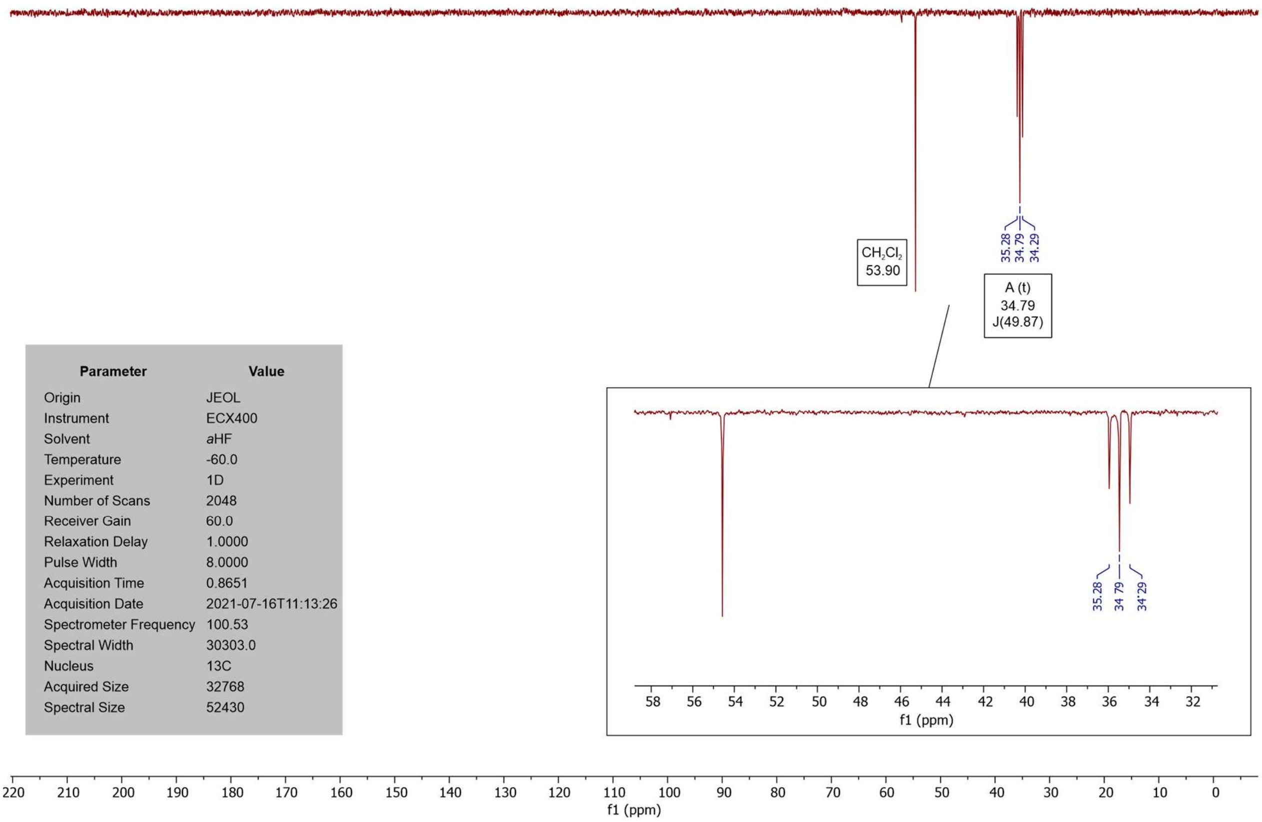

Parameter	Value
Origin	JEOL
Instrument	ECX400
Solvent	*a*HF
Temperature	-60.0
Experiment	1D
Number of Scans	2048
Receiver Gain	60.0
Relaxation Delay	1.0000
Pulse Width	8.0000
Acquisition Time	0.8651
Acquisition Date	2021-07-16T11:13:26
Spectrometer Frequency	100.53
Spectral Width	30303.0
Nucleus	13C
Acquired Size	32768
Spectral Size	52430

^{19}F NMR - [FOC−CH$_2$−C(OH)F][SbF$_6$] (2) in *a*HF

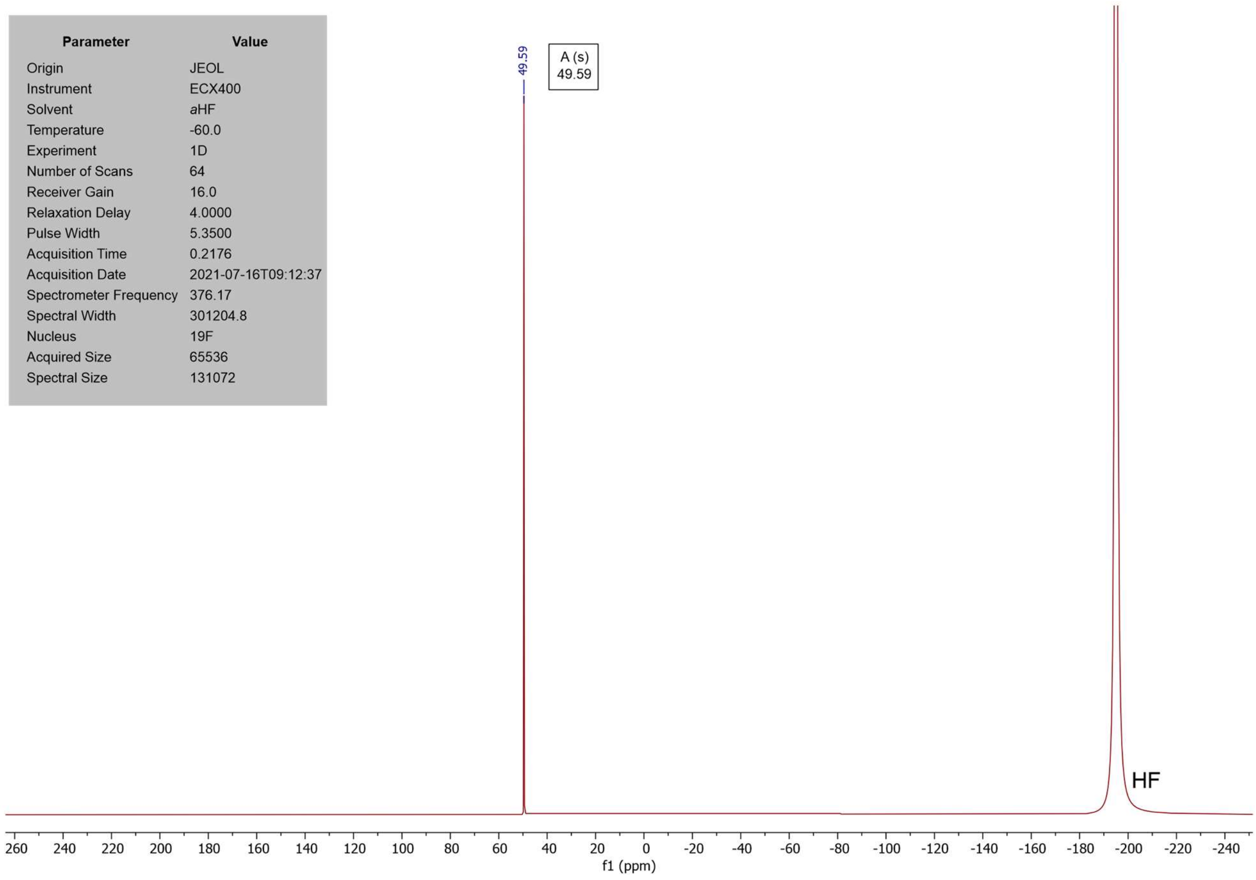

Parameter	Value
Origin	JEOL
Instrument	ECX400
Solvent	*a*HF
Temperature	-60.0
Experiment	1D
Number of Scans	64
Receiver Gain	16.0
Relaxation Delay	4.0000
Pulse Width	5.3500
Acquisition Time	0.2176
Acquisition Date	2021-07-16T09:12:37
Spectrometer Frequency	376.17
Spectral Width	301204.8
Nucleus	19F
Acquired Size	65536
Spectral Size	131072

4.3 Diprotonated Malonyl Difluoride

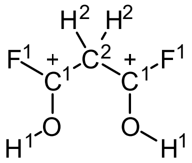

$[F(HO)C{-}CH_2{-}C(OH)F][SbF_6]_2$:

^{1}H NMR (400 MHz, *a*HF) δ [ppm] = 10.08–9.68 (m, H1), 4.25 (s, H2).
^{13}C NMR (101 MHz, *a*HF) δ [ppm] = 169.01 (dd, *J*=367.0 Hz, 13.9 Hz, C1), 35.13 (t, *J*=47.5 Hz, C2)
^{19}F NMR (376 MHz, *a*HF) δ [ppm] = 50.18 (s, F1).

^{1}H NMR - $[F(OH)C{-}CH_2{-}C(OH)F][SbF_6]_2$ (4) in *a*HF

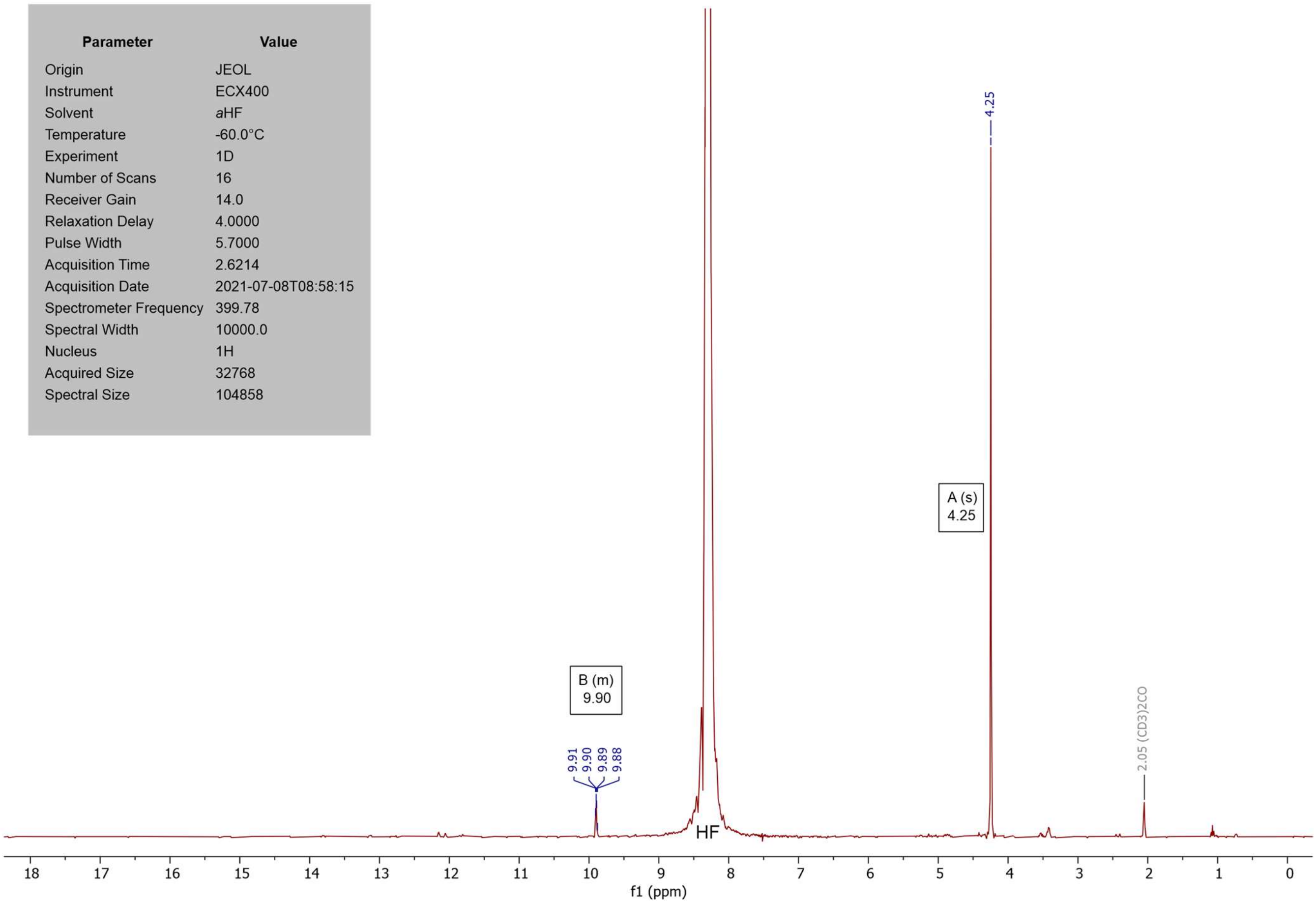

Parameter	Value
Origin	JEOL
Instrument	ECX400
Solvent	*a*HF
Temperature	-60.0°C
Experiment	1D
Number of Scans	16
Receiver Gain	14.0
Relaxation Delay	4.0000
Pulse Width	5.7000
Acquisition Time	2.6214
Acquisition Date	2021-07-08T08:58:15
Spectrometer Frequency	399.78
Spectral Width	10000.0
Nucleus	1H
Acquired Size	32768
Spectral Size	104858

^{13}C NMR - [F(OH)C−CH$_2$−C(OH)F][SbF$_6$]$_2$ (4) in *a*HF

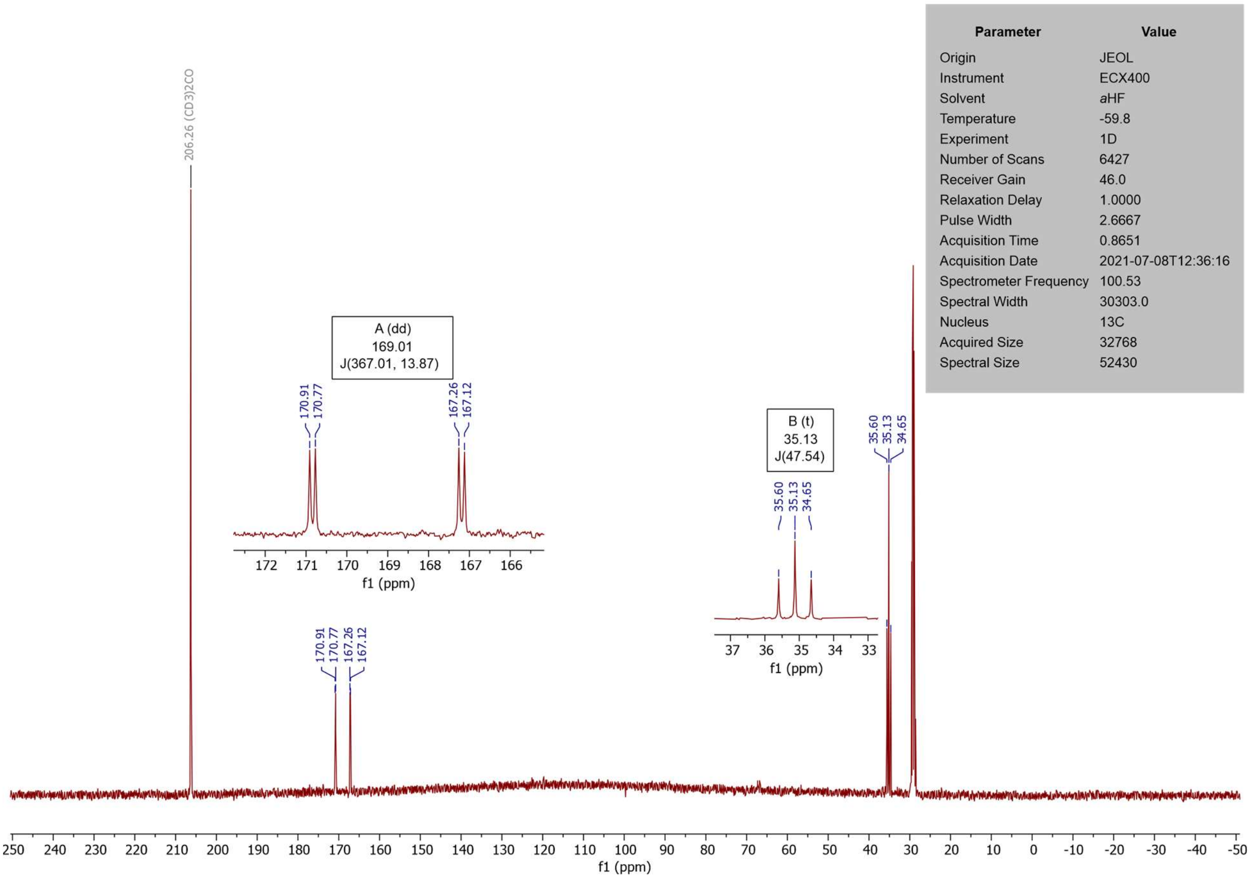

Parameter	Value
Origin	JEOL
Instrument	ECX400
Solvent	*a*HF
Temperature	-59.8
Experiment	1D
Number of Scans	6427
Receiver Gain	46.0
Relaxation Delay	1.0000
Pulse Width	2.6667
Acquisition Time	0.8651
Acquisition Date	2021-07-08T12:36:16
Spectrometer Frequency	100.53
Spectral Width	30303.0
Nucleus	13C
Acquired Size	32768
Spectral Size	52430

^{19}F NMR - [F(OH)C−CH$_2$−C(OH)F][SbF$_6$]$_2$ (4) in *a*HF

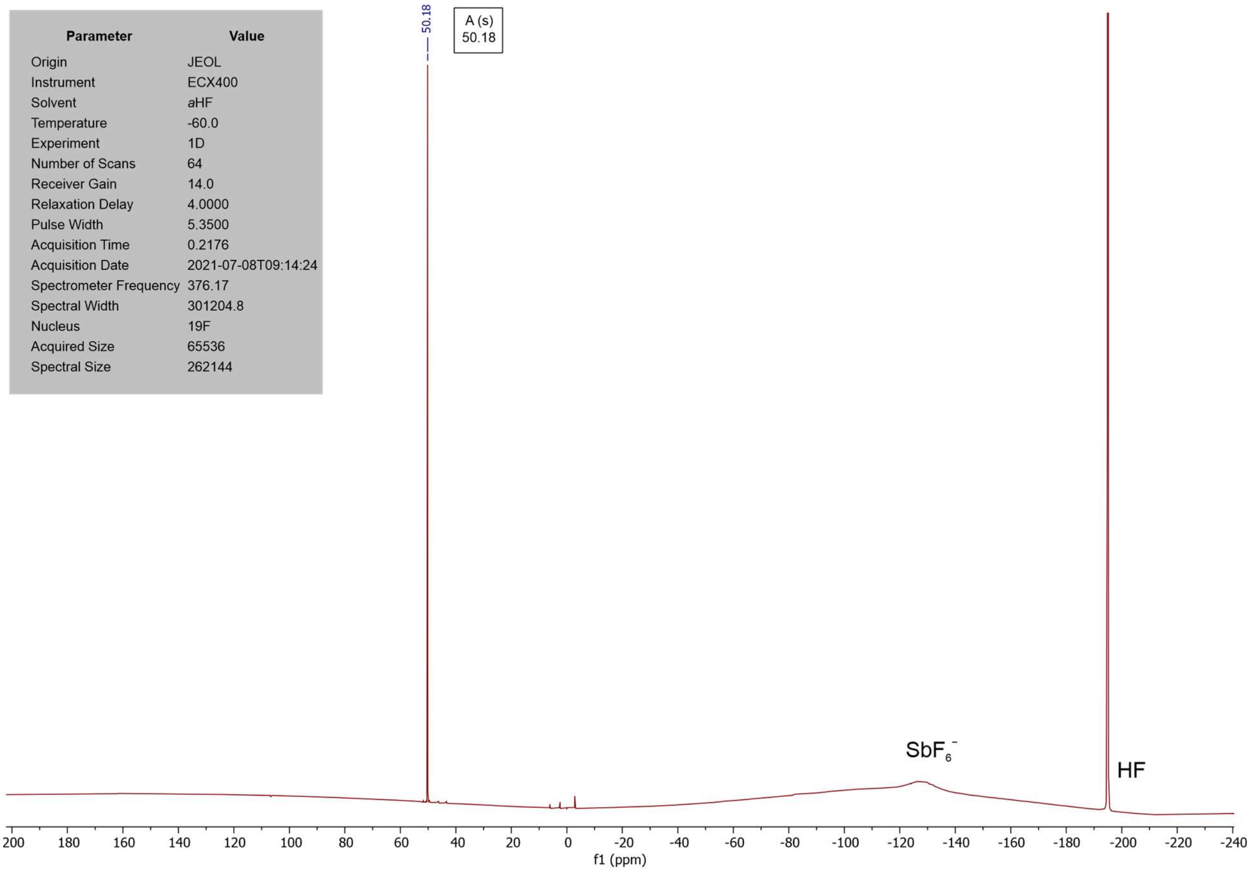

Parameter	Value
Origin	JEOL
Instrument	ECX400
Solvent	*a*HF
Temperature	-60.0
Experiment	1D
Number of Scans	64
Receiver Gain	14.0
Relaxation Delay	4.0000
Pulse Width	5.3500
Acquisition Time	0.2176
Acquisition Date	2021-07-08T09:14:24
Spectrometer Frequency	376.17
Spectral Width	301204.8
Nucleus	19F
Acquired Size	65536
Spectral Size	262144

5 Quantum Chemical Calculations

The optimized structures are given with their cartesian coordinates x, y, z in angstrom. An illustration of the respective structures together with calculated bond lengths in angstrom is shown next to the tables.

[FOC−CH$_2$−COF]$_U$ (U-gauche)

Energy (M06-2X/aug-cc-pVTZ): −465.692983 Hartree

C	0.000000	1.256998	-0.066104
C	-0.000000	0.000000	0.758463
H	-0.873706	-0.018470	1.410723
H	0.873706	0.018470	1.410723
C	-0.000000	-1.256998	-0.066104
O	-0.394916	-1.423432	-1.157983
O	0.394916	1.423432	-1.157983
F	0.491821	-2.274149	0.663819
F	-0.491821	2.274149	0.663819

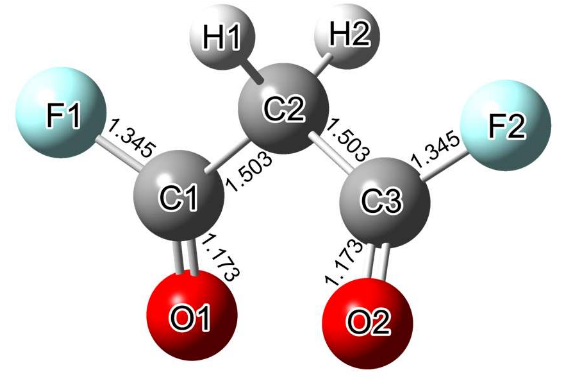

[FOC−CH$_2$−COF]$_S$ (S-gauche)

Energy (M06-2X/aug-cc-pVTZ): −465.695093 Hartree

C	1.280113	-0.202372	0.013413
C	-0.060851	-0.810124	0.315786
H	-0.159391	-0.988890	1.386820
H	-0.157310	-1.759784	-0.206353
C	-1.177860	0.098533	-0.117886
O	-1.107838	1.124779	-0.685978
O	2.071950	-0.565518	-0.775883
F	-2.358761	-0.436334	0.224269
F	1.509359	0.853930	0.803124

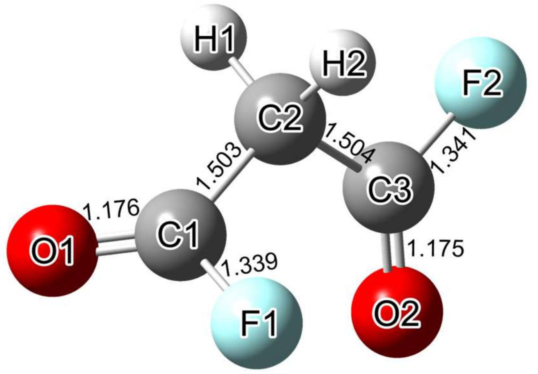

[(FOC−CH$_2$−COF)$_2$H]$^+$

Energy (M06-2X/aug-cc-pVTZ): −931.704295 Hartree

F	-1.829696	-1.290467	-1.030374
F	-5.432113	0.286341	0.369391
O	-1.054082	-0.069832	0.581093
O	-3.787116	1.031255	-0.891472
C	-1.989301	-0.671989	0.093236
C	-3.354834	-0.734947	0.676216
C	-4.187963	0.302473	-0.059124
H	-3.325279	-0.498163	1.738282
H	-3.788981	-1.724049	0.527081
H	-0.000004	-0.000010	0.000009
F	1.829692	1.290442	1.030394
F	5.432116	-0.286309	-0.369414
O	1.054074	0.069817	-0.581078
O	3.787140	-1.031253	0.891460
C	1.989294	0.671977	-0.093224
C	3.354820	0.734953	-0.676215
C	4.187970	-0.302461	0.059112
H	3.325258	0.498172	-1.738282
H	3.788957	1.724059	-0.527080

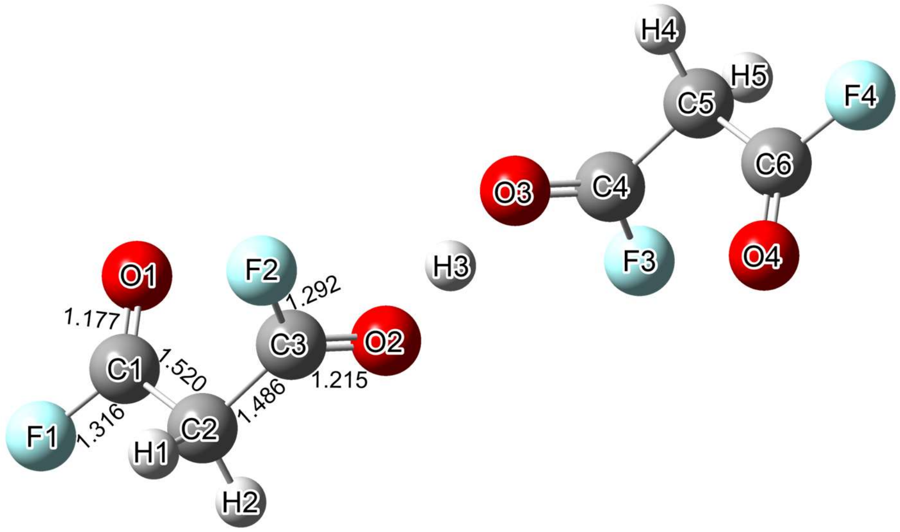

$[FOC{-}CH_2{-}C(OH)F \cdot HF]^{+}$

Energy (M06-2X/aug-cc-pVTZ): −566.444965 Hartree

O	-1.344735	1.379315	0.160161
F	-3.074064	0.056101	-0.188957
C	-0.972165	-0.964741	-0.182656
H	-1.279822	-1.688384	0.573853
H	-1.094810	-1.383455	-1.180551
C	-1.798271	0.313139	-0.043131
F	0.829942	-0.409685	1.241242
O	1.216929	-0.319036	-0.883988
C	0.430661	-0.554933	0.041450
H	2.140324	0.010426	-0.615537
F	3.479916	0.452682	-0.094915
H	4.173262	0.926509	-0.497470

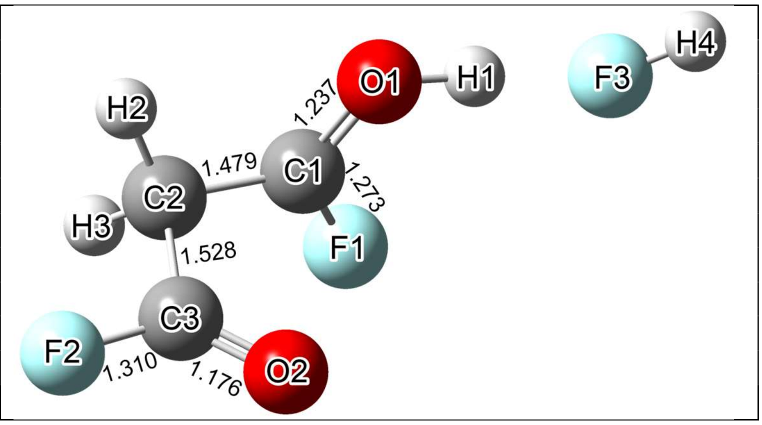

$[FOC{-}CH_2{-}C(OD)F \cdot HF]^{+}$

Energy (M06-2X/aug-cc-pVTZ): −566.447971 Hartree

F	-1.019382	2.377785	0.000020
F	2.647926	-0.464301	0.000013
O	-1.491087	0.317114	-0.000005
O	0.647051	-1.360879	0.000010
C	-0.607608	1.173655	0.000009
C	1.342967	-0.405865	0.000012
C	0.868129	1.024037	0.000012
H	1.259400	1.563466	0.870423
H	1.259403	1.563469	-0.870395
D	-1.254248	-0.672347	-0.000016
F	-1.926648	-2.127980	-0.000056
H	-1.450248	-2.924967	-0.000049

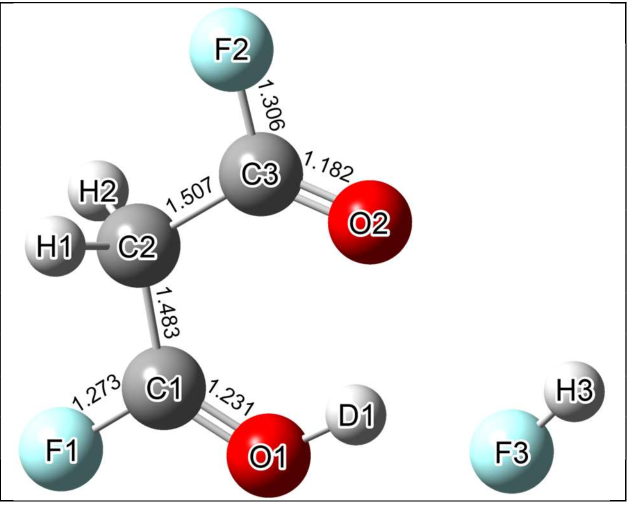

$[F(HO)C{-}CH_2{-}C(OH)F \cdot 2HF]^{2+}$

Energy (M06-2X/aug-cc-pVTZ): −667.068175 Hartree

F	2.318556	-1.315389	-0.000222
F	-2.318556	-1.315389	0.000219
O	1.388403	0.643775	0.000145
O	-1.388403	0.643776	-0.000142
C	1.284719	-0.577178	-0.000027
C	-1.284719	-0.577178	0.000028
C	0.000000	-1.338637	0.000001
H	-0.000027	-2.017318	-0.867108
H	0.000027	-2.017316	0.867112
H	2.373340	1.057339	0.000126
H	-2.373340	1.057339	-0.000124
F	3.674278	1.427449	0.000058
H	4.065181	2.280218	0.000232
F	-3.674278	1.427449	-0.000061
H	-4.065181	2.280218	-0.000227

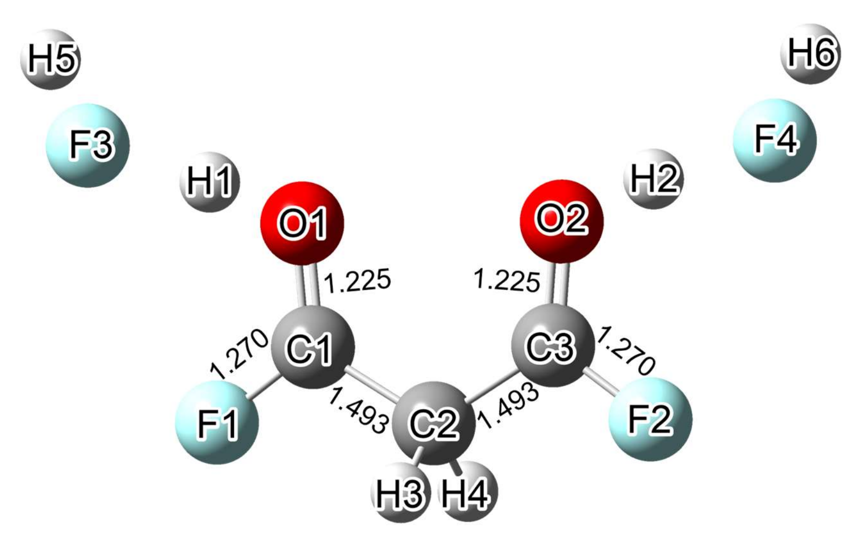

$[F(DO)C{-}CH_2{-}C(OD)F \cdot 2HF]^{2+}$

Energy (M06-2X/aug-cc-pVTZ): −667.068175 Hartree

F	-2.318557	1.315392	-0.000028	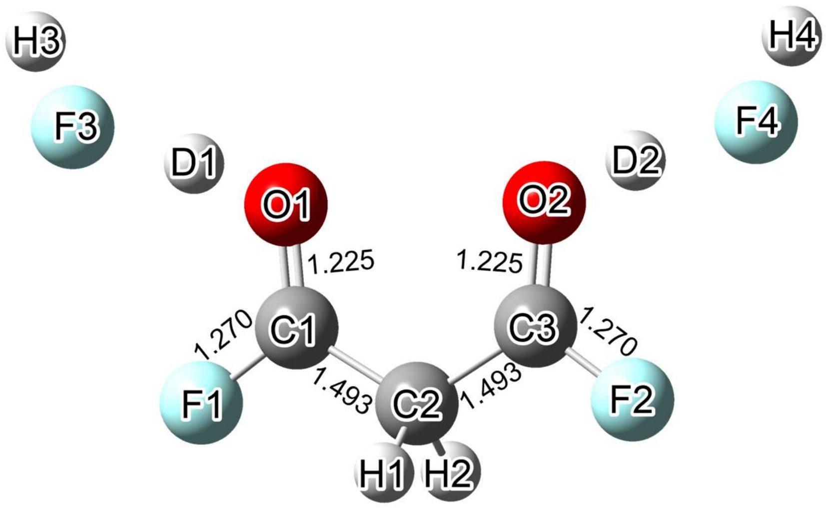
F	2.318557	1.315392	0.000028	
O	-1.388399	-0.643771	0.000067	
O	1.388399	-0.643771	-0.000066	
C	-1.284718	0.577184	0.000013	
C	1.284718	0.577183	-0.000013	
C	0.000000	1.338643	0.000000	
H	-0.000006	2.017323	-0.867110	
H	0.000006	2.017323	0.867110	
D	-2.373335	-1.057341	0.000078	
D	2.373335	-1.057340	-0.000077	
F	-3.674267	-1.427460	0.000081	
H	-4.065160	-2.280234	0.000135	
F	3.674267	-1.427460	-0.000081	
H	4.065161	-2.280233	-0.000134	

Calculations on the MP2/aug-cc-pVTZ level of theory

The following structures were optimized on the MP2/aug-cc-pVTZ level of theory. Subsequent vibrational analysis confirmed the optimized geometries as true energy minimum structures. The structures were employed to further calculate their respective single-point energy on the CCSD(t)/aug-cc-pVTZ level of theory.

$[FOC{-}CH_2{-}C(OH)F]^+$ (I)

Energy (MP2/aug-cc-pVTZ): −465.294899 Hartree; Energy (CCSD(t)/aug-cc-pVTZ): −465.363509 Hartree;

O	0.944845	1.259654	-0.402299	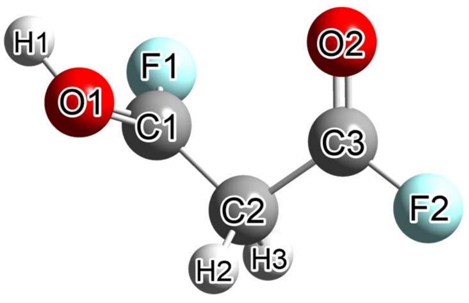
F	2.417291	-0.341751	0.071654	
C	0.157378	-0.924561	0.233552	
H	0.241721	-1.750115	-0.471538	
H	0.272777	-1.280804	1.257726	
C	1.204911	0.146076	-0.073192	
F	-1.583909	0.472853	1.032878	
O	-1.790810	-0.300075	-0.991530	
C	-1.135567	-0.233970	0.076547	
H	-2.607547	0.249104	-0.997785	

$[FOC{-}CH_2{-}C(OH)F]^+$ (II)

Energy (MP2/aug-cc-pVTZ): −465.310131 Hartree; Energy (CCSD(t)/aug-cc-pVTZ): −465.377713 Hartree;

O	1.206050	1.210210	-0.000025	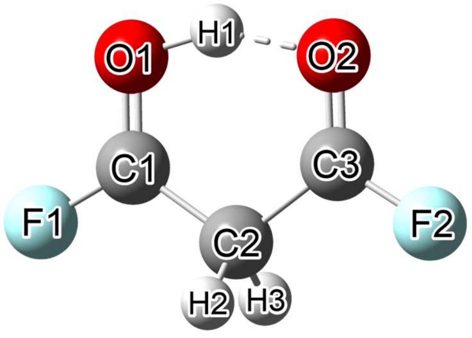
F	2.353521	-0.660690	0.000011	
C	0.017426	-0.880391	0.000012	
H	0.014202	-1.537786	-0.875338	
H	0.014205	-1.537771	0.875372	
C	1.240037	-0.000450	-0.000002	
F	-2.335287	-0.668295	0.000021	
O	-1.232419	1.184950	-0.000021	
C	-1.220952	-0.053366	0.000003	
H	-0.200640	1.480394	-0.000029	

$[F(HO)C{-}CH{-}C(OH)F]^+$ (III)

Energy (MP2/aug-cc-pVTZ): −465.310375 Hartree; Energy (CCSD(t)/aug-cc-pVTZ): −465.377931 Hartree;

F	-0.000187	-2.298614	0.795020	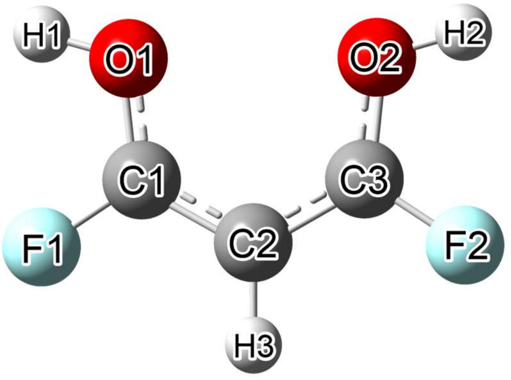
C	0.000000	0.000000	0.759307	
H	0.000000	0.000000	1.836378	
C	0.000000	-1.208977	0.094465	
F	0.000187	2.298614	0.795020	
O	0.000158	1.347990	-1.184332	
C	0.000000	1.208977	0.094465	
H	0.000229	2.289274	-1.443422	
O	-0.000158	-1.347990	-1.184332	
H	-0.000229	-2.289274	-1.443422	

6 References

[1] L. Bayersdorfer, R. Minkwitz, J. Jander, *Z. Anorg. Allg. Chem.* **1972**, *392*, 137.

[2] Rigaku Oxford Diffraction, CrysAlisPro Software System, *Version 1.171.39.46e*, Rigaku Corporation,Oxford, UK, **2018**.

[3] G. M. Sheldrick, *Acta crystallographica. Section A, Foundations and advances* **2015**, *71*, 3.

[4] G. M. Sheldrick, *Acta crystallographica. Section C, Structural chemistry* **2015**, *71*, 3.

[5] L. J. Farrugia, *J. Appl. Crystallogr.* **1999**, *32*, 837.

[6] A. L. Spek, *J. Appl. Crystallogr.* **2003**, *36*, 7.

[7] *SCALE3 ABSPACK, An Oxford Diffraction Program*, Oxford Diffraction Ltd, UK, **2005**.

[8] C. F. Macrae, I. Sovago, S. J. Cottrell, P. T. A. Galek, P. McCabe, E. Pidcock, M. Platings, G. P. Shields, J. S. Stevens, M. Towler et al., *J. Appl. Crystallogr.* **2020**, *53*, 226.

[9] Mestrelab Research S.L., *MestReNova Version 14.0.0*, **2019**.

[10] a) M. J. Frisch, G. W. Trucks, H. B. Schlegel, G. E. Scuseria, M. A. Robb, J. R. Cheeseman, G. Scalmani, V. Barone, B. Mennucci, G. A. Petersson, H. Nakatsuji, M. Caricato, X. Li, H. P. Hratchian, A. F. Izmaylov, J. Bloino, G. Zheng, J. L. Sonnenberg, M. Hada, M. Ehara, K. Toyota, R. Fukuda, J. Hasegawa, M. Ishida, T. Nakajima, Y. Honda, O. Kitao, H. Nakai, T. Vreven, J. A. Montgomery, J. E. Peralta, F. Ogliaro, M. Bearpark, J. J. Heyd, E. Brothers, K. N. Kudin, V. N. Staroverov, R. Kobayashi, J. Normand, K. Raghavachari, A. Rendell, J. C. Burant, S. S. Iyengar, J. Tomasi, M. Cossi, N. Rega, J. M. Millam, M. Klene, J. E. Knox, J. B. Cross, V. Bakken, C. Adamo, J. Jaramillo, R. Gomperts, R. E. Stratmann, O. Yazyev, A. J. Austin, R. Cammi, C. Pomelli, J. W. Ochterski, R. L. Martin, K. Morokuma, V. G. Zakrzewski, G. A. Voth, P. Salvador, J. J. Dannenberg, S. Dapprich, A. D. Daniels, O. Farkas, J. B. Foresman, J. V. Ortiz, J. Cioslowski, D. J. Fox, *Gaussian09, Revision A.02*, Gaussian, Inc, Wallingford CT, **2009**; b) M. J. Frisch, G. W. Trucks, H. B. Schlegel, G. E. Scuseria, M. A. Robb, J. R. Cheeseman, G. Scalmani, V. Barone, G. A. Petersson, H. Nakatsuji et al., *Gaussian16 Revision C.01*, **2016**.

[11] Roy Dennington, Todd A. Keith, John M. Millam, *GaussView Version 6*, **2019**.

[12] A. Jin, H. G. Mack, A. Waterfeld, H. Oberhammer, *J. Am. Chem. Soc.* **1991**, *113*, 7847.

[13] a) K. O. Christe, P. Charpin, E. Soulie, R. Bougon, J. Fawcett, D. R. Russell, *Inorg. Chem.* **1984**, *23*, 3756; b) K. O. Christe, C. J. Schack, R. D. Wilson, *Inorg. Chem.* **1975**, *14*, 2224.

Acylium Cations of Malonyl Difluoride: Synthesis and Characterization of the $C_3O_2H^+$ Cation

Christoph Jessen,[a,b] Dirk Hollenwäger,[a] Florian Zischka,[b] and Andreas J. Kornath*[a,b]

[a] C. Jessen, D. Hollenwäger, Dr. F. Zischka, Prof. Dr. A. J. Kornath
Department Chemie
Ludwig-Maximilians-Universität München
Butenandtstr. 5–13, 81377 München, Germany
E-mail: andreas.kornath@cup.uni-muenchen.de

[b] C. Jessen, Prof. Dr. A. J. Kornath
F-Select GmbH
Semmelweisstrasse 5
82152 Planegg

Supporting information for this article is given via a link at the end of the document.

Abstract: Three different acylium species deriving from malonyl difluoride were synthesized in the solid state. The monoacylium species $[FOC{-}CH_2{-}CO][Sb_2F_{11}]$ was obtained upon the reaction of malonyl difluoride with SbF_5 in the solvent 1,1,1,2-tetrafluoroethane (R-134a). The salt was employed for further reactions to the enol tautomeric species $F(HO)C{=}CH{-}CO^+$ in the solvents R-134a and SO_2ClF. Reacting $[FOC{-}CH_2{-}CO][Sb_2F_{11}]$ with $SO_2{\cdot}SbF_5$ in the solvent SO_2 afforded protonated carbon suboxide as the salt $[C_3O_2H][Sb_2F_{11}]$. Single crystals of the compounds allowed X-ray structure analyses of the salts $[FOC{-}CH_2{-}CO]_4[SbF_6][Sb_2F_{11}]_3{\cdot}SO_2$, $[F(HO)C{=}CH{-}CO][M_2F_{11}]$ (M = As, Sb), and $[C_3O_2H][Sb_2F_{11}]$. The respective acylium cations were characterized by vibrational spectroscopy and in the case of $FOC{-}CH_2{-}CO^+$ and $C_3O_2H^+$ by NMR spectroscopy. The $C_3O_2H^+$ cation is compared structurally and spectroscopically with the isoelectronic cations $OCNCO^+$ and N_5^+. Quantum chemical calculations were performed to discuss the Lewis structure of the cations $F(HO)C{=}CH{-}CO^+$ and $C_3O_2H^+$ as well as the electron distribution and orbital interactions in the latter.

Introduction

The reaction of acyl fluorides with boron trifluoride was the starting point for *Olah*'s search for stable carbocations.[1] In the course of his career, *Olah* investigated a variety of different acylium and even diacylium cations.[2,3] However, one of those publications particularly caught our attention. Reacting compounds with two acyl fluoride groups with the Lewis acid SbF_5 either leads to $R(COF{\cdots}SbF_5)_2$ donor-acceptor complexes, diacylium cations $R(CO)_2^{2+}$, or mixtures of both depending on the size of R.[3] *Olah* and *Klumpp* later picked up on this reaction in "*Superelectrophiles and Their Chemistry*" and described that the reaction of malonyl difluoride with SbF_5 leads to the diacylium cation $OC{-}CH_2{-}CO^{2+}$.[4] However, in the publication cited therein, the products of this reaction are described as unstable, which did not allow their investigation.[3] The diacylium cation $OC{-}CH_2{-}CO^{2+}$ is particularly interesting because it is the diprotonated species of carbon suboxide. The first and second proton affinities of carbon suboxide indicate that a monoprotonation could be achieved in highly acidic media, whereas a diprotonation is very unlikely, even in superacids.[5,6] Quantum chemical calculations about monoprotonated carbon suboxide (C_3O_2) have been reported in the literature due to its observation in mass spectrometry experiments.[6–9] In a work about the electronic structure and bonding of the $C_3O_2H^+$ cation on a high theoretical level, the authors conclude that the $C_3O_2H^+$ cation could be isolable in the solid state, with a suitable anion and proper experimental conditions.[10] *Frenking et al.* reported on the detection of the $C_3O_2H^+$ cation in the gas phase in a mass spectrometry experiment and achieved to measure vibrational frequencies of the gas phase complex $[HC_3O_2{\cdot}CO]^+$ via infrared photodissociation spectroscopy.[9] However, the protonation of carbon suboxide in the condensed phase is extremely difficult due to the high reactivity of the starting material. Carbon suboxide readily reacts with water, hydrogen chloride, and other nucleophiles like carboxylic acids.[11] In our opinion, this also excluded the possibility of successful protonation in the binary superacidic system HF/SbF_5. This prompted us to reinvestigate the reaction of malonyl difluoride with SbF_5 and further investigate the resulting products at low temperatures with the objective to isolate acylium cations or even gaining access to protonated carbon suboxide.

Results and Discussion

Syntheses

From the reaction of malonyl difluoride with the Lewis superacid SbF_5 in the solvent 1,1,1,2-tetrafluoroethane (R-134a) the monoacylium cation $FOC{-}CH_2{-}CO^+$ was obtained as the salt $[FOC{-}CH_2{-}CO][Sb_2F_{11}]$ ([**1**][Sb_2F_{11}]). The reaction is shown in Scheme 1. When less than two equivalents of SbF_5 were used, the reaction was not complete and side products like a donor-acceptor complex ($FOC{-}CH_2{-}C(O{\cdot}SbF_5)F$) were observed. However, even with a tenfold excess of SbF_5, the respective diacylium cation $OC{-}CH_2{-}CO^{2+}$ was not observed, as described by *Olah* and *Klumpp*.[4]

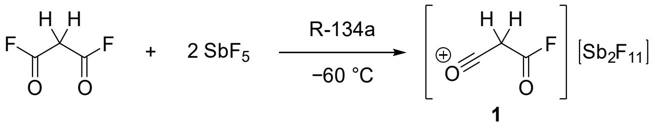

1

Scheme 1. Synthesis of the monoacylium cation $FOC{-}CH_2{-}CO^+$.

The salt $[FOC{-}CH_2{-}CO][Sb_2F_{11}]$ slowly decomposes at 18 °C under nitrogen atmosphere and is moderately soluble in the solvents R-134a or SO_2ClF and highly soluble in SO_2. When suspensions of $[\mathbf{1}][Sb_2F_{11}]$ in R-134a or SO_2ClF are kept at −50 °C for several days the formation of a new compound was observed. Under these conditions, the acylium cation $FOC{-}CH_2{-}CO^+$ reacts under the formation of the isomeric monoacylium cation $F(HO)C{=}CH{-}CO^+$, which was isolated as the salt $[F(HO)C{=}CH{-}CO][Sb_2F_{11}]$ ($[\mathbf{2}][Sb_2F_{11}]$) and the salt $[F(HO)C{=}CH{-}CO][As_2F_{11}]$ ($[\mathbf{2}][As_2F_{11}]$). The reaction is shown in Scheme 2. Two pathways were considered for this reaction with the first one being a formal proton shift, resembling keto-enol tautomerism, since the $F(HO)C{=}CH{-}CO^+$ cation is the enol tautomer of $FOC{-}CH_2{-}CO^+$. The second pathway proceeds via HF elimination to form the intermediate $C_3O_2H^+$ cation, which then reacts back with the released HF to form $F(HO)C{=}CH{-}CO^+$.

The possible intermediate $C_3O_2H^+$ from the reaction above is obtainable as the salt $[C_3O_2H][Sb_2F_{11}]$ ($[\mathbf{3}][Sb_2F_{11}]$). For this, the starting material $[\mathbf{1}][Sb_2F_{11}]$ was dissolved in SO_2 together with a twofold stoichiometric amount of the complex $SO_2{\cdot}SbF_5$ and the solution was kept at −30 °C for several days. Subsequently, all volatile compounds were removed *in vacuo* to obtain a mixture of $[\mathbf{3}][Sb_2F_{11}]$ and a side product. The idea was to capture the released HF (Equation 1) with the complex $SO_2{\cdot}SbF_5$ under the formation of the salt $[FS(OH)_2][SbF_6]$ (Equation 2). We reported this reaction (Equation 2) in a previous work of our group.[12]

$$FOC{-}CH_2{-}CO^+ \longrightarrow C_3O_2H^+ + HF \tag{1}$$

$$SO_2{\cdot}SbF_5 + 2\,HF \rightleftharpoons [FS(OH)_2][SbF_6] \tag{2}$$

However, instead of $[FS(OH)_2][SbF_6]$ a different compound was formed as a byproduct, as detected by NMR and Raman spectroscopy and assumed to be a protonated fluorosulfinic ester of malonyl fluoride ($[C_3H_4F_2O_4S][Sb_2F_{11}]_2$ ($[\mathbf{4}][Sb_2F_{11}]_2$)). The formation of $[\mathbf{3}][Sb_2F_{11}]$ and $[\mathbf{4}][Sb_2F_{11}]_2$ is shown in Scheme 3. The salt $[C_3O_2H][Sb_2F_{11}]$ was isolated from a mixture of $[\mathbf{3}][Sb_2F_{11}]$ and $[\mathbf{4}][Sb_2F_{11}]_2$ by recrystallization in R-134a. The compounds $[\mathbf{2}][Sb_2F_{11}]$ and $[\mathbf{3}][Sb_2F_{11}]$ were also found as products of the thermal decomposition of $[\mathbf{1}][Sb_2F_{11}]$ at room temperature.

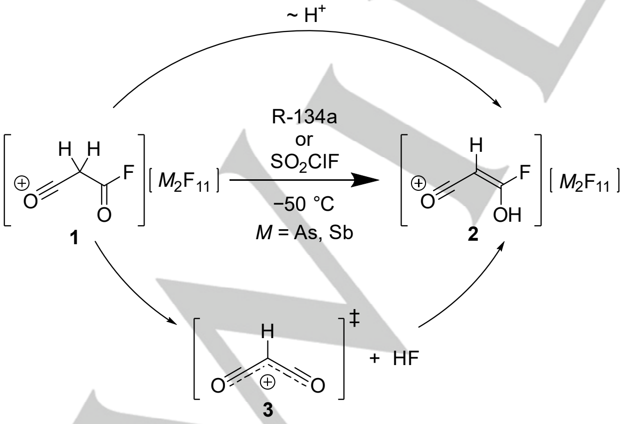

Scheme 2. Synthesis of the monoacylium cation $F(HO)C{=}CH{-}CO^+$.

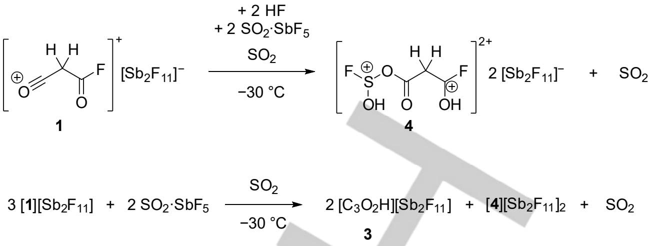

Scheme 3. Synthesis of protonated carbon suboxide ($[\mathbf{3}][Sb_2F_{11}]$) from $[FOC{-}CH_2{-}CO][Sb_2F_{11}]$.

Interestingly, acylium cations **1**, **2**, and **3** react with hydrogen fluoride when dissolved in anhydrous hydrogen fluoride (*a*HF) to form monoprotonated malonyl difluoride (*A Neutron Makes the Difference - Structures of Malonyl Difluoride and its Protonated Species in Condensed Media* (C. Jessen, D. Hollenwäger, A. J. Kornath, work in preparation)). The reactions are given in Equation 3, Equation 4, and Equation 5, respectively. This proves the difficulty to isolate protonated carbon suboxide from the superacidic system HF/SbF_5.

$$[FOC{-}CH_2{-}CO][Sb_2F_{11}] + HF \xrightarrow[-60\ ^\circ C]{aHF} [FOC{-}CH_2{-}C(OH)F][Sb_2F_{11}] \tag{3}$$

$$[F(HO)C{=}CH{-}CO][Sb_2F_{11}] + HF \xrightarrow[-60\ ^\circ C]{aHF} [FOC{-}CH_2{-}C(OH)F][Sb_2F_{11}] \tag{4}$$

$$[C_3O_2H][Sb_2F_{11}] + 2\,HF \xrightarrow[-60\ ^\circ C]{aHF} [FOC{-}CH_2{-}C(OH)F][Sb_2F_{11}] \tag{5}$$

Crystal Structures

Single-crystals were obtained of the salts $[\mathbf{1}]_4[SbF_6][Sb_2F_{11}]_3{\cdot}SO_2$, $[\mathbf{2}][Sb_2F_{11}]$, $[\mathbf{2}][As_2F_{11}]$, and $[\mathbf{3}][Sb_2F_{11}]$, which allowed single crystal X-ray structure analysis of the respective compounds.

The acylium cation **1** was only successfully crystallized as the salt $[FOC{-}CH_2{-}CO]_4[SbF_6][Sb_2F_{11}]_3{\cdot}SO_2$ in a mixture of SO_2/SO_2ClF at −78 °C. The salt crystallizes in the monoclinic space group *Pm* with one formula unit per unit cell. The formula unit is shown in Figure 1.

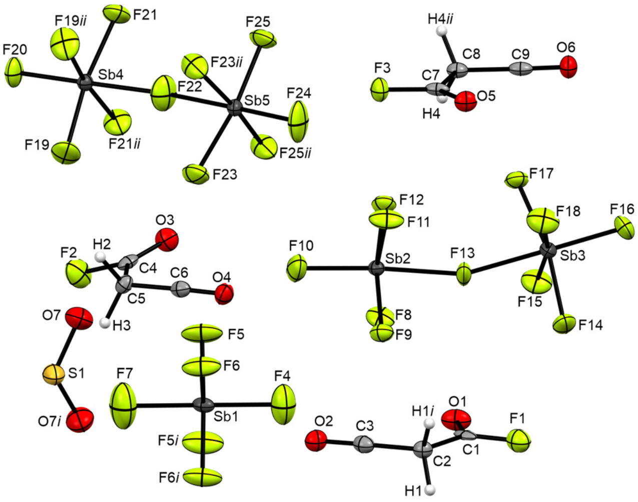

Figure 1. Formula unit of $[FOC{-}CH_2{-}CO]_4[SbF_6][Sb_2F_{11}]_3{\cdot}SO_2$ with 50% probability displacement ellipsoids. Symmetry code: *i* = x,−y,z; *ii* = x,1−y,z.

The crystal structure contains three symmetry-independent $[FOC{-}CH_2{-}CO]^+$ cations, two of which lie on mirror planes and therefore show C_s symmetry. The third $[FOC{-}CH_2{-}CO]^+$ cation lies in a general position and exhibits C_1 symmetry. The respective geometric parameters of the three cations are within their standard uncertainties. However, the estimated standard deviations are unsatisfyingly high probably due to the poor quality of the crystal or unresolvable disorders. A detailed comparison with other acylium cations from the literature or this work is therefore not very meaningful. Further details on the crystal structure of the salt $[\mathbf{1}]_4[SbF_6][Sb_2F_{11}]_3{\cdot}SO_2$ are found in the Supporting Information.

Two single-crystal X-ray structure analyses were performed on salts containing the acylium cation $F(HO)C{=}CH{-}CO^+$ (**2**). The salts $[\mathbf{2}][Sb_2F_{11}]$ and $[\mathbf{2}][As_2F_{11}]$ crystallize in the monoclinic space group $P2_1/c$ with four formula units per unit cell, respectively. The geometric parameters of the cations in the two salts are identical. However, the salt $[\mathbf{2}][As_2F_{11}]$ afforded better single crystals, resulting in an overall higher quality of the crystal structure. In the following the $F(HO)C{=}CH{-}CO^+$ cation is discussed with the geometric parameters of $[\mathbf{2}][As_2F_{11}]$. The formula unit is shown in Figure 2. Selected bond lengths and bond angles of the cation are depicted in Figure 3.

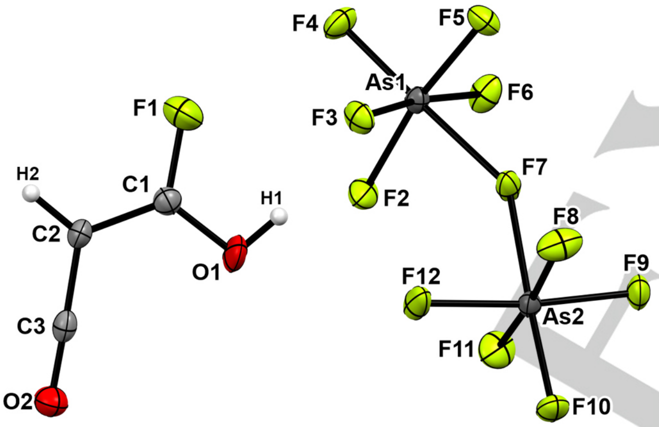

Figure 2. Formula unit of $[F(HO)C{=}CH{-}CO][As_2F_{11}]$ with 50% probability displacement ellipsoids.

All bond distances of the $F(HO)C{=}CH{-}CO^+$ cation differ significantly from the parent compound malonyl difluoride. Most obvious is the short C3−O2 bond (1.118(3) Å) of the acylium group, which is in the range between a formal C=O double (1.19 Å) and a formal C≡O triple bond (1.07 Å).[13] The C3−O2 distance of **2** is comparable with reported acylium cations from the literature.[14–18] The acylium group shows the expected linear geometry with an O2−C3−C2 angle of 178.6(2)°. The C1−C2 (1.366(3) Å) and C2−C3 (1.364(3) Å) bond lengths are equally long and are significantly shorter than the C−C bond length in malonyl difluoride (1.502(5) Å).[19] The C−C distance is in the range of a formal C=C double bond (1.33 Å).[13] This indicates a double bond character of the C−C bonds, which is not observed in malonyl difluoride and which also affects the CC(OH)F moiety of **2**. The C1−O1 bond length (1.277(3) Å) and the C1−F1 bond length (1.296(3) Å) also differ significantly from the respective bonds in malonyl difluoride.[19] Therefore, the CC(OH)F moiety in **2** seems comparable to protonated acyl fluorides. The recently reported structure of monoprotonated fumaryl fluoride is particularly well suited for comparison containing a protonated acyl fluoride group attached to an sp^2-carbon.[20]However, in monoprotonated fumaryl fluoride, the C−C bond (1.454(7) Å) of the $CC(OH)F^+$ moiety is significantly longer compared to **2**. Additionally, the C1−O1 bond (1.277(3) Å) of $F(HO)C{=}CH{-}CO^+$ is significantly longer than the C−O bond lengths of reported protonated acyl fluorides.[20,21]

Hence, describing the CC(OH)F moiety of **2** as a protonated acyl fluoride group fits the geometric parameters of the $F(HO)C{=}CH{-}CO^+$ cation very poorly. Instead, **2** is better described as the enol tautomer of the keto species $FOC{-}CH_2{-}CO^+$ (**1**). This is very surprising since acyl fluoride groups are known to highly favor the keto tautomer.[19,22] To our knowledge, cation **2** is in fact the first example of an isolated compound containing a 1-fluoro-1-en-1-ol moiety.

The $F(HO)C{=}CH{-}CO^+$ cation exhibits C_1 symmetry with a slight twist of the C(OH)F group out of the C1−C2−C3 plane (C3−C2−C1−F1: 177.8(2)°). In the crystal, the cation forms several interionic contacts with the surrounding $As_2F_{11}^-$ anions. The observed contacts are shown in Figure S4 in the Supporting Information.

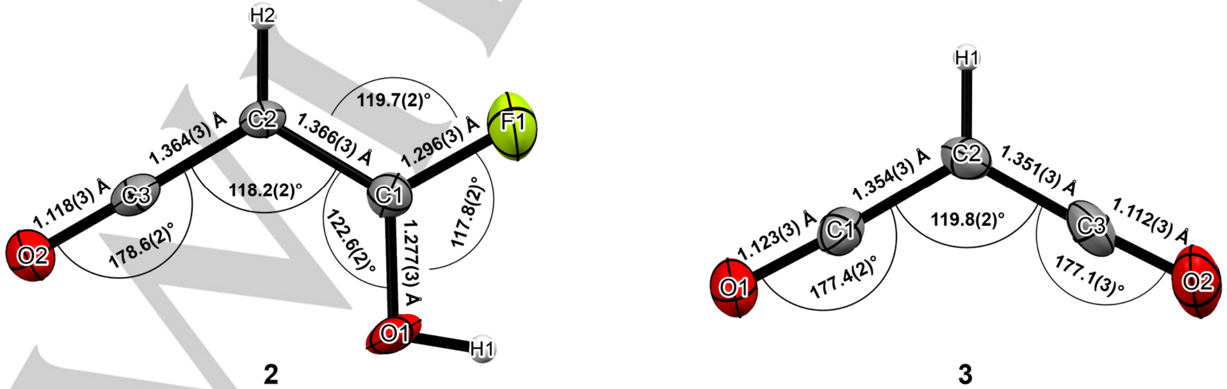

2 **3**

Figure 3. Structures of the cations from the crystal structures of the salts $[F(HO)C{=}CH{-}CO][Sb_2F_{11}]$ and $[C_3O_2H][Sb_2F_{11}]$ with selected geometric parameters (50% probability displacement ellipsoids).

Three O−H···F hydrogen bonds with donor-acceptor distances of 2.774(3) Å, 2.824(2) Å, and 3.050(2) Å are observed as well as two C−H···F hydrogen bonds with donor-acceptor distances of 3.092(3) Å and 3.204(3) Å. These hydrogen bonds are moderate to weak following the classification of *Jeffrey*.[23] Furthermore, six C···F contacts below the sum of the Van-der-Waals radii are observed in [**2**][As_2F_{11}].[24] Two C···F contacts with distances of 2.977(3) Å and 3.109 Å are directed toward the C1 atom. The C3 atom of the acylium group is surrounded by four contacting fluorine atoms with C···F distances of 2.864(3) Å, 2.903(3) Å, 2.963(3) Å, and 2.963(3) Å. Comparable C···F contacts are observed in the monoacylium cation of fumaryl fluoride.[18]

The salt [C_3O_2H][Sb_2F_{11}] crystallizes in the monoclinic space group $P2_1/n$ with four formula units per unit cell. The formula unit is shown in Figure 4. The observed bond lengths and angles of **3** are depicted in Figure 3 and listed in Table 1. The $C_3O_2H^+$ cation is the protonated species of carbon suboxide. Quantum chemical calculations on protonated carbon suboxide indicate that protonation of the central carbon atom results in the energetically most favored structure.[7] In the crystal structure, the cation has C_{2v} symmetry with an angled structure around the C2 atom containing a C1−C2−C3 angle of 119.8(2)°. On the contrary, carbon suboxide exhibits a quasilinear structure in the solid state and the gas phase.[25]

The C1−C2 and C2−C3 bonds in **2** are equally long with distances of 1.354(3) Å and 1.351(3) Å, respectively. This is in the range of a formal C=C double bond (1.33 Å)[13] and comparable to the C−C bond lengths in the F(HO)C=CH−CO$^+$ cation. The C-C bond lengths of carbon suboxide in the solid state are between 1.2475(15) Å and 1.2564(15) Å and therefore significantly shorter than in the protonated species **3**.[25] A very similar C−C bond length is however observed in the gas phase structure of ketene.[26] The C−C bond length in ketene amounts to 1.323(2) Å which is only slightly shorter than the C−C distances in the $C_3O_2H^+$ cation.[26]

The C1−O1 (1.123(3) Å) and C3−O2 (1.112(3) Å) distances do not differ significantly. The C−O bonds are in the range between a formal C=O double (1.19 Å) and a C≡O triple bond (1.07 Å),[13] and also comparable with reported acylium cations from the literature and **2**.[14–18] In comparison, the C−O distances in **3** are only slightly shorter than the C−O distances in the neutral compound C_2O_3 (1.1442(13) Å − 1.1479(12) Å)[25] or ketene (1.154(3) Å).[26] The C−C−O bond angles (177.4(2)°, 177.1(3)°) are close to the expected linear geometry of acylium groups.[14–18]

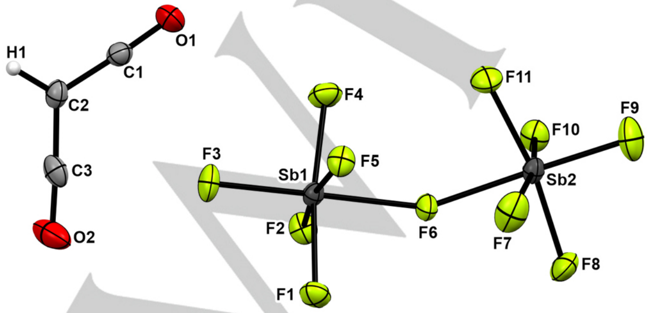

Figure 4. Formula unit of [**3**][Sb_2F_{11}] with 50% probability displacement ellipsoids.

The surrounding of $C_3O_2H^+$ in the crystal structure of **3** shows several interionic contacts between the cation and $Sb_2F_{11}^-$ anions. These contacts are depicted in Figure S6 in the Supporting Information. Two C−H···F hydrogen bonds (donor-acceptor distances: 3.010(3) Å, 3.045(3) Å) are observed, which are characterized as moderate to weak following the classification of *Jeffrey*.[23] Furthermore, seven C···F contacts below the sum of the Van-der-Waals radii are observed with C···F distances between 2.690(3) Å and 3.045(3) Å.[24] These are comparable with the interionic interactions of the acylium cation in [**2**][As_2F_{11}]. The C···F contacts are exclusively between the acylium carbons C1 and C3 and surrounding anions. Interestingly, no C···F contacts are present between anions and the central carbon atom C2, which bears the acidic proton.

The structure of $C_3O_2H^+$ shows similarities to the structures of the isoelectronic cations N_5^+ and OCNCO$^+$.[14,27,28] The three cations can be summarized with the formula $ZYXYZ^+$ (X = CH, N; Y = C, N; Z = N, O). Selected geometrical parameters of the cations are compared in Table 1. The biggest difference between the $ZYXYZ^+$ cations is the X−Y bond distance (C−C, C−N, N−N), which is shortest for OCNCO$^+$ and longest for $C_3O_2H^+$. This is probably due to the electronegativity difference between carbon and nitrogen.[14] On the contrary, the Y−Z distances referring to the acylium groups in $C_3O_2H^+$ do not differ significantly. All three cations show an angled structure around the central atom. The Y−X−Y angle of $C_3O_2H^+$ is in the range between that of the other two cations.

Table 1. Bond lengths and angles of $ZYXYZ^+$ type cations (X = CH, N; Y = C, N; Z = N, O) from this work ($C_3O_2H^+$) and the literature (OCNCO$^+$, N_5^+).

	$C_3O_2H^+$[a]	OCNCO$^+$[b][25]	N_5^+[c][28]
X−Y [Å]	1.354(3) (C2−C1) 1.351(3) (C2−C3)	1.250(4) (N1−C1) 1.250(5) (N1−C2)	1.303(19) (N3−N2) 1.295(19) (N3−N4)
Y−Z [Å]	1.123(3) (C1−O1) 1.112(3) (C3−O2)	1.118(4) (C1−O1) 1.114(5) (C2−O2)	1.102(19) (N2−N1) 1.107(19) (N4−N5)
X−Y−Z [°]	177.4(2) (C2−C1−O1) 177.1(3) (C2−C3−O2)	173.7(4) (N1−C1−O1) 173.1(4) (N1−C2−O2)	168.1(15) (N3−N2−N1) 166.3(−)[d] (N3−N4−N5)
Y−X−Y [°]	119.8(2) (C1−C2−C3)	130.7(2) (C1−N1−C2)	111.2(11) (N2−N3−N4)

[a] as salt [C_3O_2H][Sb_2F_{11}]. [b] as salt [OCNCO][Sb_3F_{16}]. [c] as salt [N_5][Sb_2F_{11}]. [d] the estimated standard deviation is not given in the reported data.

Vibrational Spectroscopy

In addition to the X-ray structure analyses, the salts [**1**][Sb_2F_{11}], [**2**][Sb_2F_{11}], [**2**][As_2F_{11}], and [**3**][Sb_2F_{11}] were investigated by Raman and infrared (IR) spectroscopy. The assignment of the experimental frequencies was supported by calculated frequencies. The geometries of the cations FOC−CH_2−CO$^+$, F(HO)C=CH−CO$^+$, and $C_3O_2H^+$ were first optimized on the M06-2X/aug-cc-pVTZ level of theory. Subsequently, the found geometries were confirmed as true minima by frequency analyses on the same level of theory. The calculated structures agree very well with the data from the crystal structures and are found in the Supporting Information. The salt [**1**][Sb_2F_{11}] was characterized by Raman and IR spectroscopy, while the salts [**2**][Sb_2F_{11}] and [**2**][As_2F_{11}] were characterized by Raman spectroscopy only. We were able to isolate an appreciable amount of [C_3O_2H][Sb_2F_{11}] for the measurement of Raman and IR spectra, but these contain a significant amount of impurity, which was assigned to compound

4 (Scheme 3). By comparison with the calculated frequencies and values from the literature, distinctive vibrational frequencies are still undoubtedly assigned to the $C_3O_2H^+$ cation. Complete lists of the observed experimental and calculated vibrational frequencies of the discussed compounds are found in the Supporting Information. Selected vibrational frequencies of the cations $FOC{-}CH_2{-}CO^+$, $F(HO)C{=}CH{-}CO^+$, and $C_3O_2H^+$ from the respective salts are listed in Table 2. In the following, only the $C_3O_2H^+$ cation is discussed in detail.

All three acylium cations $FOC{-}CH_2{-}CO^+$, $F(HO)C{=}CH{-}CO^+$, and $C_3O_2H^+$ are most noticeably detected by their Raman active CO stretching vibrations of the acylium groups. Figure 5 shows the region of the Raman spectrum containing the acylium ν(CO) vibrations of the cations. The calculated frequencies of the characteristic CO stretching vibrations are blue-shifted from the observed frequencies, even after applying a scaling factor of 0.956.[29] This finding is assumably caused by interionic contacts between the acylium carbons and anions in the solid state. Such C⋯F interactions were observed in all crystal structures in this work. Nevertheless, the calculated and experimental frequencies agree very well relative to each other.

The $C_3O_2H^+$ cation exhibits C_{2v} symmetry in the crystal structure of [**3**][Sb_2F_{11}] as well as the calculated structure. Therefore, 12 fundamental vibrations ($\Gamma_{vib}(C_{2v}) = 5\,A_1 + 1\,A_2 + 2\,B_1 + 5\,B_2$) are expected for the cation. All vibrational modes are IR and Raman active, except for the IR inactive A_2 mode.

Table 2. Selected experimental vibrational frequencies of the salts [**1**][Sb_2F_{11}], [**2**][As_2F_{11}], and [**3**][Sb_2F_{11}] together with the calculated vibrational frequencies of the respective cations.

	$FOC{-}CH_2{-}CO^+$ (**1**)	$F(HO)C{=}CH{-}CO^+$ (**2**)	$C_3O_2H^+$ (**3**)
	exp. IR / Raman[a] *[calc. (IR/Raman)]*[b]	exp. Raman[a] *[calc. (IR/Raman)]*[b]	exp. IR / Raman[a] *[calc. (IR/Raman)]*[b]
ν(CH)	2922 (w) / 2927 (19) *[2952 (74/41)]*	3081 (11) *[3085 (111/65)]*	3020 (m) / 3017 (17) *[3026 (175/76)]*
ν(CH)	2864 (w) / 2867 (33) *[2905 (83/102)]*		
ν(CO)	2328 (w) / 2332 (40) *[2357 (193/57)]*	2228 (92) *[2276 (659/57)]*	2291 (w) / 2296 (50) *[2335 (114/68)]*
ν(CO)	1850 (m) / 1851 (14) *[1897 (253/11)]*	1641 (5) *[1606 (903/6)]*	2191 (m) / 2191 (15) *[2242 (1320/26)]*
ν(CF)	1198 (w) / 1201 (4) *[1152 (118/3)]*	1469 (3) *[1491 (314/1)]*	
ν(CC)	916 (m) / 919 (3) *[877 (2/2)]*	1203 (2) *[1267 (40/0)]*	1369 (m) / 1352 (5) *[1354 (124/0)]*
ν(CC)	891 (m) / 894 (19) *[841 (33/10)]*	974 (41) *[959 (24/16)]*	n. o. / 990 (18) *[976 (3/13)]*

[a] Abbreviations for IR intensities: m = medium, w = weak, n.o. = not observed. Experimental Raman intensities are relative to a scale of 1 to 100. [b] Calculated on the M06-2X/aug-cc-pVTZ level of theory. Scaling factor: 0.956. Calculated IR intensities in km/mol; calculated Raman intensities in Å⁴/u.

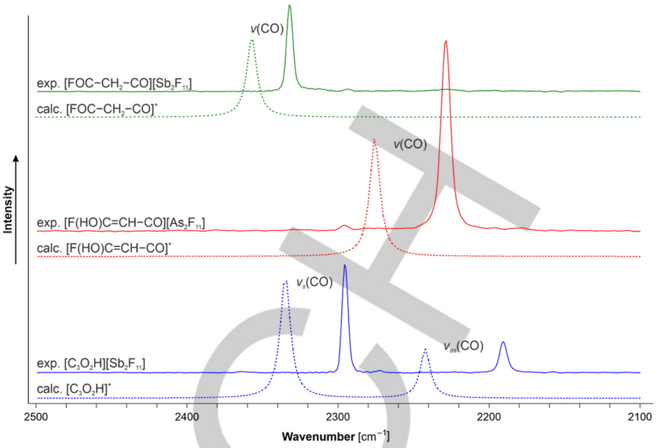

Figure 5. Stacked excerpts of the experimental low-temperature Raman spectra of [**1**][Sb_2F_{11}], [**2**][As_2F_{11}], [**3**][Sb_2F_{11}], and calculated Raman spectra (dashed) of the cations $FOC{-}CH_2{-}CO^+$, $F(HO)C{=}CH{-}CO^+$, and $C_3O_2H^+$. The frequencies were calculated on the M06-2X/aug-cc-pVTZ level of theory and scaled by the factor 0.956.

The CH stretching vibration of $C_3O_2H^+$ is observed at 3020 cm^{-1} in the IR spectrum and 3017 cm^{-1} in the Raman spectrum. The ν_s(CO) mode of $C_3O_2H^+$ is observed at 2291 cm^{-1} in the IR and 2296 cm^{-1} in the Raman spectrum, respectively. Whereas, the ν_{as}(CO) mode is observed at 2191 cm^{-1} in the IR and 2191 cm^{-1} in the Raman spectrum, respectively. *Frenking et al.* measured vibrational frequencies of $C_3O_2H^+$ from the gas phase complex $[HC_3O_2{\cdot}CO]^+$ via infrared photodissociation spectroscopy in a mass spectrometer.[9] They detected bands at 3044 cm^{-1}, 2292 cm^{-1}, and 2208 cm^{-1} and assigned them to the ν(CH), ν_s(CO), and ν_{as}(CO) modes, respectively.[9] These vibrational frequencies agree very well with the measured frequencies of [C_3O_2H][Sb_2F_{11}] in this work. The slight shifts are probably caused by interactions in the solid state. The CC stretching vibrations are also observed in the spectra of [**3**][Sb_2F_{11}]. The ν_{as}(CC) mode is detected in the IR spectrum at 1369 cm^{-1} and in the Raman spectrum at 1352 cm^{-1}, respectively. The symmetric CC stretching vibration is only observed in the Raman spectrum at 990 cm^{-1}. An additional band at 1076 cm^{-1} in the IR spectrum and a line at 1081 cm^{-1} in the Raman spectrum are assigned to a CCH deformation vibration. The interesting CCC deformation vibration of $C_3O_2H^+$ is calculated at a frequency of 651 cm^{-1}. However, the intensive SbF stretching vibrations of the $Sb_2F_{11}^-$ anion are observed in this region of the spectra. Therefore, an assignment of the CCC deformation vibration is not feasible.

Due to the structural similarity of $C_3O_2H^+$ with the isoelectronic cations N_5^+ and $OCNCO^+$, we were interested, if the vibrational spectra of these cations are also comparable. The cation N_5^+ was fully characterized by IR and Raman spectroscopy by *Christe et al.*[27] In the salt [N_5][Sb_2F_{11}] the symmetrical terminal NN stretching vibrations are observed at 2260 cm^{-1} (IR) and 2261 cm^{-1} (Raman), whereas the antisymmetrical terminal NN stretching vibrations are observed at 2203 cm^{-1} (IR) and 2202 cm^{-1} (Raman), respectively.[27] These modes are well comparable to the ν_s(CO) and ν_{as}(CO) vibrations of $C_3O_2H^+$. The central ν_{as}(NN) and ν_s(NN) vibrations of the N_5^+ cation, were observed at 1064 cm^{-1} (IR) and 867 cm^{-1} (IR), 866 cm^{-1} (Raman), respectively.[27] The corresponding CC stretching vibrations of $C_3O_2H^+$ (1352 cm^{-1} and 990 cm^{-1}, Raman) are significantly blue-shifted in comparison. For the $OCNCO^+$ cation, the Raman frequencies are reported without an assignment.[14] In the spectra of the salt $[OCNCO][Sb_3F_{16}]$, Raman lines at 2359 cm^{-1}, 2320 cm^{-1}, and 914 cm^{-1} were reported, which agree well with the frequencies of the stretching vibrations of $C_3O_2H^+$ and N_5^+.[14,27]

Quantum Chemical Calculations

Quantum chemical calculations were performed to understand the unique structural features of the cations $F(HO)C{=}CH{-}CO^+$ and $C_3O_2H^+$ and to clarify the electron distribution in each of them. All following calculations concerning the cations **2** and **3** were performed on the MP2/aug-cc-pVTZ level of theory, including geometry optimization and subsequent frequency analysis. The first question we wanted to address was: how to draw these cations as Lewis structures? For this reason, the natural resonance theory (NRT) analysis of the cations was studied, using NBO 6.0.[30] The respective three leading Lewis resonance structures of the two cations are shown in Figure 6. All Lewis structures with weightings over 5% are shown in Figure S9 and Figure S10 in the Supporting Information.

For **2** the highest weighted resonance Lewis structure of the cation can be described as enol species with an attached acylium group. Since this is consistent with the crystal structure results, we conclude that **2-I** (Figure 6) is the most fitting way to describe cation **2** with a single Lewis structure. Overall, seven Lewis resonance structures show weightings over 5%, so the delocalization of the π-electrons and thus the positive charge in **2** plays an eminent role in the cation. This also explains the higher stability of $F(HO)C{=}CH{-}CO^+$ compared to the other acylium species $FOC{-}CH_2{-}CO^+$ (**1**) in which the positive charge is very poorly stabilized.

The NRT analysis shows that the cation $C_3O_2H^+$ is even more difficult to describe with a single Lewis structure. The three leading Lewis structures have weightings of around 27%. Structure **3-I** with the highest weighting can be described as diacylium methanide with two acylium groups and a lone pair on the central carbon atom. The Lewis resonance structures **3-II** and **3-III** which are degenerate, correspond to an acylium ketene structure. The weightings of the resonance structures **3-II** and **3-III** add up to a value of around 55%, which underlines the ketene-like character of the $C_3O_2H^+$ cation. The similarity to ketene is supported by the experimental results of the C−C and C−O bond distances in the crystal structure and the ^{13}C NMR resonances in the NMR spectrum. The ^{13}C NMR resonances and respective bond distances of $C_3O_2H^+$ and ketene are compared in Table 3.

This raises the question of which of these Lewis resonance structures is the most fitting for the $C_3O_2H^+$ cation. Structure **3-I** appears counterintuitive at first but there are arguments to describe $C_3O_2H^+$ with this particular Lewis structure. First, it is the only symmetrical Lewis structure among those listed. Second, a high electron density on the central carbon atom is not surprising when the cation is compared to similar structures. The isoelectronic dicyanomethanide ($NCC(H)CN^-$) is a well-described and stable anion.[31] The neutral compound carbon suboxide has a negatively polarized central carbon atom, which even exhibits a negative ^{13}C NMR chemical shift in its ^{13}C NMR spectrum.[32] Furthermore, the two before-mentioned cations N_5^+ and $OCNCO^+$ both contain negatively polarized central nitrogen atoms.[14,28] The bonding situation in the N_5^+ cation has been thoroughly discussed in the literature.[33]

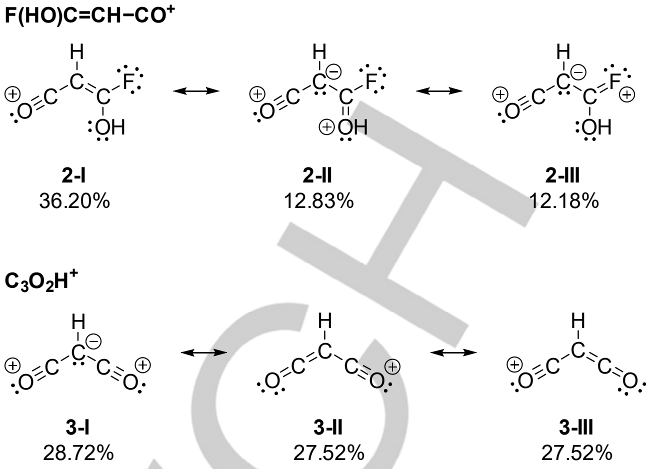
$F(HO)C{=}CH{-}CO^+$

2-I 36.20%

2-II 12.83%

2-III 12.18%

$C_3O_2H^+$

3-I 28.72%

3-II 27.52%

3-III 27.52%

Figure 6. Leading Lewis resonance structures of the cations **2** and **3** along with their weightings from the NRT analysis.

Table 3. Bond lengths of $C_3O_2H^+$ in [**3**][Sb_2F_{11}] and ketene[26] and ^{13}C NMR resonances of both compounds.

bond lengths[a]	$C_3O_2H^+$ (solid)	$H_2C{=}C{=}O$ (gas)[a]
C−C	1.354(3) (C2−C1) 1.351(3) (C2−C3)	1.323(2) Å
C−O	1.123(3) (C1−O1) 1.112(3) (C3−O2)	1.154(3) Å
^{13}C NMR resonance	$C_3O_2H^+$ (solution)[b]	$H_2C{=}C{=}O$ (solution)[c]
H**C**(CO)$_2^+$ / H_2**C**=C=O	11.17 ppm	2.5 ppm
HC(**CO**)$_2^+$ / H_2C=**C**=O	158.91 ppm	194.0 ppm

[a] bond lengths of ketene from gas electron diffraction,[26] [b] [**3**][Sb_2F_{11}] measured in liquid SO_2 at −40 °C, [c] ketene measured at −60 °C in $CDCl_3$.[34]

The bonding situation in $C_3O_2H^+$ is discussed in detail in two studies in the literature.[9] *Frenking et al.* argue that **3** can be described as the dicarbonyl complex of the methylidyne cation with strong σ-donations of the carbonyl ligands into the CH^+ moiety ($OC{\rightarrow}CH^+{\leftarrow}CO$) and additional weaker π-backdonations ($OC{\leftarrow}CH^+{\rightarrow}CO$).[9]

In the notation as dicarbonyl of the methylidyne cation, the central carbon atom bears the positive charge as CH^+ moiety.[9] This is contradictory to the results from the NRT calculations, where the highest weighted resonance Lewis structure contains a central carbon atom with a formal negative charge. While the description of the bonding situation in $C_3O_2H^+$ as dicarbonyl of CH^+ may be accurate, it fails to describe the properties of the $C_3O_2H^+$ cation towards its chemical surrounding. This is negligible when the cation is studied in the gas phase, but of fundamental importance in the condensed phase. This prompted us to investigate the $C_3O_2H^+$ cation with additional results from the NBO analysis as well as its electrostatic potential.

Figure 7 shows the NPA charges in the $C_3O_2H^+$ cation, which indicate positively charged acylium carbon atoms (+1.033 *e*) as well as a negatively charged central carbon atom (−0.770 *e*). The mapped molecular electrostatic potential (MEP) of $C_3O_2H^+$ draws a similar picture in this matter with the highest electron deficiencies being situated around the acylium carbons. A similar finding was observed in the monoacylium cation of fumaryl fluoride.[18]

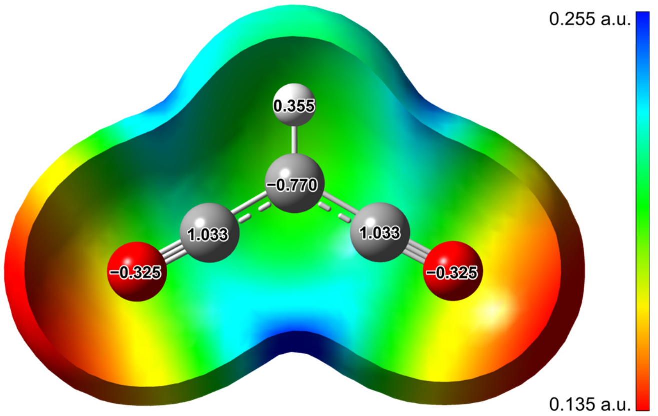

Figure 7. MEP mapped on the electron density isosurface (0.0004 Bohr^{-3}) of the $C_3O_2H^+$ cation along with NPA charges of the respective atoms. The MEP is illustrated in a color range from 0.135 a.u. (red) to 0.255 a.u. (blue). The NPA charges are given in *e*.

The molecular electrostatic potential around the central carbon atom is less positive, especially perpendicular to the plane of the cation. The NRT resonance structures and the NPA charges indicate a high electron density on the central carbon atom even though it is bound to the acidic proton. To understand the origin of the high electron density on the central carbon atom from the natural bond orbital (NBO) analysis, the involved orbitals were studied.

Figure 8 shows five NBOs critical for the π-system of $C_3O_2H^+$, which stabilizes the positive charge in the cation. The canonical molecular orbitals (CMOs) that result from the mixing of these NBOs along with their respective energies and occupancies are depicted below. The three relevant Lewis-type NBOs are the π_{CO} NBOs with occupancies of 1.99 electrons and the n_C NBO, which corresponds to a lone pair on the central carbon atom with an occupancy of 1.44 electrons. The two relevant non-Lewis-type NBOs are the π^*_{CO} NBOs with occupancies of 0.27 electrons. The not fully occupied n_C orbital together with the partially occupied π^*_{CO} orbitals indicate a delocalization of the electrons between these orbitals. Indeed from the second-order perturbation analysis, the interactions $n_C \rightarrow \pi^*_{CO}$ between the donating orbital n_C and the acceptor orbitals π^*_{CO} are present. The stabilization energy of this interaction is 741.6 kJ/mol, respectively. The $n_C \rightarrow \pi^*_{CO}$ interactions correspond to the π-backdonations ($OC \leftarrow CH^+ \rightarrow CO$) in *Frenking*'s description.[9]

The consideration of the π-stabilization of the positive charge in $C_3O_2H^+$ using canonical molecular orbitals, leads to the five MOs shown in Figure 8. The NBO composition of the HOMO (Ψ_3) is approximately expressed as:

$$MO(\Psi_3) = 0.791\ n_C - 2 \times 0.243\ \pi_{CO} + 2 \times 0.352\ \pi^*_{CO}$$

The HOMO is primarily composed of the lone pair n_C (62.6% = 0.791^2), antibonding contributions of the π_{CO} NBOs (11.8% = 2 × 0.243^2), and significant bonding contributions of the π^*_{CO} NBOs (24.7% = 2 × 0.352^2). Again the $n_C \rightarrow \pi^*_{CO}$ interaction is observed, mainly affecting the HOMO of $C_3O_2H^+$ in the perspective of canonical molecular orbitals. The NBO compositions of the other depicted CMOs are shown in Figure S10.

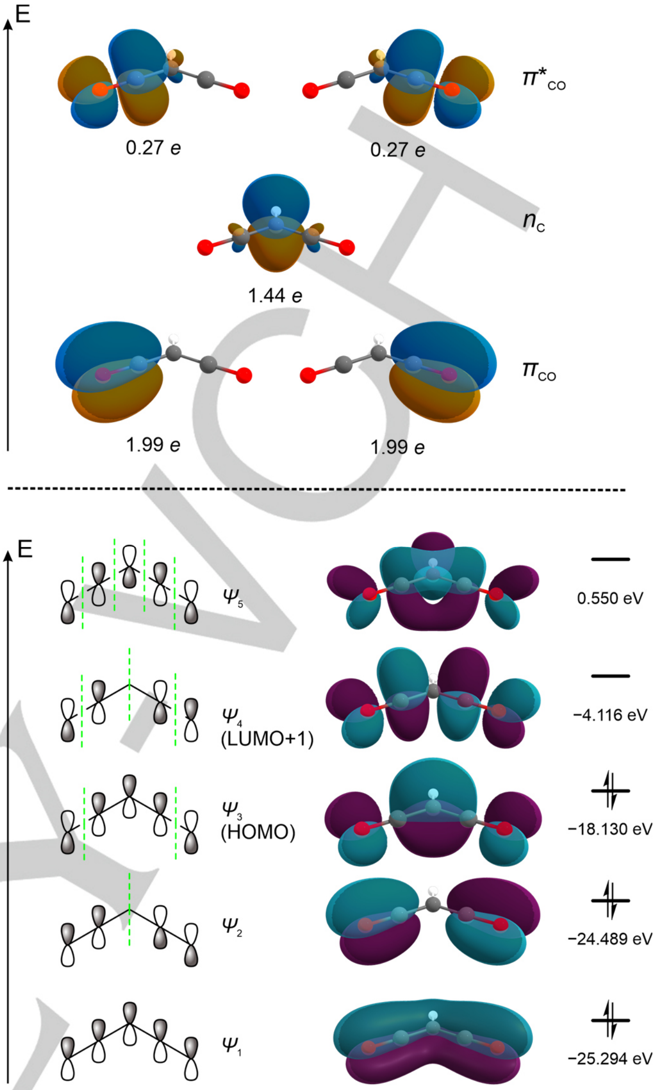

Figure 8. Top: Illustration of the NBOs corresponding to the p_z-orbitals of $C_3O_2H^+$ along with their occupancies between 0.00 to 2.00 electrons. Bottom: CMOs of the mixed p_z-orbitals of $C_3O_2H^+$ with an illustration of the number of nodes (green dashed lines), occupancies, and energy, respectively.

In summary, the Lewis resonance structure **3-I** of the $C_3O_2H^+$ cation is well justifiable. In terms of chemical intuition, it indicates how the cation would interact with its surrounding in condensed media. An example are the interionic contacts with the $Sb_2F_{11}^-$ anions in the crystal structure of [**3**][Sb_2F_{11}] (Figure S6). The anion-cation contacts are observed between the acylium carbon atoms C1 and C3, and fluorine atoms of the anion. No relevant interactions are observed between the surrounding anions and the C2 atom, which is the site of protonation in the cation.

Conclusion

The salts [$FOC{-}CH_2{-}CO$][Sb_2F_{11}], [$F(HO)C{=}CH{-}CO$][Sb_2F_{11}], and [C_3O_2H][Sb_2F_{11}] were obtained from the reaction of malonyl difluoride with the Lewis superacid SbF_5 under respective conditions. The acylium cations were characterized by vibrational spectroscopy and NMR spectroscopy. Furthermore, with single crystals of the salts [$FOC{-}CH_2{-}CO$]$_4$[SbF_6][Sb_2F_{11}]$_3 \cdot SO_2$, [$F(HO)C{=}CH{-}CO$][M_2F_{11}] (M = As, Sb), and [C_3O_2H][Sb_2F_{11}], the solid-state structures of these compounds were elucidated for the first time by single-crystal X-ray structural analyses. The cation $F(HO)C{=}CH{-}CO^+$ is the enol tautomer of the keto species $FOC{-}CH_2{-}CO^+$. Since the keto-enol tautomerism in acid fluorides is almost exclusively shifted to the keto species, this is the first example of an isolated 1-fluoro-1-en-1-ol moiety that we know of. This is supported by calculated results from an NRT analysis. The $C_3O_2H^+$ cation is the monoprotonated species of carbon suboxide and was isolated for the first time in the condensed phase. The cation shows remarkable similarities to the isoelectronic cations $OCNCO^+$ and N_5^+. To support the experimental results, quantum chemical calculations were performed for the assignment of the vibrational frequencies and to elucidate the interesting electron distribution in $C_3O_2H^+$. The NBO analysis reveals a high electron density at the central carbon atom, even though it bears the acidic proton. We conclude that this justifies the description of $C_3O_2H^+$ with a Lewis resonance structure that can be described as diacylium methanide.

Experimental Section

All experimental data and procedures are found in the Supporting Information.

Deposition Numbers 2220802 ($[FOC{-}CH_2{-}CO]_4[SbF_6][Sb_2F_{11}]_3{\cdot}SO_2$), 2220803 ($[FOC{-}CH_2{-}CO][Sb_2F_{11}]$), 2220804 ($[FOC{-}CH_2{-}CO][As_2F_{11}]$), and 2220805 ($[C_3O_2H][Sb_2F_{11}]$) contain the supplementary crystallographic data for this paper. These data are provided free of charge by the joint Cambridge Crystallographic Data Centre and Fachinformationszentrum Karlsruhe Access Structures service www.ccdc.cam.ac.uk/structures.

Acknowledgments

We are grateful to the Department of Chemistry of the Ludwig-Maximilian University, Munich, the Deutsche Forschungsgemeinschaft (DFG), and the F-Select GmbH for the support of this work.

Keywords: acylium cation; protonated carbon suboxide; single-crystal X-ray structure analysis; vibrational spectroscopy, NBO analysis

[1] G. A. Olah, *J. Org. Chem.* **2001**, *66*, 5943.

[2] a) G. A. Olah, W. S. Tolgyesi, S. J. Kuhn, M. E. Moffatt, I. J. Bastien, E. B. Baker, *J. Am. Chem. Soc.* **1963**, *85*, 1328; b) G. A. Olah, S. J. Kuhn, W. S. Tolgyesi, E. B. Baker, *J. Am. Chem. Soc.* **1962**, *84*, 2733; c) G. A. Olah, A. Germain, H. C. Lin, *J. Am. Chem. Soc.* **1975**, *97*, 5481.

[3] G. A. Olah, M. B. Comisarow, *J. Am. Chem. Soc.* **1966**, *88*, 3313.

[4] G. A. Olah, D. A. Klumpp, *Superelectrophiles and Their Chemistry*, John Wiley & Sons, Inc, Hoboken, NJ, USA, **2007**.

[5] R. Tonner, G. Heydenrych, G. Frenking, *ChemPhysChem* **2008**, *9*, 1474.

[6] J. Tortajada, G. Provot, J.-P. Morizur, J.-F. Gal, P.-C. Maria, R. Flammang, Y. Govaert, *Int. J. Mass Spectrom. Ion Processes* **1995**, *141*, 241.

[7] J. B. Westmore, W. D. Buchannon, L. Plaggenborg, B. W. Wenclawiak, *J. Am. Soc. Mass Spectrom.* **1998**, *9*, 29.

[8] M. Lang, F. Holzmeier, I. Fischer, P. Hemberger, *J. Phys. Chem. A* **2014**, *118*, 11235.

[9] J. Jin, L. Zhao, X. Wu, W. Li, Y. Liu, D. M. Andrada, M. Zhou, G. Frenking, *J. Phys. Chem. A* **2017**, *121*, 2903.

[10] A. Papakondylis, A. Mavridis, *J. Phys. Chem. A* **2005**, *109*, 6549.

[11] a) O. Diels, L. Lalin, *Ber. Dtsch. Chem. Ges.* **1908**, *41*, 3426; b) O. Diels, K. Hansen, *Ber. Dtsch. Chem. Ges. B* **1926**, *59*, 2555; c) O. Diels, B. Wolf, *Ber. Dtsch. Chem. Ges.* **1906**, *39*, 689; d) T. Kappe, E. Ziegler, *Angew. Chem.* **1974**, *86*, 529.

[12] A. Kornath, R. Seelbinder, R. Minkwitz, *Angew. Chem., Int. Ed.* **2005**, *44*, 973.

[13] A. F. Holleman, E. Wiberg, N. Wiberg, G. Fischer, *Anorganische Chemie*, De Gruyter, Berlin, Boston, **2017**.

[14] I. Bernhardi, T. Drews, K. Seppelt, *Angew. Chem., Int. Ed.* **1999**, *38*, 2232.

[15] F. P. Boer, *J. Am. Chem. Soc.* **1968**, *90*, 6706.

[16] J. M. Le Carpentier, R. Weiss, *Acta Crystallogr., Sect. B: Struct. Crystallogr. Cryst. Chem.* **1972**, *28*, 1421.

[17] J. M. Le Carpentier, R. Weiss, *Acta Crystallogr., Sect. B: Struct. Crystallogr. Cryst. Chem.* **1972**, *28*, 1430.

[18] M. C. Bayer, N. Greither, C. Jessen, A. Nitzer, A. J. Kornath, *Eur. J. Inorg. Chem.* **2022**, *2022*.

[19] A. Jin, H. G. Mack, A. Waterfeld, H. Oberhammer, *J. Am. Chem. Soc.* **1991**, *113*, 7847.

[20] M. C. Bayer, C. Kremser, C. Jessen, A. Nitzer, A. J. Kornath, *Chem. - Eur. J.* **2022**, *28*, e202104422.

[21] S. Steiner, C. Jessen, A. J. Kornath, *Z. Anorg. Allg. Chem.* **2022**, *648*.

[22] a) N. V. Belova, H. Oberhammer, X. Zeng, M. Gerken, H. Willner, R. J. F. Berger, S. A. Hayes, N. W. Mitzel, *Phys. Chem. Chem. Phys.* **2010**, *12*, 11445; b) N. V. Belova, V. V. Sliznev, H. Oberhammer, G. V. Girichev, *J. Mol. Struct.* **2010**, *978*, 282; c) N. Heinrich, W. Koch, G. Frenking, H. Schwarz, *J. Am. Chem. Soc.* **1986**, *108*, 593.

[23] G. A. Jeffrey, *An introduction to hydrogen bonding*, Oxford Univ. Press, New York, **1997**.

[24] A. Bondi, *J. Phys. Chem.* **1964**, *68*, 441.

[25] A. Ellern, T. Drews, K. Seppelt, *Z. Anorg. Allg. Chem.* **2001**, *627*, 73.

[26] S. J. Atkinson, R. Noble-Eddy, S. L. Masters, *J. Phys. Chem. A* **2016**, *120*, 2041.

[27] K. O. Christe, W. W. Wilson, J. A. Sheehy, J. A. Boatz, *Angew. Chem., Int. Ed.* **1999**, *38*, 2004.

[28] A. Vij, W. W. Wilson, V. Vij, F. S. Tham, J. A. Sheehy, K. O. Christe, *J. Am. Chem. Soc.* **2001**, *123*, 6308.

[29] R. D. Johnson, *Computational Chemistry Comparison and Benchmark Database, NIST Standard Reference Database 101*, National Institute of Standards and Technology, **2002**.

[30] E. D. Glendening, C. R. Landis, F. Weinhold, *J. Comput. Chem.* **2013**, *34*, 1429.

[31] a) H. Brand, J. F. Liebman, A. Schulz, P. Mayer, A. Villinger, *Eur. J. Inorg. Chem.* **2006**, *2006*, 4294; b) W. Hiller, S. Frey, J. Strähle, G. Boche, W. Zarges, K. Harms, M. Marsch, R. Wollert, K. Dehnicke, *Chem. Ber.* **1992**, *125*, 87; c) K. Jens, J. Kopf, N. P. Lorenzen, E. Weiss, *Chem. Ber.* **1988**, *121*, 1201.

[32] a) E. A. Williams, J. D. Cargioli, A. Ewo, *J. Chem. Soc., Chem. Commun.* **1975**, 366; b) J. F. Olsen, L. Burnelle, *J. Phys. Chem.* **1969**, *73*, 2298.

[33] a) T. M. Klapötke, *Angew. Chem., Int. Ed.* **1999**, *38*, 2536; b) M. T. Nguyen, T.-K. Ha, *Chem. Phys. Lett.* **2000**, *317*, 135; c) X. Wang, H. Hu, A. Tian, N. B. Wong, S.-H. Chien, W.-K. Li, *Chem. Phys. Lett.* **2000**, *329*, 483; d) R. Ponec, J. Roithová, X. Gironés, K. Jug, *J. Mol. Struct.: THEOCHEM* **2001**, *545*, 255; e) I. S. K. Kerkines, A. Papakondylis, A. Mavridis, *J. Phys. Chem. A* **2002**, *106*, 4435; f) R. D. Harcourta, T. M. Klapötke, *Z. Naturforsch., B: J. Chem. Sci.* **2002**, *57*, 983.

[34] J. Firl, W. Runge, *Angew. Chem., Int. Ed.* **1973**, *12*, 668.

Entry for the Table of Contents

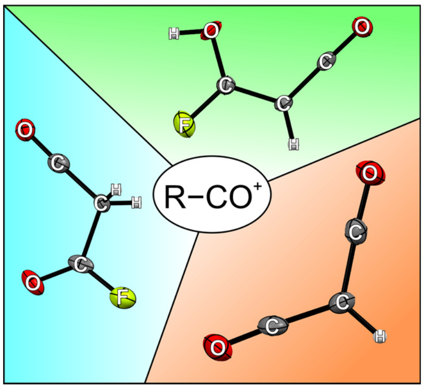

The acylium cations FOC−CH$_2$−CO$^+$, F(HO)C=CH−CO$^+$, and C$_3$O$_2$H$^+$ were synthesized and isolated as salts. The compounds were characterized by vibrational spectroscopy, single-crystal X-ray structure analysis, and NMR spectroscopy, respectively. The C$_3$O$_2$H$^+$ cation is the difficult to access protonated species of carbon suboxide and is described in condensed phase for the first time. Its unique structure is elucidated by experimental and theoretical results.

Supporting Information

Acylium Cations of Malonyl Difluoride: Synthesis and Characterization of the $C_3O_2H^+$ Cation

Christoph Jessen, Dirk Hollenwäger, Florian Zischka, and Andreas J. Kornath*

Table of Contents

1 Experimental Details ... 3

1.1 Apparatus and Materials ... 3

1.2 Computational Methods ... 3

1.3 Experimental Procedures ... 4

2 Crystallographic Data ... 5

2.1 $[FOC-CH_2-CO]_4[SbF_6][Sb_2F_{11}]_3\cdot SO_2$ ... 6

2.2 $[F(HO)C=CH-CO][Sb_2F_{11}]$ ... 8

2.3 $[F(HO)C=CH-CO][As_2F_{11}]$ ... 10

2.4 $[C_3O_2H][Sb_2F_{11}]$ ... 12

3 Vibrational Data ... 14

3.1 $[FOC-CH_2-CO]^+$ (1) ... 14

3.2 $[F(HO)C=CH-CO]^+$ (2) ... 15

3.3 $[C_3O_2H]^+$ (3) ... 16

3.4 $[C_3H_4F_2O_4S]^{2+}$ (4) ... 17

4 NMR ... 19

4.1 $[FOC-CH_2-CO][Sb_2F_{11}]$ ... 19

4.2 $[C_3H_4F_2O_4S][Sb_2F_{11}]$ (4) ... 21

4.3 $[C_3O_2H][Sb_2F_{11}]$ ... 23

5 Quantum Chemical Calculations ... 27

6 References ... 32

1 Experimental Details

Caution! Note that any contact with the described compounds should be avoided. Hydrolysis of malonyl difluoride, SbF_5, AsF_5, SO_2ClF and all described products may form hydrogen fluoride which burns skin and causes irreparable damage. Safety precautions should be taken while handling these compounds.

1.1 Apparatus and Materials

All reactions were carried out by employing standard Schlenk techniques on a stainless steel vacuum line. The syntheses of the salts were performed using FEP/PFA reactors with stainless steel valves. Before each reaction or NMR measurement, the stainless steel vacuum line and the reactors were dried with fluorine.

For Raman measurements a Bruker MultiRam FT-Raman spectrometer with Nd:YAG laser excitation (λ = 1064 nm) was used. The measurement was performed after transferring the sample into a cooled (−196°C) glass cell under a nitrogen atmosphere and subsequent evacuation of the glass cell.

Low-temperature IR-spectroscopic investigations were carried out with a Bruker Vertex-80V FTIR spectrometer using a cooled cell with a single-crystal CsBr plate on which small amounts of the samples were placed.[1]

The single-crystal X-ray diffraction studies were performed with an Oxford XCalibur3 diffractometer equipped with a Spellman generator (voltage 50 kV, current 40 mA) and a KappaCCD detector, operating with Mo-Kα radiation (λ = 0.7107 Å) The measurements were performed between 103-110 K. The program CrysAlisPro 1.171.39.46e (Rigaku Oxford Diffraction, 2018) was employed for the data collection and reduction.[2] Deviations from this version are given in the CIF files of the respective crystal structure. The structures were solved utilizing SHELXT[3] and SHELXL-2018/3[4] of the WINGX software package.[5] The structures were checked using the software PLATON.[6] The absorption correction was performed using the SCALE3 ABSPACK multiscan method.[7] Visualization was done with the software Mercury.[8]

NMR spectra were recorded on either a Jeol ECX400 NMR instrument or a Bruker AV400 NMR instrument. The spectrometer was externally referenced to $CFCl_3$ for ^{19}F NMR and to tetramethylsilane for ^{1}H NMR spectra. For visualization and evaluation, the software MestReNova Version 14.0.4 was used.[9] The spectra were recorded inside 4 mm FEP tube inliners. The NMR samples were prepared by transferring the SO_2-solution of the respective compound into a dried 4 mm FEP tube inliner under a nitrogen atmosphere. Then the FEP tube was frozen at −196 °C. The FEP tube was evacuated, flame sealed and kept at −196 °C. Immediately before the NMR measurement, the sealed FEP tube was put in a standard glass NMR tube loaded with 0.2 mL acetone-d_6 as an external reference and warmed to the designated temperature.

1.2 Computational Methods

Quantum chemical calculations were carried out using the software packages Gaussian09 and Gaussian16.[10,11] For visualization and illustration of the calculated structures, the software GaussView 6 was used.[12] The NBO analysis was performed with the NBO 6.0 program.[13,14] The visualization of NBOs and CMOs was done with the software Chemcraft 1.8.[15]

1.3 Experimental Procedures

For the following procedures applies R-134a = 1,1,1,2-tetrafluoroethane.

Malonyl difluoride

Malonyl difluoride (FOC−CH$_2$−COF) was prepared according to the literature.[16] Malonyl difluoride was stored in a glass flask with a grease-free stopcock at −20 °C.

Monoacylium cation (1)

[FOC−CH$_2$−CO][Sb$_2$F$_{11}$]

SbF$_5$ (1.0 mmol) was condensed into an FEP reactor vessel together with 1 mL R-134a at −196 °C. The reactor was warmed to −60°C and mixed until the SbF$_5$ was completely dissolved. Then the reactor was cool to −78 °C with dry ice and malonyl difluoride (0.5 mmol) was added under nitrogen atmosphere using a syringe. The reactants were warmed to −60°C and mixed until no more precipitation of the product as a colorless solid was observed. Subsequently, volatile components were removed at −78 °C in a dynamic vacuum. The product [FOC−CH$_2$−CO][Sb$_2$F$_{11}$] was obtained as a colorless solid. The decomposition of the salt was observed upon warming to 18 °C.

[FOC−CH$_2$−CO]$_4$[SbF$_6$][Sb$_2$F$_{11}$]$_3$·SO$_2$

Single crystals of the salt [**1**]$_4$[SbF$_6$][Sb$_2$F$_{11}$]$_3$·SO$_2$ were obtained by recrystallization of [**1**][Sb$_2$F$_{11}$] in a 1:4 mixture of SO$_2$/SO$_2$ClF at −70 °C.

Monoacylium cation (2)

[F(HO)C=CH−CO][Sb$_2$F$_{11}$]

SbF$_5$ (1.0 mmol) was condensed into an FEP reactor vessel together with 1 mL R-134a at −196 °C. The reactor was warmed to −60°C and mixed until the SbF$_5$ was completely dissolved. Then the reactor was cooled to −78 °C with dry ice and malonyl difluoride (0.5 mmol) was added under a nitrogen atmosphere using a syringe. The reactants were warmed to −60°C and mixed until no more precipitation of the product as a colorless solid was observed. The reaction mixture was kept at −50 °C for 3-5 days and then cooled to −70 °C for one week. At −70 °C the growth of colorless crystals was observed. Subsequently, all volatile components were removed at −78 °C in a dynamic vacuum to obtain the salt [F(HO)C=CH−CO][Sb$_2$F$_{11}$] as a crystalline colorless solid.

[F(HO)C=CH−CO][As$_2$F$_{11}$]

AsF$_5$ (4.0 mmol) was condensed into an FEP reactor vessel together with 1 mL R-134a at −196 °C. The reactor was warmed to −60°C and mixed until complete dissolution of AsF$_5$. Then the reactor was frozen and malonyl difluoride (0.5 mmol) was added under nitrogen atmosphere using a syringe. The reactants were warmed to −60°C and mixed until no more precipitation of the product as a colorless solid was observed. The reaction mixture was kept at −50 °C for two days and then cooled to −70 °C for one week. At −70 °C the growth of colorless crystals was observed. Subsequently, all volatile components were removed at −78 °C in a dynamic vacuum to obtain the salt [F(HO)C=CH−CO][As$_2$F$_{11}$] as a colorless crystalline solid.

Protonated carbon suboxide (3)

[C$_3$O$_2$H][Sb$_2$F$_{11}$]

In an FEP reactor vessel, freshly prepared [FOC−CH$_2$−CO][Sb$_2$F$_{11}$] (0.5 mmol) was dissolved together with SO$_2$·SbF$_5$ (0.5 mmol) in SO$_2$ (1 mL) at −30 °C. The solution was kept at −30 °C for three days. Then, all volatile components were removed at −78 °C in a dynamic vacuum to obtain a yellow oily residue. The residue was frozen at −196 °C and carefully pulverized by knocking on the FEP reactor. Subsequently, the solid was again exposed to a dynamic vacuum at −30 °C. By repeating the last two steps three to five times, the product was obtained as an off-white solid. To grow single crystals the solid was redissolved in R-134a (2 mL) and recrystallized from −40 °C to −70 °C.

2 Crystallographic Data

Table S1. Crystal data and structure refinement of $[FOC{-}CH_2{-}CO]_4[SbF_6][Sb_2F_{11}]_3\cdot SO_2$, $[F(HO)C{=}CH{-}CO][Sb_2F_{11}]$, $[F(HO)C{=}CH{-}CO][As_2F_{11}]$, $[C_3O_2H][Sb_2F_{11}]$.

	$[\mathbf{1}]_4[SbF_6][Sb_2F_{11}]_3\cdot SO_2$	$[\mathbf{2}][Sb_2F_{11}]$	$[\mathbf{2}][As_2F_{11}]$	$[\mathbf{3}][Sb_2F_{11}]$
Molecular Formula	$C_{12}H_8F_{43}O_{10}SSb_7$	$C_3H_2F_{12}O_2Sb_2$	$C_3H_2As_2F_{12}O_2$	$C_3HF_{11}O_2Sb_2$
M_r[g·mol^{-1}]	2013.49	541.55	447.89	521.54
Crystal size [mm^3]	0.24 × 0.09 × 0.07	0.33 × 0.22 × 0.20	0.53 × 0.44 × 0.33	0.287 × 0.206 × 0.138
Crystal system	monoclinic	monoclinic	monoclinic	monoclinic
Space group	Pm	$P2_1/c$	$P2_1/c$	$P2_1/n$
a [Å]	5.3633(2)	7.3045(2)	7.1642(3)	7.4127(2)
b [Å]	14.8916(4)	11.2097(4)	10.8796(4)	11.4560(3)
c [Å]	13.8536(5)	14.1404(4)	13.8832(5)	13.2666(3)
α [°]	5.3633(2)	90	90	90
β [°]	14.8916(4)	97.382(3)	96.287(3)	94.848(2)
γ [°]	13.8536(5)	90	90	90
V [Å^3]	1106.40(6)	1148.24(6)	1075.60(7)	1122.57(5)
Z	1	4	4	4
ρ_{calc} [g·cm^{-3}]	3.022	3.133	2.766	3.086
μ [mm^{-1}]	4.479	4.863	6.381	4.949
$\lambda_{MoK\alpha}$ [Å]	0.71073	0.71073	0.71073	0.71073
F(000)	920	984	840	944
T [K]	103(2)	110(2)	108(2)	106(2)
h, k, l range	-7:7,-21:16,-18:19	-10:10,-15:16,-18:20	-10:9,-15:15,-19:19	-10:10,-17:16,-19:19
Reflections collected	11316	11503	10658	12523
Independent reflections	5795	3510	3283	3710
R_{int}	0.0401	0.0553	0.0303	0.0210
Parameters	362	175	176	163
R(F)/wR(F^2)[a] (all data)	0.0433/0.0661	0.0427/0.0769	0.0354/0.0621	0.0237/0.0451
Weighting scheme[b]	0.0179/0.0000	0.0274/0.0000	0.0253/0.4114	0.0206/0.2230
S (Gof)[c]	1.003	1.051	1.089	1.075
Residual density [e·Å^{-3}]	1.402/-0.795	0.891/-1.494	0.557/-0.732	0.687/-0.416
Device	Oxford XCalibur	Oxford XCalibur	Oxford XCalibur	Oxford XCalibur
CCDC	2220802	2220803	2220804	2220805

[a] $R_1 = \Sigma||F_0|-|F_c||/\Sigma|F_0|$.

[b] $wR_2 = [\Sigma[w(F_0^2-F_c^2)^2]/\Sigma[w(F_0)^2]]^{1/2}$; $w = [\sigma_c^2(F_0^2)+(xP)^2+yP]-1$; $P = (F_0^2+2F_c^2)/3$.

[c] GoF = $\{\Sigma[w(F_o^2-F_c^2)^2]/(n-p)\}^{1/2}$ (n = number of reflections; p = total number of parameters).

2.1 [FOC−CH$_2$−CO]$_4$[SbF$_6$][Sb$_2$F$_{11}$]$_3$·SO$_2$

Table S2. Structural parameters of [FOC−CH$_2$−CO]$_4$[SbF$_6$][Sb$_2$F$_{11}$]$_3$·SO$_2$

Bond lengths [Å]		Bond angles [°]		Torsion angles [°]	
F1−C1	1.302(18)	O1−C1−F1	121.9(12)	O1−C1−C2−C3	0
O2−C3	1.138(18)	O1−C1−C2	127.9(14)	F1−C1−C2−C3	180
O1−C1	1.197(17)	F1−C1−C2	110.2(11)	C6−C5−C4−O3	-16.5(13)
C1−C2	1.470(15)	C3−C2−C1	113.8(11)	C6−C5−C4−F2	163.4(8)
C2−C3	1.42(2)	O2−C3−C2	178.1(13)	C9−C8−C7−O5	0
F2−C4	1.308(11)	O4−C6−C5	178.3(10)	C9−C8−C7−F3	180
O4−C6	1.109(12)	C6−C5−C4	111.4(8)		
O3−C4	1.157(11)	O3−C4−F2	123.5(9)		
C6−C5	1.425(14)	O3−C4−C5	128.0(10)		
C5−C4	1.540(13)	F2−C4−C5	108.5(8)		
O6−C9	1.101(17)	O6−C9−C8	176.6(14)		
O5−C7	1.159(16)	C9−C8−C7	110.2(11)		
F3−C7	1.325(16)	O5−C7−F3	124.5(11)		
C9−C8	1.451(18)	O5−C7−C8	128.3(13)		
C8−C7	1.535(16)	F3−C7−C8	107.2(11)		
Sb1−F4	1.829(10)	F4−Sb1−F7	179.4(5)		
Sb1−F7	1.841(11)	F4−Sb1−F5	90.8(3)		
Sb1−F5	1.857(6)	F7−Sb1−F5	89.7(4)		
Sb1−F5	1.857(6)	F4−Sb1−F5	90.8(3)		
Sb1−F6	1.865(6)	F7−Sb1−F5	89.7(4)		
Sb1−F6	1.865(6)	F5−Sb1−F5	89.7(4)		
Sb2−F10	1.827(7)	F4−Sb1−F6	90.9(3)		
Sb2−F12	1.850(5)	F7−Sb1−F6	88.7(3)		
Sb2−F11	1.850(5)	F5−Sb1−F6	178.2(4)		
Sb2−F8	1.854(5)	F5−Sb1−F6	89.8(2)		
Sb2−F9	1.860(5)	F4−Sb1−F6	90.9(3)		
Sb2−F13	2.008(6)	F7−Sb1−F6	88.7(3)		
Sb3−F18	1.838(6)	F5−Sb1−F6	89.8(2)		
Sb3−F16	1.841(6)	F5−Sb1−F6	178.2(4)		
Sb3−F14	1.849(6)	F6−Sb1−F6	90.7(4)		
Sb3−F15	1.858(6)	F10−Sb2−F12	96.4(3)		
Sb3−F17	1.873(5)	F10−Sb2−F11	96.0(3)		
Sb3−F13	2.028(6)	F12−Sb2−F11	89.6(3)		
Sb4−F20	1.838(9)	F10−Sb2−F8	94.1(3)		
Sb4−F19	1.843(6)	F12−Sb2−F8	89.9(2)		
Sb4−F19	1.843(6)	F11−Sb2−F8	169.9(3)		
Sb4−F21	1.848(5)	F10−Sb2−F9	92.8(3)		
Sb4−F21	1.849(5)	F12−Sb2−F9	170.8(3)		
Sb4−F22	2.000(11)	F11−Sb2−F9	90.2(3)		
Sb5−F24	1.830(10)	F8−Sb2−F9	88.8(3)		
Sb5−F25	1.838(5)	F10−Sb2−F13	176.0(3)		
Sb5−F25	1.838(5)	F12−Sb2−F13	87.1(2)		
Sb5−F23	1.852(5)	F11−Sb2−F13	86.0(3)		
Sb5−F23	1.852(5)	F8−Sb2−F13	83.8(3)		
Sb5−F22	2.005(11)	F9−Sb2−F13	83.7(2)		
S1−O7	1.414(7)	F18−Sb3−F16	96.0(3)		
S1−O7	1.414(7)	F18−Sb3−F14	91.2(3)		
		F16−Sb3−F14	96.8(3)		
		F18−Sb3−F15	167.9(3)		
		F16−Sb3−F15	96.0(3)		
		F14−Sb3−F15	89.2(3)		
		F18−Sb3−F17	89.1(3)		
		F16−Sb3−F17	94.1(3)		
		F14−Sb3−F17	169.0(3)		
		F15−Sb3−F17	88.3(3)		
		F18−Sb3−F13	84.7(3)		
		F16−Sb3−F13	179.1(3)		

F14−Sb3−F13	83.8(2)
F15−Sb3−F13	83.3(3)
F17−Sb3−F13	85.2(2)
Sb2−F13−Sb3	159.1(3)
F20−Sb4−F19	95.0(3)
F20−Sb4−F19	95.0(3)
F19−Sb4−F19	90.3(4)
F20−Sb4−F21	94.4(3)
F19−Sb4−F21	170.6(3)
F19−Sb4−F21	89.3(3)
F20−Sb4−F21	94.4(3)
F19−Sb4−F21	89.3(3)
F19−Sb4−F21	170.6(3)
F21−Sb4−F21	89.5(4)
F20−Sb4−F22	178.3(4)
F19−Sb4−F22	86.2(3)
F19−Sb4−F22	86.2(3)
F21−Sb4−F22	84.4(3)
F21−Sb4−F22	84.4(3)
F24−Sb5−F25	95.2(3)
F24−Sb5−F25	95.2(3)
F25−Sb5−F25	89.7(4)
F24−Sb5−F23	94.0(3)
F25−Sb5−F23	170.7(3)
F25−Sb5−F23	90.1(3)
F24−Sb5−F23	94.0(3)
F25−Sb5−F23	90.1(3)
F25−Sb5−F23	170.7(3)
F23−Sb5−F23	88.6(4)
F24−Sb5−F22	178.0(4)
F25−Sb5−F22	86.2(3)
F25−Sb5−F22	86.2(3)
F23−Sb5−F22	84.6(3)
F23−Sb5−F22	84.6(3)
Sb4−F22−Sb5	170.2(6)
O7−S1−O7	119.1(6)

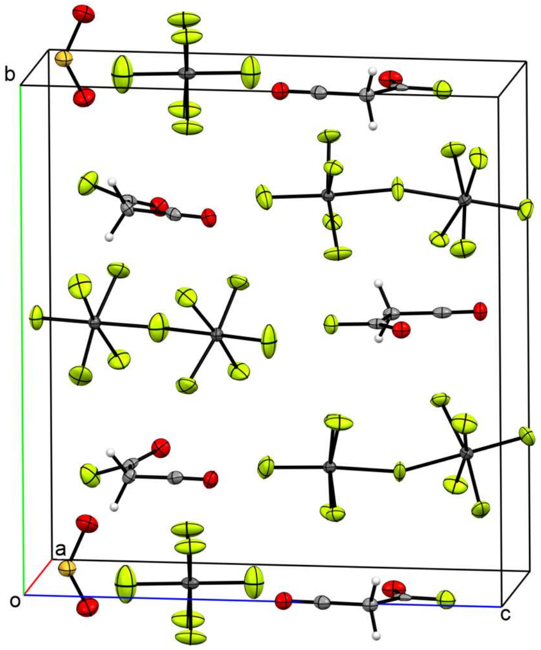

Figure S1. Crystal packing of $[FOC{-}CH_2{-}CO]_4[SbF_6][Sb_2F_{11}]_3 \cdot SO_2$ with 50% probability displacement ellipsoids.

2.2 [F(HO)C=CH−CO][Sb$_2$F$_{11}$]

Table S3. Structural parameters of [F(HO)C=CH−CO][Sb$_2$F$_{11}$].

Bond lengths [Å]		Bond angles [°]		Torsion angles [°]	
Sb1−F4	1.849(2)	F4−Sb1−F3	95.51(12)	O1−C1−C2−C3	1.2(7)
Sb1−F3	1.850(2)	F4−Sb1−F6	96.25(11)	F1−C1−C2−C3	-178.4(4)
Sb1−F6	1.852(2)	F3−Sb1−F6	168.18(12)		
Sb1−F2	1.858(2)	F4−Sb1−F2	92.83(12)		
Sb1−F5	1.865(2)	F3−Sb1−F2	90.33(12)		
Sb1−F7	2.040(2)	F6−Sb1−F2	90.32(12)		
Sb2−F8	1.851(2)	F4−Sb1−F5	94.64(11)		
Sb2−F12	1.852(3)	F3−Sb1−F5	88.95(11)		
Sb2−F11	1.855(2)	F6−Sb1−F5	88.88(12)		
Sb2−F10	1.860(2)	F2−Sb1−F5	172.53(11)		
Sb2−F9	1.863(3)	F4−Sb1−F7	178.52(10)		
Sb2−F7	2.025(2)	F3−Sb1−F7	84.02(11)		
F1−C1	1.304(4)	F6−Sb1−F7	84.26(11)		
O2−C3	1.121(5)	F2−Sb1−F7	85.77(11)		
O1−C1	1.270(5)	F5−Sb1−F7	86.76(10)		
C1−C2	1.359(5)	F8−Sb2−F12	91.41(12)		
C3−C2	1.361(6)	F8−Sb2−F11	171.14(11)		
		F12−Sb2−F11	90.78(13)		
		F8−Sb2−F10	92.93(11)		
		F12−Sb2−F10	92.91(12)		
		F11−Sb2−F10	95.53(11)		
		F8−Sb2−F9	88.48(12)		
		F12−Sb2−F9	172.50(11)		
		F11−Sb2−F9	88.24(12)		
		F10−Sb2−F9	94.59(12)		
		F8−Sb2−F7	85.63(10)		
		F12−Sb2−F7	85.25(11)		
		F11−Sb2−F7	85.99(10)		
		F10−Sb2−F7	177.63(10)		
		F9−Sb2−F7	87.26(11)		
		Sb2−F7−Sb1	145.96(12)		
		O1−C1−F1	117.3(3)		
		O1−C1−C2	123.7(4)		
		F1−C1−C2	119.0(4)		
		O2−C3−C2	178.1(5)		
		C1−C2−C3	119.4(4)		

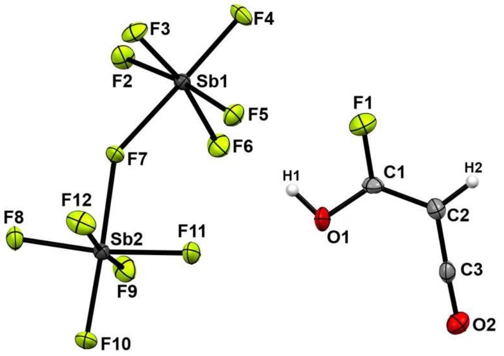

Figure S2. Formula unit of [F(HO)C=CH−CO][Sb$_2$F$_{11}$] with 50% probability displacement ellipsoids.

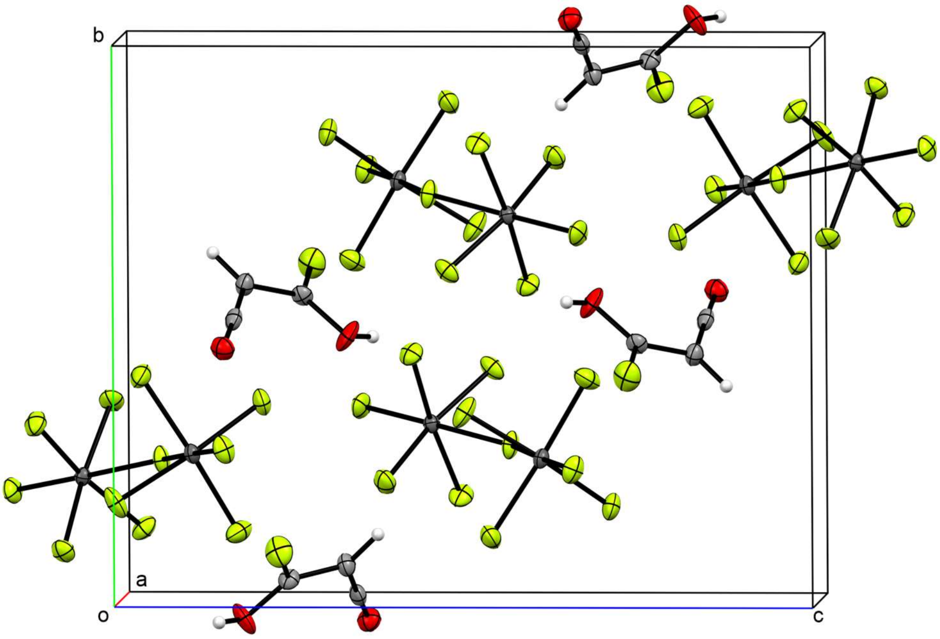

Figure S3. Crystal packing of [F(HO)C=CH−CO][Sb_2F_{11}] with 50% probability displacement ellipsoids.

2.3 [F(HO)C=CH−CO][As$_2$F$_{11}$]

Table S4. Structural parameters of [F(HO)C=CH−CO][As$_2$F$_{11}$].

Bond lengths [Å]		Bond angles [°]		Torsion angles [°]	
As1−F4	1.6813(14)	F4−As1−F5	94.78(7)	C3−C2−C1−O1	-1.4(4)
As1−F5	1.6914(14)	F4−As1−F2	95.51(8)	C3−C2−C1−F1	177.8(2)
As1−F2	1.6927(15)	F5−As1−F2	169.61(7)		
As1−F6	1.6984(15)	F4−As1−F6	93.95(8)		
As1−F3	1.7127(14)	F5−As1−F6	90.34(8)		
As1−F7	1.9296(14)	F2−As1−F6	90.38(8)		
As2−F8	1.6943(16)	F4−As1−F3	94.02(8)		
As2−F9	1.6945(14)	F5−As1−F3	89.06(7)		
As2−F12	1.6951(15)	F2−As1−F3	88.79(7)		
As2−F10	1.6958(14)	F6−As1−F3	172.03(7)		
As2−F11	1.7013(16)	F4−As1−F7	178.47(7)		
As2−F7	1.9062(14)	F5−As1−F7	83.96(7)		
F1−C1	1.297(3)	F2−As1−F7	85.77(7)		
O2−C3	1.117(3)	F6−As1−F7	85.19(7)		
O1−C1	1.276(3)	F3−As1−F7	86.84(7)		
C2−C3	1.364(3)	F8−As2−F9	90.46(8)		
C2−C1	1.366(3)	F8−As2−F12	90.40(9)		
		F9−As2−F12	172.04(7)		
		F8−As2−F10	93.68(8)		
		F9−As2−F10	93.21(7)		
		F12−As2−F10	94.63(7)		
		F8−As2−F11	172.38(8)		
		F9−As2−F11	89.10(8)		
		F12−As2−F11	88.99(9)		
		F10−As2−F11	93.94(8)		
		F8−As2−F7	85.19(7)		
		F9−As2−F7	85.07(7)		
		F12−As2−F7	87.11(7)		
		F10−As2−F7	177.93(6)		
		F11−As2−F7	87.19(7)		
		As2−F7−As1	146.01(8)		
		C3−C2−C1	118.2(2)		
		O2−C3−C2	178.6(3)		
		O1−C1−F1	117.7(2)		
		O1−C1−C2	122.6(2)		
		F1−C1−C2	119.7(2)		

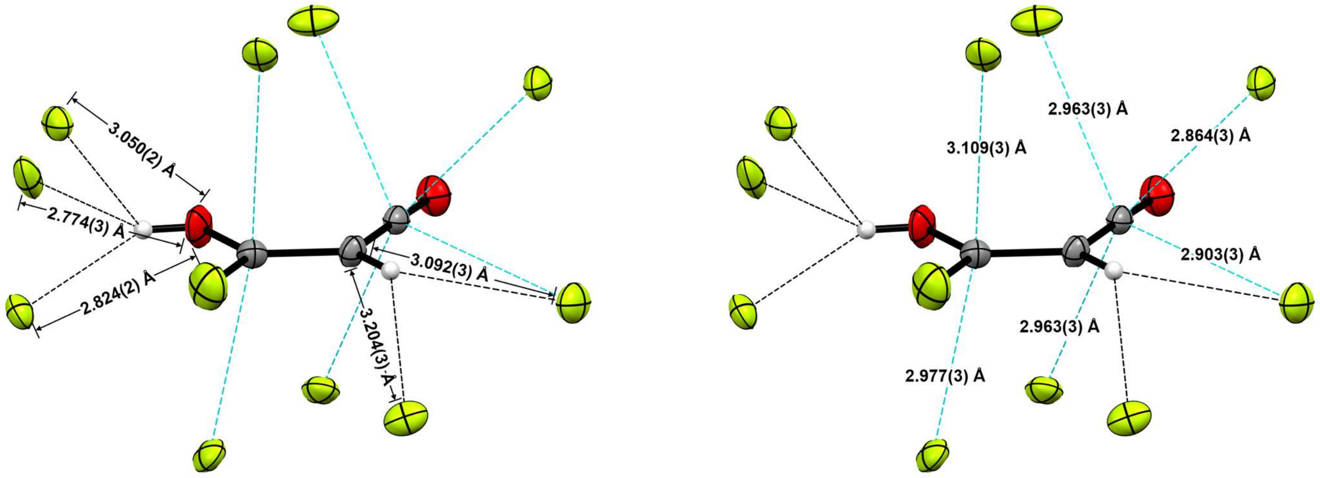

Figure S4. Selected interionic contacts of [F(HO)C=CH−CO][As$_2$F$_{11}$] with 50% probability displacement ellipsoids. The As$_2$F$_{11}^-$ anions are reduced to the contacting fluorine atoms for better visualization. The donor-acceptor distances of observed hydrogen bonds (black dashed lines) are shown on the left side and the distances of C···F contacts (blue dashed lines) below the sum of the Van der Waals radii are shown on the right side.

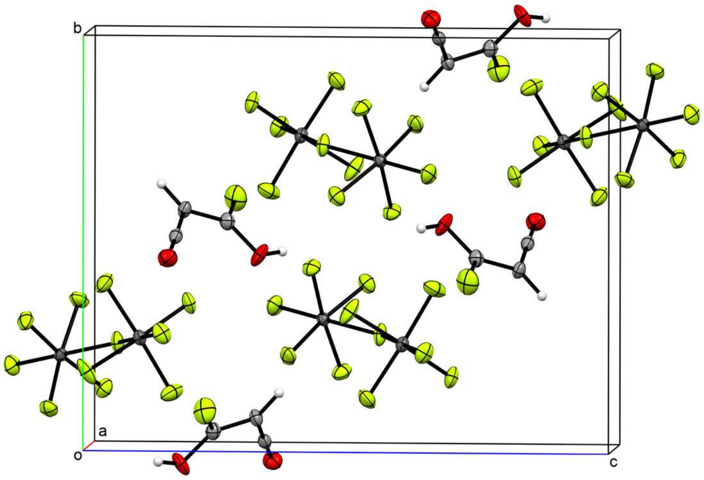

Figure S5. Crystal packing of [F(HO)C=CH−CO][As_2F_{11}] with 50% probability displacement ellipsoids.

2.4 $[C_3O_2H][Sb_2F_{11}]$

Table S5. Structural parameters of $[C_3O_2H][Sb_2F_{11}]$.

Bond lengths [Å]		Bond angles [°]	
Sb1−F1	1.8538(13)	F1−Sb1−F5	89.71(6)
Sb1−F5	1.8562(13)	F1−Sb1−F4	172.38(6)
Sb1−F4	1.8566(14)	F5−Sb1−F4	90.11(7)
Sb1−F2	1.8611(13)	F1−Sb1−F2	89.99(6)
Sb1−F3	1.8642(13)	F5−Sb1−F2	170.43(6)
Sb1−F6	2.0210(12)	F4−Sb1−F2	88.91(6)
Sb2−F9	1.8438(15)	F1−Sb1−F3	93.82(6)
Sb2−F10	1.8498(13)	F5−Sb1−F3	94.89(6)
Sb2−F7	1.8577(14)	F4−Sb1−F3	93.79(7)
Sb2−F11	1.8598(14)	F2−Sb1−F3	94.68(6)
Sb2−F8	1.8605(15)	F1−Sb1−F6	85.94(6)
Sb2−F6	2.0408(13)	F5−Sb1−F6	86.02(6)
O1−C1	1.123(3)	F4−Sb1−F6	86.44(6)
O2−C3	1.111(3)	F2−Sb1−F6	84.42(6)
C2−C3	1.352(3)	F3−Sb1−F6	179.06(6)
C2−C1	1.354(3)	F9−Sb2−F10	96.15(7)
		F9−Sb2−F7	95.80(7)
		F10−Sb2−F7	168.04(7)
		F9−Sb2−F11	95.30(8)
		F10−Sb2−F11	89.53(6)
		F7−Sb2−F11	89.57(7)
		F9−Sb2−F8	94.14(8)
		F10−Sb2−F8	90.08(7)
		F7−Sb2−F8	88.85(7)
		F11−Sb2−F8	170.54(7)
		F9−Sb2−F6	178.76(7)
		F10−Sb2−F6	83.75(6)
		F7−Sb2−F6	84.29(6)
		F11−Sb2−F6	85.93(6)
		F8−Sb2−F6	84.63(6)
		Sb1−F6−Sb2	145.53(8)
		C3−C2−C1	119.7(2)
		O1−C1−C2	177.3(3)
		O2−C3−C2	177.1(2)

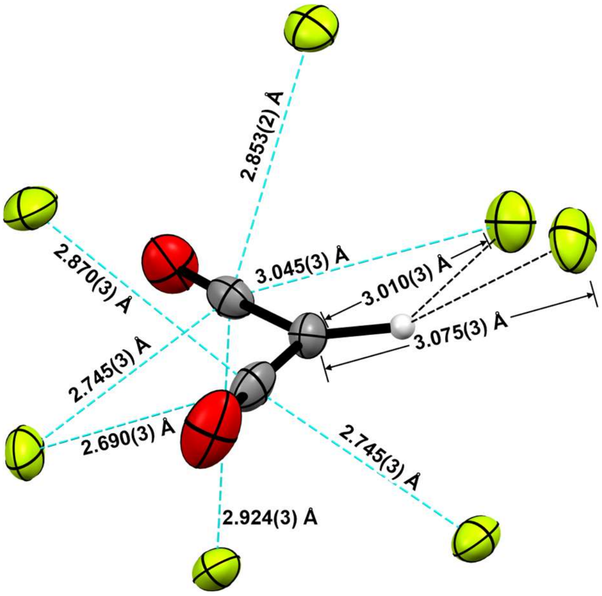

Figure S6. Selected interionic contacts of $[C_3O_2H][Sb_2F_{11}]$ with 50% probability displacement ellipsoids. The $Sb_2F_{11}^-$ anions are reduced to the contacting fluorine atoms for better visualization. The donor-acceptor distance of the hydrogen bond (black dashed line) and the distances of C···F contacts (blue dashed lines) below the sum of the Van der Waals radii are noted next to the respective contacts.

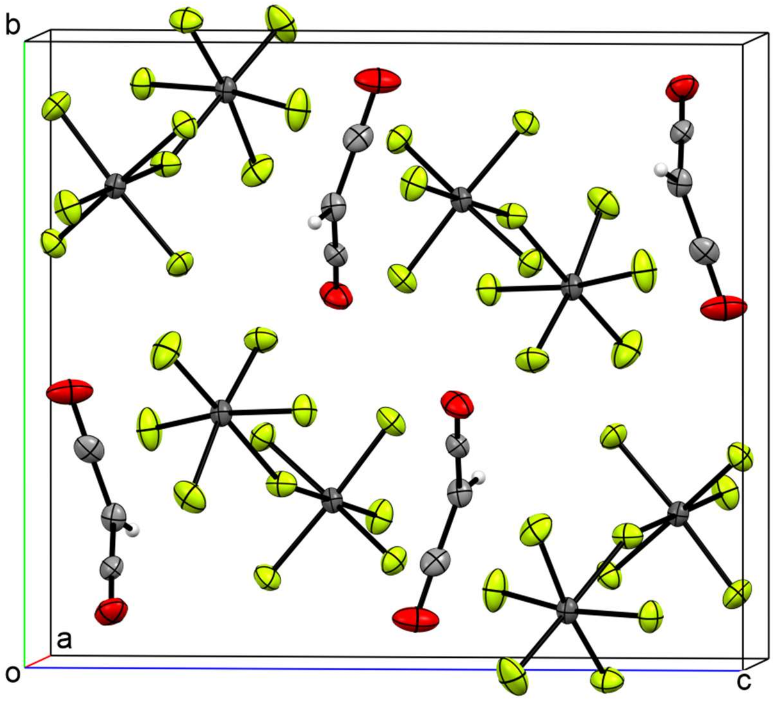

Figure S7. Crystal packing of $[C_3O_2H][Sb_2F_{11}]$ with 50% probability displacement ellipsoids.

3 Vibrational Data

3.1 $[FOC-CH_2-CO]^+$ (1)

Table S6. Experimental vibrational frequencies [cm^{-1}] of $[FOC-CH_2-CO][Sb_2F_{11}]$ and calculated vibrational frequencies [cm^{-1}] of $[FOC-CH_2-CO]^+$.

$[FOC-CH_2-CO][Sb_2F_{11}]$ exp.[a]		$[FOC-CH_2-CO]^+$ calc.[b,c]	Assignment		
IR	Raman	IR/Raman			
2922 (w)	2927 (19)	2952 (74/41)	ν_{13}	A''	ν_{as}(CH)
2864 (w)	2867 (33)	2905 (83/102)	ν_1	A'	ν_s(CH)
2328 (w)	2332 (40)	2357 (193/57)	ν_2	A'	ν(CO)
2226 (w)					Impurity **2**
2195 (w)					Impurity **3**
1850 (m)	1851 (14)	1897 (253/11)	ν_3	A'	ν(CO)
1630 (w)					Impurity **2**
1414 (w)					
1377 (w)					
1348 (m)	1349 (7)	1330 (44/7)	ν_4	A'	$\delta(CH_2)$
1310 (m)	1313 (6)	1247 (292/8)	ν_5	A'	$\omega(CH_2)$
1198 (w)	1201 (4)	1152 (118/3)	ν_6	A'	ν(CF)
1169 (m)	1171 (6)	1147 (0/2)	ν_{14}	A''	$\tau(CH_2)$
966 (w)	940 (1)	887 (21/0)	ν_{15}	A''	$\rho(CH_2)$
916 (m)	919 (3)	877 (2/2)	ν_7	A'	ν(CC)
891 (m)	894 (19)	841 (33/10)	ν_8	A'	ν(CC)
716 (vs)	712 (4)	657 (10/3)	ν_9	A'	δ(CCC)
505 (s)	518 (1)	520 (0/1)	ν_{16}	A''	γ(COF)
484 (s)	487 (15)	474 (26/4)	ν_{10}	A'	δ(CCO)
	383 (6)	381 (4/0)	ν_{17}	A''	δ(CCO)
374 (m)	372 (5)	340 (3/0)	ν_{11}	A'	δ(CCF)
		131 (7/1)	ν_{12}	A'	δ(CCC)
		63 (7/0)	ν_{18}	A''	τ(COF)
Vibrations of the anion $Sb_2F_{11}^-$					
	703 (7)				$Sb_2F_{11}^-$
687 (vs)	687 (78)				$Sb_2F_{11}^-$
	673 (4)				$Sb_2F_{11}^-$
	668 (5)				$Sb_2F_{11}^-$
	654 (100)				$Sb_2F_{11}^-$
	600 (11)				$Sb_2F_{11}^-$
598 (m)	593 (10)				$Sb_2F_{11}^-$
559 (m)	563 (2)				$Sb_2F_{11}^-$
	302 (23)				$Sb_2F_{11}^-$
	284 (6)				$Sb_2F_{11}^-$
	270 (6)				$Sb_2F_{11}^-$

[a] Abbreviations for IR intensities: vs = very strong, s = strong, m = medium, w = weak. Experimental Raman intensities are relative to a scale of 1 to 100. [b] Calculated on the M06-2X/aug-cc-pVTZ level of theory. Scaling factor: 0.956. [c] IR intensities in km/mol; Raman intensities in Å^4/u.

3.2 $[F(HO)C{=}CH{-}CO]^+$ (2)

Table S7. Experimental vibrational frequencies [cm^{-1}] of $[F(HO)C{=}CH{-}CO][Sb_2F_{11}]$ and $[F(HO)C{=}CH{-}CO][As_2F_{11}]$ and calculated vibrational frequencies [cm^{-1}] of $[F(HO)C{=}CH{-}CO]^+$.

$[F(HO)C{=}CH{-}CO][Sb_2F_{11}]$ exp.[a]	$[F(HO)C{=}CH{-}CO][As_2F_{11}]$ exp.[a]	$[F(HO)C{=}CH{-}CO]^+$ calc.[b,c]	Assignment		
Raman	Raman	IR/Raman			
		3552 (449/74)	ν_1	A'	ν(OH)
3099 (2)	3081 (11)	3085 (111/65)	ν_2	A'	ν(CH)
2295 (1)	2296 (3)				Impurity **3**
2230 (11)	2228 (92)	2276 (659/57)	ν_3	A'	ν(CO)
1634 (1)	1641 (5)	1606 (903/6)	ν_4	A'	ν(CO)
	1498 (2)				
1460 (1)	1469 (3)	1491 (314/1)	ν_5	A'	ν(CF)
1371 (1)					
1333 (3)	1338 (2)				
1231 (1)	1203 (2)	1267 (40/0)	ν_6	A'	ν(CC)
1143 (1)	1139 (2)	1115 (159/2)	ν_7	A'	δ(COH)
1063 (1)	1070 (8)	1058 (4/3)	ν_8	A'	δ(CCH)
977 (5)	974 (41)	959 (24/16)	ν_9	A'	ν(CC)
941 (10)	940 (55)				
913 (2)					
860 (1)					
741 (1)	747 (10)	744 (84/1)	ν_{14}	A''	γ(COF)
		642 (15/7)	ν_{10}	A'	δ(CCC)
602 (3)	602 (4)	612 (55/0)	ν_{15}	A''	δ(CCH)
588 (4)	586 (4)	588 (1/0)	ν_{16}	A''	δ(CCO)
560 (2)	561 (12)	495 (29/2)	ν_{11}	A'	δ(FCO)
517 (3)	517 (14)	491 (111/1)	ν_{17}	A''	δ(COH)
423 (3)	427 (15)	410 (3/2)	ν_{12}	A'	δ(CCF)
		135 (3/3)	ν_{13}	A'	δ(CCC)
		134 (0/0)	ν_{18}	A''	τ(COF)
Vibrations of the anions $Sb_2F_{11}^-$ and $As_2F_{11}^-$					
684 (24)	739 (9)				$Sb_2F_{11}^-$; $As_2F_{11}^-$
673 (100)	717 (8)				$Sb_2F_{11}^-$; $As_2F_{11}^-$
651 (23)	693 (66)				$Sb_2F_{11}^-$; $As_2F_{11}^-$
638 (10)	685 (100)				$Sb_2F_{11}^-$; $As_2F_{11}^-$
622 (3)	670 (30)				$Sb_2F_{11}^-$; $As_2F_{11}^-$
614 (4)	531 (11)				$Sb_2F_{11}^-$; $As_2F_{11}^-$
402 (1)	394 (5)				$Sb_2F_{11}^-$; $As_2F_{11}^-$
363 (1)	374 (29)				$Sb_2F_{11}^-$; $As_2F_{11}^-$
302 (15)	357 (6)				$Sb_2F_{11}^-$; $As_2F_{11}^-$
282 (9)	314 (4)				$Sb_2F_{11}^-$; $As_2F_{11}^-$
266 (4)	276 (1)				$Sb_2F_{11}^-$; $As_2F_{11}^-$

[a] The experimental Raman intensities are corrected to a scale of 1 to 100 [b] Calculated on the M06-2X/aug-cc-pVTZ level of theory. Scaling factor: 0.956. [c] IR intensities in km/mol; Raman intensities in Å^4/u.

3.3 [C_3O_2H]$^+$ (3)

Table S8. Experimental vibrational frequencies [cm^{-1}] of [C_3O_2H][Sb_2F_{11}] and impurity **4** and calculated vibrational frequencies [cm^{-1}] of [C_3O_2H]$^+$.

[C_3O_2H][Sb_2F_{11}] (**4**) exp.[a]		[C_3O_2H]$^+$ calc.[b,c]	Assignment		
IR	Raman	IR/Raman			
3020 (m)	3017 (17)	3026 (175/76)	ν_1	A_1	ν(CH)
	2970 (6)				**4**[d]
2932 (m)	2928 (5)				**4**[d]
2361 (w)					
2291 (w)	2296 (50)	2335 (114/68)	ν_2	A_1	ν_s(CO)
2191 (m)	2191 (15)	2242 (1320/26)	ν_9	B_2	ν_{as}(CO)
1811 (m)	1817 (5)				**4**[d]
1697 (m)					
1678 (m)					**4**d]
1630 (m)					
1591 (m)					
1554 (m)					
1483 (w)					**4**[d]
1369 (m)	1352 (5)	1354 (124/0)	ν_{10}	B_2	ν_{as}(CC)
1337 (w)					**4**[d]
	1317 (3)				**4**[d]
1213 (m)	1222 (3)				**4**[d]
1167 (m)	1152 (2)				**4**[d]
	1104 (3)				**4**[d]
1076 (w)	1081 (3)	1065 (3/3)	ν_{11}	B_2	δ(CCH)
	990 (18)	976 (3/13)	ν_3	A_1	ν_s(CC)
957 (w)					**4**[d]
	941 (1)				**4**[d]
928 (w)					**4**[d]
901 (w)	902 (7)				**4**[d]
851 (w)					**4**[d]
795 (w)					**4**[d]
756 (w)					**4**[d]
		651 (5/7)	ν_4	A_1	δ(CCC)
		602 (89/0)	ν_6	A_2	γ(CC(H)C)
	532 (2)	536 (0/0)	ν_7	B_1	δ(CCO)
492 (m)		450 (2/0)	ν_{12}	B_2	δ(CCO)
	422 (4)	418 (9/0)	ν_8	B_1	δ(CCH)
		145 (9/4)	ν_5	A_1	δ(CCC)
Vibrations of the anion $Sb_2F_{11}^-$					
	704 (7)				$Sb_2F_{11}^-$
	697 (13)				$Sb_2F_{11}^-$
	689 (43)				$Sb_2F_{11}^-$
	670 (28)				$Sb_2F_{11}^-$
	664 (14)				$Sb_2F_{11}^-$
658 (vs)	655 (100)				$Sb_2F_{11}^-$
	629 (4)				$Sb_2F_{11}^-$
	608 (6)				$Sb_2F_{11}^-$
588 (m)	598 (14)				$Sb_2F_{11}^-$
	388 (2)				$Sb_2F_{11}^-$
	298 (20)				$Sb_2F_{11}^-$
	285 (6)				$Sb_2F_{11}^-$
	272 (5)				$Sb_2F_{11}^-$

[a] Abbreviations for IR intensities: vs = very strong, m = medium, w = weak. Experimental Raman intensities are relative to a scale of 1 to 100. [b] Calculated on the M06-2X/aug-cc-pVTZ level of theory. Scaling factor: 0.956. [c] IR intensities in km/mol; Raman intensities in Å^4/u. [d] Impurity of the compound [$C_3H_4F_2O_4S$][Sb_2F_{11}]$_2$ (**4**).

3.4 $[C_3H_4F_2O_4S]^{2+}$ (4)

Table S9. Calculated vibrational frequencies [cm^{-1}] of $[C_3H_4F_2O_4S]^{2+}$ for the assignment of the vibrational frequencies of $[C_3H_4F_2O_4S][Sb_2F_{11}]_2$ ([**4**]$[Sb_2F_{11}]_2$).

$[C_3H_4F_2O_4S]^{2+}$ calc.[a,b] IR/Raman	Assignment		
3443 (563/71)	ν_1	A	ν(OH)
3266 (519/41)	ν_2	A	ν(OH)
2926 (63/36)	ν_3	A	ν(CH)
2897 (84/99)	ν_4	A	ν(CH)
1822 (233/10)	ν_5	A	ν(CO)
1645 (190/2)	ν_6	A	ν(CO)
1495 (390/4)	ν_7	A	ν(CF)
1326 (56/3)	ν_8	A	$\delta(CH_2)$
1316 (66/6)	ν_9	A	$\omega(CH_2)$
1185 (1/2)	ν_{10}	A	$\tau(CH_2)$
1124 (145/3)	ν_{11}	A	δ(COH)
1081 (526/5)	ν_{12}	A	ν(CO)
1052 (98/4)	ν_{13}	A	δ(SOH)
961 (240/7)	ν_{14}	A	ν(SO)
932 (31/0)	ν_{15}	A	γ(carboxyl)
927 (164/11)	ν_{16}	A	ν(SF)
914 (174/1)	ν_{17}	A	ν(CC)
890 (1/12)	ν_{18}	A	ν(CC)
820 (71/0)	ν_{19}	A	δ(COH)
781 (219/11)	ν_{20}	A	ν(SO)
730 (38/1)	ν_{21}	A	δ(OCO)
608 (1/0)	ν_{22}	A	γ(carboxyl)
581 (7/3)	ν_{23}	A	δ(FCO)
496 (12/1)	ν_{24}	A	δ(OSO)
446 (2/0)	ν_{25}	A	$\rho(CH_2)$
416 (16/1)	ν_{26}	A	δ(SOH)
375 (10/1)	ν_{27}	A	δ(CCO)
370 (11/1)	ν_{28}	A	δ(CCC)
295 (96/1)	ν_{29}	A	δ(OSO)
237 (2/2)	ν_{30}	A	δ(CCO)
224 (60/0)	ν_{31}	A	δ(CCC)
117 (26/0)	ν_{32}	A	skeletal torsion
112 (1/0)	ν_{33}	A	skeletal torsion
91 (2/0)	ν_{34}	A	δ(COS)
54 (0/0)	ν_{35}	A	skeletal torsion
44 (3/1)	ν_{36}	A	skeletal torsion

[a] Calculated on the M06-2X/aug-cc-pVTZ level of theory. Scaling factor: 0.956. [b] IR intensities in km/mol; Raman intensities in Å^4/u.

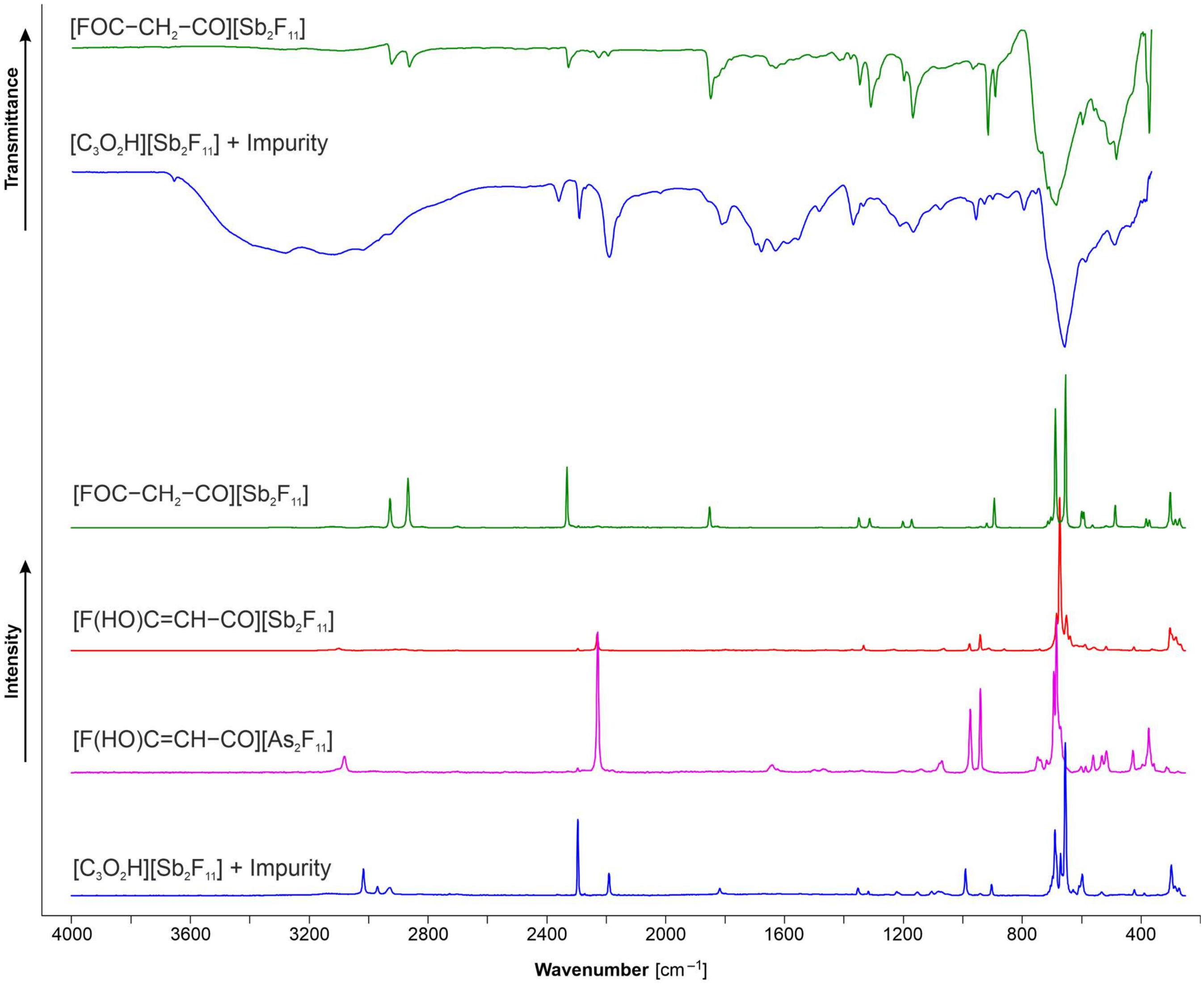

Figure S8. Low-temperature and Raman spectra of [**1**][Sb_2F_{11}], [**2**][Sb_2F_{11}], [**2**][As_2F_{11}], [**3**][Sb_2F_{11}] and low-temperature IR spectra of [**1**][Sb_2F_{11}] and [**3**][Sb_2F_{11}].

4 NMR

4.1 [FOC−CH$_2$−CO][Sb$_2$F$_{11}$]

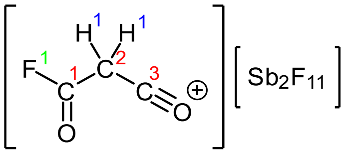

^{1}**H NMR** (400 MHz, SO$_2$) δ [ppm] = 5.96 (d, *J*=2.4 Hz, H1).
^{13}**C-{^{1}H} NMR** (101 MHz, SO$_2$) δ [ppm] = 145.14 (d, *J*=9.5 Hz, C3), 144.68 (d, *J*=357.5 Hz, C1), 30.79 (d, *J*=80.6 Hz, C2).
^{19}**F NMR** (376 MHz, SO$_2$) δ [ppm] = 51.99 (s, F1).

^{1}H NMR - [FOC−CH$_2$−CO][Sb$_2$F$_{11}$] in SO$_2$

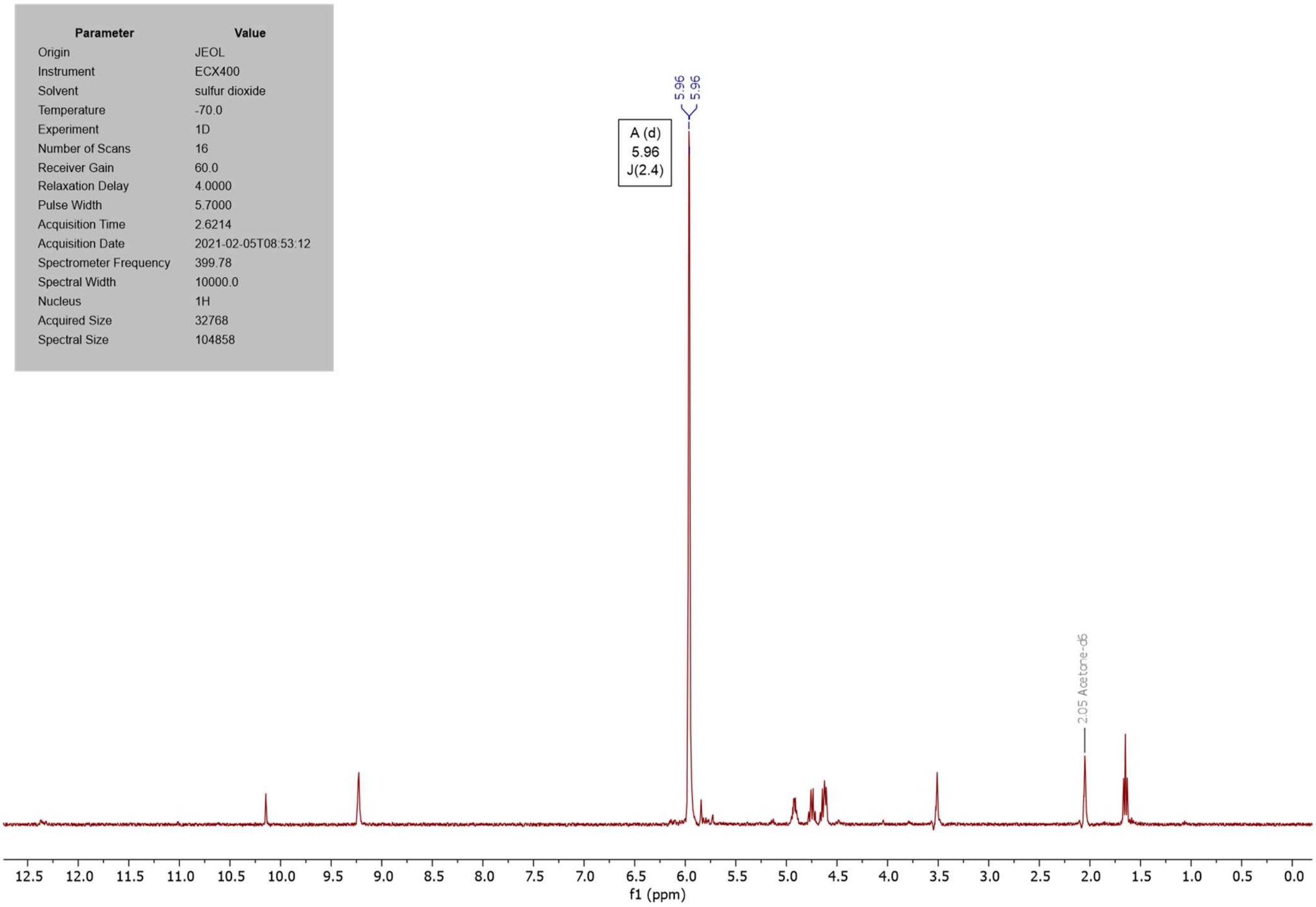

Parameter	Value
Origin	JEOL
Instrument	ECX400
Solvent	sulfur dioxide
Temperature	-70.0
Experiment	1D
Number of Scans	16
Receiver Gain	60.0
Relaxation Delay	4.0000
Pulse Width	5.7000
Acquisition Time	2.6214
Acquisition Date	2021-02-05T08:53:12
Spectrometer Frequency	399.78
Spectral Width	10000.0
Nucleus	1H
Acquired Size	32768
Spectral Size	104858

^{13}C-{^{1}H} NMR - [FOC−CH$_2$−CO][Sb$_2$F$_{11}$] in SO$_2$

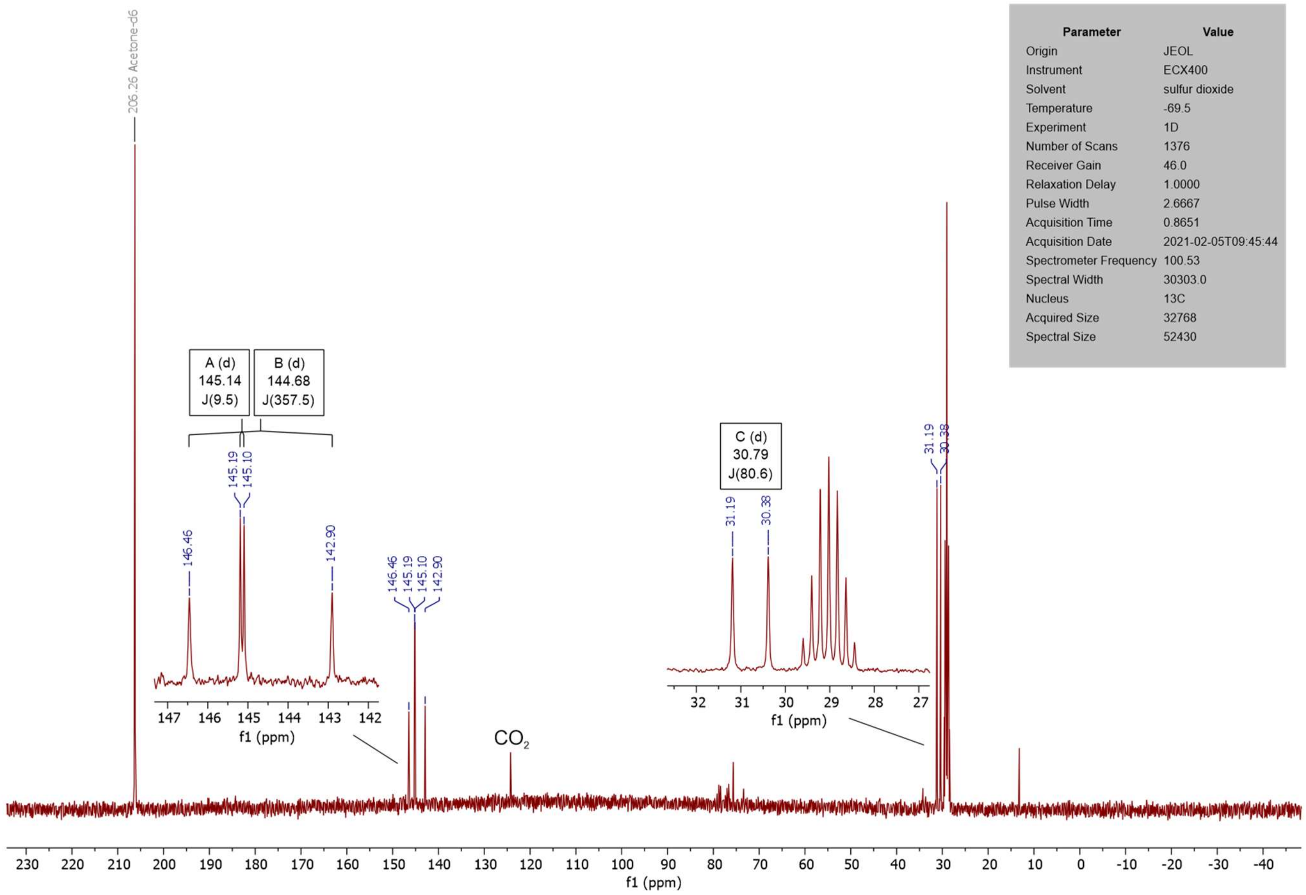

Parameter	Value
Origin	JEOL
Instrument	ECX400
Solvent	sulfur dioxide
Temperature	-69.5
Experiment	1D
Number of Scans	1376
Receiver Gain	46.0
Relaxation Delay	1.0000
Pulse Width	2.6667
Acquisition Time	0.8651
Acquisition Date	2021-02-05T09:45:44
Spectrometer Frequency	100.53
Spectral Width	30303.0
Nucleus	13C
Acquired Size	32768
Spectral Size	52430

^{19}F NMR - [FOC−CH$_2$−CO][Sb$_2$F$_{11}$] in SO$_2$

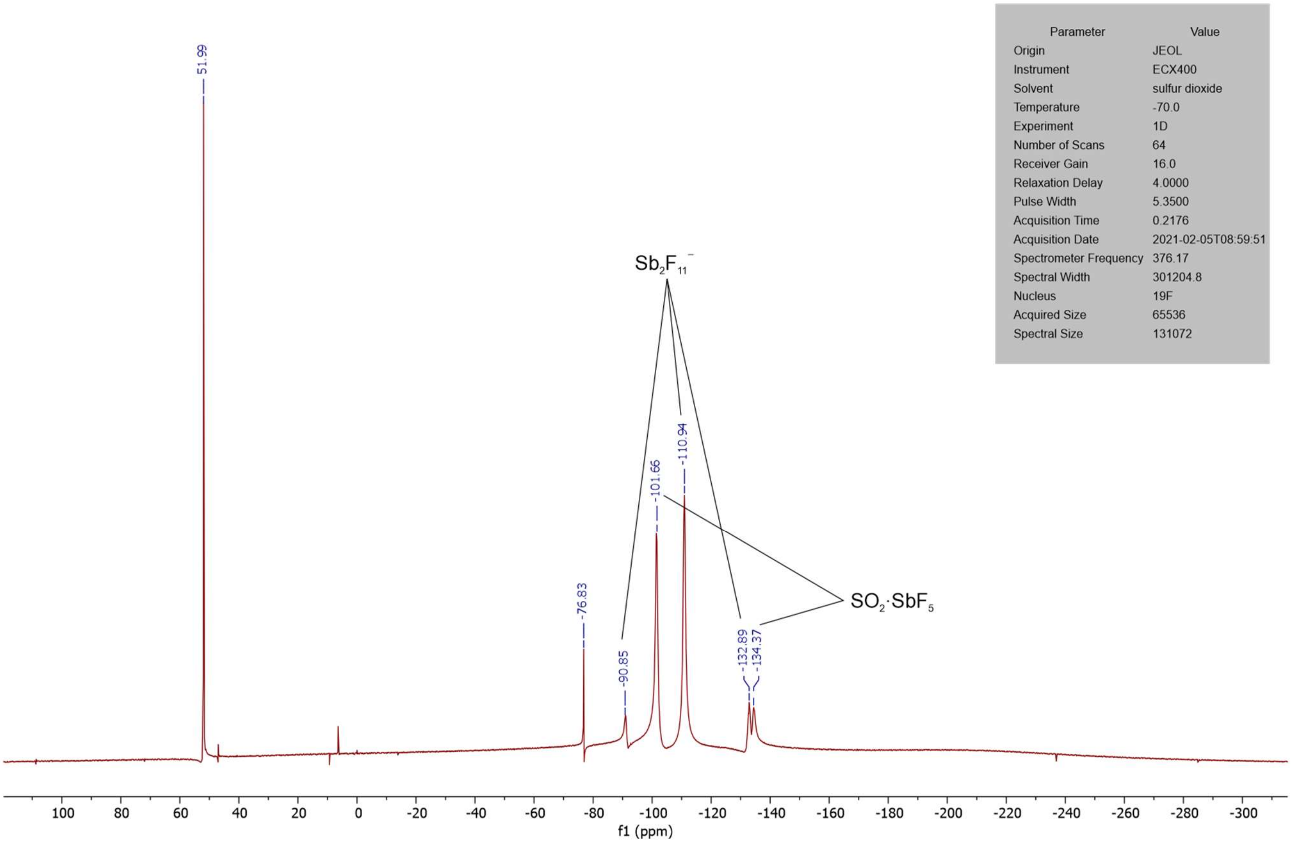

Parameter	Value
Origin	JEOL
Instrument	ECX400
Solvent	sulfur dioxide
Temperature	-70.0
Experiment	1D
Number of Scans	64
Receiver Gain	16.0
Relaxation Delay	4.0000
Pulse Width	5.3500
Acquisition Time	0.2176
Acquisition Date	2021-02-05T08:59:51
Spectrometer Frequency	376.17
Spectral Width	301204.8
Nucleus	19F
Acquired Size	65536
Spectral Size	131072

4.2 $[C_3H_4F_2O_4S][Sb_2F_{11}]$ (4)

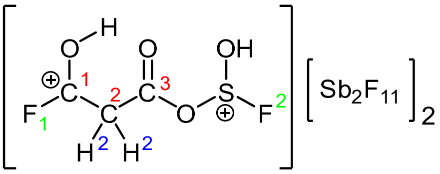

^{1}H NMR (400 MHz, SO_2) δ [ppm] = 14.52 (s), 13.18 (s), 4.68 (d, *J*=4.5 Hz, H2).
^{13}C NMR (101 MHz, SO_2) δ [ppm] = 187.13 (d, *J*=13.9 Hz, C3), 162.24 (d, *J*=355.0 Hz, C1), 34.78 (d, *J*=60.4 Hz, C2).
^{19}F NMR (376 MHz, SO_2) δ [ppm] = 72.66 (F2), 46.87 (F1).

^{1}H NMR - $[C_3H_4F_2O_4S][Sb_2F_{11}]_2$ (4) in SO_2

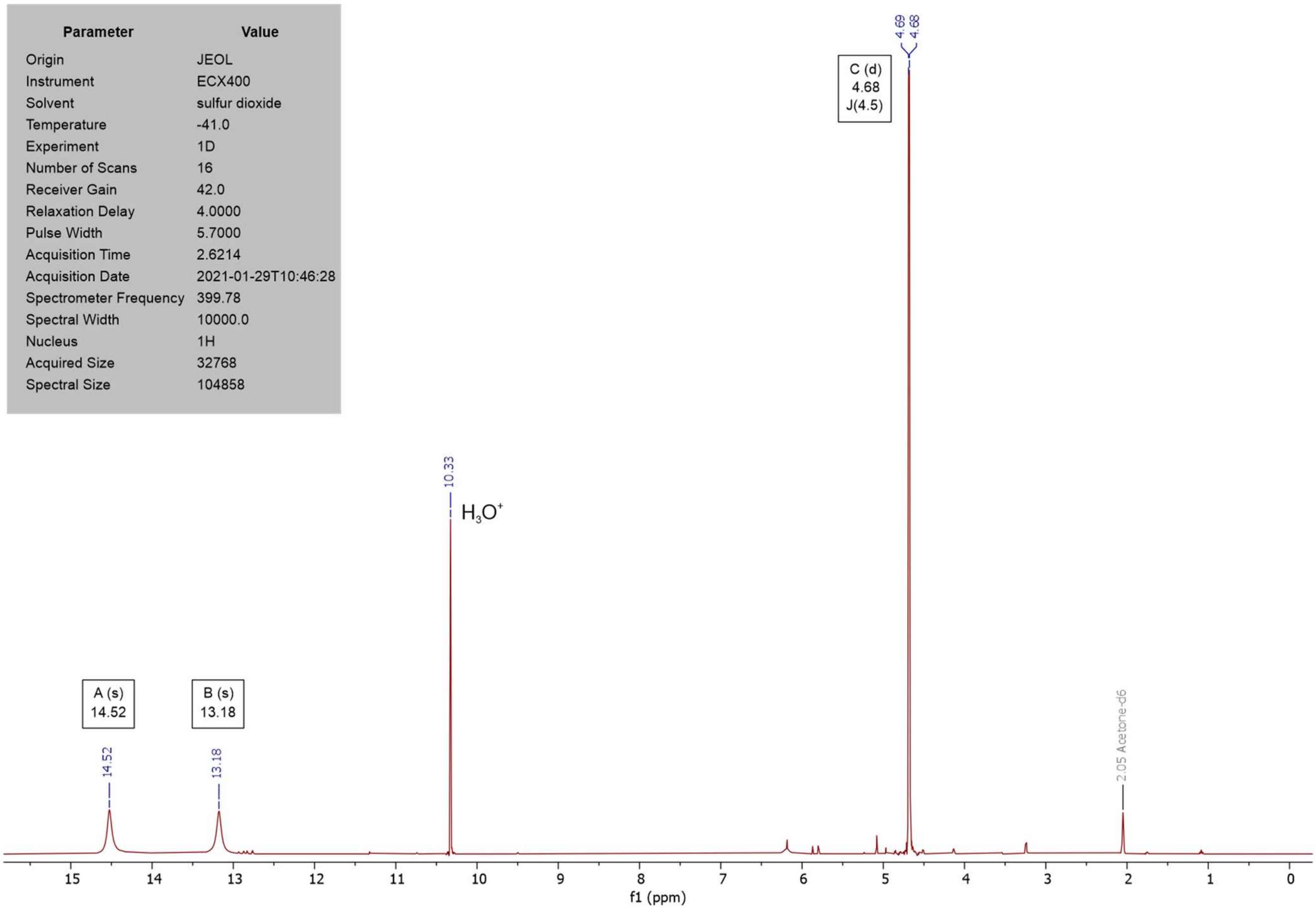

Parameter	Value
Origin	JEOL
Instrument	ECX400
Solvent	sulfur dioxide
Temperature	-41.0
Experiment	1D
Number of Scans	16
Receiver Gain	42.0
Relaxation Delay	4.0000
Pulse Width	5.7000
Acquisition Time	2.6214
Acquisition Date	2021-01-29T10:46:28
Spectrometer Frequency	399.78
Spectral Width	10000.0
Nucleus	1H
Acquired Size	32768
Spectral Size	104858

^{13}C-{^{1}H} NMR - $[C_3H_4F_2O_4S][Sb_2F_{11}]_2$ (4) in SO_2

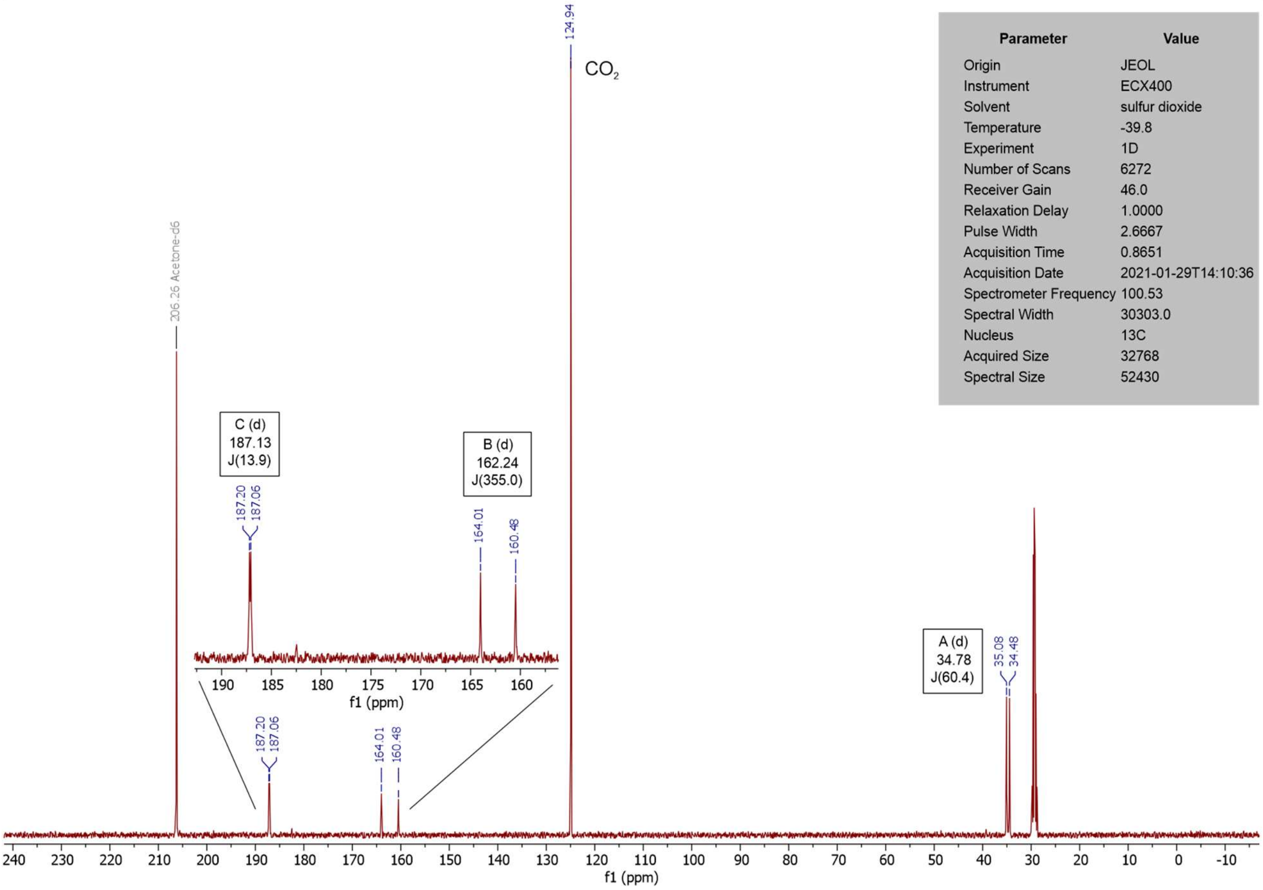

Parameter	Value
Origin	JEOL
Instrument	ECX400
Solvent	sulfur dioxide
Temperature	-39.8
Experiment	1D
Number of Scans	6272
Receiver Gain	46.0
Relaxation Delay	1.0000
Pulse Width	2.6667
Acquisition Time	0.8651
Acquisition Date	2021-01-29T14:10:36
Spectrometer Frequency	100.53
Spectral Width	30303.0
Nucleus	13C
Acquired Size	32768
Spectral Size	52430

^{19}F NMR - $[C_3H_4F_2O_4S][Sb_2F_{11}]_2$ (4) in SO_2

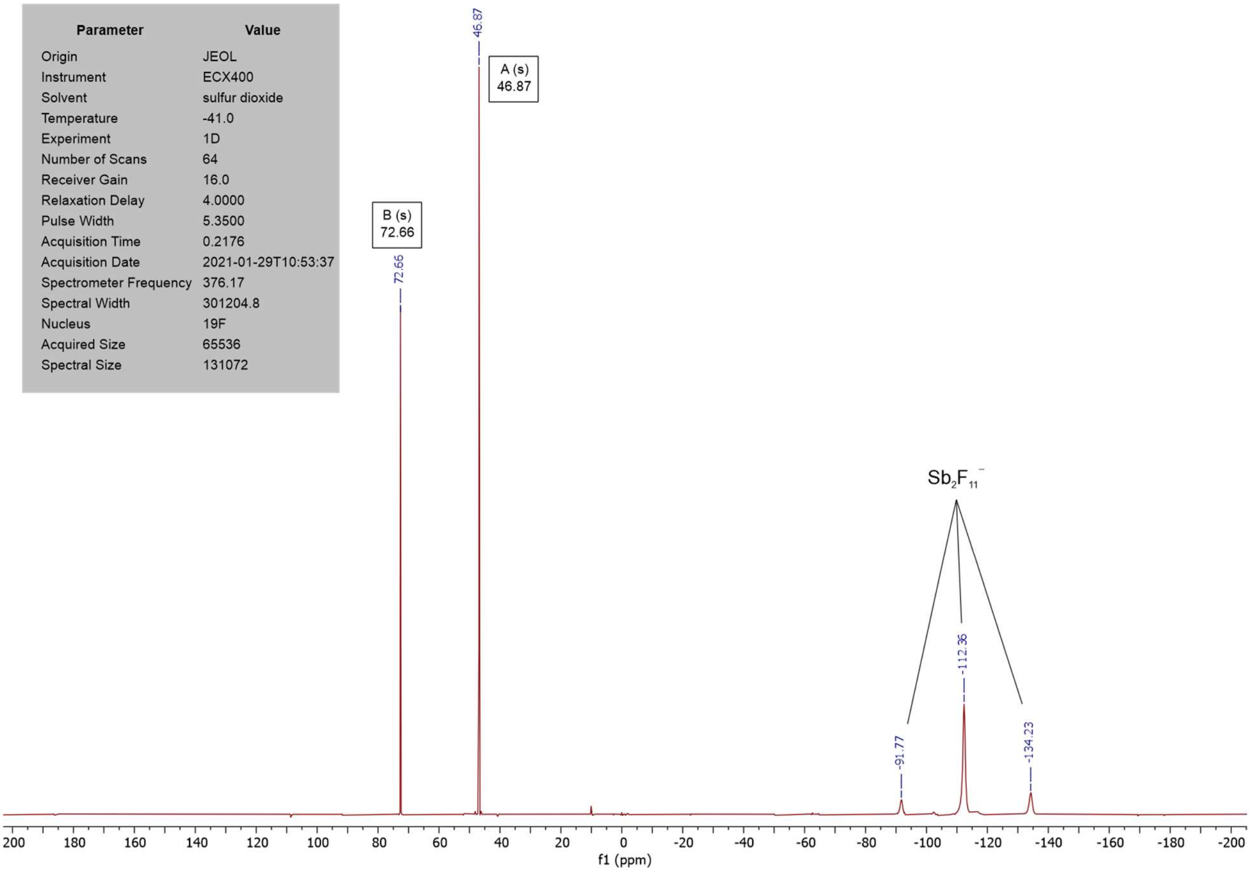

Parameter	Value
Origin	JEOL
Instrument	ECX400
Solvent	sulfur dioxide
Temperature	-41.0
Experiment	1D
Number of Scans	64
Receiver Gain	16.0
Relaxation Delay	4.0000
Pulse Width	5.3500
Acquisition Time	0.2176
Acquisition Date	2021-01-29T10:53:37
Spectrometer Frequency	376.17
Spectral Width	301204.8
Nucleus	19F
Acquired Size	65536
Spectral Size	131072

4.3 $[C_3O_2H][Sb_2F_{11}]$

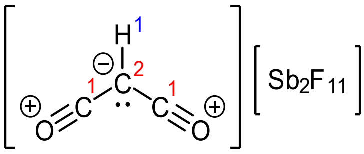

^{1}H NMR (400 MHz, SO_2) δ [ppm] = 6.17 (s, H1).
^{13}C-{^{1}H} NMR (101 MHz, SO_2) δ [ppm] = 158.91 (s, C1), 11.17 (s, C2).

^{1}H NMR - $[C_3O_2H][Sb_2F_{11}]$ (3) & $[C_3H_4F_2O_4S][Sb_2F_{11}]_2$ in SO_2

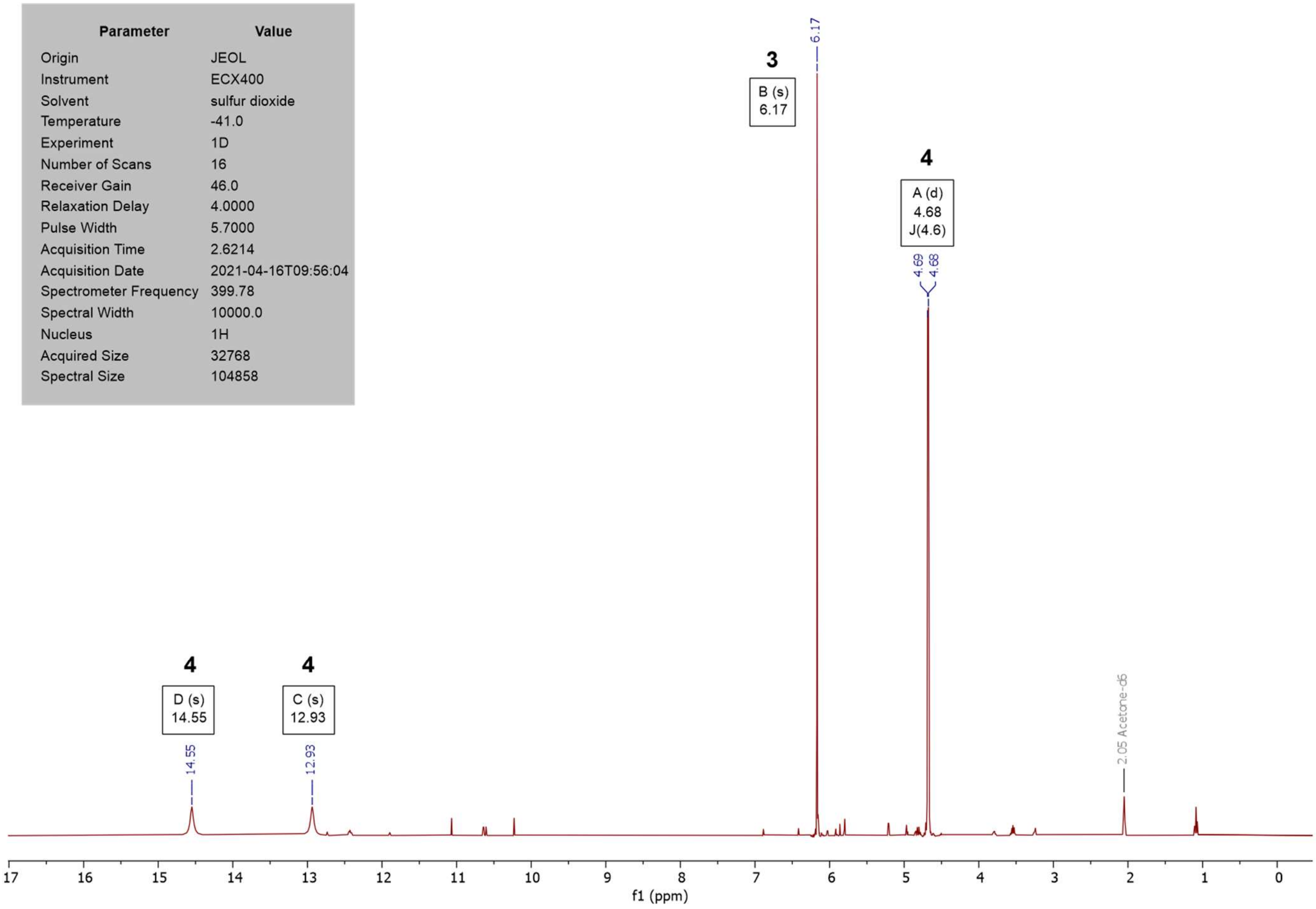

Parameter	Value
Origin	JEOL
Instrument	ECX400
Solvent	sulfur dioxide
Temperature	-41.0
Experiment	1D
Number of Scans	16
Receiver Gain	46.0
Relaxation Delay	4.0000
Pulse Width	5.7000
Acquisition Time	2.6214
Acquisition Date	2021-04-16T09:56:04
Spectrometer Frequency	399.78
Spectral Width	10000.0
Nucleus	1H
Acquired Size	32768
Spectral Size	104858

^{13}C-{^{1}H} NMR - $[C_3O_2H][Sb_2F_{11}]$ (3) & $[C_3H_4F_2O_4S][Sb_2F_{11}]_2$ (4) in SO_2

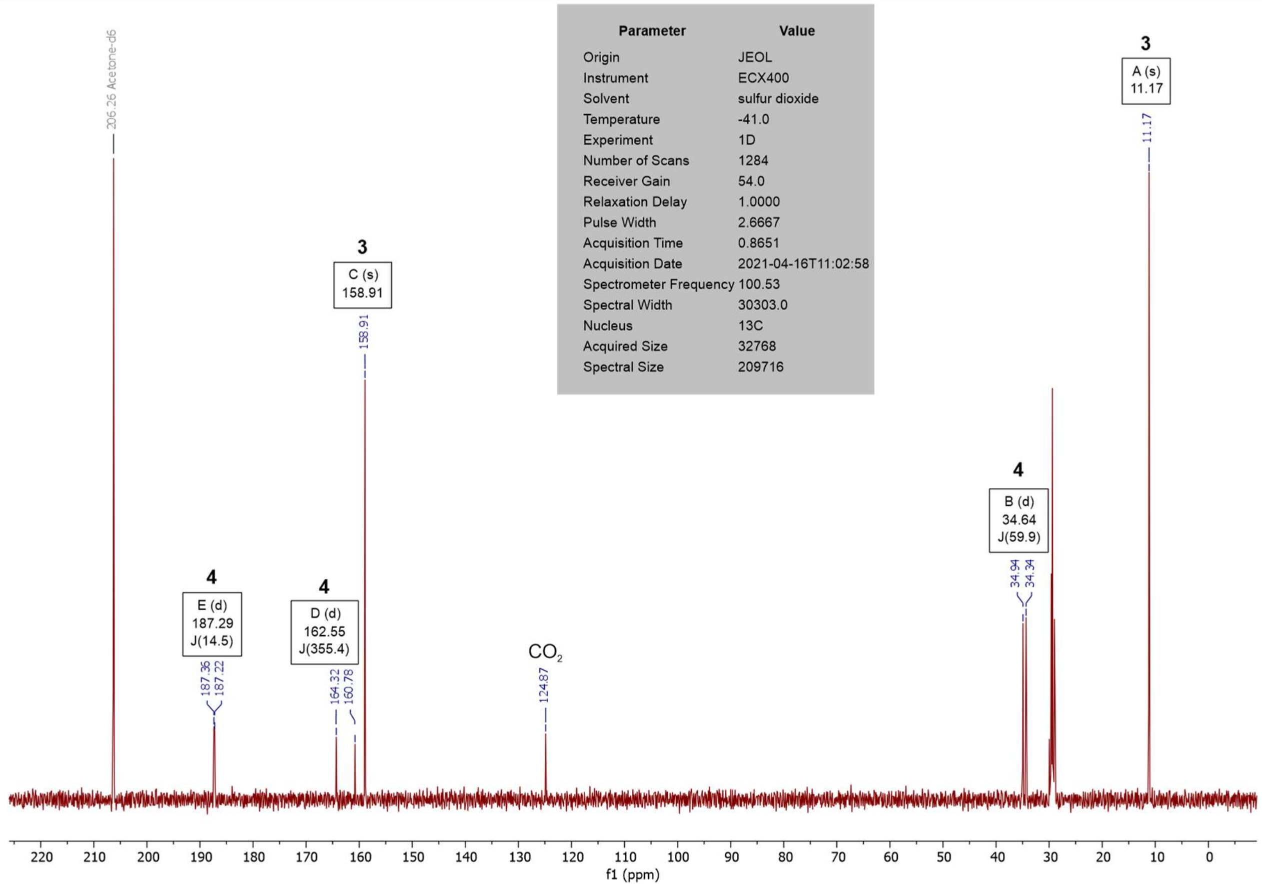

Parameter	Value
Origin	JEOL
Instrument	ECX400
Solvent	sulfur dioxide
Temperature	-41.0
Experiment	1D
Number of Scans	1284
Receiver Gain	54.0
Relaxation Delay	1.0000
Pulse Width	2.6667
Acquisition Time	0.8651
Acquisition Date	2021-04-16T11:02:58
Spectrometer Frequency	100.53
Spectral Width	30303.0
Nucleus	13C
Acquired Size	32768
Spectral Size	209716

^{13}C-{^{1}H} NMR - $[C_3O_2H][Sb_2F_{11}]$ (3) & $[C_3H_4F_2O_4S][Sb_2F_{11}]_2$ (4) in SO_2

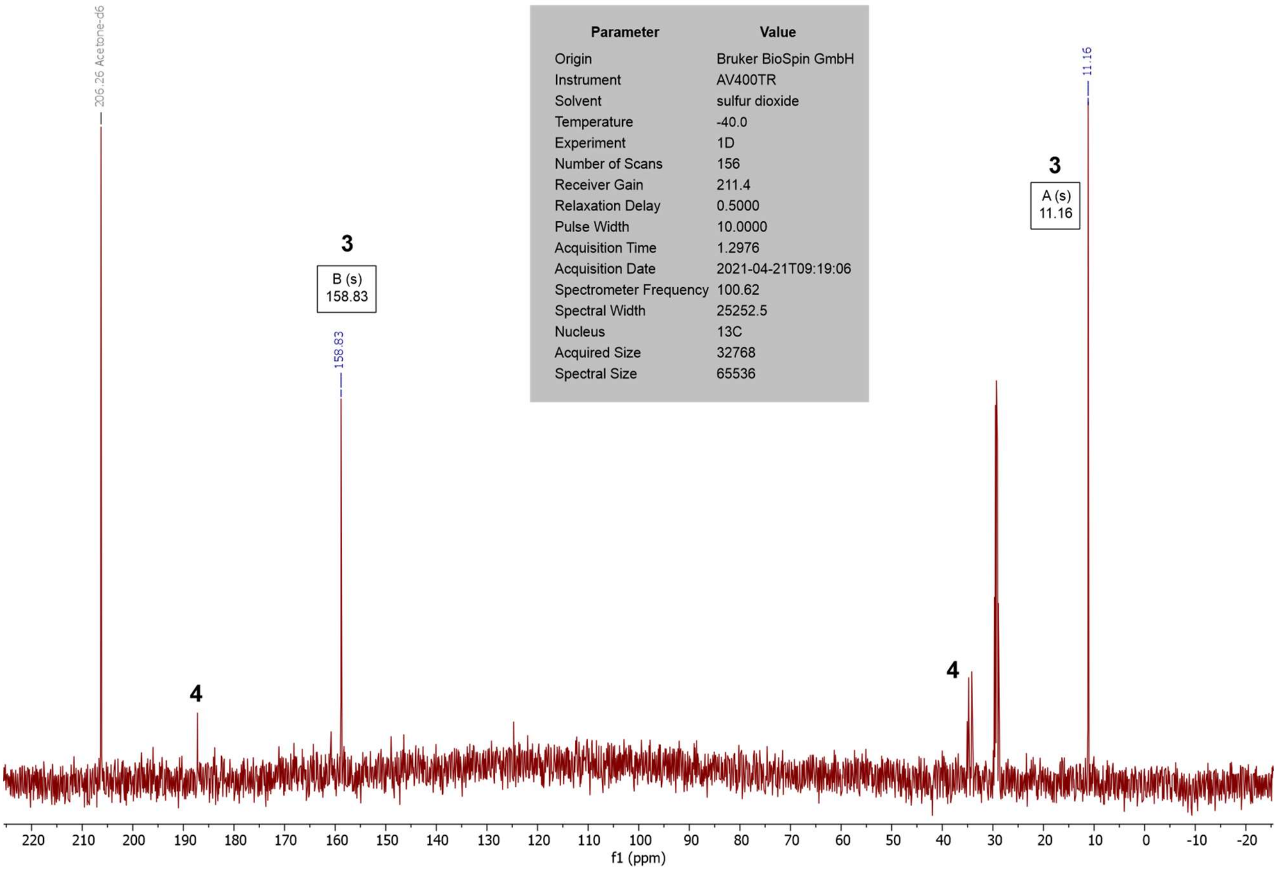

Parameter	Value
Origin	Bruker BioSpin GmbH
Instrument	AV400TR
Solvent	sulfur dioxide
Temperature	-40.0
Experiment	1D
Number of Scans	156
Receiver Gain	211.4
Relaxation Delay	0.5000
Pulse Width	10.0000
Acquisition Time	1.2976
Acquisition Date	2021-04-21T09:19:06
Spectrometer Frequency	100.62
Spectral Width	25252.5
Nucleus	13C
Acquired Size	32768
Spectral Size	65536

HSQC NMR - $[C_3O_2H][Sb_2F_{11}]$ (3) & $[C_3H_4F_2O_4S][Sb_2F_{11}]_2$ (4) in SO_2

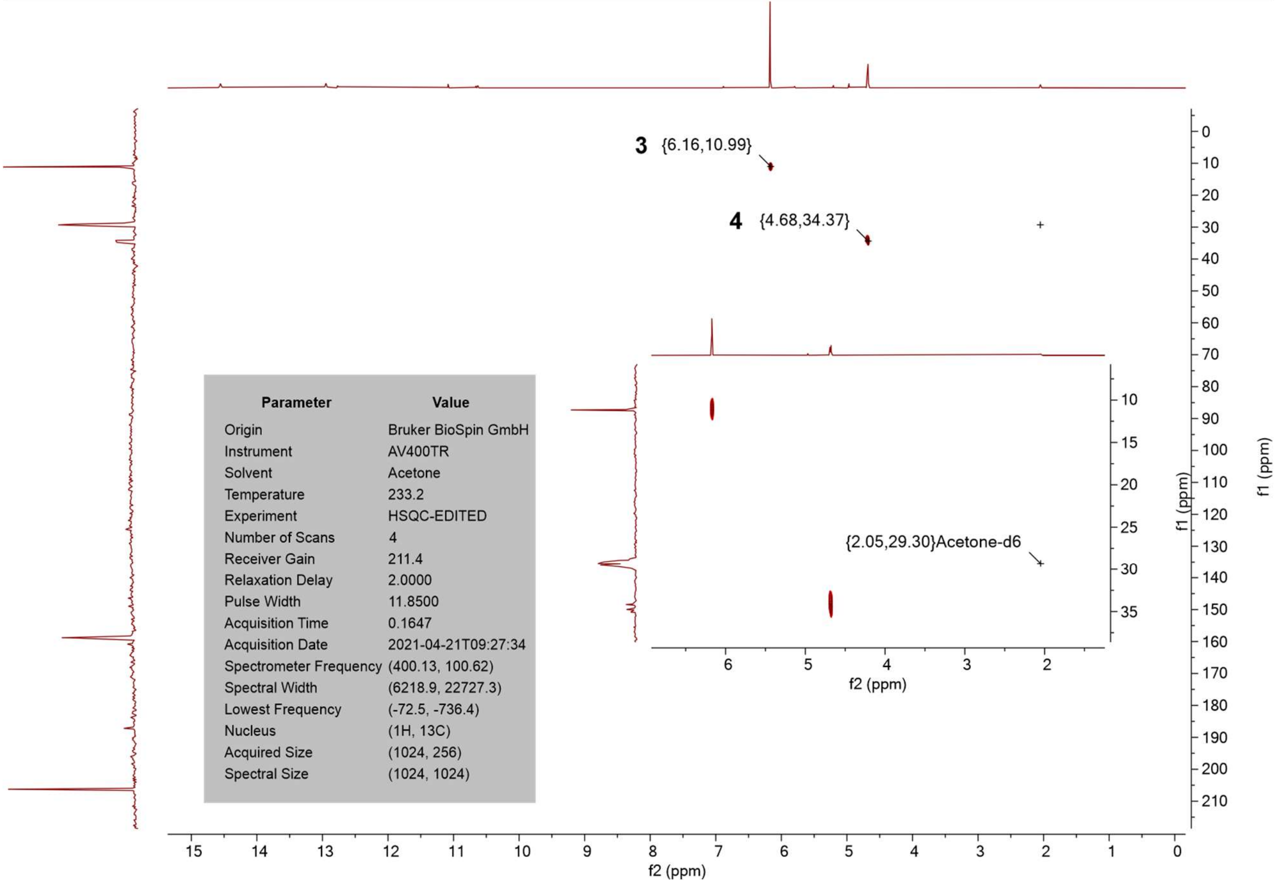

Parameter	Value
Origin	Bruker BioSpin GmbH
Instrument	AV400TR
Solvent	Acetone
Temperature	233.2
Experiment	HSQC-EDITED
Number of Scans	4
Receiver Gain	211.4
Relaxation Delay	2.0000
Pulse Width	11.8500
Acquisition Time	0.1647
Acquisition Date	2021-04-21T09:27:34
Spectrometer Frequency	(400.13, 100.62)
Spectral Width	(6218.9, 22727.3)
Lowest Frequency	(-72.5, -736.4)
Nucleus	(1H, 13C)
Acquired Size	(1024, 256)
Spectral Size	(1024, 1024)

HMBC NMR - $[C_3O_2H][Sb_2F_{11}]$ (3) & $[C_3H_4F_2O_4S][Sb_2F_{11}]_2$ (4) in SO_2

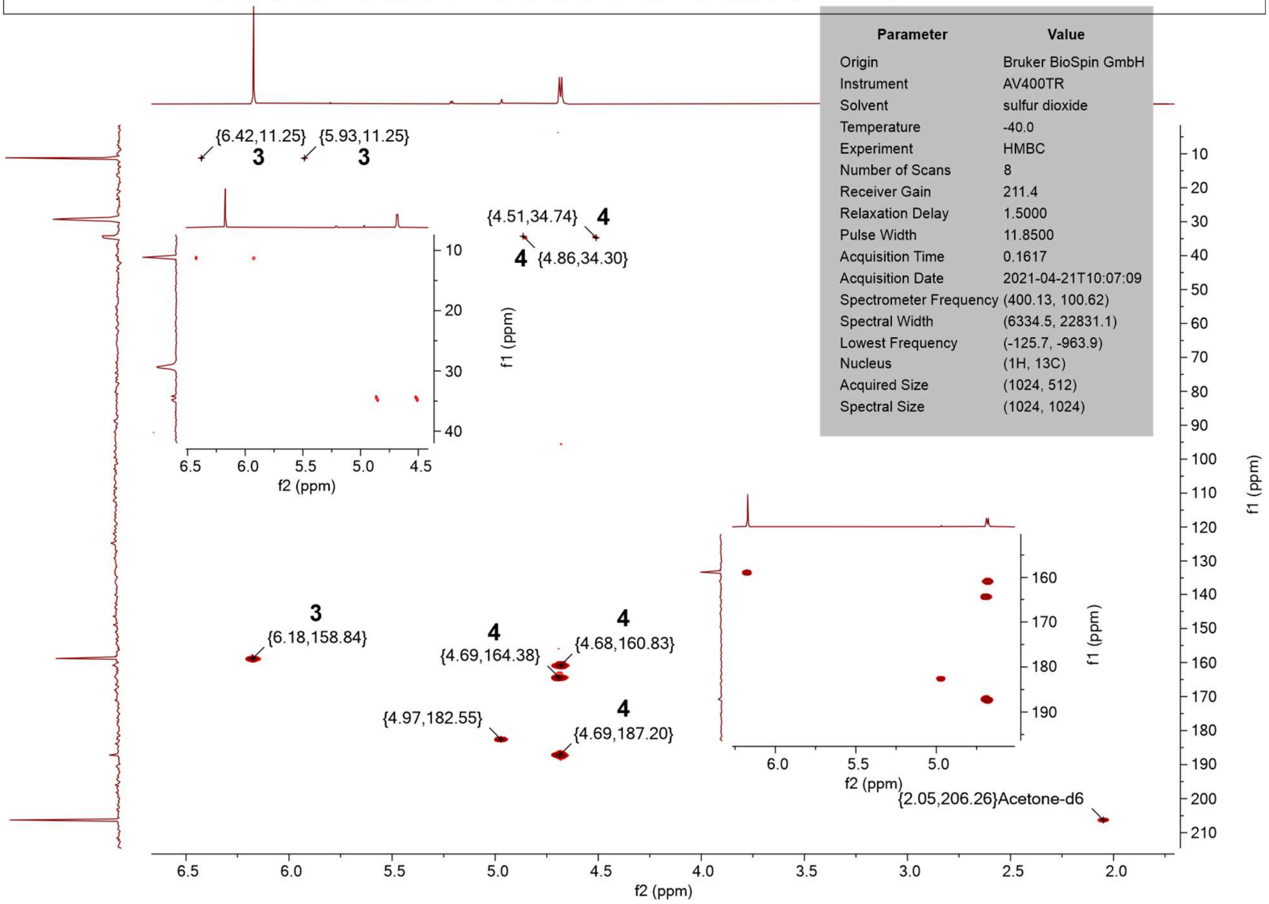

Parameter	Value
Origin	Bruker BioSpin GmbH
Instrument	AV400TR
Solvent	sulfur dioxide
Temperature	-40.0
Experiment	HMBC
Number of Scans	8
Receiver Gain	211.4
Relaxation Delay	1.5000
Pulse Width	11.8500
Acquisition Time	0.1617
Acquisition Date	2021-04-21T10:07:09
Spectrometer Frequency	(400.13, 100.62)
Spectral Width	(6334.5, 22831.1)
Lowest Frequency	(-125.7, -963.9)
Nucleus	(1H, 13C)
Acquired Size	(1024, 512)
Spectral Size	(1024, 1024)

^{19}F NMR - $[C_3O_2H][Sb_2F_{11}]$ (3) & $[C_3H_4F_2O_4S][Sb_2F_{11}]_2$ (4) in SO_2

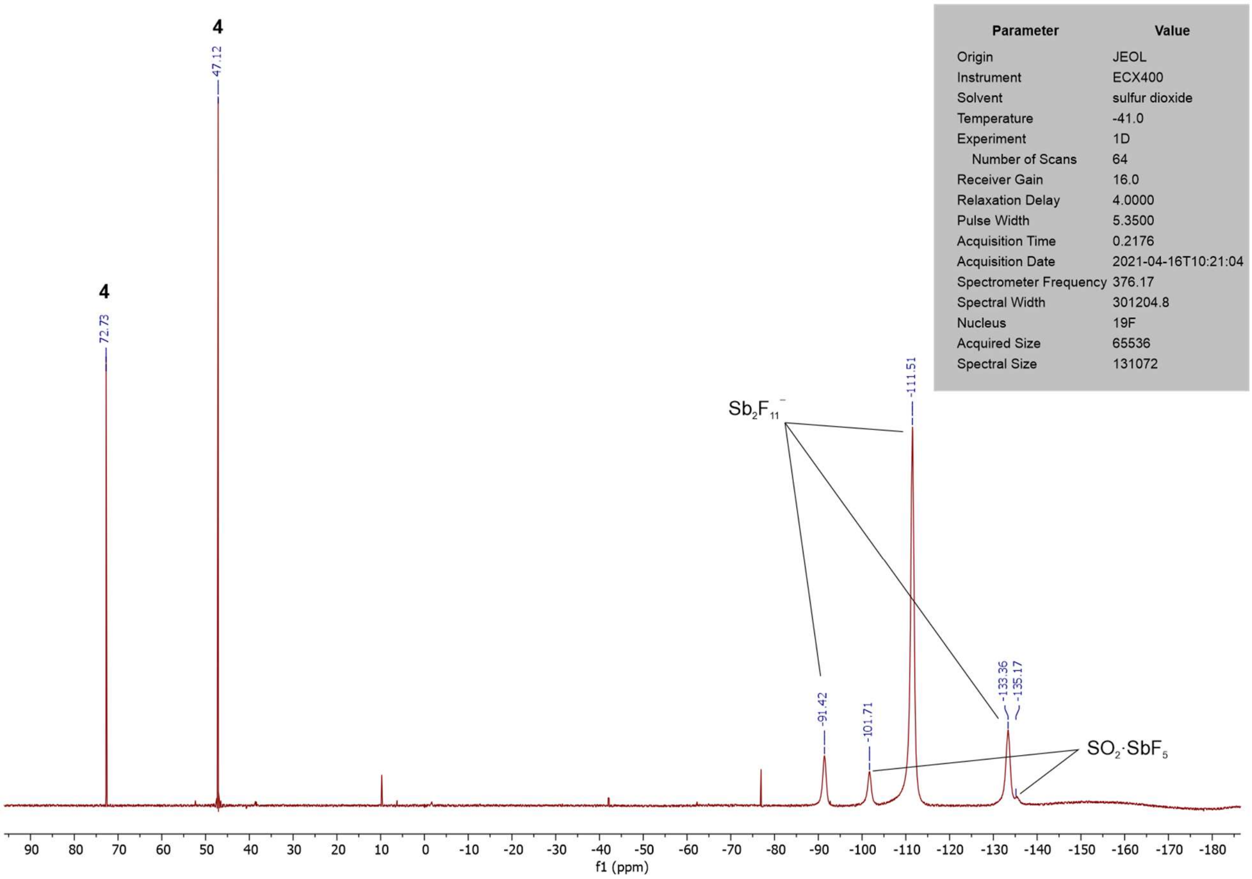

Parameter	Value
Origin	JEOL
Instrument	ECX400
Solvent	sulfur dioxide
Temperature	-41.0
Experiment	1D
Number of Scans	64
Receiver Gain	16.0
Relaxation Delay	4.0000
Pulse Width	5.3500
Acquisition Time	0.2176
Acquisition Date	2021-04-16T10:21:04
Spectrometer Frequency	376.17
Spectral Width	301204.8
Nucleus	19F
Acquired Size	65536
Spectral Size	131072

5 Quantum Chemical Calculations

The following structures were optimized on the M06-2X/aug-cc-pVTZ or MP2/aug-cc-pVTZ level of theory. Subsequent vibrational analysis confirmed the optimized geometries as true energy minimum structures with no imaginary frequencies. The optimized structures are given with their cartesian coordinates x, y, z in angstrom. An illustration of the respective structures is shown next to the tables. The NBO analysis was carried out on the MP2/aug-cc-pVTZ level of theory.

M06-2X/aug-cc-pVTZ level of theory

[FOC−CH$_2$−CO]$^+$

Energy (M06-2x/aug-cc-pVTZ): −365.485663288 Hartree

C	1.462741	-0.268750	0.000001	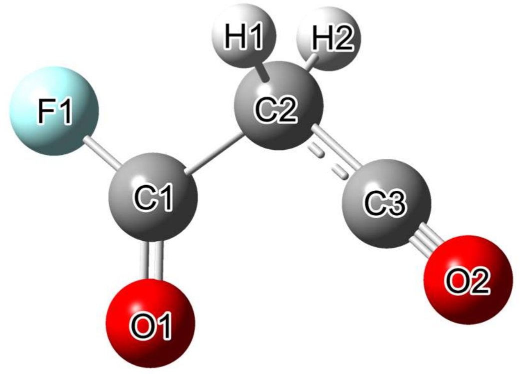
C	0.174417	-0.922144	0.000003	
C	-0.906359	0.183724	-0.000000	
F	-2.080954	-0.381299	0.000002	
O	2.441854	0.242605	-0.000001	
O	-0.676985	1.330838	-0.000004	
H	0.112422	-1.556418	-0.892851	
H	0.112423	-1.556412	0.892861	

[F(HO)C=CH−CO]$^+$

Energy (M06-2x/aug-cc-pVTZ): −365.507033639 Hartree

F	2.003258	-0.564907	0.000056	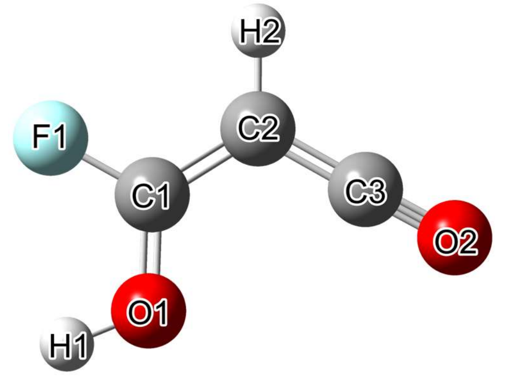
O	-2.525087	0.219962	-0.000006	
O	0.792377	1.259357	-0.000185	
C	0.840192	-0.020219	-0.000005	
C	-1.505000	-0.242086	0.000051	
C	-0.273787	-0.826778	0.000122	
H	-0.202923	-1.905456	0.000270	
H	1.666856	1.689558	-0.000257	

[C$_3$O$_2$H]$^+$

Energy (M06-2x/aug-cc-pVTZ): −265.017897733 Hartree

C	6	-0.074773	1.175441	0.000000	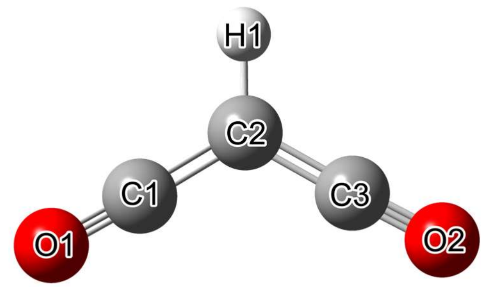
O	8	0.455356	2.161147	0.000000	
C	6	-0.757434	-0.000000	0.000000	
H	1	-1.843815	-0.000000	0.000000	
C	6	-0.074773	-1.175441	0.000000	
O	8	0.455356	-2.161147	0.000000	

$[C_3H_4F_2O_4S]^+$

Energy (M06-2x/aug-cc-pVTZ): −1014.75923714 Hartree

F	3.818957	-0.830973	0.267554	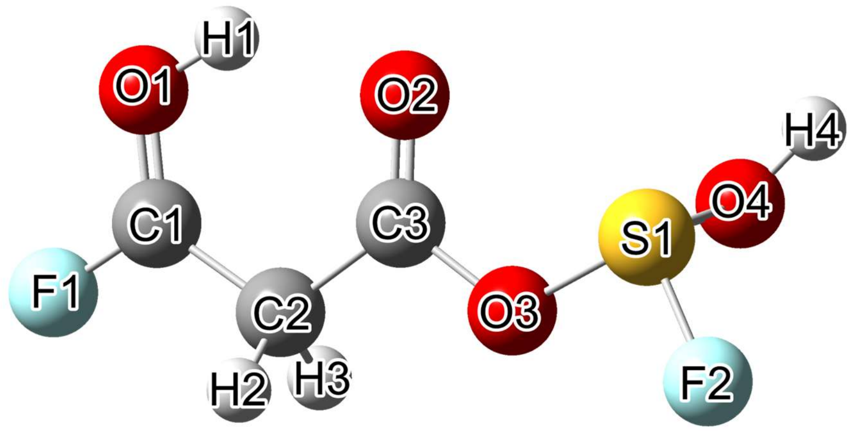
C	2.806473	-0.119602	0.048081	
C	0.317741	0.094083	-0.098405	
O	-0.874203	-0.597736	0.031373	
C	1.489030	-0.812583	0.174481	
H	1.426933	-1.243445	1.183287	
H	1.490875	-1.673755	-0.507483	
S	-2.251611	0.161293	-0.333737	
O	0.355882	1.246018	-0.381719	
F	-3.075561	-1.119048	-0.309770	
O	-2.540836	0.758785	1.051854	
H	-3.150803	1.530319	1.068363	
O	3.019917	1.065820	-0.246034	
H	2.202660	1.601902	-0.413176	

MP2/aug-cc-pVTZ level of theory

[F(HO)C=CH−CO]$^+$

Energy (MP2/aug-cc-pVTZ): −364.954121 Hartree

F	-0.000029258	0.000006048	0.000002138
O	0.000038941	-0.000015314	-0.000000207
O	-0.000009016	-0.000013453	0.000001118
C	0.000053274	0.000018907	-0.000006436
C	-0.000059706	0.000039773	0.000000801
C	0.000007238	-0.000041911	0.000001701
H	0.000004275	0.000007469	0.000000053
H	-0.000005748	-0.000001519	0.000000833

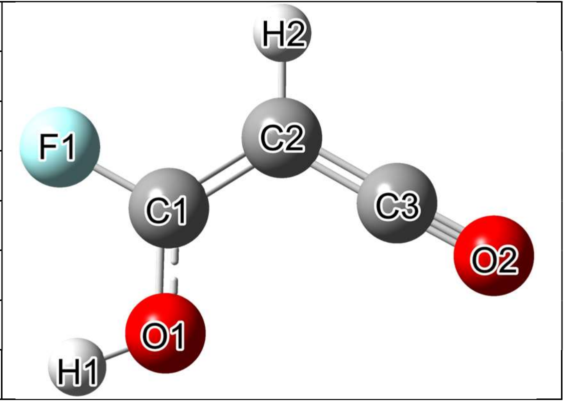

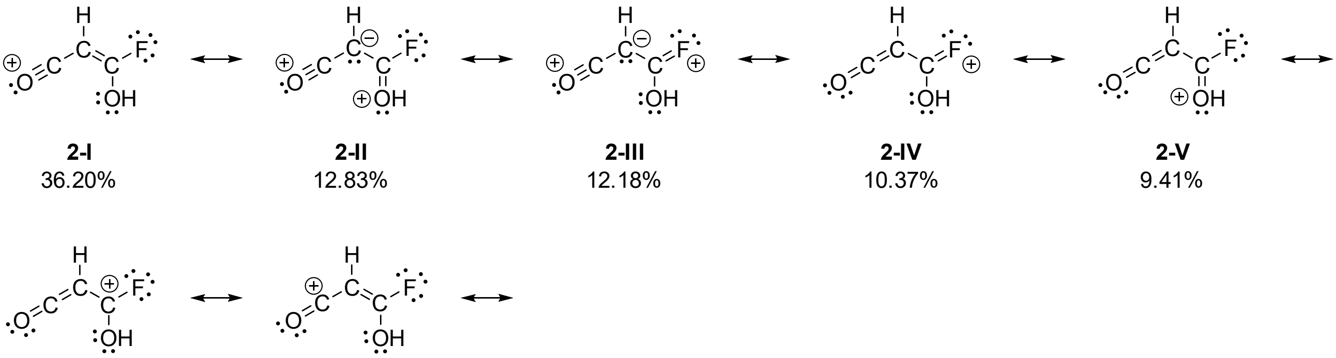

2-I
36.20%

2-II
12.83%

2-III
12.18%

2-IV
10.37%

2-V
9.41%

2-VI
7.13%

2-VII
5.09%

other[a]
6.79%

Figure S9. Lewis resonance structures of the NRT analysis of [F(HO)C=CH−CO]$^+$ along with their respective weightings. The remark [a] corresponds to the sum of other Lewis resonance structures with weightings over 5%.

$[C_3O_2H]^+$

Energy (MP2/aug-cc-pVTZ): −264.590447 Hartree

C	1.177821	0.077777	0.000000
O	2.182848	-0.459298	0.000000
C	-0.000000	0.761527	0.000000
H	0.000004	1.846264	0.000000
C	-1.177821	0.077778	0.000000
O	-2.182848	-0.459296	0.000000

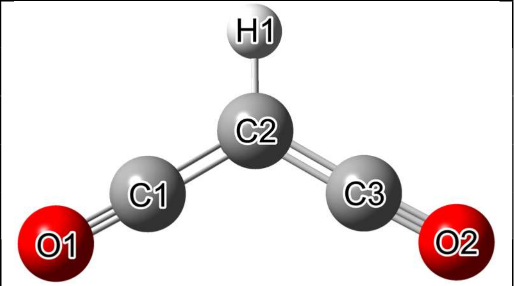

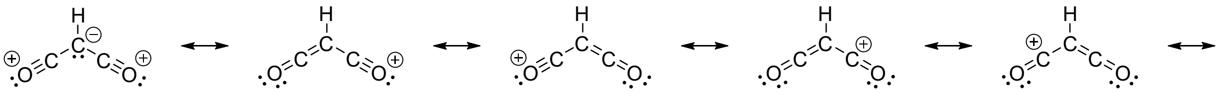

3-I	3-II	3-III	3-IV	3-V	other[a]
28.72%	27.52%	27.52%	5.94%	5.94%	4.36%

Figure S9. Lewis resonance structures of the NRT analysis of $[C_3H_2H]^+$ along with their respective weightings. The remark [a] corresponds to the sum of other Lewis resonance structures with weightings over 5%.

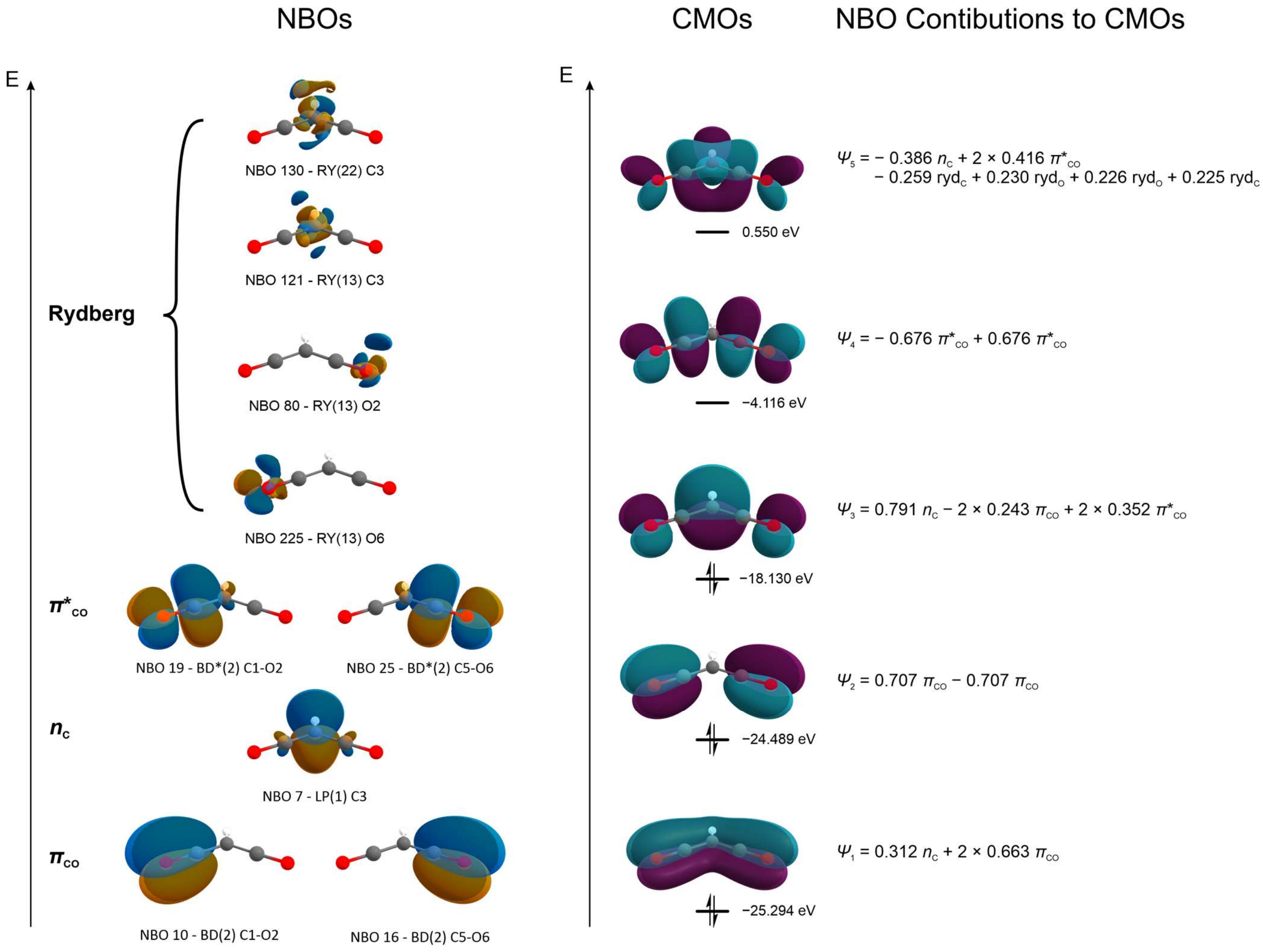

Figure S10. Selected natural bond orbitals (NBOs), canonical molecular orbitals (CMOs) of $C_3O_2H^+$, and NBO contributions to the respective CMOs. The designation of the NBOs corresponds to Table S10 from the NBO analysis. The occupancies and energies are given below the CMOs, respectively.

Table S10. Excerpt of the NBO analysis of $C_3O_2H^+$.

NATURAL BOND ORBITALS (Summary):

	NBO		Occupancy	Energy	Principal Delocalizations (geminal,vicinal,remote)
Molecular unit 1 (C3HO2)					
------ Lewis ---					
1	CR(1)	C1	1.99939	-11.55547	70(v), 111(v), 23(v)
2	CR(1)	O2	1.99974	-20.61457	27(v), 21(v)
3	CR(1)	C3	1.99869	-11.40927	18(v), 24(v), 27(v), 172(v) 150(v)
4	CR(1)	C5	1.99939	-11.55547	215(v), 111(v), 21(v)
5	CR(1)	O6	1.99974	-20.61457	172(v), 23(v)
6	LP(1)	O2	1.98227	-1.29534	27(v), 21(v)
7	LP(1)	C3	1.44525	-0.48082	19(v), 25(v), 120(g), 28(v) 173(v), 125(g), 32(v), 177(v) 68(r), 213(r), 76(r), 221(r) 185(v), 127(g), 152(v)
8	LP(1)	O6	1.98227	-1.29534	172(v), 23(v)
9	BD(1)	C1-O2	1.99858	-1.84454	21(g), 27(g), 112(v)
10	BD(2)	C1-O2	1.99634	-0.89701	109(v), 19(g)
11	BD(3)	C1-O2	1.99320	-0.88195	23(v), 22(v), 111(v), 110(v)
12	BD(1)	C1-C3	1.98544	-1.33118	24(v), 69(v), 26(v), 175(v) 18(g), 22(g), 151(v), 174(v) 23(g), 172(v), 159(v), 27(g) 30(g)
13	BD(1)	C3-H4	1.94520	-0.99304	20(v), 26(v), 18(v), 24(v) 175(v), 30(v), 29(v), 174(v) 23(g), 21(g), 116(g), 151(g) 27(v), 172(v), 22(g), 159(g) 181(v), 36(v), 211(v), 112(g) 128(g)
14	BD(1)	C3-C5	1.98544	-1.33119	18(v), 214(v), 20(v), 30(v) 24(g), 22(g), 151(v), 29(v) 21(g), 27(v), 159(v), 172(g) 175(g)
15	BD(1)	C5-O6	1.99858	-1.84454	23(g), 172(g), 112(v)
16	BD(2)	C5-O6	1.99634	-0.89701	109(v), 25(g)
17	BD(3)	C5-O6	1.99320	-0.88195	21(v), 22(v), 111(v), 110(v)
------ non-Lewis --					
18	BD*(1)	C1-O2	0.00738	0.77316	
19	BD*(2)	C1-O2	0.27128	-0.0851	
20	BD*(3)	C1-O2	0.02772	-0.03506	
21	BD*(1)	C1-C3	0.01202	0.56345	
22	BD*(1)	C3-H4	0.00779	0.37506	
23	BD*(1)	C3-C5	0.01202	0.56346	
24	BD*(1)	C5-O6	0.00738	0.77316	
25	BD*(2)	C5-O6	0.27128	-0.0851	
26	BD*(3)	C5-O6	0.02772	-0.03506	
.					
80	RY(13)	O2	0.00000	0.96795	
.					
121	RY(13)	C3	0.00000	1.91202	
.					
130	RY(22)	C3	0.00000	2.09312	
.					
225	RY(13)	O6	0.00000	0.81677	
.					

	Total Lewis		33.29907	(97.9385%)	
	Valence non-Lewis		0.64461	(1.8959%)	
	Rydberg non-Lewis		0.05631	(0.1656%)	

	Total unit 1		34.00000	(100.0000%)	
	Charge unit 1		1.00000		

6 References

[1] L. Bayersdorfer, R. Minkwitz, J. Jander, *Z. Anorg. Allg. Chem.* **1972**, *392*, 137.

[2] Rigaku Oxford Diffraction, CrysAlisPro Software System, *Version 1.171.39.46e*, Rigaku Corporation,Oxford, UK, **2018**.

[3] G. M. Sheldrick, *Acta Crystallogr., Sect. A: Found. Adv.* **2015**, *71*, 3.

[4] G. M. Sheldrick, *Acta Crystallogr., Sect. C: Struct. Chem.* **2015**, *71*, 3.

[5] L. J. Farrugia, *J. Appl. Crystallogr.* **1999**, *32*, 837.

[6] A. L. Spek, *J. Appl. Crystallogr.* **2003**, *36*, 7.

[7] *SCALE3 ABSPACK, An Oxford Diffraction Program*, Oxford Diffraction Ltd, UK, **2005**.

[8] C. F. Macrae, I. Sovago, S. J. Cottrell, P. T. A. Galek, P. McCabe, E. Pidcock, M. Platings, G. P. Shields, J. S. Stevens, M. Towler et al., *J. Appl. Crystallogr.* **2020**, *53*, 226.

[9] Mestrelab Research S.L., *MestReNova Version 14.0.0*, **2019**.

[10] M. J. Frisch, G. W. Trucks, H. B. Schlegel, G. E. Scuseria, M. A. Robb, J. R. Cheeseman, G. Scalmani, V. Barone, B. Mennucci, G. A. Petersson, H. Nakatsuji, M. Caricato, X. Li, H. P. Hratchian, A. F. Izmaylov, J. Bloino, G. Zheng, J. L. Sonnenberg, M. Hada, M. Ehara, K. Toyota, R. Fukuda, J. Hasegawa, M. Ishida, T. Nakajima, Y. Honda, O. Kitao, H. Nakai, T. Vreven, J. A. Montgomery, J. E. Peralta, F. Ogliaro, M. Bearpark, J. J. Heyd, E. Brothers, K. N. Kudin, V. N. Staroverov, R. Kobayashi, J. Normand, K. Raghavachari, A. Rendell, J. C. Burant, S. S. Iyengar, J. Tomasi, M. Cossi, N. Rega, J. M. Millam, M. Klene, J. E. Knox, J. B. Cross, V. Bakken, C. Adamo, J. Jaramillo, R. Gomperts, R. E. Stratmann, O. Yazyev, A. J. Austin, R. Cammi, C. Pomelli, J. W. Ochterski, R. L. Martin, K. Morokuma, V. G. Zakrzewski, G. A. Voth, P. Salvador, J. J. Dannenberg, S. Dapprich, A. D. Daniels, O. Farkas, J. B. Foresman, J. V. Ortiz, J. Cioslowski, D. J. Fox, *Gaussian09, Revision A.02*, Gaussian, Inc, Wallingford CT, **2009**.

[11] M. J. Frisch, G. W. Trucks, H. B. Schlegel, G. E. Scuseria, M. A. Robb, J. R. Cheeseman, G. Scalmani, V. Barone, G. A. Petersson, H. Nakatsuji et al., *Gaussian16 Revision C.01*, **2016**.

[12] Roy Dennington, Todd A. Keith, John M. Millam, *GaussView Version 6*, **2019**.

[13] E. D. Glendening, C. R. Landis, F. Weinhold, *J. Comput. Chem.* **2013**, *34*, 1429.

[14] E. D. Glendening, C. R. Landis, F. Weinhold, *J. Comput. Chem.* **2013**, *34*, 2134.

[15] G. A. Zhurko, *Chemcraft - graphical program for visualization of quantum chemistry computations. Version: 1.8*, Russia, **2005**.

[16] A. Jin, H. G. Mack, A. Waterfeld, H. Oberhammer, *J. Am. Chem. Soc.* **1991**, *113*, 7847.